NASA Contractor Report 170417

Model Reduction for Control System Design

Dale Enns

March 1985

National Aeronautics and
Space Administration

NASA Contractor Report 170417

Model Reduction for Control System Design

Dale Enns
Stanford Electronics Laboratories, Stanford University, Stanford, California

1985

National Aeronautics and
Space Administration
Ames Research Center
Dryden Flight Research Facility
Edwards, California 93523

This Page Intentionally Left Blank

MODEL REDUCTION FOR CONTROL SYSTEM DESIGN

Dale Enns, Ph.D.
Stanford University, 1984

In a number of applications areas, the control engineer is faced with controlling a physical system for which an analytical model can be derived in the form of a very large number of coupled, first order, linear, time invariant differential equations. This high order analytical model is an input to the controller design process for any design technique.

This thesis develops an approach and a technique for effectively obtaining reduced order mathematical models of a given large order model for the purposes of synthesis, analysis and implementation of control systems.

This approach involves the use of an error criterion which is the H-infinity norm of a frequency weighted error between the full and reduced order models. The weightings are chosen to take into account the purpose for which the reduced order model is intended.

A previously unknown error bound in the H-infinity norm for reduced order models obtained from internally balanced realizations was obtained. This motivated further development of the balancing technique to include the frequency dependent weightings. This resulted in the frequency weighted balanced realization and a new model reduction technique.

Two new approaches to designing reduced order controllers were also developed. The first involves reducing the order of a high order controller with an appropriate weighting. The second involves linear-quadratic-Gaussian synthesis based on a reduced order model obtained with an appropriate weighting.

Several numerical examples are used to illustrate the theoretical developments of the thesis. These examples include aircraft and large space structure problems. The examples clearly illustrate the usefulness of this research for practical problems.

ACKNOWLEDGMENTS

Certainly the biggest influence with respect to background, motivation, direction and philosophy for the practical, theoretical and numerical issues of this thesis has been obtained as a result of my association with the Honeywell Systems and Research Center. I have especially benefited from working with Mike Barrett, Tom Cunningham, John Doyle, Chris Greene, Norm Lehtomaki, Steve Pratt, Gunter Stein and Joe Wall.

I would like to express my gratitude to my major advisor at Stanford, Professor Gene Franklin for having time to listen to me and for his comments, questions and advise throughout the course of this research. I want to thank Professors Arthur Bryson and Robert Cannon for their constructive comments and questions during the final phases of this manuscript. In general, I would like to thank all of my professors at Stanford and the University of Minnesota for the quality instruction I have received in their classes.

I have also benefited from many discussions with fellow classmates, notably: Doug Bernard, Uy-Loi Ly, Kevin Petersen, Dan Rosenthal, Eric Schmitz and Bong Wie.

I am also very thankful for the diligent and excellent typing of Ms. Mieko Parker that enabled a timely completion of this thesis.

Most of all I would like to express my deepest gratitude to Laurie, my wife. I am grateful for the cheerful encouragement she gives me and for putting up

with my conversation when the thesis material dominated my thoughts.

The thesis work was supported by Honeywell Internal Research and Development and supported under the grant NAG 2-223 and monitored by Kevin Petersen from the NASA Dryden Flight Research Facility.

TABLE OF CONTENTS

LIST OF FIGURES

LIST OF TABLES

LIST OF SYMBOLS

A	dynamics matrix
B	input matrix
C	output matrix
D	feedthru matrix
E_∞	scalar model reduction error
F	dynamics matrix
G	input matrix
G_F	grammian for $F(t)$
H	output matrix
I	identity matrix
j	square root of –1, i.e. $j^2 = -1$
J	performance index
k	integer index
K	gain matrix
M	process noise spectral intensity
n	number of states
N	measurement noise spectral intensity
P	Riccati solution
q	scalar recovery parameter
Q	state weighting matrix
r	number of states in reduced order model
R	input weighting matrix

s	Laplace transform variable
S_c	controllable set
S_o	observable set
t	time
T	similarity transformation
u	input vector
U	controllability grammian
U	weighted controllability grammian
v	eigenvector
V	eigenvector matrix
W	orthogonal matrix
x	state vector
$\hat{x}$	state vector estimate
y	output vector
$\hat{y}$	output vector estimate
Y	observability grammian
Y	weighted observability grammian
z	transmission zero
z	state vector
Γ	process noise input matrix
Δ	perturbation
ς	damping ratio
η	measurement noise vector
λ_i	(i,i) element of Λ

Λ diagonal matrix

ξ process noise vector

σ_i (i,i) element of Σ

Σ diagonal matrix

τ time

ω angular frequency

LIST OF FUNCTIONS

$A(s)$ all pass transfer function

$d(t)$ disturbance

$e(s)$ error Laplace transform

$e(t)$ error

$f(s)$ function of Laplace transform variable

$f(t)$ function of time

$f(U)$ plant order reduction fixed point function

$F(s)$ function of Laplace transform variable

$F(t)$ impulse response matrix

$G(s)$ transfer function

$H(s)$ closed loop transfer function

$K(s)$ compensator transfer function

$l(\omega)$ uncertainty bound

$L(s)$ loop transfer function

$L(s)$ left factor of perturbation Laplace transform

$n(t)$ sensor noise

$P(s)$ all pass transfer function

$P(s)$ loop transfer function

$R(s)$ right factor of perturbation Laplace transform

$S(s)$ sensitivity transfer function

$T(s)$ transfer function

$u(s)$ input Laplace transform

$w(\omega)$	frequency response of weighting
$W(s)$	weighting Laplace transform
$y(s)$	output Laplace transform
$y_c(t)$	output command
$\delta(t)$	unit impulse function
$\Delta(s)$	perturbation Laplace transform
$\eta(t)$	output of output model reduction weighting
$\mu(t)$	input to input model reduction weighting

LIST OF OPERATORS

$\det[\bullet]$	determinant of $\bullet$
$\mathrm{Im}[\bullet]$	imaginary part of $\bullet$
$L[\bullet](s)$	Laplace transform of $\bullet$
$L^{-1}[\bullet](t)$	inverse Laplace transform of $\bullet$
$\mathrm{Re}[\bullet]$	real part of $\bullet$
$tr[\bullet]$	trace of $\bullet$
$\lambda[\bullet]$	eigenvalues of $\bullet$
$\sigma[\bullet]$	singular values of $\bullet$
$\bar{\sigma}[\bullet]$	maximum singular value of $\bullet$
$\underline{\sigma}[\bullet]$	minimum singular value of $\bullet$
$[\dot{\bullet}]$	$\frac{d}{dt}[\bullet]$
$\lvert\bullet\rvert$	absolute value of $\bullet$
$\lVert\bullet\rVert$	vector norm of $\bullet$
$\lVert\bullet\rVert_2$	L_2 norm of $\bullet$
$\lVert\bullet\rVert_\infty$	L_∞/H_∞ norm of $\bullet$
$\lVert\bullet\rVert_H$	Hankel norm of $\bullet$

LIST OF SUBSCRIPTS

act	actuator
c	command
c	control
cl	closed loop
d	disturbance
e	error
f	filter
H	Hankel
i	input
i	integer index
ib	internally balanced
in	input
k	integer index
l	loop
m	number of inputs
max	maximum
n	integer
n	number of states
n	sensor noise
p	number of outputs
p	perturbed
o	output

ol	open loop
out	output
r	number of states in reduced order model
r	reduced
s	stable
sr	stable reduced
true	true system
u	input
us	unstable
w	weighting
y	output
∞	infinity
+	some poles in right half plane
–	no poles in right half plane

LIST OF SUPERSCRIPTS

H	complex conjugate transpose
m	number of inputs
n	number of states
N	number of states
p	number of outputs
T	transpose
$*$	complex conjugate
-1	inverse

LIST OF ABBREVIATIONS

DC	zero frequency (direct current)
GM	gain margin
LQ	linear quadratic
LQG	linear quadratic gaussian
MIMO	multiple input - multiple output
PM	phase margin
SISO	single input - single output

I. INTRODUCTION

In a number of applications areas, the control engineer is faced with controlling a physical system for which an analytical model can be derived in the form of a very large number of coupled, first order, linear, time invariant differential equations. This high order analytical model is an input to the controller design process for any design technique.

Two important control law design techniques: linear quadratic gaussian (LQG) [Refs. 1-5] and H_∞ optimization,[Ref. 5] result in high order control laws that are at least as complex (same number of equations) as the differential equation model of the system to be controlled. These control laws are typically overly complex and simpler designs are sought.

Because of computational and other practical limitations, the order (number of equations) of such a model or controller must be reduced for synthesis, analysis and implementation of the control system. Nowhere is this need more clear than in the area of flexible vehicle control (aircraft or large space structures) where an infinite number of resonant frequencies (hence, equations) characterize the flexible vehicle.

Using model reduction as a part of the controller design process is in effect a technique for designing a reduced order controller. The reduced order model must characterize the physical system with sufficient fidelity such that performance objectives (including, but not limited to stability) for the controlled

physical system can be met by designing control laws with the reduced order model.

The intent of this thesis is to develop well understood tools for effectively obtaining reduced order mathematical models of a given large order model for the purposes of synthesis, analysis and implementation of control systems.

Related Literature

There is an enormous amount (e.g. see reference list of Ref. 6) of model reduction literature, however, very few of the researchers have studied this problem from the perspective of controller design based on the reduced order model. Indeed, most present their results without any mention of the controller and the impact of the model reduction on stability or other performance objectives.

The most common approach cited is to minimize the integral squared impulse response error between the full and reduced order model (e.g. Refs. 7-10). For some unknown reason this error criterion was adopted and algorithms for solving the minimization problem have been developed. Unfortunately, a closed form solution to this problem has not been found and the iterative algorithms suffer from such difficulties as: choice of starting guesses, convergence, multiple local minima, etc. This approach is somewhat dissatisfying since there is no good reason for choosing such an error criterion and its lack of desirable solution properties.

Another approach to the model reduction problem is to neglect states of the internally balanced realization of the full order model [Ref. 11]. This technique does not attempt to minimize any error criterion. Rather, it is based on transforming the realization of the full order model into balanced coordinates where the states of the balanced realization are as controllable as observable in a well defined sense. The reduced order model is then obtained by neglecting the states which are weakly controllable/observable. In contrast to the previous approach, this technique permits a closed form solution involving standard matrix software.

A closely related approach is the Hankel norm model reduction technique, [Refs. 12-14]. For any error criterion this is the only model reduction technique which results in a closed form solution for the optimal reduced order model. Optimal here is in the sense of the Hankel norm which will be defined in a later chapter.

A characteristic common to all of these approaches is that the ultimate use for which a reduced order model is sought is not formally a part of the model reduction process. For the purposes of this thesis, the ultimate use is for design, analysis and implementation of feedback control systems.

Thesis Contributions

An approach to the model reduction problem where control design is a formal part of the model reduction process was developed. This approach

involves the use of an error criterion which is the H_∞ norm of a frequency weighted error between the full and reduced order models. The motivation for choosing this error criterion (to be defined precisely in a later chapter) was the relation between model uncertainty and closed loop system behavior.

The balancing technique was extended to include the frequency dependent weightings. The weightings are added in the context of the balancing method i.e. controllability/observability aspects of a weighted system.

A previously unknown error bound (in the H_∞ norm) for the internally balanced realization was discovered. This bound provides the missing error criterion for the balancing technique. This bound was compared to an error bound (in the H_∞ norm) for the Hankel norm technique which was obtained by Glover [Ref. 15]. Unfortunately a corresponding, simple error bound (in the H_∞ norm) for the weighted case was not obtained.

An explicit weighting for reducing the order of a controller was developed. This results in a straightforward reduced order controller design algorithm, however, the full order controller must first be designed with the full order model.

Another approach to the reduced order controller design problem, where a reduced order model is used to design the low order controller directly was also developed. This approach, however, requires an iterative solution for the reduced order model.

The theoretical approaches were applied to several example problems to illustrate the methodology. A significant design/demonstration example was carried out for the ACOSS II large space structure. This example clearly demonstrates the effectiveness of the developments of this thesis. This example also shows the usefulness of this research for application to practical problems.

Organization of the Thesis

The remainder of this thesis is organized into five chapters. Chapter II will cover the necessary background material on control system design and model reduction. Chapter III will cover the new model reduction technique. Chapter IV will cover control system design with reduced order models. Chapter V will present the examples and Chapter VI the conclusions and recommendations for further research.

Chapter II will serve as a reference for the work that follows. In the area of feedback controller design some feedback fundamentals as well as the LQG synthesis procedure will be discussed. In the area of model reduction the internally balanced realization technique will be discussed. No attempt will be made at completeness, rather, only those aspects that directly relate to this work will be addressed.

Chapter III will discuss the new model reduction approach and techniques. An algorithm for computing the frequency weighted balanced realization will be

derived. The properties of the resulting reduced order models will also be discussed.

Chapter IV will develop two new approaches to reduced order controller design. Both of these approaches are developed by connecting model reduction and controller design together with the relationship between model uncertainty and robust design. The first approach involves compensator order reduction and the second involves plant order reduction.

Chapter V will present several design examples in detail. The control objectives will be stated and reduced order controllers are designed to meet these objectives using the techniques developed in this thesis.

II. BACKGROUND MATERIAL

The purpose of this chapter is to cover background material in the areas of model reduction and feedback control system design. Some mathematical analysis notation and tools will be covered briefly.

Notation

The transpose of the matrix, A will be denoted by A^T. The complex conjugate of the matrix, A will be denoted by A^*. The conjugate transpose of the matrix, A will be denoted by A^H. Eigenvalues and singular values of the matrix, A will be denoted by $\lambda[A]$ and $\sigma[A]$ respectively. The maximum and minimum singular values of the matrix, A will be denoted by $\bar{\sigma}[A]$ and $\underline{\sigma}[A]$ respectively. The trace and determinant of the matrix, A will be denoted by $tr[A]$ and $det[A]$ respectively. A positive definite matrix, A will be denoted by $A > 0$ and a positive semi-definite matrix, A will be denoted by $A \geq 0$. Real and imaginary parts of the complex matrix A will be denoted by $\mathrm{Re}[A]$ and $\mathrm{Im}[A]$ respectively. That is $A = \mathrm{Re}[A] + j\ \mathrm{Im}[A]$ where $j^2 = -1$. An $n \times n$ identity matrix will be denoted by I_n or I depending on context. A diagonal matrix, A will be denoted by $A = \mathrm{diag}\ \{a_i\}$ where a_i is the (i,i) element of the matrix A. The notation: block col $\{A_i\}$ and block row $\{A_i\}$ is defined

$$\text{block col}\{A_i\} = [A_1\, A_2 \cdots A_n]$$

$$\text{block row}\{A_i\} = \begin{bmatrix} A_1 \\ A_2 \\ \cdot \\ \cdot \\ \cdot \\ A_n \end{bmatrix}$$

where A_i are matrices of compatible dimensions.

The symbol, $\triangleq$ is read equals by definition. The symbol, $\forall$ is read for any or for all. The symbol, $\mathbf{R}$ represents the field of real scalars. The symbol, $\mathbf{R}^n$ represents the space of $n \times 1$ real vectors. The symbol, ϵ is read is an element of (e.g. $x \epsilon \mathbf{R}^n$). The symbol, $\delta(t)$ stands for the Dirac delta function (also called the unit impulse function).

Linear Systems Terminology

Consider the linear system given by

$$\dot{x} = Ax + Bu \qquad x \epsilon \mathbf{R}^n \qquad u \epsilon \mathbf{R}^m$$
$$y = Cx + Du \qquad y \epsilon \mathbf{R}^p \quad .$$

The order of the system is the integer, n. The system has m inputs and p outputs. The transfer function of the system is given by $C(sI-A)^{-1}B + D$. The symbols $\{A,B,C,D\}_n$ or $\{A,B,C,D\}$ (when $D=0$, $\{A,B,C\}_n$ or $\{A,B,C\}$) represent a realization (above differential equations) of the transfer function of the system. Note that realizations are not unique. The statements (A,B) controllable and (A,C) observable have the standard meaning, [Ref. 34]. The

statement (A,B) stabilizable will mean that the uncontrollable modes of the system are stable. The statement (A,C) detectable will mean that the unobservable modes of the system are stable. The realization $\{A,B,C,D\}$ will be said to be minimal if it is completely controllable and observable. The system is said to be asymptotically stable if $\mathrm{Re}[\lambda[A]] < 0$. The system is said to be minimum phase if $\mathrm{Re}[z] < 0$ where z is a transmission zero of the system. Transmission zeros are defined for minimal systems to be the values of z such that

$$\begin{bmatrix} zI-A & -B \\ -C & -D \end{bmatrix} \text{ loses rank} \quad .$$

The Laplace transform of the function, $f(t)$ will be denoted by $\mathbf{L}[\mathrm{f}(\mathrm{t})](\mathrm{s})$, or when context permits $f(s)$, and t will be used exclusively to denote time and s will be used exclusively to denote the Laplace variable. This is an abuse of notation but context will always determine whether the function or the transform is meant.

The function, $f(t)$ which is the inverse Laplace transform of the function, $F(s)$ will be denoted by $\mathbf{L}^{-1}[\mathrm{F}(\mathrm{s})](\mathrm{t})$. That is

$$\begin{aligned} f(t) &= \mathbf{L}^{-1}[\mathrm{F}(\mathrm{s})](\mathrm{t}) \\ F(s) &= \mathbf{L}[\mathrm{f}(\mathrm{t})](\mathrm{s}) \quad . \end{aligned}$$

Singular values will be used throughout this thesis and to make the thesis self contained some definitions, identities, inequalities and theorems are tabulated in Appendix A.

Analysis Tools

The analysis tools needed for the development of the thesis ideas are several norms. These norms will now be defined.

Absolute value: The absolute value of the complex scalar, z will be denoted by $|z|$ and is defined by $|z|^2 \triangleq zz^*$.

Vector norm: The norm of the complex vector, x will be denoted by $||x||$ and is defined by $||x||^2 \triangleq x^H x$.

Maximum singular value: The maximum singular value (sometimes called the spectral norm) of the complex matrix, A will be denoted by $\bar{\sigma}[A]$ and is defined by $\bar{\sigma}^2[A] \triangleq \lambda_{\max}[A^H A]$.

L_2 norm: The L_2 norm of the complex matrix valued function, $f(x)$ of a single real variable, x will be denoted by $||f(x)||_2$ and is defined by $||f(x)||_2^2 \triangleq \int_o^\infty tr[f^H(x)f(x)]dx$.

L_∞: The L_∞ norm of the complex matrix valued function, $f(x)$ of a single real variable, x will be denoted by $||f(x)||_\infty$ and is defined by $||f(x)||_\infty = \sup_x \bar{\sigma}[f(x)]$.

H_∞ norm: The H_∞ norm of the complex matrix valued function, $f(s)$ of a single complex variable, s which is analytic in the closed right half plane will be denoted by $||f(s)||_\infty$ and is defined by $||f(s)||_\infty = \sup_\omega \bar{\sigma}[f(j\omega)]$.

Hankel norm: The Hankel norm of the complex matrix valued function, $f(s)$ of a single complex variable, s which is analytic in the closed right half plane will be denoted by $\|f(s)\|_H$ and is defined by $\|f(s)\|_H^2 \triangleq \lambda_{\max}[UY]$ where $f(s)$ is assumed to have a state space realization: $f(s) = C(sI-A)^{-1}B$ and U, Y satisfy the Lyapunov equations:

$$\begin{aligned} AU + UA^T + BB^T &= 0 \\ A^TY + YA + C^TC &= 0 \quad . \end{aligned}$$

Note that this definition is equivalent to other definitions of the Hankel norm given in the literature. A finite dimensional realization of $f(s)$ was assumed as a convenience for this thesis.

General Framework for Control Systems Analysis and Synthesis

The purpose of this section is to briefly review a new framework for analysis and synthesis of control systems developed by Doyle, [Ref. 5]. This review will state the assumptions which imply the use of the specific analysis and synthesis tools to be used in this thesis. The point is that other assumptions could just as well be made and they in turn would require other analysis and synthesis tools.

A general control system is depicted in Fig. II.1. The diagram already

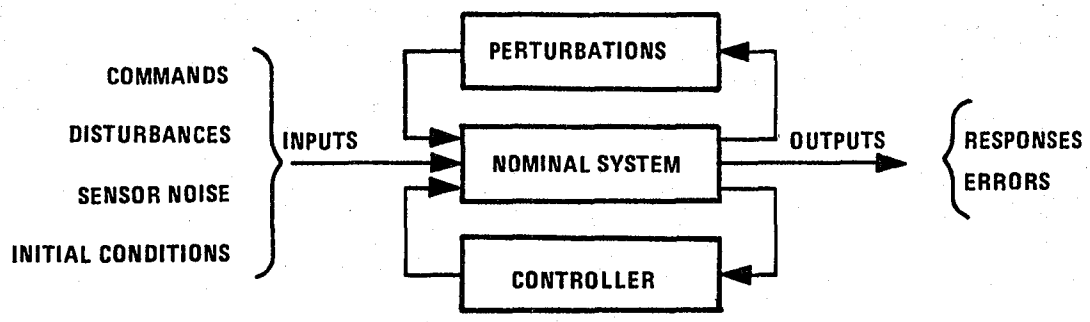

Fig. II.1 General Control System

makes the assumption that the actual physical system can be represented as a nominal system plus perturbations. This assumption is necessary since it is desirable for the nominal model (typically linear, time invariant ordinary differential equations) of the system to be as simple as possible (otherwise we cannot do much analysis, let alone synthesis). This is also the motivation for model reduction.

Typically the input signals are given for a control problem. That is their magnitude, energy, frequency content, ... are specified in some way. The output signals on the other hand are functions of the inputs and the rest of the system. Typically some desirable output signal magnitude, energy, frequency content, ... are specified. These specifications mathematically take the form of frequency weighted norms.

The perturbations denoted by Δ can typically be bounded in some way. In general, these bounds mathematically take the form of frequency weighted norms. A simple example is the system in Fig. II.2 where the time constant of the nominal linear system

$$\begin{aligned} \dot{x}(t) &= ax(t) + u(t) \\ y(t) &= x(t) \end{aligned}$$

is uncertain but bounded above and below with the absolute value norm, i.e.

$$|\Delta| \leq \frac{1}{10} |a| \quad \text{where} \quad a = \text{constant} \quad .$$

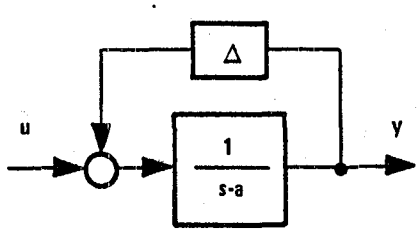

Fig. II.2 Simple Uncertain System

Another less trivial example is an actuator with a finite bandwidth and rate limit shown in Fig. II.3. This system can be nominally modeled as unity

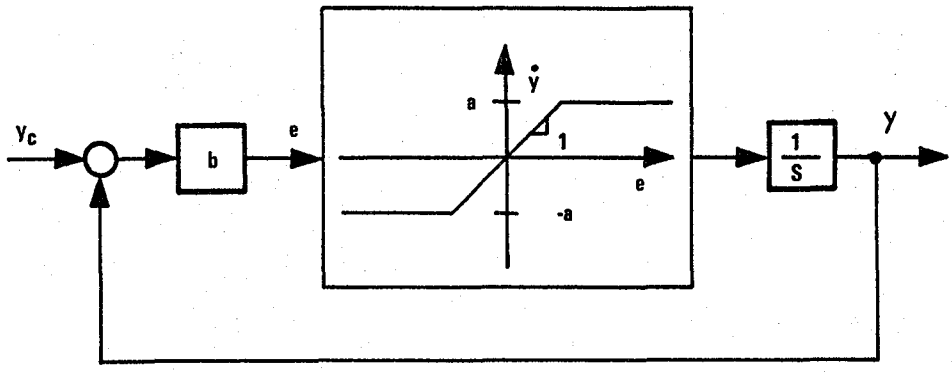

Fig. II.3 Finite Bandwidth Actuator with a Rate Limit

plus a perturbation as shown in Fig. II.4. In this case the uncertainty is bounded using the absolute value and $\mathbf{L}_\infty$ norms and is expressed [Ref. 16]

$$\|e(t)\|_\infty \leq \eta a \quad \Rightarrow$$

$$|\Delta(j\omega)| \leq \frac{\frac{\omega}{b}\left[\sqrt{\frac{\omega^2}{b^2} + \frac{1}{4}(1+\frac{1}{\eta})^2} + \frac{1}{2}(1-\frac{1}{\eta})\right]}{\left(\frac{\omega^2}{b^2} + \frac{1}{\eta}\right)}$$

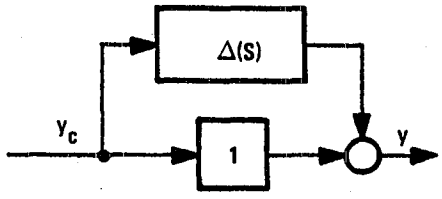

Fig. II.4 Actuator Nominal Model Plus a Perturbation

Note that the bound for $\Delta(s)$ depends on the signal level.

Without elaborating any further here (see Ref. 5 for more details) Doyle's Table will be introduced now and is shown as Table II.1. This table lists out various assumptions and the analysis and synthesis tools that result. The assumptions that will be used for the remainder of this thesis are found in the second and third rows of Table II.1.

The second row assumes the input signals have bounded $\mathbf{L}_2$ norms and that the output specifications are expressed in terms of L_2 norms. Actually the frequency content of these signals is also of interest but without loss of generality the weightings for this frequency content can be absorbed into the nominal model. The perturbations are assumed to be zero. These assumptions result in the use of Bode plots of singular values as the analysis tool and for this thesis loop shaping as a synthesis tool.

Table II.1 Assumptions and Corresponding Analysis and Synthesis Tools

Assumptions

Nominal Plant	Inputs	Output Spec.	Perturbations	Analysis	Synthesis	
Linear Time-Invariant	White Noise	Covariance	$\Delta = 0$	Covariance	Wiener-Hopf-Kalman LQG	Special Cases
	L_2	L_2	$\Delta = 0$	Singular Values	H_∞ (Zames, et al.)	Special Cases
	—	stable	L_2 conic sector	Bode Plots	Loop Shaping	Special Cases
	L_2	L_2	Multiple L_2 Conic Sectors (Structured)	μ Structured Singular Value	New H_∞ Results	New General Framework

The third row assumes zero inputs and guaranteed stability as the only output specification. However, a specific class of perturbations is permitted. These assumptions also result in Bode plots of singular values and loop shaping as analysis and synthesis tools respectively.

Note that for these two rows performance and stability robustness are treated separately. This is, in fact, one of the weaknesses of loop shaping as a design tool and singular values as an analysis tool. Singular values can be used in general but may be too conservative. In general, the weakness of loop shaping is that we are typically concerned with properties of more than one of the feedback system's loops simultaneously.

This weakness is eliminated with the use of the structured singular value [Refs. 17, 18]. The structured singular value permits the non-conservative evaluation of robust performance. That is, it answers the question of whether or not the performance specification is met in the face of the perturbations (not necessarily small). This is not otherwise possible.

Although the structured singular value and H_∞ synthesis techniques [Ref. 19] are very promising tools, they were considered beyond the scope of this thesis.

Why Bode Plots of Singular Values?

As already indicated in Table II.1, using Bode plots of singular values is a consequence of the assumptions of the second and third rows of Table II.1. The purpose of this section is to develop these consequences in more detail.

Performance

Let $G(s)$ be the asymptotically stable transfer function from the input, u to the output, y, i.e.

$$y(s) = G(s)u(s) \quad .$$

Then the following two statements are equivalent [Ref. 20]:

$$||y(t)||_2 \leq 1 \qquad \text{for all} \qquad ||u(t)||_2 \leq 1$$

and

$$||G(s)||_\infty \leq 1 \quad .$$

In other words, the H_∞ norm of the transfer function (or the L_∞ norm of the transfer function's frequency response) measures the worst case gain of the system. The idea is that for an arbitrary input, $u(t)$, with unit L_2 norm, the transfer function's H_∞ norm gives the worst case L_2 norm of the output, $y(t)$.

Typically frequency content is also important and the utility of this approach to measuring performance is increased by introducing the weighting transfer functions $W_y(s)$ and $W_u(s)$ respectively. In this case the following two statements are equivalent [Ref. 20]:

$$||\mathbf{L}^{-1}[\mathrm{W_y(s)y(s)}](\mathrm{t})||_2 \leq 1 \qquad \text{for all} \qquad ||\mathbf{L}^{-1}[\mathrm{W_u(s)u(s)}]\,(\mathrm{t})||_2 \leq 1$$

and

$$\| W_y(s) G(s) W_u^{-1}(s) \|_\infty \leq 1 \quad .$$

The Bode plot of the singular values of $G(j\omega)$ or $W_y(j\omega)\ G(j\omega) W_u^{-1}(j\omega)$ is just a graphical means of assessing performance (because the magnitude of the highest peak of the frequency response is the H_∞ norm). Often the weightings are not explicitly constructed, rather, the singular values of $G(j\omega)$ are plotted and the effect of certain weightings can be readily assessed by the shape of the frequency response.

Stability Robustness

The stability robustness of a MIMO control system can be determined with Bode plots of singular values with the aid of the following theorem. Consider the perturbed feedback system shown in Fig. II.5 where $G(s)$ is the nominal open loop transfer function and $\Delta(s)$ is the

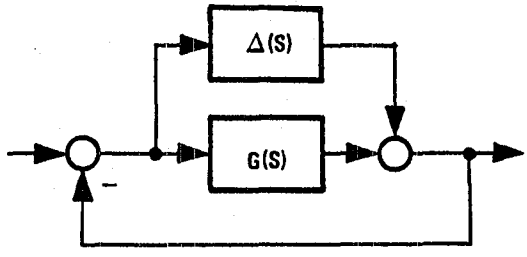

Fig. II.5 Perturbed MIMO Feedback System

transfer function of the additive perturbation.

Stability Robustness Theorem:

Assume that the nominal closed loop system is stable i.e. $G(s)[I + G(s)]^{-1}$ has no poles in the closed right half plane. Then for any stable $\Delta(s)$ such that

$$||L(s)\ \Delta(s)\ R^{-1}(s)||_\infty \leq 1$$

if

$$||R(s)[I + G(s)]^{-1}\ L^{-1}(s)||_\infty < 1$$

the perturbed closed loop system is stable [Ref. 18].

Note that this test evaluates closed loop stability of the perturbed system for a large class of perturbations with a single test.

Actually the Stability Robustness Theorem stated above is a special case of a more general theorem in Reference 18 but it will be adequate for the purposes of this thesis.

Three stronger requirements for robust stability are:

$$\begin{aligned}
\underline{\sigma}[I + G(j\omega)] &> \bar{\sigma}[\Delta(j\omega)] && \forall\omega \\
\underline{\sigma}[I + G^{-1}(j\omega)] &> \bar{\sigma}[G^{-1}(j\omega)\Delta(j\omega)] && \forall\omega \\
\underline{\sigma}[I + G^{-1}(j\omega)] &> \bar{\sigma}[\Delta(j\omega)\ G^{-1}(j\omega)] && \forall\omega
\end{aligned}$$

i.e. satisfaction of any of these three requirements implies that the condition of the stability robustness theorem is satisfied. A proof of this statement is given in Appendix B.

The advantage of these more conservative requirements is that bounds for

the perturbation by itself or the perturbation normalized by the nominal are most times easily obtained or estimated and then can be readily compared to something that depends only on the nominal system.

The Bode plot of singular values is again just a graphical means for checking whether the control system has stability robustness with respect to a given set of perturbations. For example consider the set of perturbations

$$\{\Delta(s) \quad \text{such that} \quad \bar{\sigma}[G^{-1}(j\omega)\Delta(j\omega)] < l(\omega) \qquad \forall\omega\}$$

where $l(\omega)$ is a known function of frequency. Then if the Bode plot of $\underline{\sigma}[I + G^{-1}(j\omega)]$ lies above the Bode plot of $l(\omega)$ the perturbed closed loop system is guaranteed to be stable for any perturbation in this set.

Closed Loop Responses

The purpose of this section is to derive expressions for a MIMO control system's closed loop responses. Consider the MIMO feedback control system shown in Fig. II.6 where $G(s)$ is the plant transfer function; $K(s)$ is the compensator transfer function; y_c is the commanded value for the output, y; u is the plant input; d is the disturbance and n is the sensor noise.

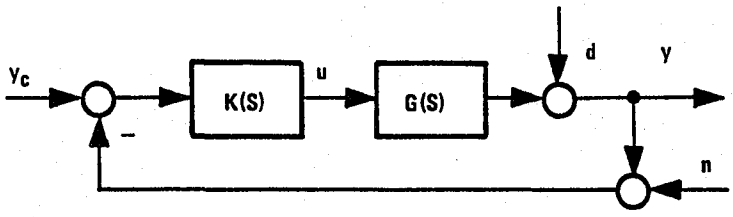

Fig. II.6 MIMO Feedback Control System

Employing standard feedback algebra results in the following closed loop responses where for notational convenience, the Laplace variable notation, s has been suppressed:

$$
\begin{aligned}
y &= d + GK[y_c - (n+y)] \\
&= (I + GK)^{-1}\,[d + GK(y_c - n)] \\
e &\triangleq y_c - y \\
&= -(I+GK)^{-1}d + [I - (I+GK)^{-1}GK]\, y_c + (I+GK)^{-1}\, GK\, n \\
&= (I+GK)^{-1}\,(y_c - d) + (I+GK)^{-1}\, GK\, n \\
u &= K[y_c - (n+d+Gu)] \\
&= (I+KG)^{-1}\, K(y_c - n - d) \quad .
\end{aligned}
$$

Desensitization

One important goal of feedback is to accomplish desensitization. Desensitization means making a system or system component insensitive to changes in operating conditions. A classic example is the feedback amplifier

where some of its component's dynamic characteristics vary widely with temperature, however, with feedback this variation can be made negligible.

The purpose of this section is to quantify the effect of feedback in accomplishing this desensitization. Note that this will not be a stability robustness analysis (which requires another analysis), here, stability is assumed.

To quantify the desensitizing effect of feedback in the multivariable case, the comparison sensitivity approach will be used [Refs. 21, 22]. In order that we compare "apples to apples," the relative sizes of perturbations to two transfer functions (open and closed loop) which are nominally the same will be compared. To facilitate this comparison, constant pre- or post-compensation will be used such that the nominal closed loop transfer function will be identical to the nominal open loop transfer function.

Output Sensitivity

For the effects of a perturbation on the output consider the open loop system in Fig. II.7 and the closed loop system in Fig. II.8 where $G(s)$ is

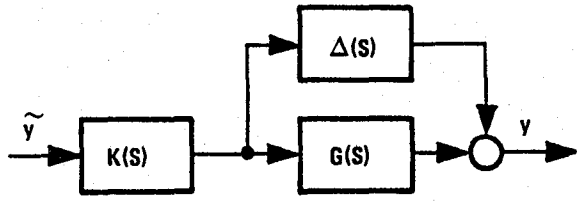

Fig. II.7 Open Loop System With Perturbation

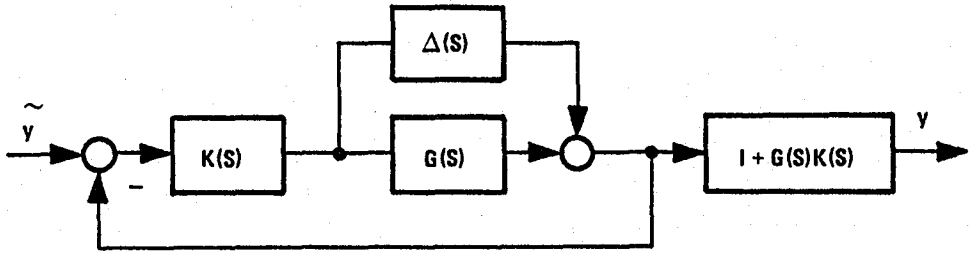

Fig. II.8 Closed Loop System With Perturbation and Post-compensation

the nominal plant transfer function, $K(s)$ and $\Delta(s)$ are the transfer functions of the compensator and perturbation respectively.

For notational convenience, the Laplace variable notation, s will be dropped. Let the perturbed plant be denoted by

$$\begin{aligned} G_p &\triangleq G + \Delta \\ &= (I + P_o)^{-1} G \end{aligned}$$

where

$$P_o \triangleq -\Delta G_p^{-1}$$

is a normalized (from the right) version of $\Delta(s)$ (i.e. % error).

Then the transfer functions from $\tilde{y}$ to y for Figs. II.7 and II.8 are given by

$$T_{ol} = G_p K = \text{open loop transfer function}$$
$$T_{cl} = (I+ GK)(I+ G_p K)^{-1} G_p K = \text{closed loop transfer function} \quad .$$

It can be verified that when $\Delta = 0$ (i.e. nominal condition) the two transfer functions: T_{ol} and T_{cl} are the same. What is of interest here is the effect of the perturbation on T_{ol} and T_{cl}. The effect of the perturbation on the open loop transfer function is given by

$$T_{ol} = (I+ P_o)^{-1} GK \quad .$$

To obtain an analogous expression for the closed loop transfer function, substitute for G_p and perform the following algebra:

$$\begin{aligned}
T_{cl} &= (I+ GK)[I + (I+ P_o)^{-1} GK]^{-1} (I+ P_o)^{-1} GK \\
&= (I+ GK)[(I+ P_o)^{-1} (I+ P_o+ GK)]^{-1} (I+ P_o)^{-1} GK \\
&= (I+ GK)(I+ GK+ P_o)^{-1} GK \\
&= (I+ GK) \{[I + P_o(I+ GK)^{-1}] (I+ GK) \}^{-1} GK \\
&= [I + P_o(I+ GK)^{-1}]^{-1} GK \\
&= [I + (P_o)_{cl}]^{-1} GK
\end{aligned}$$

where

$$(P_o)_{cl} \triangleq P_o(I+GK)^{-1} \quad .$$

At this point the effect of feedback on the perturbation is readily seen. The closed loop perturbation is essentially a scaled version of the open loop perturbation. In terms of the spectral norm we have

$$\begin{aligned} \bar{\sigma}[(P_o)_{cl}] &= \bar{\sigma}[P_o(I+GK)^{-1}] \\ &\leq \bar{\sigma}[P_o]\,\bar{\sigma}[(I+GK)^{-1}] \\ &= \bar{\sigma}[P_o]\,\frac{1}{\underline{\sigma}[I+GK]} \quad . \end{aligned}$$

That is if $\underline{\sigma}[I+GK] > 1$ holds at some frequency ($s=j\omega$) then the use of feedback accomplishes desensitization at that frequency. Bode plots of singular values again can be used as a graphical means of assessing a feedback system's desensitization properties.

Input Sensitivity

For the effects of the perturbation on the input consider the open loop system in Fig. II.9 and the closed loop system in Fig. II.10.

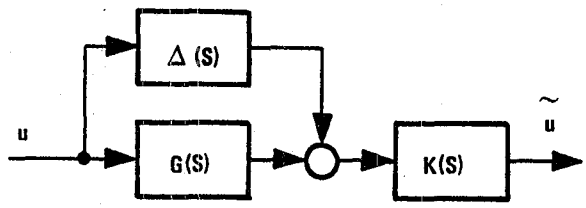

Fig. II.9 Open Loop System With Perturbation

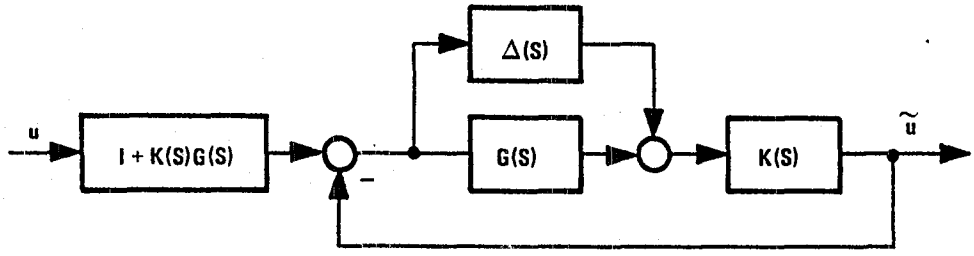

Fig. II.10 Closed Loop System With Perturbation and Pre-compensation

Let the perturbation be normalized from the left, then

$$G_p \;=\; G(I+P_i)^{-1}$$

where

$$P_i \;\triangleq\; -G_p^{-1}\,\Delta \quad .$$

Performing the same steps as for the output results in the closed loop

perturbation being given by

$$(P_i)_{cl} \triangleq (I+KG)^{-1} P_i \quad .$$

At this point the effect of feedback on the perturbation is readily seen. The closed loop perturbation is essentially a scaled version of the open loop perturbation. In terms of the spectral norm we have

$$\begin{aligned} \bar{\sigma}[(P_i)_{cl}] &= \bar{\sigma}[(I+KG)^{-1} P_i] \\ &\leq \bar{\sigma}[(I+KG)^{-1}\,]\,\bar{\sigma}[P_i] \\ &= \bar{\sigma}[P_i]\,\frac{1}{\underline{\sigma}[I+KG]} \quad . \end{aligned}$$

That is if $\underline{\sigma}[I+KG] > 1$ holds at some frequency ($s=j\omega$) then the use of feedback accomplishes desensitization at that frequency. Bode plots of singular values again can be used as a graphical means of assessing a feedback system's desensitization properties.

Feedback System Transfer Functions

The purpose of this section is to define some special transfer functions which will be used for assessing a feedback system's performance, desensitization and stability robustness properties. The following terminology will now be attached to some of the transfer functions from above. Let

$$L_o(s) \triangleq G(s)K(s) = \text{output loop transfer function}$$

$$L_i(s) \triangleq K(s)G(s) = \text{input loop transfer function}$$

$$I + G(s)K(s) = \text{output return difference}$$

$$I + K(s)G(s) = \text{input return difference}$$

$$S_o(s) \triangleq [I + G(s)K(s)]^{-1} = \text{output sensitivity}$$

$$S_i(s) \triangleq [I + K(s)G(s)]^{-1} = \text{input sensitivity}$$

$$H_o(s) \triangleq [I + G(s)K(s)]^{-1} G(s)K(s) = \text{output closed loop}$$

$$H_i(s) \triangleq K(s)G(s)[I + K(s)G(s)]^{-1} = \text{input closed loop}$$

$$I + [G(s)K(s)]^{-1} = H_o^{-1}(s) = \text{output inverse-return difference}$$

$$I + [K(s)G(s)]^{-1} = H_i^{-1}(s) = \text{input inverse-return difference} \quad .$$

The feedback properties are summarized in Table II.2.

Typical Control System Design Problem

The design problem assumes that the external inputs (commands, disturbances, sensor noise) are specified in some way (weighted L_2 norm bounds). An assumption regarding the uncertainty of the nominal model (frequency response error bound) is also required. It is also assumed that the objective of the design problem (small error between the output and commanded output) is specified in some way (weighted L_2 norm bounds again). Another objective may be that control energy is minimized in meeting the small error objective. Satisfying the control energy objective will be treated as a secondary objective and will only be mentioned briefly in a later section.

Mathematically the control design problem takes the following form.

Table II.2 Summary of Feedback System Properties

Closed Loop Responses:

$$\begin{bmatrix} y(s) \\ e(s) \\ u(s) \end{bmatrix} = \begin{bmatrix} H_o(s) & S_o(s) & -H_o(s) \\ S_o(s) & -S_o(s) & H_o(s) \\ H_i(s)G^{-1}(s) & -H_i(s)G^{-1}(s) & -H_i(s)G^{-1}(s) \end{bmatrix} \begin{bmatrix} y_c(s) \\ d(s) \\ n(s) \end{bmatrix}$$

Stability Robustness:

$$\bar{\sigma}\left[H_i^{-1}(j\omega)\right] > \bar{\sigma}\left[G^{-1}(j\omega)\Delta(j\omega)\right] \qquad \forall\omega$$

$$\bar{\sigma}\left[H_o^{-1}(j\omega)\right] > \bar{\sigma}\left[\Delta(j\omega)G^{-1}(j\omega)\right] \qquad \forall\omega$$

Desensitization:

$$\bar{\sigma}\left[(P_i)_{cl}(j\omega)\right] \leq \bar{\sigma}\left[P_i(j\omega)\right]\bar{\sigma}\left[S_i(j\omega)\right] \qquad \forall\omega$$

$$\bar{\sigma}\left[(P_o)_{cl}(j\omega)\right] \leq \bar{\sigma}\left[P_o(j\omega)\right]\bar{\sigma}\left[S_o(j\omega)\right] \qquad \forall\omega$$

Assume that weightings have been obtained such that the magnitude and frequency content of the commands, disturbances and sensor noise for the control problem are described by

$$\|\mathbf{L}^{-1}\,[W_{y_c}(s)y_c(s)]\,(t)\|_2 \leq 1$$
$$\|\mathbf{L}^{-1}[W_d(s)d(s)]\,(t)\|_2 \leq 1$$
$$\|\mathbf{L}^{-1}[W_n(s)n(s)]\,(t)\|_2 \leq 1 \quad .$$

Likewise assume that a weighting has been obtained such that the acceptable magnitude and frequency content of the error (i.e. $e \triangleq y_c - y$) is described by

$$\|\mathbf{L}^{-1}[W_e(s)e(s)]\,(t)\|_2 \leq 1 \quad .$$

Assume that the modeling process has produced a nominal model of the plant, $G(s)$ (transfer function corresponding to linear, time invariant, ordinary differential equations) and one or both of the input and/or output scalar, frequency dependent, multiplicative uncertainty bounds $l_i(\omega)$ and/or $l_o(\omega)$. These bounds describe the uncertainty between the nominal model, $G(s)$ and the true system $G_{\text{true}}(s)$ as follows. Although the true system is not precisely known we will assume it belongs to one or both of the sets:

$$\{G_{\text{true}}(s):\ \bar{\sigma}[G^{-1}(j\omega)\,[G_{\text{true}}(j\omega) - G(j\omega)]\,] \leq l_i(\omega)\,\}$$
$$\{G_{\text{true}}(s):\ \bar{\sigma}[[G_{\text{true}}(j\omega) - G(j\omega)]\,G^{-1}(j\omega)] \leq l_o(\omega)\,\} \quad .$$

Given the weightings $W_{y_c}(s)$, $W_d(s)$, $W_n(s)$ and $W_e(s)$, the nominal model, $G(s)$ and its uncertainty bounds, $l_i(\omega)$ and $l_o(\omega)$ the control system design

problem is to find the compensator transfer function such that the performance objective is satisfied for the feedback system of Fig. II.11.

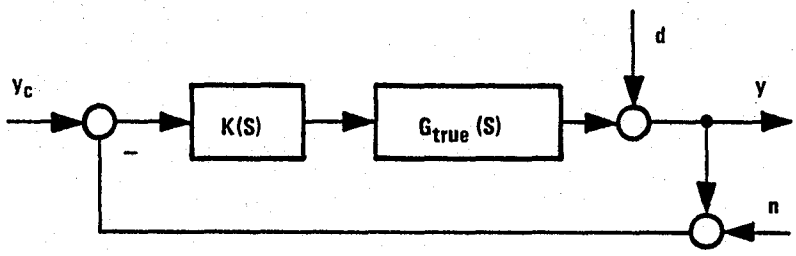

Fig. II.11 Feedback Control System Block Diagram

Although Doyle's structured singular value and H_∞/L_∞ synthesis method [Refs. 5, 17, 18, 19] solve this problem, the theoretical background required is far beyond the scope of this work, hence, this thesis will only discuss an approximate solution. In addition to the substantial theoretical understanding required, the H_∞/L_∞ synthesis method requires significantly more numerical computations to obtain the compensator transfer function, $K(s)$.

A major simplifying assumption is to require only that the performance objective be satisfied for the nominal system (second row of Table II.1) although stability is required for the true system (3rd row of Table II.1). The other simplification is that no formal optimization will be attempted.

Performance and Uncertainty Requirements

To meet the performance objective for each one of the command, disturbance and sensor noise individually requires that

$$\begin{aligned} \| W_e(s)[I + L_o(s)]^{-1} W_{y_c}^{-1}(s) \|_\infty &\leq 1 \\ \| W_e(s)[I + L_o(s)]^{-1} W_d^{-1}(s) \|_\infty &\leq 1 \\ \| W_e(s)[I + L_o(s)]^{-1} L_o(s) W_n^{-1}(s) \|_\infty &\leq 1 \quad . \end{aligned}$$

To satisfy the output stability robustness requirement, requires that

$$\underline{\sigma}[I + L_o^{-1}(j\omega)] > l_o(\omega) \quad .$$

To gain a clearer picture of these requirements, note that they are satisfied if

$$\begin{aligned} w_e(\omega) w_{y_c}^{-1}(\omega) &\leq \underline{\sigma}[I + L_o(j\omega)] \\ w_e(\omega) w_d^{-1}(\omega) &\leq \underline{\sigma}[I + L_o(j\omega)] \\ \bar{\sigma}[[I + L_o(j\omega)]^{-1} L_o(j\omega)] &\leq w_e^{-1}(\omega) w_n(\omega) \\ \bar{\sigma}[[I + L_o(j\omega)]^{-1} L_o(j\omega)] &< l_o^{-1}(\omega) \end{aligned}$$

where

$$\begin{aligned} w_e(\omega) &\triangleq \bar{\sigma}[W_e(j\omega)] \\ w_k(\omega) &\triangleq \underline{\sigma}[W_k(j\omega)] \qquad k = y_c, d, n \quad . \end{aligned}$$

It will be helpful to choose the simple performance objective

$$\begin{aligned} \| e(t) \|_2 &\triangleq \| y_c(t) - y(t) \|_2 < \epsilon \\ &\Rightarrow W_e(s) = \frac{1}{\epsilon} \end{aligned}$$

and plot $\frac{1}{\epsilon} w_{y_c}^{-1}(\omega)$, $\frac{1}{\epsilon} w_d^{-1}(\omega)$, $\epsilon w_n(\omega)$ and $l_o^{-1}(\omega)$ versus frequency. Such a plot is shown in Fig. II.12 where a log-log scale has been used.

Satisfying the requirements for the commands and disturbances requires that a plot of $\underline{\sigma}[I + L_o(j\omega)]$ lie above the command and disturbance curves in Fig. II.12. Satisfying the requirements for the sensor noise and uncertainty requires that a plot of $\bar{\sigma}[\,[I + L_o(j\omega)]^{-1} L_o(j\omega)\,]$ lie below the sensor noise and uncertainty curves in Fig. II.12.

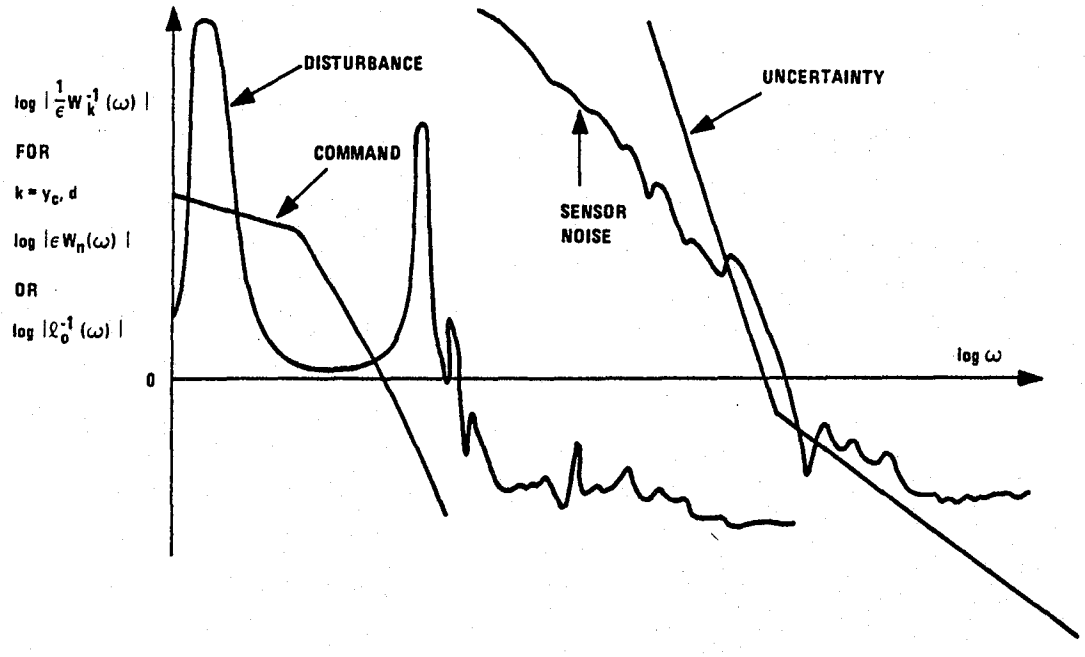

Fig. II.12 Typical Magnitude and Frequency Content of Commands, Disturbances, Sensor Noise and Uncertainty

Large and Small Loop Gain Approximations

Although the requirements are in terms of $\underline{\sigma}[I + L_o(j\omega)]$ and $\bar{\sigma}[\,[I + L_o(j\omega)]^{-1} L_o(j\omega)]$ they can be well approximated by requirements on large and small loop gains as follows. Note that if $\underline{\sigma}[I + L_o(j\omega)]$ is large (i.e. $>> 1$) then $\underline{\sigma}[L_o(j\omega)]$ is also large in fact

$$\underline{\sigma}[I + L_o(j\omega)] \cong \underline{\sigma}[L_o(j\omega)]$$

when

$$\underline{\sigma}[L_o(j\omega)] >> 1 \quad .$$

Also note that if $\bar{\sigma}[[I + L_o(j\omega)]^{-1} L_o(j\omega)]$ is small (i.e. $<< 1$) then $\bar{\sigma}[L_o(j\omega)]$ is also small in fact

$$\bar{\sigma}[[I + L_o(j\omega)]^{-1} L_o(j\omega)] \cong \bar{\sigma}[L_o(j\omega)]$$

when

$$\bar{\sigma}[L_o(j\omega)] << 1 \quad .$$

These observations suggest that Fig. II.12 can be used to determine graphically the suitability of any $L_o(s)$ and thus of any compensator, $K(s)$ (since $L_o(s) = G(s)K(s)$) by simply sketching the singular values of $L_o(j\omega)$. Such a plot is shown in Fig. II.13.

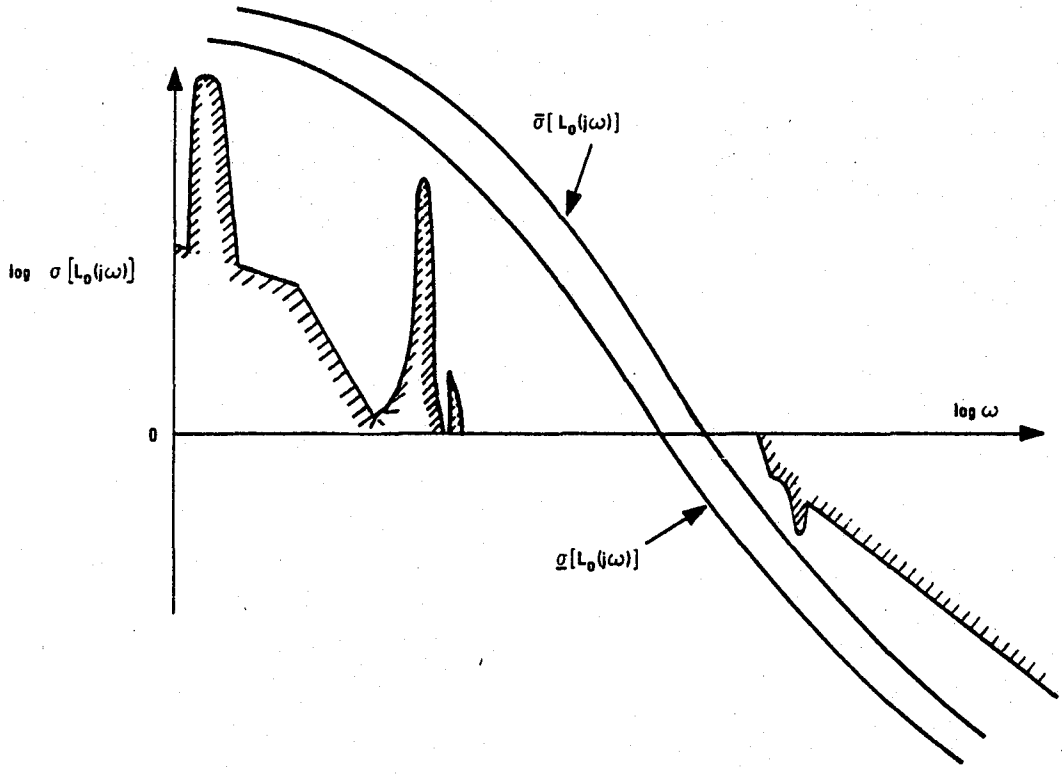

Fig. II.13 Loop Shape Constraints and Trial Design

The secondary objective of minimizing control energy can be approximately satisfied by having the $\bar{\sigma}[L_o(j\omega)]$ line follow as closely as possible to the command and disturbance limits.

Crossover Requirements

The large and small loop gain approximations are not valid when the singular values of the loop transfer function are near unity (i.e. crossover) and thus additional constraints are required for crossover. These constraints are that the minimum singular values of the return difference and the inverse return difference don't get too much smaller than unity near crossover. This is such that performance and stability robustness are not compromised for frequencies in the crossover region. Recall that when the minimum singular value of the return difference is less than unity, disturbance and command responses of the error and sensitivity are amplified compared to open loop. When the minimum singular value of the inverse-return difference is much less than unity the closed loop system could be unstable for small perturbations.

SISO Interpretation

The crossover requirements for SISO systems have historically [Ref.23] been expressed in terms of gain and phase margins. The relationships between the gain and phase margins and the magnitudes of the return difference and the inverse-return difference will now be derived.

Phase Margin

By the definition of the phase margin, PM of the loop transfer function, $L(s)$; $L(j\omega) = -(\cos \text{PM} + j \sin \text{PM})$ for some frequency, ω. In this case the

magnitude of the return difference and the inverse-return difference are the same which can be seen by

$$|1 + L(j\omega)| = \frac{|1 + L(j\omega)|}{|L(j\omega)|} = |1 + L^{-1}(j\omega)| \quad .$$

In terms of the phase margin they are given by

$$\begin{aligned} |1 + L(j\omega)| = |1 + L^{-1}(j\omega)| &= \sqrt{(1 - \cos \mathrm{PM})^2 + \sin^2 \mathrm{PM}} \\ &= \sqrt{2}\sqrt{1 - \cos \mathrm{PM}} \quad . \end{aligned}$$

Thus clearly a small phase margin (say $|PM| < 30$ deg.) implies a small return difference and inverse-return difference magnitude.

Gain Margin

By the definition of the gain margin, GM of the loop transfer function, $L(s)$; $L(j\omega) = -10^{GM}$ for some frequency, ω. In this case the magnitude of the return difference is given by

$$|1 + L(j\omega)| = |1 - 10^{GM}|$$

and the magnitude of the inverse-return difference is given by

$$|1 + L^{-1}(j\omega)| = |1 - 10^{-GM}| \quad .$$

Thus clearly a small gain margin (say $|GM| < 0.3$) implies a small return difference and inverse-return difference magnitude. Historically the gain margin, GM as defined above is multiplied by 20 to give its value in dB. That is $GM = 1$ and $GM = 20dB$ are equivalent.

LQG Loop Shaping

The process of obtaining satisfactory (in terms of Fig. II.13) Bode plots of the singular values of the loop transfer function is called loop shaping. The LQG design methodology can be a remarkably effective tool for achieving the loop shaping demanded by Fig. II.13. A detailed description of the manner in which LQG can be used to solve multivariable control problems is given in Reference 24. Some of the properties of LQG loops which make the LQG methodology effective for loop shaping will be briefly summarized below. In addition to LQG properties, some algorithms for loop shaping and two simple examples will also be discussed.

LQ Regulator

The linear quadratic (LQ) regulator problem assumes that a model of the system

$$\dot{x} = Ax + Bu \qquad x \in \mathbf{R}^n \qquad u \in \mathbf{R}^m$$

and a performance index

$$J = \frac{1}{2}\int_0^\infty \{x^T Q x + u^T R u\}\, dt \qquad Q \geq 0 \ , \qquad R > 0$$

have been specified where the objective is to minimize J. This results [Refs. 1-5] in the control law $u = -K_c x$ where K_c is obtained from the positive semi-definite solution, P_c of the Riccati equation:

$$A^T P_c + P_c A + Q - P_c B R^{-1} B^T P_c = 0$$

as $K_c = R^{-1} B^T P_c$ where it is assumed that (A,B) is stabilizable.

It was shown in Reference 25 that there is no loss of generality in taking $Q = H^T H$ where H is an $m \times n$ matrix. That is for any Q,R the full state feedback matrix, K_c could also have been obtained for some H where $Q = H^T H$. Thus the designer's only input to the LQ regulator problem will be taken to be H. To insure a stable regulator H is always taken to be such that (A,H) is detectable.

The LQ regulator's block diagram is shown in Fig. II.14. It is well known

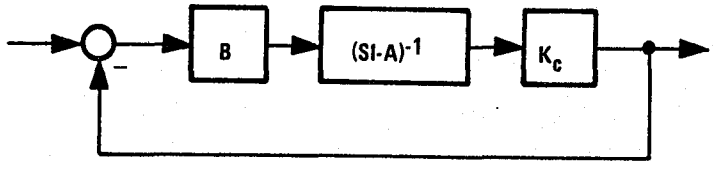

Fig. II.14 LQ Regulator Block Diagram

[Ref. 1-5] that if (A,H) is detectable the regulator is stable. Other theoretical properties of interest here can be derived from the Riccati equation as follows. For notational convenience let

$$\phi(s) \triangleq (sI-A)^{-1}$$
$$L_i(s) \triangleq K_c(sI-A)^{-1}B$$
$$W_c(s) \triangleq H(sI-A)^{-1}B \quad .$$

Note that $L_i(s)$ is just the regulator's loop transfer function and $W_c(s)$ is the transfer function corresponding to the weighting in the LQ performance index which the designer can specify. Starting with the Riccati equation we have

$$A^TP_c + P_cA + H^TH - P_cBB^TP_c = 0$$
$$(-j\omega I-A^T)P_c + P_c(j\omega I-A) - H^TH + K_c^TK_c = 0$$
$$P_c\phi + \phi^HP_c - \phi^HH^TH\phi + \phi^HK_c^TK_c\phi = 0$$
$$B^TP_c\phi B + B^T\phi^HP_cB - B^T\phi^HH^TH\phi B + B^T\phi^HK_c^TK_c\phi B = 0$$
$$K_c\phi B + B^T\phi^HK_c^T - W_c^H(j\omega)\,W_c(j\omega) + L_i^H(j\omega)L_i(j\omega) = 0$$
$$[I + L_i(j\omega)]^H[I + L_i(j\omega)] = I + W_c^H(j\omega)W_c(j\omega) \qquad (II.LQ) \quad .$$

Two important properties of the LQ regulator can be determined from this final equation and they are

LQ Property 1: $\underline{\sigma}[I + L_i(j\omega)] \geq 1 \qquad \forall\omega$

LQ Property 2: $\sigma[L_i(j\omega)] \cong \sigma[W_c(j\omega)]$
when $\underline{\sigma}[W_c(j\omega)] >> 1 \quad .$

The first can be seen by observing that the right hand side of (II.LQ) has eigenvalues which are all greater than or equal to unity (since $W_c^H(j\omega)\,W_c(j\omega) \geq 0 \quad \forall\omega$) together with the definition of singular values applied to the left hand side. The second can be seen be observing that the identity matrices are negligible when $\underline{\sigma}[W_c(j\omega)]$ is large (i.e. $>> 1$).

The first property is important since it implies that the LQ regulator's input return difference has a minimum singular value which is larger than or equal to unity for any frequency. This in turn implies that the regulator has desirable disturbance rejection and desensitization properties (i.e. both are equal to or better than open loop for any frequency!).

The second property is important since the command and disturbance requirements of Fig. II.13 are for large loop gain. Thus the regulator loop transfer function's high gain characteristics can be specified *a priori* by choosing the LQ weighting matrix, H such that $W_c(s) = H(sI-A)^{-1}B$ has the required high gain characteristic.

To achieve the high gain performance requirement with $H(sI-A)^{-1}B$ it may also be necessary to append additional dynamics. For example, to achieve zero steady state errors may require additional integrators in the plant (i.e. integral control). This is equivalent to frequency dependent weighting [Ref. 26].

It is also well known [Ref. 27, 28] that the LQ regulator has certain guaranteed stability robustness properties. This is also a consequence of $\underline{\sigma}[I + L_i(j\omega)] \geq 1 \quad \forall\omega$. It is the multivariable generalization of avoiding the -1 critical point on the Nyquist diagram for SISO systems. It implies that LQ regulator loops provide reasonable transition or "crossover" between the low and high frequency regions shown in Fig. II.13.

Finally we note that at high frequencies the LQ loop transfer function approaches [Ref. 24]

$$\bar{\sigma}[L_i(j\omega)] \cong \frac{1}{\omega}\bar{\sigma}[HB]$$

when HB is full rank. This shows how the high frequency roll-off characteristics are related to H. This is a relatively slow attenuation rate and is the price the regulator pays for its excellent return difference properties. We recognize that no physical system can maintain a $\frac{1}{\omega}$ characteristic indefinitely [Ref. 29]. This is not a concern since $L_i(s)$ is only a design function and will have to be approximated by the full state loop transfer recovery procedure.

Full State Loop Transfer Recovery

The next step of the design process is to provide estimates of the states by processing the output measurements with a Kalman filter. This procedure is also well known [Refs. 1-5]. It involves the model of the system:

$$\begin{aligned} \dot{x} &= Ax + Bu + \xi \qquad x\epsilon\ \mathbf{R}^n \qquad u\epsilon\ \mathbf{R}^m \\ y &= Cx + \eta \qquad y\epsilon\ \mathbf{R}^p \end{aligned}$$

where ξ and η are uncorrelated white noise processes with spectral intensities given by

$$\begin{aligned} E[\xi(t)\xi^T(\tau)] &= \delta(t-\tau)M \qquad \text{where} \quad M \geq 0 \\ E[\eta(t)\eta^T(\tau)] &= \delta(t-\tau)N \qquad \text{where} \quad N \geq 0 \end{aligned}$$

the estimation equations

$$\dot{\hat{x}} = A\hat{x} + Bu + K_f(y-\hat{y})$$
$$\hat{y} = C\hat{x}$$

and the performance index

$$J = \lim_{t\to\infty} tr\ E[\,(x(t) - \hat{x}(t))\,(x(t) - \hat{x}(t))^T\,]$$

where J is to be minimized by choice of K_f.

The solution for the constant matrix, K_f is well known [Refs. 1-5] and is obtained from the positive semi-definite solution, P_f of the Riccati equation:

$$AP_f + P_f A^T + M - P_f C^T N^{-1} C P_f = 0$$

as $K_f = P_f C^T N^{-1}$ where it is assumed that (A,C) is observable.

Using the estimates of the state in the control law i.e. $u = -K_c\hat{x}$ results in the compensator transfer function

$$K(s) = K_c(sI-A + BK_c + K_f C)^{-1}K_f \quad .$$

It is also well known that this compensator results in a stable closed loop system for any noise parameters: M,N. For the purposes of this thesis these noise intensities will be treated as design parameters which can be manipulated by the designer and not as some sacrosanct noise intensities for the system. By duality with the LQ results [Ref. 25] there is no loss of generality in taking $M = \Gamma\Gamma^T$ and $N = I$ where Γ is an $n \times m$ matrix.

For full state loop transfer recovery, the following value for Γ will be used:

$$\Gamma = qB$$

where q is a scalar design parameter. Then as q becomes large (assuming $G(s) \triangleq C(sI-A)^{-1}B$ is minimum phase) it has been shown in Reference 30 that the filter gain behaves in such a way that

$$\lim_{q\to\infty} K(s)G(s) = K_c(sI-A)^{-1}B$$

where the convergence is pointwise in s.

This design procedure essentially inverts the plant from the left i.e.

$$\lim_{q\to\infty} K(s) = K_c(sI-A)^{-1}B\ G^{-1}(s) \quad .$$

This inversion, intuitively is why $G(s)$ is not allowed to have zeros in the right half plane. In practice the recovery procedure is effective as long as $G(s)$ has no right half plane zeros with magnitudes in frequency ranges where high loop gain is required. The limitations on the achievable performance of feedback systems because of non-minimum phase zeros is discussed in Ref. 31.

It has been suggested [Refs. 32,33] that an improved recovery is obtained by using colored rather than white process noise. This procedure however does not recover the LQ loop transfer function i.e.

$$\lim_{q\to\infty} K(s)G(s) \neq K_c(sI-A)^{-1}B$$

when colored noise is used. The reason the authors of References 32 and 33

concluded that an improvement was obtained is that although their LQ loop transfer function, $K_c(sI-A)^{-1}B$ did not satisfy the requirements of Fig. II.13, their LQG loop transfer function $K(s)G(s)$ (obtained with colored noise) did satisfy the requirements of Fig. II.13. The point is that the desirable $K(s)G(s)$ loop transfer function could have been recovered with white noise if the LQ loop transfer function had in fact been desirable.

SISO Double Integrator Example

The design methodology will now be illustrated with a simple example. Assume the desired loop shape must satisfy the requirements shown in Fig. II.15 where $G(s) = \frac{1}{s^2}$. The state space matrices are

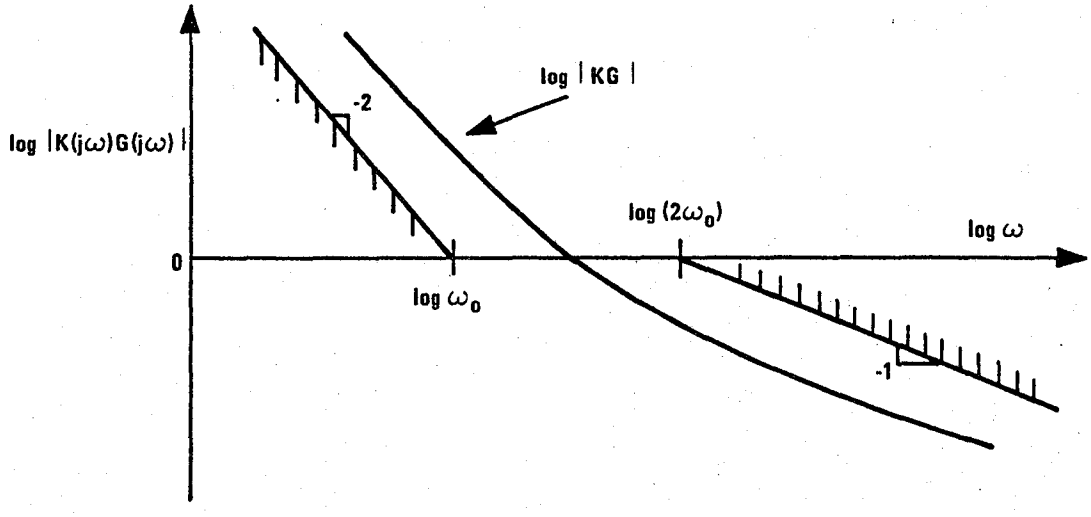

Fig. II.15 Desired Loop Shape For Double Integrator Plant

given by

$$A = \begin{bmatrix} 0 & 1 \\ 0 & 0 \end{bmatrix} \quad B = \begin{bmatrix} 0 \\ 1 \end{bmatrix} \quad C = [1 \quad 0] \quad .$$

The first step is to choose H such that $H(sI-A)^{-1}B$ satisfies the low frequency requirement. This is obtained by choosing

$$H = [\omega_o^2 \quad 0]$$

as can be seen from the plot in Fig. II.16.

Solving the LQ Riccati equation gives

$$K_c = \begin{bmatrix} \omega_o^2 & \sqrt{2}\ \omega_o \end{bmatrix} \quad \text{and}$$

the LQ loop transfer function is given by

$$K_c(sI-A)^{-1}B = \frac{\omega_o^2}{s^2} \frac{\left(s + \frac{\omega_o}{\sqrt{2}}\right)}{\left(\frac{\omega_o}{\sqrt{2}}\right)} \quad .$$

That it satisfies the requirements of Fig. II.15, can be verified by examining the plot of $|K_c(j\omega I-A)^{-1}B|$ shown in Fig. II.16. LQ Property 2 can also be verified by comparing

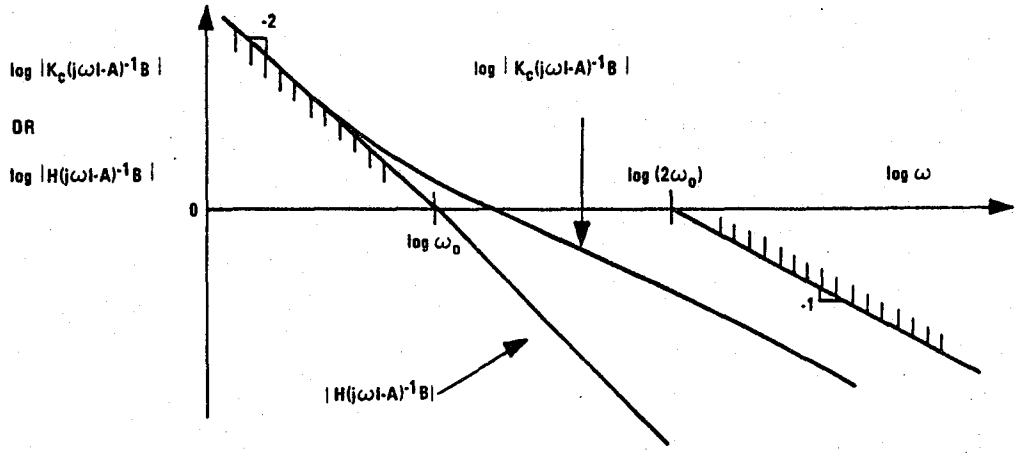

Fig. II.16 LQ Loop Transfer Function for Double Integrator

$|H(j\omega I-A)^{-1}B|$ and $|K_c(j\omega I-A)^{-1}B|$ for frequencies $\omega \ll \omega_o$ (i.e. where $|H(j\omega I-A)^{-1}B| \gg 1$).

Solving the filter Riccati equation gives

$$K_f = \begin{bmatrix} \sqrt{2q} \\ q \end{bmatrix} .$$

Computing the compensator transfer function results in

$$K(s) = \sqrt{2}\,\omega_o\sqrt{q}\,(\omega_o+\sqrt{q})\,\frac{\left[s + \dfrac{\omega_o\sqrt{q}}{\sqrt{2}\,(\omega_o+\sqrt{q})}\right]}{\left[s^2 + \sqrt{2}\,(\omega_o+\sqrt{q})s + (\omega_o+\sqrt{q})^2\right]} \quad .$$

Finally the input loop transfer function is given by

$$K(s)G(s) = \frac{\dfrac{\omega_o^2\,q}{(\omega_o+\sqrt{q})^2}}{s^2}\,\frac{\left[s + \dfrac{\omega_o\sqrt{q}}{\sqrt{2}\,(\omega_o+\sqrt{q})}\right]}{\left[\dfrac{\omega_o\sqrt{q}}{\sqrt{2}\,(\omega_o+\sqrt{q})}\right]}$$

$$\frac{(\omega_o + \sqrt{q})^2}{\left[s^2 + \sqrt{2}\,(\omega_o+\sqrt{q})s + (\omega_o+\sqrt{q})^2\right]}$$

and its magnitude for $s = j\omega$ is sketched in Fig. II.17 for several values of q. The LQ loop transfer function is also sketched in Fig. II.17 for comparison.

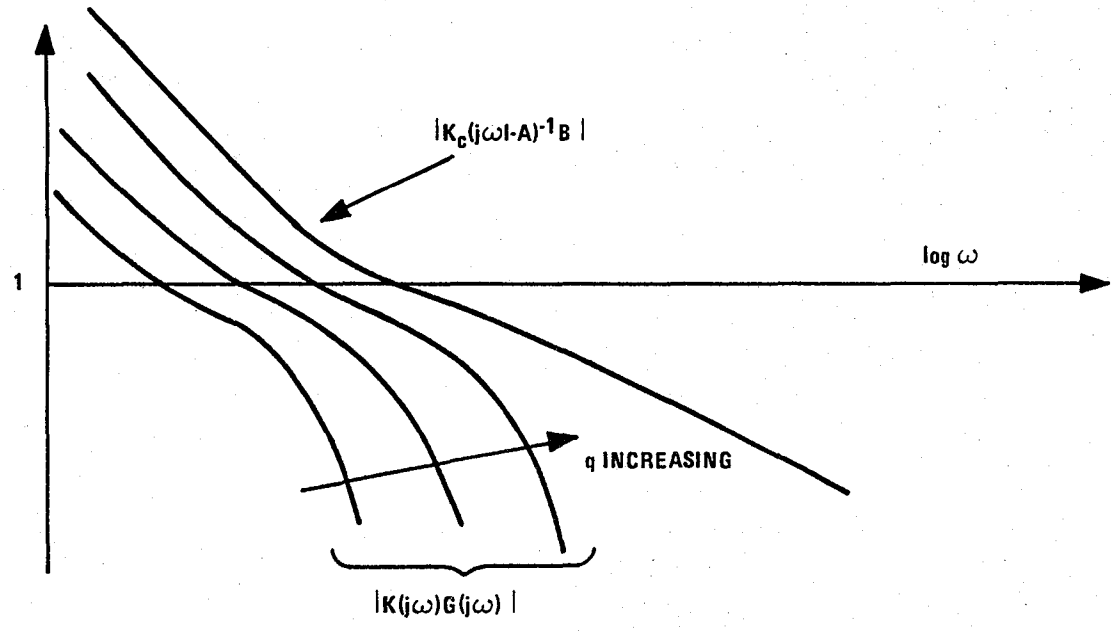

Fig. II.17 LQG Recovery for Double Integrator

From the expression for $K(s)G(s)$ above it can be seen that

$$\lim_{q\to\infty} K(s)G(s) = \frac{\omega_o^2}{s^2}\frac{\left(s+\frac{\omega_o}{\sqrt{2}}\right)}{\frac{\omega_o}{\sqrt{2}}} = K_c(sI-A)^{-1}B \quad .$$

The convergence of $K(s)G(s)$ to $K_c(sI-A)^{-1}B$ as q goes to infinity occurs pointwise on s not uniformly on s. This means that for finite q the approximation $K(s)G(s) \cong K_c(sI-A)^{-1}B$ will be valid only over a restricted frequency range. Outside that range the approximation can be quite poor. This is evident from the plots in Fig. II.17. Practically of course the errors at high

frequency cause little concern provided $|K(j\omega)\ G(j\omega)|$ stays small.

Designing a full state LQ regulator and then recovering the full state design with the Kalman filter has just been discussed. This approach was followed because it is the usual sequence one considers for LQG design. This process allows the designer to shape the input loop transfer function $K(s)G(s)$.

A dual procedure for shaping the output loop transfer function $G(s)K(s)$ is to design the filter first and recover with the regulator. The equations for this alternate procedure are mathematical "duals" of the ones given above. The subtle differences between the two procedures are discussed in Reference 31.

The filter loop transfer function, $L_o(s) = C(sI-A)^{-1}K_f$ shown in block diagram form in Fig. II.18, enjoys the same properties as the LQ loop transfer function. These properties are summarized in Table II.3.

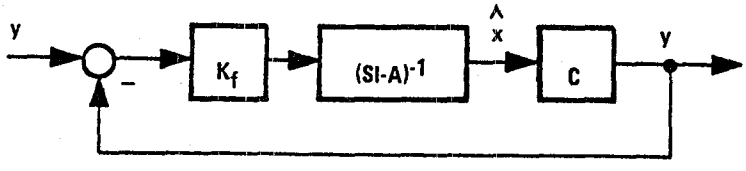

Fig. II.18 Filter Loop Transfer Function

Table II.3 Regulator and Filter Loop Transfer Function Properties

	Input	Output
Minimal Parameterization	$Q = H^T H \qquad R = I$ where H is $m \times n$	$M = \Gamma\Gamma^T \quad N = I$ where Γ is $n \times m$
Definitions	$L_i(s) = K_c(sI-A)^{-1}B$ $W_c(s) = H(sI-A)^{-1}B$	$L_o(s) = C(sI-A)^{-1}K_f$ $W_f(s) = C(sI-A)^{-1}\Gamma$
Return Difference Bound	$\underline{\sigma}\left[I + L_i(j\omega)\right] \geq 1$	$\underline{\sigma}\left[I + L_o(j\omega)\right] \geq 1$
Inverse-Return Difference Bound	$\underline{\sigma}\left[I + L_i^{-1}(j\omega)\right] \geq 1/2$	$\underline{\sigma}\left[I + L_o^{-1}(j\omega)\right] \geq 1/2$
Near Equality of $W(s)$ and $L(s)$ (useful for design)	$\sigma\left[L_i(j\omega)\right] \cong \sigma\left[W_c(j\omega)\right]$ when $\underline{\sigma}\left[W_c(j\omega)\right] >> 1$	$\sigma\left[L_o(j\omega)\right] \cong \sigma\left[W_f(j\omega)\right]$ when $\underline{\sigma}\left[W_f(j\omega)\right] >> 1$
High Frequency Characteristics (useful for design)	$\bar{\sigma}\left[L_i(j\omega)\right] \cong \frac{1}{\omega}\bar{\sigma}\left[HB\right]$ $\omega \to \infty$ (A,H) observable HB full rank	$\bar{\sigma}\left[L_o(j\omega)\right] \cong \frac{1}{\omega}\bar{\sigma}\left[C\Gamma\right]$ for $\omega \to \infty$ (A,Γ) controllable $C\Gamma$ full rank

The duality of these two design procedures is easy to see in the SISO double integrator example given above by interchanging the roles of ω_o^2 and q. That is since they appear symmetrically, let ω_o go to infinity while holding q fixed to give the desired loop shape (either $K(s)G(s)$ or $G(s)K(s)$ since they are the same for SISO).

The LQG input and output loop shaping procedures are summarized in Table II.4.

Advanced Loop Shaping

The *LQG* loop shaping procedures just discussed required that the plant have the dynamics of the desired loop shape i.e. the poles of either $K_c(sI-A)^{-1}B$ or $C(sI-A)^{-1}K_f$ are the same as those of the plant. Actually, as already alluded to, dynamics may be appended if they are not already present in the plant. Advanced loop shaping just formalizes this process.

Assume the high gain characteristics of the desired loop shape are given by $C_l(sI-A_l)^{-1}B_l$ i.e. A_l, B_l, C_l are all three specified by the designer to satisfy the high gain requirements of Fig. II.13. The plant transfer function will still be given by $C(sI-A)^{-1}B$. This desired loop shape can be approximately obtained for either the input or output loop transfer function with the appropriate one of the following two dual procedures.

The procedure for the input will now be discussed and the other will follow by duality. The augmented plant state space realization is given by

Table II.4 LQG Input and Output Loop Shaping Procedure

	Input	Output
append additional dynamics if necessary and choose H or Γ such that the indicated transfer function has satisfactory high gain characteristics	$H(sI-A)^{-1}B$	$C(sI-A)^{-1}\Gamma$
solve the Riccati and gain equations	$A^TP_c + P_cA + H^TH - P_cBB^TP_c = 0$ $K_c = B^TP_c$	$AP_f + P_fA^T + \Gamma\Gamma^T - P_fC^TCP_f = 0$ $K_f = P_fC^T$
to obtain the ideal loop transfer function	$K_c(sI-A)^{-1}B$	$C(sI-A)^{-1}K_f$
choose a scalar q and solve the Riccati and gain equations	$AP_f + P_fA^T + q^2BB^T - P_fC^TCP_f = 0$ $K_f = P_fC^T$	$A^TP_c + P_cA + q^2C^TC - P_cBB^TP_c = 0$ $K_c = B^TP_c$
then if $G(s) = C(sI-A)^{-1}B$ is minimum phase	$K(s)G(s) \to K_c(sI-A)^{-1}B$ as $q \to \infty$	$G(s)K(s) \to C(sI-A)^{-1}K_f$ as $q \to \infty$

$$\bar{A}_i = \begin{bmatrix} A & 0 \\ 0 & A_l \end{bmatrix} \qquad \bar{B}_i = \begin{bmatrix} B \\ B_l \end{bmatrix}$$
$$\bar{C}_i = [C \quad 0] \quad .$$

Note that this does not change the input-output transmission of the plant i.e.

$$G(s) = C(sI-A)^{-1}B = \bar{C}_i(sI-\bar{A}_i)^{-1}\bar{B}_i \quad .$$

Now to obtain an LQ loop transfer function which has the high gain characteristics of $C_l(sI-A_l)^{-1}B_l$ let

$$\bar{H}_i = [0 \quad C_l]$$

and solve the regulator Riccati equation for $\bar{P}_c \geq 0$:

$$\bar{A}_i^T\bar{P}_c + \bar{P}_c\bar{A}_c + \bar{H}_i^T\bar{H}_i - \bar{P}_c\bar{B}_i\bar{B}_i^T\bar{P}_c = 0$$

to obtain the full state gain

$$\bar{K}_c = \bar{B}_i^T\bar{P}_c \quad .$$

When A is stable $\bar{K}_c$ is given by

$$\bar{K}_c = [0 \quad K_c]$$

with $K_c = B_l^TP_c$ where $P_c \geq 0$ is the solution to the (lower order) Riccati equation:

$$A_l^TP_c + P_cA_l + C_l^TC_l - P_cB_lB_l^TP_c = 0 \quad .$$

Note that when the plant is stable it is not involved in the computations so far. That is only A_l, B_l, C_l (typically of lower dimension than A,B,C) have to be

manipulated.

Next the full state feedback recovery procedure is used as follows. Let

$$\bar{\Gamma}_i \;=\; q\,\bar{B}_i$$

where q is the scalar design parameter used for recovery and solve the filter Riccati equation for $\bar{P}_f \geq 0$:

$$\bar{A}_i\bar{P}_f \;+\; \bar{P}_f\bar{A}_i^T \;+\; \bar{\Gamma}_i\bar{\Gamma}_i^T - \bar{P}_f\,\bar{C}_i^T\bar{C}_i\bar{P}_f \;=\; 0$$

to obtain the filter gain

$$\bar{K}_f \;=\; \bar{P}_f\,\bar{C}_i^T \quad .$$

The compensator transfer function is obtained as usual from

$$K(s) \;=\; \bar{K}_c(sI-\bar{A}_i \;+\; \bar{B}_i\bar{K}_c \;+\; \bar{K}_f\,\bar{C}_i)^{-1}\,\bar{K}_f \quad .$$

Assuming $G(s)$ is minimum phase and stable we have

$$\lim_{q\to\infty} K(s)G(s) \;=\; K_c(sI-A_l)^{-1}\,B_l$$

where $\sigma[K_c(j\omega-A_l)^{-1}\,B_l] \;\cong\; \sigma[C_l(j\omega I-A_l)^{-1}\,B_l]$ for ω such that $\underline{\sigma}[C_l(j\omega I-A_l)^{-1}\,B_l] >> 1$ which was the design objective.

The comments regarding the minimum phase assumption in a previous section covering ordinary full state feedback recovery apply here as well. That is the desirable properties of the LQ loop function $K_c(sI-A_l)^{-1}\,B_l$ will be recovered for frequencies other than those near the magnitudes of right half plane zeros.

Using the procedure for an unstable system results in a loss of accuracy in the approximation of the desired loop shape. This is consistent with the fact that [Ref. 29] arbitrary loop shapes are not possible for unstable systems. Thus the procedure is still applicable to unstable systems but the choice of A_l, B_l, C_l must be made with attention to the limits to achievable performance.

SISO First Order Example

A simple example will now be discussed to help clarify the steps of this procedure. Let the plant be given by

$$G(s) = \frac{2}{s+1}, \; A = -1, \; B = 2, \; C = 1 \quad .$$

Let the desired loop transfer function be given by

$$C_l(sI-A_l)^{-1} B_l = \frac{100}{s} \qquad A_l = 0, B_l = 100, C_l = 1 \quad .$$

The plant is stable and $\overline{K}_c$ can be verified to be given by

$$\overline{K}_c = [0 \quad K_c] = [0 \quad 1] \quad .$$

This results in the desired loop transfer function being achieved exactly by the LQ loop transfer function i.e.

$$K_c(sI-A_l)^{-1} B_l = \frac{100}{s} = C_l(sI-A_l)^{-1} B_l \quad .$$

The filter gain can be verified to be given by

$$\bar{K}_f = \begin{bmatrix} \sqrt{1+4q^2} & -1 \\ \dfrac{200q^2}{\sqrt{1+4q^2}} & \end{bmatrix}$$

from which it can be seen that

$$\lim_{q\to\infty} \bar{K}_f = \begin{bmatrix} 2q & \\ 100q & \end{bmatrix} .$$

Using this limiting expression for $\bar{K}_f$ to compute $K(s)$ it can be seen that

$$\begin{aligned} \lim_{q\to\infty} K(s)G(s) &= \lim_{q\to\infty} \frac{100q(s+1)}{s^2 + (101+2q)s + 1} \begin{pmatrix} 2 \\ \hline s+1 \end{pmatrix} \\ &= \lim_{q\to\infty} \frac{200}{\dfrac{s^2}{q} + \left(\dfrac{101}{q} + 2\right)s + \dfrac{1}{q}} \\ &= \frac{100}{s} . \end{aligned}$$

As already alluded to, this procedure has a dual for shaping the output loop transfer function $G(s)K(s)$. Both procedures are summarized in Table II.5.

The design procedures just discussed are very powerful for shaping either the input or output open loop transfer functions. However, in most design problems both loops must have desirable properties. Thus, one major weakness of the design procedures is that only the properties of one open loop transfer function may be formally tailored. Of course for SISO problems the input and output loop transfer functions are the same since $G(s)$ and $K(s)$ commute.

Table II.5 Advanced LQG Input and Output Loop Shaping Procedure

	Input	Output
Form the augmented state space realization	$\bar{A}_i = \begin{bmatrix} A & 0 \\ 0 & A_\ell \end{bmatrix}$ $\bar{B}_i = \begin{bmatrix} B \\ B_\ell \end{bmatrix}$ $\bar{C}_i = [C \quad 0]$ $\bar{H}_i = [0 \quad C_\ell]$	$\bar{A}_o = \begin{bmatrix} A & 0 \\ 0 & A_\ell \end{bmatrix}$ $\bar{B}_o = \begin{bmatrix} B \\ 0 \end{bmatrix}$ $\bar{\Gamma}_o = \begin{bmatrix} 0 \\ B_\ell \end{bmatrix}$ $\bar{C}_o = [C \quad C_\ell]$
solve the Riccati and gain equation to obtain either Regulator Loop Transfer: $\bar{K}_c(sI-\bar{A}_i)^{-1}\bar{B}_i$ or Filter Loop Transfer: $\bar{C}_o(sI-\bar{A}_o)^{-1}\bar{K}_f$	$\bar{A}_i^T\bar{P}_c+\bar{P}_c\bar{A}_i+\bar{H}_i^T\bar{H}_i-\bar{P}_c\bar{B}_i\bar{B}_i^T\bar{P}_c = 0$ $\bar{P}_c \geq 0 \qquad K_c = \bar{B}_i^T\bar{P}_c$ $\Updownarrow$ A stable $A_\ell^TP_c+P_cA_\ell+C_\ell^TC_\ell-P_cB_\ell B_\ell^TP_c = 0$ $P_c \geq 0 \quad \bar{K}_c=[0 \; K_c] \quad K_c=B_\ell^TP_c$	$\bar{A}_o\bar{P}_f+\bar{P}_f\bar{A}_o^T+\bar{\Gamma}_o\bar{\Gamma}_o^T-\bar{P}_f\bar{C}_o^T\bar{C}_o\bar{P}_f = 0$ $\bar{P}_f \geq 0 \qquad \bar{K}_f = \bar{P}_f\bar{C}_o^T$ $\Updownarrow$ A stable $A_\ell P_f+P_fA_\ell^T+B_\ell B_\ell^T-P_fC_\ell^TC_\ell P_f = 0$ $P_f \geq 0 \quad \bar{K}_f = \begin{bmatrix} 0 \\ K_f \end{bmatrix} \quad K_f = P_fC_\ell^T$
solve the Riccati and gain equation	$\bar{A}_i\bar{P}_f+\bar{P}_f\bar{A}_i^T+q^2\bar{B}_i\bar{B}_i^T-\bar{P}_f\bar{C}_i^T\bar{C}_i\bar{P}_f=0$ $\bar{P}_f \geq 0 \qquad \bar{K}_f = \bar{P}_f\bar{C}_i^T$	$\bar{A}_o^T\bar{P}_c+\bar{P}_c\bar{A}_o+q^2\bar{C}_o^T\bar{C}_o-\bar{P}_c\bar{B}_o\bar{B}_o^T\bar{P}_c = 0$ $\bar{P}_c \geq 0 \qquad \bar{K}_c = \bar{B}_o^T\bar{P}_c$
Form K(s)	$K(s)=\bar{K}_c(sI-\bar{A}_i+\bar{B}_i\bar{K}_c+\bar{K}_f\bar{C}_i)^{-1}\bar{K}_f$	$K(s) = \bar{K}_c(sI-\bar{A}_o+\bar{B}_o\bar{K}_c+\bar{K}_f\bar{C}_o)^{-1}\bar{K}_f$
then if G(s) is minimum phase	$\lim_{q\to\infty} K(s)G(s) = \bar{K}_c(sI-\bar{A}_i)^{-1}\bar{B}_i$ $= K_c(sI-A_\ell)^{-1}B_\ell$ for A stable	$\lim_{q\to\infty} G(s)K(s) = \bar{C}_o(sI-\bar{A}_o)^{-1}\bar{K}_f$ $= C_\ell(sI-A_\ell)^{-1}K_f$ for A stable

Motivation For Model Reduction

As we have seen a powerful design technique (LQG loop shaping) exists to formally solve the control problem. However, this design technique requires the manipulation of matrices with dimensions greater than or equal to that of the plant model. Also it results in a compensator transfer function which has order equal to or greater than that of the plant.

For many problems the order of the plant is so high, as to prohibit a successful design of the compensator (either by cost of computations or accuracy of computations). Even when the design process can be carried out it may be desirable to simplify the compensator (i.e. reduce its order) for implementation purposes. This could be to save implementation computer time and memory, provide ease of checkout and verification of the implementation, eliminate excessive gain scheduling, or for any of many other practical reasons.

Thus we are led to search for reduced order models to simplify the design, analysis and implementation of the control system. Many methods of obtaining a reduced order model exist [Refs. 6-15] and the fundamental ideas of the internally balanced realization method will be discussed next.

Internally Balanced Realizations

Balanced realizations will be used throughout the sequel. When the adjective internally is used, it represents the essentially unique realization of an asymptotically stable MIMO transfer function defined by B. C. Moore [Ref. 11].

A geometric interpretation of the balanced realization, an algorithm for computing the realization and some of its properties will now be discussed.

A state space realization of the system to be balanced is given by

$$\begin{aligned} \dot{x} &= Fx + Gu \qquad x \epsilon \mathbf{R}^N \qquad u \epsilon \mathbf{R}^m \\ y &= Hx \qquad\qquad y \epsilon \mathbf{R}^p \quad . \end{aligned}$$

It is assumed that the system is asymptotically stable, i.e. $Re[\lambda[F]] < 0$. The minimal order of the system will be taken to be n where $n \leq N$. That is the given system may be uncontrollable and/or unobservable.

Geometric Interpretation

With reference to the block diagram shown in Fig. II.19 ask the following two

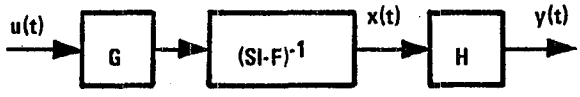

Fig. II.19 Block Diagram for Internally Balanced Realization Discussion

(dual) questions. What set of points in the x-state space could be part of the zero initial condition response for some input, $u(t)$ such that $||u(t)||_2 \leq 1$? and what set of points in the x-state space as initial conditions could produce an

output, $y(t)$ such that $||y(t)||_2 \leq 1$ with zero external input?

Moore showed that these two sets are in general different ellipsoids. The following general theorem was proved by Moore, [Ref. 11].

Grammian-Ellipsoid Theorem

Let $F(t)$ be an impulse response matrix of some asymptotically stable, linear, time invariant system. Let

$$G_F \triangleq \int_o^\infty F(t)F^T(t)\,dt \geq 0$$

$$S_c \triangleq \left\{x(t):\ x(t) = \int_o^t F(t-\tau)u(\tau)d\tau,\ \forall t,\ ||u(t)||_2 \leq 1\right\}$$

$$S_o \triangleq \left\{x(o):\ y(t) = \int_o^t F^T(t-\tau)x(o)\delta(\tau)d\tau,\ \forall t,\ ||y(t)||_2 = 1\right\}$$

the grammian, controllable set and observable set for $F(t)$ respectively. Furthermore let the eigenvalue decomposition of the grammian be given by

$$G_F = V\sum V^T,\ V^TV = I,\ \sum = \text{diag}\,\{\sigma_i\},\ V = \text{block col}[v_i] \quad .$$

Then

$$S_c = \text{ellipsoid with semi-axes given by } \sqrt{\sigma_i}\,v_i$$

and

$$S_o = \text{ellipsoid with semi-axes given by} \frac{1}{\sqrt{\sigma_i}}\,v_i \quad .$$

For the first question let $F(t) = e^{Ft}G$, then the answer is the controllable

set, S_c. For the second question let $F(t) = e^{F^T t} H^T$, then the answer is the observable set, S_o. These grammians have been given special names [Refs. 11, 34, 35]:

$$U = \int_o^\infty e^{Ft} GG^T e^{F^T t}\, dt = \text{controllability grammian}$$
$$Y = \int_o^\infty e^{F^T t} H^T H e^{Ft}\, dt = \text{observability grammian} \quad .$$

It is well known [Refs. 11, 34, 35] that these grammians can be computed from the Lyapunov equations

$$FU + UF^T + GG^T = 0 \qquad \text{(II.1a)}$$
$$F^T Y + YF + H^T H = 0 \qquad \text{(II.1b)} \quad .$$

These results are now summarized. The lengths and directions of the controllability ellipsoid semi-axes are the square roots of the eigenvalues and the eigenvectors of the controllability grammian respectively. The lengths and directions of the observability ellipsoid semi-axes are the reciprocals of the square roots of the eigenvalues and the eigenvectors of the observability grammian respectively.

It is well known [Refs. 34, 35] that a zero eigenvalue of the controllability grammian implies $\{F,G\}$ is uncontrollable and that a zero eigenvalue of the observability grammian implies $\{F,H\}$ is unobservable. The association of these grammian eigenvalues with the lengths of the ellipsoid semi-axes is intuitively pleasing in that: an uncontrollable direction would clearly correspond to an ellipsoid semi-axis of zero length and an unobservable direction would clearly

correspond to an ellipsoid semi-axis of infinite length. Hence the eigenvalues of these grammians provide scalar measures of how controllable or observable a given grammian eigenvector direction is.

Moore also showed that there exists a realization of the system obtained with a change of variables by a similarity transformation, T, such that the axes of the ellipsoids are the same (balanced) for the new state variables (say z, where $x = Tz$). For model reduction, this balancing is the key idea because it provides a basis for the n dimensional x-state space where the direction of a given basis vector is as controllable as observable in a well defined sense. The lengths of the ellipsoid's semi-axes provide a scalar measure of how controllable *and* observable a given basis vector direction is. Finally the reduced order model is obtained by neglecting the weakly controllable/observable states of the system.

Algorithm For Computing the Internally Balanced Realization

There are in fact several algorithms for computing the internally balanced realization. Most suffer from numerical difficulties when they are applied to non-trivial problems. The difficulties arise due to the squaring up nature of the problem i.e. the G and H matrices are squared to compute the grammians and as will be seen the controllability and observability grammians are then multiplied together. This is an important research area and progress has been made by Laub at USC however these results were not used for this thesis.

The algorithm for computing the internally balanced realization that will be presented here is slightly more general than Moore's in that $\{F,G,H\}$ may be uncontrollable and/or unobservable. The objective of any balancing algorithm is to find a minimal (i.e. controllable and observable) realization, $\{A,B,C\}$ of the given possibly non-minimal realization, $\{F,G,H\}$ such that the controllability and observability grammians for $\{A,B,C\}$ are equal and diagonal.

To this end consider how the original grammians change due to a similarity transformation. Starting with (II.1 ab) we have

$$\begin{aligned} T^{-1}FTT^{-1}UT^{-T} + T^{-1}UT^{-T}T^{T}F^{T}T^{-T} + T^{-1}GG^{T}T^{-T} &= 0 \\ T^{T}F^{T}T^{-T}T^{T}YT + T^{T}YTT^{-1}FT + T^{T}H^{T}HT &= 0 \end{aligned}$$

which can be rewritten as

$$\begin{aligned} \hat{F}\hat{U} + \hat{U}\hat{F}^{T} + \hat{G}\hat{G}^{T} &= 0 \\ \hat{F}^{T}\hat{Y} + \hat{Y}\hat{F} + \hat{H}^{T}\hat{H} &= 0 \end{aligned}$$

where

$$\begin{aligned} \hat{F} &\triangleq T^{-1}FT \\ \hat{G} &\triangleq T^{-1}G \\ \hat{H} &\triangleq HT \\ \hat{U} &\triangleq T^{-1}UT^{-T} \\ \hat{Y} &\triangleq T^{T}YT \quad . \end{aligned}$$

Now our objective can be stated as follows: find T such that

$$\hat{U} = T^{-1}UT^{-T} = \text{block diag } \{\sum, \sum_u\}$$
$$\hat{Y} = T^{T}YT = \text{block diag } \{\sum, \sum_y\}$$

where

$$\Sigma = \text{diag } \{\sigma_1, \sigma_2, ..., \sigma_n\}$$
$$\Sigma_u\Sigma_y = \text{diag } \{\sigma_{n+1}^2, \sigma_{n+2}^2, ..., \sigma_N^2\}$$

with $\sigma_1 \geq \sigma_2 \geq \cdots \geq \sigma_n > \sigma_{n+1} = \sigma_{n+2} = \cdots = \sigma_N = 0$. The uncontrollable and/or unobservable modes result in $\Sigma_u\Sigma_y = 0$.

The similarity transformation, T which accomplishes the objective is obtained from the eigenvector decomposition

$$UY = T\Lambda T^{-1} \quad .$$

That is the columns of T are eigenvectors (eigenvector nonuniqueness discussed below) of UY corresponding to $\Lambda = \text{diag } \{\lambda_i\}$ the real diagonal eigenvalue matrix of UY (assuming without loss of generality that the $\lambda_i's$ have been ordered such that $\lambda_1 \geq \lambda_2 \geq \cdots \geq \lambda_N$). The fact that UY has a real diagonal Jordan form is a consequence of the fact that U and Y are both positive semi-definite. It is also true that Λ is positive semi-definite. The proofs of these facts are not well known and are rather long, hence they are contained in Appendix C.

Eigenvectors are not unique since a scalar times an eigenvector is also an eigenvector and when the eigenvalues are not distinct linear combinations of eigenvectors corresponding to a repeated eigenvalue are also eigenvectors.

Specific eigenvectors can always be chosen such that

$$\begin{aligned} T^{-1}UT^{-T} &= \text{block diag } \{\Sigma,\ \Sigma_u\} \\ T^{T}YT &= \text{block diag } \{\Sigma,\ \Sigma_y\} \end{aligned}$$

where

$$\begin{aligned} \Sigma &= \text{diag } \{\sigma_1, \sigma_2, \ldots, \sigma_n\} \\ \Sigma_u\Sigma_y &= \text{diag } \{\sigma_{n+1}^2, \sigma_{n+2}^2, \ldots, \sigma_N^2\} \end{aligned}$$

with

$$\sigma_1 \geq \sigma_2 \geq \cdots \geq \sigma_n > \sigma_{n+1} = \sigma_{n+2} = \cdots = \sigma_N = 0 \quad .$$

The details of this choice of eigenvectors is messy and hence is also contained in App. C.

Fortunately any choice of eigenvectors will work for the purpose of model reduction. The eigenvector scaling just leads to a choice of scale for the individual balanced state variables (the reduced order model transfer function is independent of this scaling!). The complication, due to repeated eigenvalues of UY, is eliminated by either retaining or eliminating all the balanced states corresponding to the repeated eigenvalue of UY in the reduced order model (there is no justification for doing anything else!).

The square roots of the eigenvalues of UY are the singular values of the balanced grammian. That is

$$\sigma_i = \sqrt{\lambda_i} \qquad i = 1, 2, \ldots, N \quad .$$

Let T_n be the first n columns of T (i.e. those columns which correspond to non-zero balanced grammian singular values), likewise let S_n be the first n rows of T^{-1}, then the n^{th} order minimal internally balanced realization of $\{F,G,H\}$ is given by $\{A,B,C\} = \{S_n F T_n,\ S_n G,\ H T_n\}$. That is

$$A\sum + \sum A^T + BB^T = 0 \qquad \text{(II.2a)}$$

$$A^T\sum + \sum A + C^T C = 0 \qquad \text{(II.2b)}$$

where

$$\sum = \text{diag}\ \{\sigma_1, \sigma_2, ..., \sigma_n\} > 0 \quad .$$

Moore showed that the internally balanced realization is essentially unique when the balanced grammian singular values are distinct. Essentially unique is taken to mean unique up to a change in sign of a state variable.

The algorithm for transforming a given asymptotically stable, possibly non-minimal realization $\{F,G,H\}$ into an internally balanced, minimal realization $\{A,B,C\}$ is summarized in Table II.6.

Simple Example

A simple example will now be used to fix ideas. Consider the following 4th order non-minimal realization with one controllable and observable mode, one controllable but unobservable mode, one uncontrollable but observable mode and one uncontrollable and unobservable mode.

Table II.6 Internally Balanced Realization Algorithm

Given: F, G, H with $Re[\lambda[F]] < 0$.

Solve for U and Y from

$$FU + UF^T + GG^T = 0$$
$$F^TY + YF + H^TH = 0 \quad .$$

Solve for eigenvalues and eigenvectors of UY i.e.

$$UY = T\Lambda T^{-1} \quad .$$

Partition T, Λ and T^{-1} such that $\Sigma > 0$

$$T = \begin{bmatrix} T_n & T_{N-n} \end{bmatrix} \quad \Lambda = \begin{bmatrix} \Sigma^2 & 0 \\ 0 & 0 \end{bmatrix} \quad T^{-1} = \begin{bmatrix} S_n \\ S_{N-n} \end{bmatrix} \quad .$$

Compute A, B, C with

$$A = S_nFT_n, \quad B = S_nG, \quad C = HT_n$$

Then
$$A\Sigma + \Sigma A^T + BB^T = 0$$
$$A^T\Sigma + \Sigma A + C^TC = 0 \quad .$$

$$F = \begin{bmatrix} -1 & 0 & 0 & 0 \\ 0 & -2 & 0 & 0 \\ 0 & 0 & -3 & 0 \\ 0 & 0 & 0 & -4 \end{bmatrix} \qquad G = \begin{bmatrix} 1 \\ 1 \\ 0 \\ 0 \end{bmatrix}$$

$$H = [1 \quad 0 \quad 1 \quad 0]$$

The two grammians can be verified to be given by

$$U = \begin{bmatrix} \frac{1}{2} & \frac{1}{3} & 0 & 0 \\ \frac{1}{3} & \frac{1}{4} & 0 & 0 \\ 0 & 0 & 0 & 0 \\ 0 & 0 & 0 & 0 \end{bmatrix} \qquad Y = \begin{bmatrix} \frac{1}{2} & 0 & \frac{1}{4} & 0 \\ 0 & 0 & 0 & 0 \\ \frac{1}{4} & 0 & \frac{1}{6} & 0 \\ 0 & 0 & 0 & 0 \end{bmatrix} .$$

The similarity transformation or the eigenvector matrix of UY can be verified to be given by

$$T = \begin{bmatrix} 1 & 0 & -\frac{1}{2} & 0 \\ \frac{2}{3} & 1 & 0 & 0 \\ 0 & 0 & 1 & 0 \\ 0 & 0 & 0 & 1 \end{bmatrix} .$$

The grammian singular values can be verified to be given by

$$\Sigma = \frac{1}{2}$$

$$\Sigma_u = \text{diag}\{\frac{1}{36}, 0, 0\}$$

$$\Sigma_y = \text{diag}\{0, \frac{1}{24}, 0\} .$$

Finally a minimal realization is given by

$$A = -1 \qquad B = 1 \qquad C = 1 .$$

Some Properties of the Internally Balanced Realization

The internally balanced realization has several fascinating properties. The properties of interest here are stability, controllability and observability of reduced order models obtained from the balanced realization.

As mentioned earlier a reduced order model is obtained from the internally balanced realization by neglecting the weakly controllable/observable states of the balanced realization. The singular values of the balanced grammian provide a measure for determining how controllable/observable a given state direction is. The idea is that the states corresponding to the smallest singular values can be neglected. This is expressed by the following. Choose the order of the reduced order model, r such that $\sigma_r > \sigma_{r+1}$ then let $\sum_1 = \text{diag}\,\{\sigma_1, \sigma_2, ..., \sigma_r\}$ and $\sum_2 = \text{diag}\,\{\sigma_{r+1}, \sigma_{r+2}, ..., \sigma_n\}$. Partition A, B, C compatibly as

$$A = \begin{bmatrix} A_{11} & A_{12} \\ A_{21} & A_{22} \end{bmatrix} \quad B = \begin{bmatrix} B_1 \\ B_2 \end{bmatrix}$$
$$C = [C_1 \quad C_2]$$

then $\{A_{11}, B_1, C_1\}_r$ is the r^{th} order reduced order model of $\{A, B, C\}_n$.

Immediately from (II.2 a,b) it can be seen that the realization of the reduced order model is internally balanced i.e.

$$A_{11}\Sigma_1 + \Sigma_1 A_{11}^T + B_1 B_1^T = 0$$
$$A_{11}^T\Sigma_1 + \Sigma_1 A_{11} + C_1^T C_1 = 0 \quad .$$

Moore showed that the reduced order model is <u>generically</u> asymptotically

stable, controllable and observable. Pernebo and Silverman [Ref. 36] proved the following stronger result. The condition that $\sigma_r \neq \sigma_{r+1}$ implies that the reduced order model will be asymptotically stable, controllable and observable.

III. FREQUENCY WEIGHTED MODEL REDUCTION

One of the main points of this thesis is that model reduction and control system design are not independent of each other. That is, given that a control system will be designed, analyzed and implemented based on the reduced order model, the technique used for model reduction must be cognizant of this fact. The point is that the reduction will introduce error and the criterion used to define a small error must reflect the purposes for which the reduced order model is intended.

Model Fidelity With Respect to Control System Design

The overriding concern in control design is stability of the closed loop system. The next concern is that the performance objectives are satisfied. In Chapter II, it was shown that for good performance and robustness a loop shape must be obtained which has high gain (typically at low frequency) to satisfy disturbance attenuation, desensitization and command response specifications and low gain (always at high frequency) to satisfy sensor noise and robustness specifications. Furthermore the loop must accomplish the transition (crossover) between these two regions in a stable manner. Therefore the model reduction error criterion must assess how much the use of a reduced order model can affect the desired loop shape.

In the low frequency range, the feedback compensator should provide adequate loop gain, so the high gain of the loop shape will not be seriously

degraded by some low frequency model error. In the high frequency range the loop must be rolled off such that stability robustness to uncertainty in the full order model is maintained. Thus an accurate approximation of the full order model is not necessary in the high frequency range. This leaves the mid frequency or crossover region as the only critical region for accurately modeling the plant dynamics.

To assure stability it is also clear from the Nyquist stability criterion (and its MIMO generalization) that the reduced order model must not neglect unstable poles. Thus another requirement for model fidelity is that the reduced order model have the same number of unstable poles as that of the full order model.

These comments can be interpreted graphically for the SISO Nyquist plot shown in Fig. III.1 for the loop shape requirements:

$$\begin{aligned} |L(j\omega)| &> R & \omega &\leq \omega_l \\ |1 + L(j\omega)| &> 1 - r & \omega_l &\leq \omega \leq \omega_h \\ |L(j\omega)| &< r & \omega_h &\leq \omega \end{aligned}$$

where $L(s) = G(s)K(s) = K(s)G(s)$ and $G(s)$ and $K(s)$ are the plant and compensator transfer functions respectively. The solid line is the locus of $G_r(j\omega)K(j\omega)$ versus ω i.e. the loop is analyzed and designed with the reduced order model transfer function $G_r(s)$.

It can be readily seen from Fig. III.1 that if $G_r(j\omega)K(j\omega)$ satisfies the loop shape requirements and the error between $G(j\omega)$ and $G_r(j\omega)$ is such that the locus of $G(j\omega)K(j\omega)$ versus ω lies in the shaded region, then the loop shape

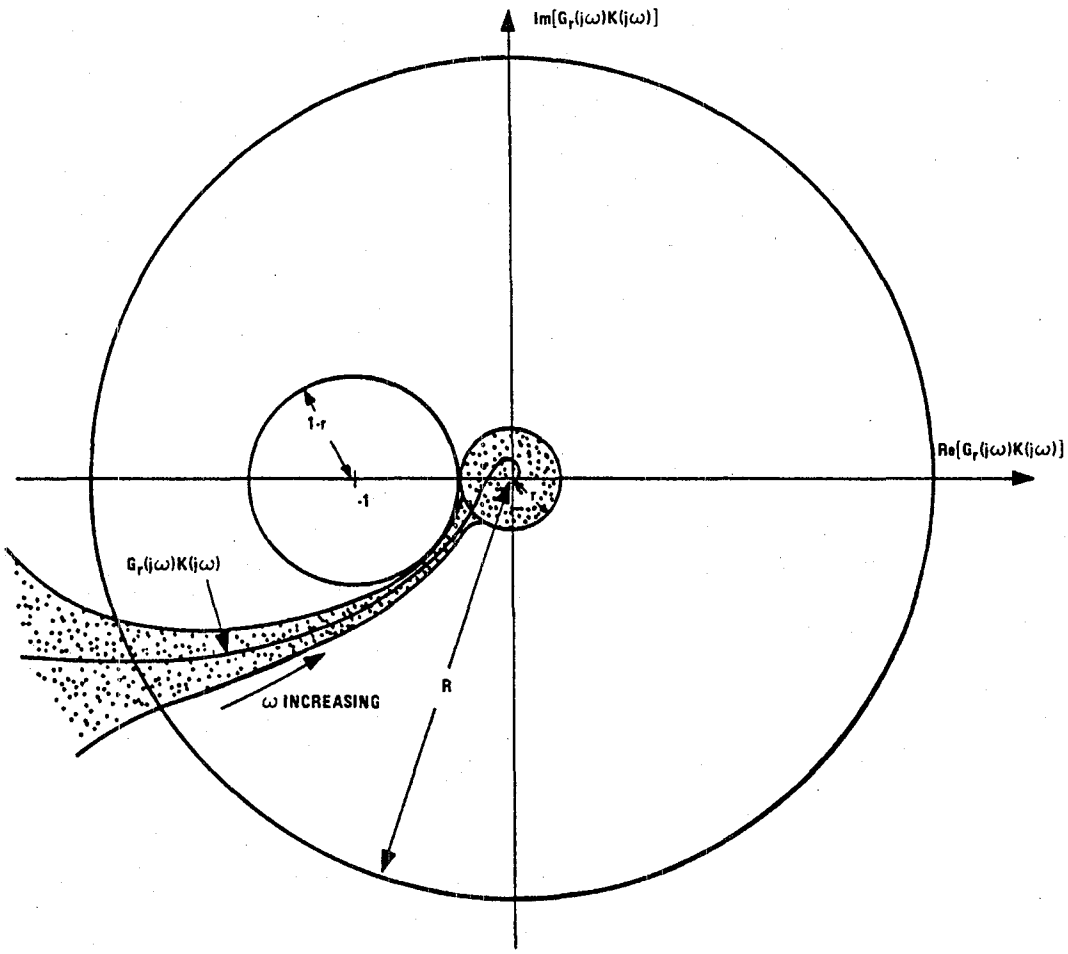

Figure III.1 Allowable Reduced Order Model Error Bound

requirements will be satisfied for $G(j\omega)K(j\omega)$ as well. Thus $G_r(s)$ is an acceptable reduced order model and the frequency dependent width of the shaded region is the frequency dependent allowable model reduction error.

Motivation For Frequency Weighted Model Reduction Error Criterion

The above comments have already indicated that for control design the model reduction error criterion must take into account the frequency dependence of the allowable error. This rather intuitive discussion will be made more formal now.

Given that the model reduction method will not neglect unstable poles and that a stable closed loop system can be designed for the reduced order model, the stability of the full order model closed loop system can be assessed with the stability robustness theorem of Chapter II.

Consider the full order model closed loop system in block diagram form shown in Fig. III.2 where $G(s)$, $G_r(s)$ and $K(s)$ are the transfer functions for the

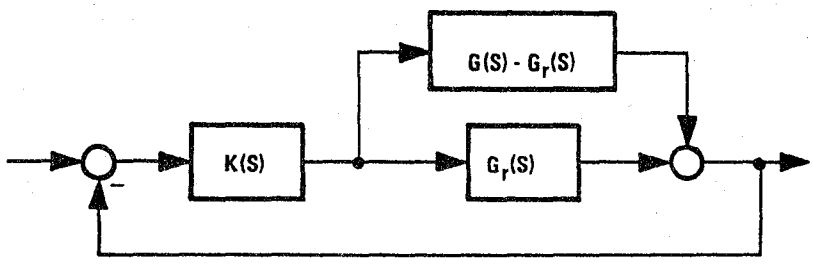

Fig. III.2 Full Order Model Closed Loop System

full order model, reduced order model and the compensator respectively. Note that, the block diagram is really just a rearranged version of the compensator and the full order model in a standard feedback configuration (i.e. $G_r(s)$ cancels out). Applying the stability robustness theorem to this configuration implies that the full order model closed loop system is stable if either

$$\| [G(s) - G_r(s)] \; W_i(s) \|_\infty < 1$$

or

$$\| W_o(s)[G(s) - G_r(s)] \|_\infty < 1$$

where

$$W_i(s) \triangleq K(s)[I + G_r(s)K(s)]^{-1}$$
$$W_o(s) \triangleq [I + K(s)G_r(s)]^{-1} K(s) \quad .$$

It is of interest to compare the magnitude of these weighting transfer functions with the intuitive discussion given above. For simplicity consider the SISO special case. Let

$$\begin{aligned} W(s) &= W_i(s) = W_o(s) \\ &= K(s)[1 + G_r(s)K(s)]^{-1} \\ &= G_r(s)K(s)[1 + G_r(s)K(s)]^{-1} G_r^{-1}(s) \quad . \end{aligned}$$

Now then $G_r(j\omega)K(j\omega)[1 + G_r(j\omega)K(j\omega)]^{-1}$ (the closed loop system frequency response) will typically have a magnitude as shown in Fig. III.3 (i.e. $| G_r(j\omega)K(j\omega) | >> 1$ for small ω and $| G_r(j\omega)K(j\omega) | << 1$ for large ω).

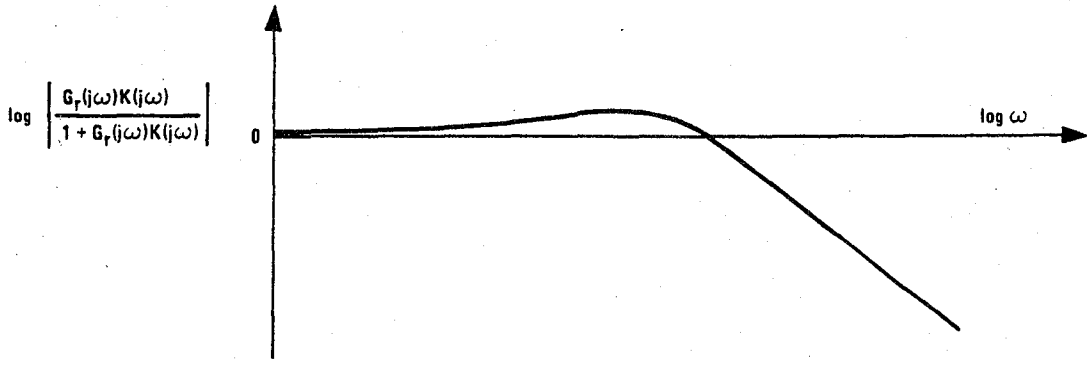

Fig. III.3 Typical Closed Loop System

Next the reduced order model transfer function, $G_r(s)$ will commonly have a magnitude plot like one of those shown in Fig. III.4.

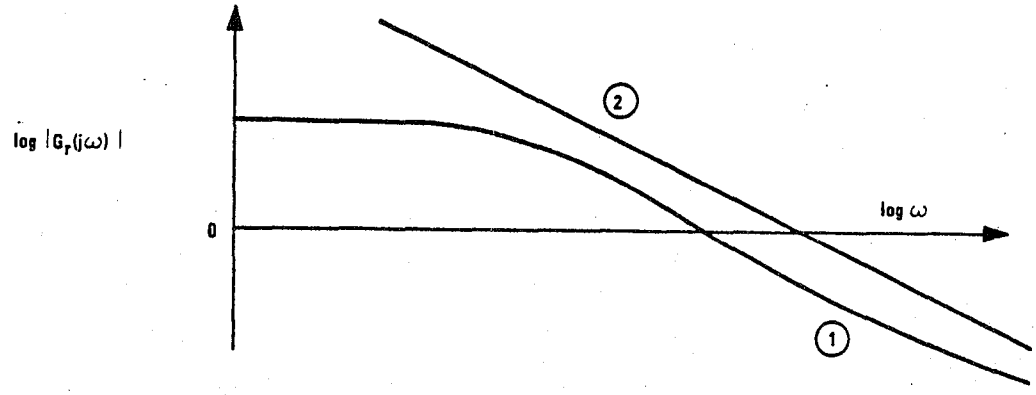

Fig. III.4 Two Common Reduced Order Models

Using Fig. III.3 the magnitudes of the weightings corresponding to the two plants in Fig. III.4 can be computed and are sketched in Fig. III.5.

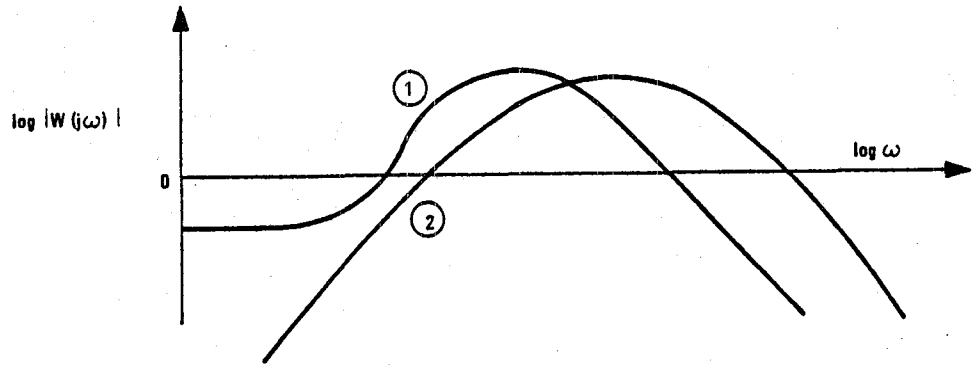

Fig. III.5 Two Common Weightings

It can be seen that these weightings indeed emphasize the crossover region and place less weight on low and high frequency error depending on the reduced order model DC gain. Thus the intuitive discussion is consistent with the formal stability analysis.

Definition of Frequency Weighted H_∞ Model Reduction Error Criterion

It has been shown that for stability, the frequency dependence of the model reduction error is important. That is, errors should be small in some frequency ranges (crossover) and can be larger in other ranges (low and high). This motivates the use of a weighted error criterion.

Stability also requires that an inequality be satisfied for every frequency, hence, it is the magnitude of the highest peak in the weighted error that is important (as opposed to some integral squared error criterion). This motivates the use of the H_∞ norm.

To obtain a formal definition of the error criterion let $G(s)$, $W_i(s)$ and $W_o(s)$ be the given full order model, input weighting and output weighting transfer functions respectively. Then the scalar model reduction error, E_∞ for the reduced order model transfer function, $G_r(s)$ is defined to be given by

$$E_\infty \triangleq \| W_o(s)[G(s) - G_r(s)]\ W_i(s) \|_\infty \quad .$$

The purpose for which the reduced order model is intended (i.e. control design) is reflected by the choice of the weighting transfer functions. The remainder of this chapter will develop the model reduction technique assuming that the weightings are given. The choice of weightings is important and will be discussed further in Chapter IV.

Model Reduction Problem

The model reduction problem will be defined to be the following. Given an nth order state space realization $\{F, G, H\}_n$ of the full order model transfer function, $G(s) = H(sI-F)^{-1}G$ and transfer functions for the input and output weightings, $W_i(s)$ and $W_o(s)$ respectively, find an r^{th} order (r specified and $r < n$) state space realization $\{A_{11}, B_1, C_1\}_r$ of the reduced order model

$G_r(s) = C_1(sI-A_{11})^{-1} B_1$ such that E_∞ is minimized and $G(s)$ and $G_r(s)$ have the same number of unstable poles.

In mathematical notation the problem is

$$\text{Given: } \{F, G, H\}_n, W_i(s), W_o(s), r < n$$
$$\text{Find: } \{A_{11}, B_1, C_1\}_r$$

such that F and A_{11} have the same number of closed right half plane eigenvalues and

$$\| W_o(s)[H(sI-F)^{-1}G - C_1(sI-A_{11})^{-1} B_1] W_i(s)\|_\infty$$

is minimized.

This problem appears to be intractable, however, the SISO special case with unity weightings and $r = n-1$ has been solved with the Hankel norm technique [Ref. 14], although the reduced order model is also required to have a constant feedthru term, D_1, i.e. $G_r(s) = C_1(sI-A_{11})^{-1} B_1 + D_1$.

Internal Balancing As An Approximate Solution

Consider the unity weightings special case and reduced order models obtained from an internally balanced realization. This also requires that the full order model is asymptotically stable. For this special case the model reduction error criterion, E_∞ can be bounded.

Internally Balanced Realization Model Reduction Error Bound

Assume that the asymptotically stable, minimal realization $\{A, B, C\}_n$ of the full order model transfer function, $G(s) = C(sI-A)^{-1}B$, is internally balanced, i.e.

$$A\Sigma + \Sigma A^T + BB^T = 0$$
$$A^T\Sigma + \Sigma A + C^TC = 0$$

where

$$\Sigma = \text{diag}\,\{\sigma_i\}$$

and

$$\sigma_1 \geq \sigma_2 \geq \cdots \geq \sigma_n \quad .$$

Let the matrices A, B, C, $\sum$ be partitioned compatibly as

$$A = \begin{bmatrix} A_{11} & A_{12} \\ A_{21} & A_{22} \end{bmatrix} \qquad B = \begin{bmatrix} B_1 \\ B_2 \end{bmatrix}$$
$$C = [C_1 \quad C_2]$$
$$\Sigma = \begin{bmatrix} \Sigma_1 & 0 \\ 0 & \Sigma_2 \end{bmatrix}$$

where the dimensions of A_{11} and Σ_1 are $r \times r$. Assuming that $\sigma_{r+1} > \sigma_r$ implies that the reduced order model $G_r(s) = C_1(sI-A_{11})^{-1}\,B_1$ is asymptotically stable and thus satisfies the model fidelity requirement that $G(s)$ and $G_r(s)$ have the same number of unstable poles (zero in this case).

Then the model reduction error criterion is bounded:

$$E_\infty \triangleq \|G(s) - G_r(s)\|_\infty \leq 2tr[\Sigma_2]$$

and for $r = n-1$ the bound is tight, i.e.

$$\|G(s) - G_{n-1}(s)\|_\infty = 2\sigma_n \quad .$$

The proof follows. Let

$$\begin{aligned}
\phi(s) &\triangleq (sI-A_{11})^{-1} \\
\Delta(s) &\triangleq sI-A_{22} - A_{21}\phi(s)A_{12} \\
\tilde{B}(s) &\triangleq A_{21}\phi(s)\, B_1 + B_2 \\
\tilde{C}(s) &\triangleq C_1\phi(s)A_{12} + C_2 \quad ,
\end{aligned}$$

then

$$\begin{aligned}
G(s) - G_r(s) &= C(sI-A)^{-1} B - C_1\phi(s)B_1 \\
&= [C_1\ C_2] \begin{bmatrix} (sI-A_{11}) & -A_{12} \\ -A_{21} & sI-A_{22} \end{bmatrix}^{-1} \begin{bmatrix} B_1 \\ B_2 \end{bmatrix} - C_1\phi(s)B_1 \quad .
\end{aligned}$$

Using the inverse of a block matrix formula [Ref. 34]

$$G(s) - G_r(s) = [C_1\ C_2]$$
$$\begin{bmatrix} \phi(s) + \phi(s)A_{12}\Delta^{-1}(s)A_{21}\phi(s) & \phi(s)A_{12}\Delta^{-1}(s) \\ \Delta^{-1}(s)A_{21}\phi(s) & \Delta^{-1}(s) \end{bmatrix} \begin{bmatrix} B_1 \\ B_2 \end{bmatrix}$$

$$- C_1\phi(s)\,B_1$$

$$= C_1\phi(s)A_{12}\Delta^{-1}(s)A_{21}\phi(s)B_1 + C_2\Delta^{-1}(s)A_{21}\phi(s)\,B_1$$

$$+ C_1\phi(s)A_{12}\Delta^{-1}(s)B_2 + C_2\Delta^{-1}(s)B_2$$

$$= \tilde{C}(s)\Delta^{-1}(s)\tilde{B}(s)$$

by algebra and the definitions of $\tilde{B}(s)$ and $\tilde{C}(s)$.

From the definition of the maximum singular value we have

$$\bar{\sigma}\left[G(j\omega) - G_r(j\omega)\right] = \lambda_{\max}^{1/2}\left[\left[G(j\omega) - G_r(j\omega)\right]\left[G(j\omega) - G_r(j\omega)\right]^H\right] .$$

Substituting for $G(j\omega) - G_r(j\omega)$ in terms of $\tilde{B}(j\omega)$, $\tilde{C}(j\omega)$ and $\Delta(j\omega)$ from above, we have

$$\bar{\sigma}\left[G(j\omega) - G_r(j\omega)\right] = \lambda_{\max}^{1/2}\left[\tilde{C}(j\omega)\Delta^{-1}(j\omega)\tilde{B}(j\omega)\tilde{B}^H(j\omega)\Delta^{-H}(j\omega)\tilde{C}^H(j\omega)\right] .$$

Using the fact that $\lambda_{\max}[AB] = \lambda_{\max}[BA]$ for any matrices A, B where the products are defined [Ref. 37], we have

$$\bar{\sigma}\left[G(j\omega) - G_r(j\omega)\right] = \lambda_{\max}^{1/2}\left[\Delta^{-1}(j\omega)\tilde{B}(j\omega)\tilde{B}^H(j\omega)\Delta^{-H}(j\omega)\tilde{C}^H(j\omega)\tilde{C}(j\omega)\right] .$$

Expressions for $\tilde{B}(j\omega)\tilde{B}^H(j\omega)$ and $\tilde{C}^H(j\omega)\tilde{C}(j\omega)$ are obtained by using the

partitioned form of the internally balanced grammian equations

$$
\begin{aligned}
A_{11}\Sigma_1 + \Sigma_1 A_{11}^T + B_1 B_1^T &= 0 \\
A_{12}\Sigma_2 + \Sigma_1 A_{21}^T + B_1 B_2^T &= 0 \\
A_{22}\Sigma_2 + \Sigma_2 A_{22}^T + B_2 B_2^T &= 0 \\
A_{11}^T\Sigma_1 + \Sigma_1 A_{11} + C_1^T C_1 &= 0 \\
A_{21}^T\Sigma_2 + \Sigma_1 A_{12} + C_1^T C_2 &= 0 \\
A_{22}^T\Sigma_2 + \Sigma_2 A_{22} + C_2^T C_2 &= 0
\end{aligned}
$$

where the first three of the above equations were obtained from $A\Sigma + \Sigma A^T + BB^T = 0$ and the last three were obtained from $A^T\Sigma + \Sigma A + C^T C = 0$.

An expression for $\tilde{B}(j\omega)\tilde{B}^H(j\omega)$ is obtained as follows. By the definition of $\tilde{B}(s)$, we have

$$
\begin{aligned}
\tilde{B}(j\omega)\tilde{B}^H(j\omega) = {} & A_{21}\phi(j\omega)B_1 B_1^T \phi^H(j\omega)A_{21}^T + A_{21}\phi(j\omega)B_1 B_2^T \\
& + B_2 B_1^T \phi^H(j\omega)A_{21}^T + B_2 B_2^T \quad .
\end{aligned}
$$

Substituting for $B_1 B_1^T$, $B_1 B_2^T$ and $B_2 B_2^T$ from the partitioned form of the grammian equations, we have

$$\tilde{B}(j\omega)\tilde{B}^H(j\omega) = -\Big\{A_{21}\phi(j\omega)\Big[A_{11}\Sigma_1+\Sigma_1A_{11}^T\Big]\phi^H(j\omega)A_{21}^T$$

$$+ A_{21}\phi(j\omega)\Big[A_{12}\Sigma_2+\Sigma_1A_{21}^T\Big]$$

$$+ \Big[A_{21}\Sigma_1+\Sigma_2A_{12}^T\Big]\phi^H(j\omega)A_{21}^T + A_{22}\Sigma_2 + \Sigma_2A_{22}^T\Big\}$$

$$= -\Big\{A_{21}\Big[\phi(j\omega)\Big[A_{11}\Sigma_1+\Sigma_1A_{11}^T\Big]\phi^H(j\omega) + \phi(j\omega)\Sigma_1$$

$$+ \Sigma_1\phi^H(j\omega)\Big]A_{21}^T$$

$$+ \Big[A_{21}\phi(j\omega)A_{12}+A_{22}\Big]\Sigma_2 + \Sigma_2\Big[A_{12}^T\phi^H(j\omega)A_{21}^T + A_{22}^T\Big]\Big\}$$

after rearranging terms. Substituting $j\omega I - \Delta(j\omega)$ for $A_{21}\phi(j\omega)A_{12} + A_{22}$ from the definition of $\Delta(s)$, we have

$$\tilde{B}(j\omega)\tilde{B}^H(j\omega) = -\Big\{A_{21}\phi(j\omega)\Big[A_{11}\Sigma_1 + \Sigma_1A_{11}^T$$

$$+ \Sigma_1\phi^{-H}(j\omega) + \phi^{-1}(j\omega)\Sigma_1\Big]\phi^H(j\omega)A_{21}^T$$

$$+ \Big[j\omega I-\Delta(j\omega)\Big]\Sigma_2 + \Sigma_2\Big[-j\omega I - \Delta^H(j\omega)\Big]\Big\}$$

where the first term was also further factored. Noting that the first term is zero by the definition of $\phi(s)$, we have

$$\tilde{B}(j\omega)\tilde{B}^H(j\omega) = \Delta(j\omega)\Sigma_2 + \Sigma_2\Delta^H(j\omega) \quad .$$

The expression for $\tilde{C}^H(j\omega)\tilde{C}(j\omega)$ is obtained analogously and is given by

$$\tilde{C}^H(j\omega)\tilde{C}(j\omega) = \Sigma_2\Delta(j\omega) + \Delta^H(j\omega)\Sigma_2 \quad .$$

These expressions for $\tilde{B}(j\omega)\tilde{B}^H(j\omega)$ and $\tilde{C}^H(j\omega)\tilde{C}(j\omega)$ are then substituted into the final expression for $\bar{\sigma}[G(j\omega) - G_r(j\omega)]$ above to obtain

$$\begin{aligned}\bar{\sigma}\Big[G(j\omega) - G_r(j\omega)\Big] &= \lambda_{\max}^{1/2}\Big[\Delta^{-1}(j\omega)\Big[\Delta(j\omega)\Sigma_2 + \Sigma_2\Delta^H(j\omega)\Big]\Delta^{-H}(j\omega) \\ &\qquad \Big[\Sigma_2\Delta(j\omega) + \Delta^H(j\omega)\Sigma_2\Big]\Big] \\ &= \lambda_{\max}^{1/2}\Big[\Big[\Sigma_2 + \Delta^{-1}(j\omega)\Sigma_2\Delta^H(j\omega)\Big] \\ &\qquad \Big[\Delta^{-H}(j\omega)\Sigma_2\Delta(j\omega) + \Sigma_2\Big]\Big]\end{aligned}$$

after algebraic simplification.

Consider order reduction by one state (i.e. $r = n-1$) then $\Sigma_2 = \sigma_n$ and

$$\bar{\sigma}[G(j\omega) - G_{n-1}(j\omega)] = \sigma_n \sqrt{[1 + A(j\omega)][1 + A^{-1}(j\omega)]}$$

where $A(j\omega) \triangleq \Delta^H(j\omega)\Delta^{-1}(j\omega)$ is an "all pass" i.e. $|A(j\omega)| = 1 \quad \forall\omega$. Thus after rearranging terms and making use of the "all pass" property of $A(j\omega)$ we have

$$\begin{aligned}\bar{\sigma}[G(j\omega) - G_{n-1}(j\omega)] &= \sigma_n \sqrt{\frac{[1 + A(j\omega)]^2}{A(j\omega)}} \\ &= \sigma_n |1 + A(j\omega)| \quad .\end{aligned}$$

By the triangle inequality we have

$$\bar{\sigma}\Big[G(j\omega) - G_{n-1}(j\omega)\Big] \leq \sigma_n\Big[1 + |A(j\omega)|\Big] = 2\sigma_n \quad .$$

This completes the proof of the bound for $r = n-1$.

The remainder of the proof is achieved by using the order reduction by one state result and by noting that $\{A_{11}, B_1, C_1\}_k$ obtained by the k^{th} order

partitioning is internally balanced with balanced grammian, $\Sigma_1 = \text{diag}\ \{\sigma_1, \sigma_2, ..., \sigma_k\}$.

Let $E_k(s) \triangleq G_{k+1}(s) - G_k(s)$ for $k = 1, 2, ..., n-1$ and let $G_n(s) \triangleq G(s)$. Then

$$\bar{\sigma}\left[E_k(j\omega)\right] \leq 2\sigma_{k+1}$$

since $G_k(s)$ is a reduced order model obtained from the internally balanced realization of $G_{k+1}(s)$ and the above bound for order reduction by one state holds.

Noting that

$$G(s) - G_r(s) = \sum_{k=r}^{n-1} E_k(s)$$

by the definition of $E_k(s)$, we have

$$\bar{\sigma}\left[G(j\omega) - G_r(j\omega)\right] = \bar{\sigma}\left[\sum_{k=r}^{n-1} E_k(j\omega)\right] \quad .$$

Using the triangle inequality we have

$$\bar{\sigma}\left[G(j\omega) - G_r(j\omega)\right] \leq \sum_{k=r}^{n-1} \bar{\sigma}\left[E_k(j\omega)\right] \quad .$$

But $\bar{\sigma}[E_k(j\omega)] \leq 2\sigma_{k+1}$ from above, hence

$$\bar{\sigma}\left[G(j\omega) - G_r(j\omega)\right] \leq 2 \sum_{k=r}^{n-1} \sigma_{k+1} = 2tr\left[\Sigma_2\right]$$

by the definition of the trace operator and Σ_2. This completes the proof of the

bound:

$$\bar{\sigma}\Big[G(j\omega) - G_r(j\omega)\Big] \leq 2tr\Big[\Sigma_2\Big] \quad .$$

Note that when $r = n-1$ by the definition of $\Delta(s)$ we have

$$\Delta(0) = A_{21} A_{11}^{-1} A_{12} - A_{22}$$

(the inverse of A_{11} exists since A_{11} has eigenvalues with strictly negative real parts). But, from the determinant of block matrices formula [Ref. 34]

$$\Delta(0) = \frac{\det A}{\det A_{11}} \quad .$$

Neither det A or det A_{11} is zero since both A and A_{11} have eigenvalues with strictly negative real parts, thus we have

$$0 < |\Delta(0)| < \infty$$

and hence

$$A(0) = \frac{\Delta(0)}{\Delta(0)} = 1 \quad .$$

Using this in the equality from above for $\omega = 0$ we have

$$\begin{aligned} \bar{\sigma}\Big[G(0) - G_{n-1}(0)\Big] &= \sigma_n |1 + A(0)| \\ &= 2\sigma_n \quad . \end{aligned}$$

Thus the bound is tight for order reduction by one state and is in fact achieved at DC, i.e. $\omega = 0$.

Tightness of the Bound For Two Special Cases

For the following two special cases the model reduction error criterion, E_∞ and the bound, $2tr[\Sigma_2]$ can be computed with a limiting process and then compared. The first example has poles and zeros which alternate along the negative real axis and the bound is tight in this case. The second example has poles and zeros which alternate along the $j\omega$ axis and the bound is not tight in this case.

Alternating Real Poles and Zeros Example

Consider the SISO system with transfer function given by

$$G(s) = \sum_{k=1}^{n} \frac{p^k}{s + p^k} \quad , \qquad p > 0 \quad .$$

For s real, the derivative of $G(s)$ with respect to s is negative so the poles and zeros must alternate along the real axis [Ref. 38]. The results in Reference 39 show that

$$\lim_{p\to\infty} G_r(s) = \sum_{k=1}^{r} \frac{p^k}{s + p^k}$$

$$\lim_{p\to\infty} \Sigma_2 = \frac{1}{2} I_{n-r}$$

$$\lim_{p\to\infty} \|G(s) - G_r(s)\|_\infty = n-r \quad .$$

Applying the bound and the above result for Σ_2 to this example results in

$$\lim_{p\to\infty} \|G(s) - G_r(s)\|_\infty \leq 2 \lim_{p\to\infty} tr[\Sigma_2] = n-r \quad .$$

Thus the actual error is equal to the bound in this limiting case.

Alternating Imaginary Poles and Zeros Example

Consider the SISO system with transfer function given by

$$G(s) = \sum_{k=1}^{n} \frac{\omega_k^2}{s^2 + 2\varsigma\omega_k s + \omega_k^2}$$

where $\varsigma > 0$ and $0 < \omega_1 < \omega_2 < \cdots < \omega_n$. Note that $\varsigma > 0$ is required such that the transfer function is asymptotically stable, but

$$\lim_{\varsigma\to 0} G(s) = \sum_{k=1}^{n} \frac{\omega_k^2}{s^2 + \omega_k^2}$$

has alternating poles and zeros along the imaginary axis (again, proved in Ref. 38). With the further assumption that the ω_i's are sufficiently separated, i.e.

$$\frac{\varsigma \max(\omega_i,\omega_j)}{|\omega_i - \omega_j|} \ll 1 \qquad \forall\, i,j = 1, n \quad , \quad i \neq j$$

the results of References 40 and 41 show that

$$\lim_{\varsigma\to 0} G_r(s) = \lim_{\varsigma\to 0} \sum_{k=1}^{r} \frac{\omega_k^2}{s^2 + 2\varsigma\omega_k s + \omega_k^2}$$

$$\lim_{\varsigma\to 0} \Sigma_2 = \frac{1}{4\varsigma} I_{2(n-r)} \quad .$$

Substituting for $G_r(s)$ and by the definition of the H_∞ norm we have

$$\lim_{\varsigma \to 0} \|G(s) - G_r(s)\|_\infty = \|G(s) - \lim_{\varsigma \to 0} G_r(s)\|_\infty$$

$$= \sup_\omega \left| \lim_{\varsigma \to 0} \sum_{k=r+1}^{n} \frac{\omega_k^2}{\omega_k^2 - \omega^2 + 2\varsigma j\omega\omega_k} \right|$$

$$= \lim_{\varsigma \to 0} \frac{1}{2\varsigma} \quad .$$

Applying the bound and the above result for $\sum_2$ to this example results in

$$\lim_{\varsigma \to 0} \|G(s) - G_r(s)\|_\infty \leq 2 \lim_{\varsigma \to 0} tr\left[\sum_2\right] = \frac{1}{\varsigma}(n-r) \quad .$$

Thus the actual error is a factor of $2(n-r)$ smaller than the bound in this limiting case.

The results for these two cases are indicated graphically in Fig. III.6.

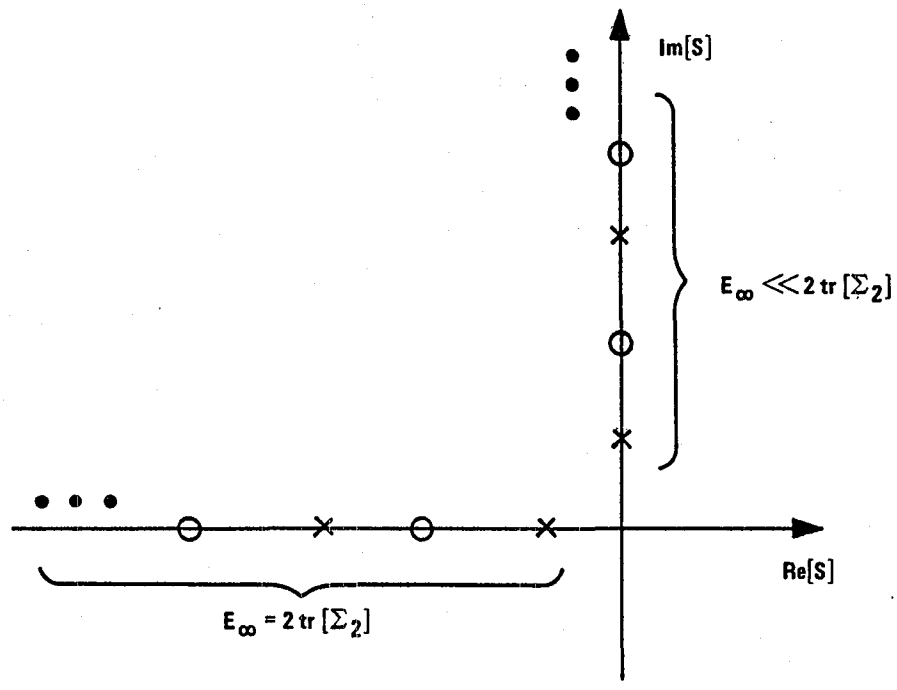

Fig. III.6 Tightness of the Error Bound For Two Special Cases

On the Question of Optimality

As already alluded to, the Hankel norm technique does provide a reduced order model for $r = n-1$ and SISO which does achieve the minimal E_∞ (with unity weightings). As was also noted this technique does require that the reduced order model have a finite D term, whereas the balancing technique uses a zero D term. With this extra degree of freedom it is expected that the E_∞ resulting from the Hankel technique would be less than or equal to that resulting from the balancing technique.

It is of interest to compare these two results for E_∞: for the Hankel technique [Ref. 14], $E_\infty = \sigma_n$ and as proved above for the balancing technique, $E_\infty = 2\sigma_n$. Thus the balancing technique yields a solution which has an error twice that of the Hankel technique which has an extra degree of freedom (i.e. the D term).

In the more general case of any $r < n$ and MIMO but with unity weightings Glover [Ref. 15] states an algorithm for model reduction based on the Hankel technique for which

$$E_\infty \leq tr\left[\Sigma_2\right]$$

where again it involves a finite D term.

It should also be noted that if the D terms for these techniques are set to zero and the reduced order model is otherwise unchanged, the following bound holds in this case

$$E_\infty \leq 2tr\left[\Sigma_2\right] \quad .$$

Thus short of knowing the optimal solution for the unweighted, zero D case, the internally balanced realization model reduction technique will be regarded as an attractive technique for performing model reduction. The computations for the Hankel technique start with a balanced realization, hence, obtaining the reduced order model from the internally balanced realization is computationally less

expensive and satisfies the same error bound as the Hankel technique for the same assumptions on the reduced order model.

Frequency Weighted Balanced Realizations

We have seen that the internally balanced realization is an attractive model reduction technique for unity weightings. An extension to the balancing technique to include weightings will now be developed.

This extension is motivated by the geometric interpretation of the internally balanced realization given in Chapter II. The n^{th} order, minimal, asymptotically stable system to be balanced with respect to the asymptotically stable input and output weightings $W_i(s)$ and $W_o(s)$ satisfies the given state equations

$$\begin{aligned} \dot{x} &= Fx + Gu \qquad x\epsilon\mathbf{R}^n \quad u\epsilon\mathbf{R}^m \\ y &= Hx \qquad\quad y\epsilon\mathbf{R}^p \quad . \end{aligned}$$

With reference to the block diagram shown in Fig. III.7, ask the following

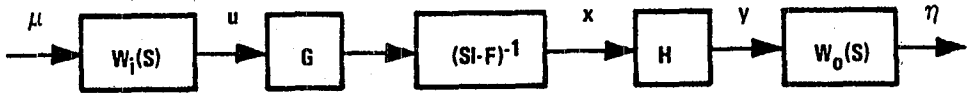

Fig. III.7 Block Diagram For Frequency Weighted Balanced Realization Discussion

two (dual) questions. What set of points in the x-state space could be part of the zero initial condition response for some weighted input, $\mu(t)$ such that $||\mu(t)||_2 \leq 1$ and zero initial conditions for the states of the input weighting? and what set of points in the x-state space as initial conditions could produce a weighted output, $\eta(t)$ such that $||\eta(t)||_2 \leq 1$ with zero input and zero initial conditions for the states of the output weighting?

These questions are again answered by appealing to the grammian-ellipsoid theorem of Chapter II. First assume asymptotically stable state space realizations for the input and output weightings are given, i.e.

$$\begin{aligned} W_i(s) &= H_i(sI-F_i)^{-1}\, G_i + D_i \\ W_o(s) &= H_o(sI-F_o)^{-1}\, G_o + D_o \quad . \end{aligned}$$

For the first question, let $F(t) = \overline{H}_i\, e^{\overline{F}_i t}\, \overline{G}_i$ where

$$\begin{aligned} \overline{F}_i &= \begin{bmatrix} F & GH_i \\ 0 & F_i \end{bmatrix} \qquad \overline{G}_i = \begin{bmatrix} GD_i \\ G_i \end{bmatrix} \\ \overline{H}_i &= [I \;\; 0] \quad , \end{aligned}$$

then the answer is the controllable set, S_c.

For the second question, let $F(t) = \overline{H}_o\, e^{\overline{F}_o t}\, \overline{G}_o$ where

$$\begin{aligned} \overline{F}_o &= \begin{bmatrix} F & 0 \\ G_oH & F_o \end{bmatrix} \; \overline{G}_o = \begin{bmatrix} I \\ 0 \end{bmatrix} \\ \overline{H}_o &= [D_oH \;\; H_o] \quad . \end{aligned}$$

The grammians corresponding to these questions are given by

$$U \triangleq \int_0^\infty \bar{H}_i e^{\bar{F}_i t}\, \bar{G}_i \bar{G}_i^T\, e^{\bar{F}_i^T t}\, \bar{H}_i^T dt$$

$$Y \triangleq \int_0^\infty \bar{G}_o^T e^{\bar{F}_o^T t}\, \bar{H}_o^T \bar{H}_o e^{\bar{F}_o t}\, \bar{G}_o\, dt$$

and thus can also be computed from the cascaded grammians

$$\bar{U} \triangleq \int_o^\infty e^{\bar{F}_i t}\, \bar{G}_i \bar{G}_i^T\, e^{\bar{F}_i^T t}\, dt$$

$$\bar{Y} \triangleq \int_o^\infty e^{\bar{F}_o^T t}\, \bar{H}_o^T \bar{H}_o\, e^{\bar{F}_o t}\, dt$$

which can be computed from the Lyapunov equations

$$\bar{F}_i \bar{U} + \bar{U}\bar{F}_i^T + \bar{G}_i \bar{G}_i^T = 0 \qquad \text{(III.1a)}$$

$$\bar{F}_o^T \bar{Y} + \bar{Y}\bar{F}_o + \bar{H}_o^T \bar{H}_o = 0 \quad . \qquad \text{(III.1b)}$$

Partition $\bar{U}$ and $\bar{Y}$ such that their upper left block is $n \times n$ as

$$\bar{U} = \begin{bmatrix} U_{11} & U_{21}^T \\ U_{21} & U_{22} \end{bmatrix} \qquad Y = \begin{bmatrix} Y_{11} & Y_{12} \\ Y_{12}^T & Y_{22} \end{bmatrix}$$

then

$$U = \bar{H}_i \bar{U} \bar{H}_i^T = U_{11}$$

$$Y = \bar{G}_o^T \bar{Y} \bar{G}_o = Y_{11} \quad .$$

Thus again, the two sets are in general different ellipsoids with n semi-axes. The lengths and directions of the weighted controllability ellipsoid semi-axes are the square roots of the eigenvalues and eigenvectors of the weighted controllability grammian U, respectively. The lengths and directions of the weighted observability ellipsoid semi-axes are the reciprocals of the square roots

of the eigenvalues and the eigenvectors of the weighted observability grammian, Y respectively.

The next step is to obtain a realization of the system such that the two ellipsoid axes are lined up (balanced). To obtain a new realization with this property a change of variables with a similarity transformation will be used i.e. $x = Tz$.

A possibly subtle point should be noted here: this is *not* the same as internally balancing the cascaded systems. That is, the $n \times n$ grammians, U and Y are balanced not $\overline{U}$ and $\overline{Y}$ which in general will not even have the same dimensions.

Algorithm For Computing the Frequency Weighted Balanced Realization

The objective of the balancing algorithm is to obtain a realization $\{A, B, C\}_n$ of $G(s) = H(sI-F)^{-1}G = C(sI-A)^{-1}B$ such that U and Y, the weighted grammians are equal and diagonal. Towards this end, consider how the original grammians change due to a similarity transformation on the full order model state variables.

Starting with III.1a in partitioned form together with $U = U_{11}$ we have

$$\begin{bmatrix} F & GH_i \\ 0 & F_i \end{bmatrix} \begin{bmatrix} U & U_{21}^T \\ U_{21} & U_{22} \end{bmatrix} + \begin{bmatrix} U & U_{21}^T \\ U_{21} & U_{22} \end{bmatrix} \begin{bmatrix} F^T & 0 \\ H_i^T G^T & F_i^T \end{bmatrix}$$
$$+ \begin{bmatrix} GD_i \\ G_i \end{bmatrix} \begin{bmatrix} D_i^T G^T & G_i^T \end{bmatrix} = \begin{bmatrix} 0 & 0 \\ 0 & 0 \end{bmatrix} .$$

Introducing the transformation, T, we have

$$\begin{bmatrix} T^{-1} & 0 \\ 0 & I \end{bmatrix} \begin{bmatrix} F & GH_i \\ 0 & F_i \end{bmatrix} \begin{bmatrix} T & 0 \\ 0 & I \end{bmatrix} \begin{bmatrix} T^{-1} & 0 \\ 0 & I \end{bmatrix} \begin{bmatrix} U & U_{21}^T \\ U_{21} & U_{22} \end{bmatrix} \begin{bmatrix} T^{-T} & 0 \\ 0 & I \end{bmatrix}$$
$$+ \begin{bmatrix} T^{-1} & 0 \\ 0 & I \end{bmatrix} \begin{bmatrix} U & U_{21}^T \\ U_{21} & U_{22} \end{bmatrix} \begin{bmatrix} T^{-T} & 0 \\ 0 & I \end{bmatrix} \begin{bmatrix} T^T & 0 \\ 0 & I \end{bmatrix} \begin{bmatrix} F^T & 0 \\ H_i^T G^T & F_i^T \end{bmatrix} \begin{bmatrix} T^{-T} & 0 \\ 0 & I \end{bmatrix}$$
$$+ \begin{bmatrix} T^{-1} & 0 \\ 0 & I \end{bmatrix} \begin{bmatrix} GD_i \\ G_i \end{bmatrix} \begin{bmatrix} D_i^T G^T & G_i^T \end{bmatrix} \begin{bmatrix} T^{-T} & 0 \\ 0 & I \end{bmatrix} = \begin{bmatrix} 0 & 0 \\ 0 & 0 \end{bmatrix}$$

which can be rewritten

$$\begin{bmatrix} A & BH_i \\ 0 & F_i \end{bmatrix} \begin{bmatrix} \hat{U} & \hat{U}_{21}^T \\ \hat{U}_{21} & \hat{U}_{22} \end{bmatrix} + \begin{bmatrix} \hat{U} & \hat{U}_{21}^T \\ \hat{U}_{21} & \hat{U}_{22} \end{bmatrix} \begin{bmatrix} A^T & 0 \\ H_i^T B^T & F_i^T \end{bmatrix}$$
$$+ \begin{bmatrix} BD_i \\ G_i \end{bmatrix} \begin{bmatrix} D_i^T B^T & G_i^T \end{bmatrix} = \begin{bmatrix} 0 & 0 \\ 0 & 0 \end{bmatrix}$$

Similarly III.1b can be rewritten

$$\begin{bmatrix} A^T & C^T G_o^T \\ 0 & F_o^T \end{bmatrix} \begin{bmatrix} \hat{Y} & \hat{Y}_{12} \\ \hat{Y}_{12}^T & \hat{Y}_{22} \end{bmatrix} + \begin{bmatrix} \hat{Y} & \hat{Y}_{12} \\ \hat{Y}_{12}^T & \hat{Y}_{22} \end{bmatrix} \begin{bmatrix} A & 0 \\ G_o C & F_o \end{bmatrix}$$
$$+ \begin{bmatrix} C^T D_o^T \\ H_o^T \end{bmatrix} \begin{bmatrix} D_o C & H_o \end{bmatrix} = \begin{bmatrix} 0 & 0 \\ 0 & 0 \end{bmatrix}$$

where

$$A \triangleq T^{-1}FT \qquad B \triangleq T^{-1}G$$
$$C \triangleq HT$$
$$\begin{bmatrix} \hat{U} & \hat{U}_{21}^T \\ \hat{U}_{21} & \hat{U}_{22} \end{bmatrix} \triangleq \begin{bmatrix} T^{-1}UT^{-T} & T^{-1}U_{21}^T \\ U_{21}T^{-T} & U_{22} \end{bmatrix}$$
$$\begin{bmatrix} \hat{Y} & \hat{Y}_{12} \\ \hat{Y}_{12}^T & \hat{Y}_{22} \end{bmatrix} \triangleq \begin{bmatrix} T^T YT & T^T Y_{12} \\ Y_{12}^T T & Y_{22} \end{bmatrix} .$$

Now the objective is to find T such that

$$\hat{U} = T^{-1}UT^{-T} = \Sigma$$
$$\hat{Y} = T^T YT = \Sigma$$

where $\Sigma = \text{diag}\{\sigma_1, \sigma_2, ..., \sigma_n\}$

with $\sigma_1 \geq \sigma_2 \geq \cdots \geq \sigma_n$.

The similarity transformation, T which accomplishes the objective is the eigenvector matrix obtained from the eigenvector decomposition

$$UY = T\Lambda T^{-1}$$

as for the internally balanced case discussed in Chapter II. Noting that

$$\overline{U} \geq 0 \qquad \Rightarrow U \geq 0$$

and

$$\overline{Y} \geq 0 \qquad \Rightarrow Y \geq 0 \quad ,$$

the result in Appendix C shows that $\Lambda \geq 0$, thus letting

$$\sigma_i \triangleq \sqrt{\lambda_i} \qquad i = 1, 2, ..., n$$

where $\Lambda = \text{diag}\,\{\lambda_i\}$ accomplishes the objective (assuming without loss of generality that the λ_i's have been ordered such that $\lambda_1 \geq \lambda_2 \geq \cdots \geq \lambda_n$).

The frequency weighted balanced realization $\{A,B,C\}$ is also unique to within a change in sign of a state variable when the singular values of the balanced grammian are distinct (i.e. $\sigma_i \neq \sigma_j$ for $i \neq j$). The proof of this fact for the weighted case is identical to that of the internally balanced case [Ref. 11] and hence is omitted.

The algorithm for transforming a given asymptotically stable, minimal realization $\{F,G,H\}_n$ into a frequency weighted balanced realization, given state space realizations for the transfer functions of the asymptotically stable input and output weightings is summarized in Table III.1.

Thus it has been shown that there exists an essentially unique realization of the system obtained by a change of variables with a similarity transformation, T, such that the axes of the ellipsoids are the same (balanced) for the new state variables (say, z where $x = Tz$). For model reduction this balancing is the key idea. It provides a basis for the n dimensional x-state space where the direction of a given basis vector is as controllable with the weighted input as observable with the weighted output in a well defined sense. The lengths of the ellipsoid's semi-axes provide a scalar measure, σ_i of how important a given basis vector direction is with respect to the weighted controllability and observability.

The reduced order model is then obtained by neglecting the states which are weakly controllable/observable with the weighted input/output. In mathematical

Table III.1 Frequency Weighted Balanced Realization Algorithm

Given: F, G, H with $R_e\left[\lambda[F]\right] < 0$

F_i, G_i, H_i, D_i with $R_e\left[\lambda[F_i]\right] < 0$

F_o, G_o, H_o, D_o with $R_e\left[\lambda[F_o]\right] < 0$

where
$$G(s) = H(sI-F)^{-1}G$$
$$W_i(s) = H_i(sI-F_i)^{-1}G_i + D_i$$
$$W_o(s) = H_o(sI-F_o)^{-1}G_o + D_o$$

Solve for U and Y from

$$\begin{bmatrix} F & GH_i \\ 0 & F_i \end{bmatrix}\begin{bmatrix} U & U_{21}^T \\ U_{21} & U_{22} \end{bmatrix} + \begin{bmatrix} U & U_{21}^T \\ U_{21} & U_{22} \end{bmatrix}\begin{bmatrix} F^T & 0 \\ H_i^T G^T & F_i^T \end{bmatrix}$$
$$+ \begin{bmatrix} GD_i \\ G_i \end{bmatrix}\begin{bmatrix} D_i^T G^T & G_i^T \end{bmatrix} = \begin{bmatrix} 0 & 0 \\ 0 & 0 \end{bmatrix}$$
$$\begin{bmatrix} F^T & H^T G_o^T \\ 0 & F_o^T \end{bmatrix}\begin{bmatrix} Y & Y_{12} \\ Y_{12}^T & Y_{22} \end{bmatrix} + \begin{bmatrix} Y & Y_{12} \\ Y_{12}^T & Y_{22} \end{bmatrix}\begin{bmatrix} F & 0 \\ G_o H & F_o \end{bmatrix}$$
$$+ \begin{bmatrix} H^T D_o^T \\ H_o^T \end{bmatrix}\begin{bmatrix} D_o H & H_o \end{bmatrix} = \begin{bmatrix} 0 & 0 \\ 0 & 0 \end{bmatrix} .$$

Solve for eigenvalues and eigenvectors of UY

i.e. $UY = T\Lambda T^{-1}$, $\Lambda = \text{diag}\{\lambda_i\}$, $\lambda_1 \geq \lambda_2 \geq \cdots \geq \lambda_n$

$\sum = \text{diag}\{\sigma_i\}$ $\sigma_i \triangleq \sqrt{\lambda_i}$ $i = 1, n$

$A = T^{-1}FT$ $B = T^{-1}G$

$B = HT$

terms this involves partitioning of the frequency weighted balanced realization, $\{A,B,C\}$:

$$A = \begin{bmatrix} A_{11} & A_{12} \\ A_{21} & A_{22} \end{bmatrix} \qquad B = \begin{bmatrix} B_1 \\ B_2 \end{bmatrix}$$
$$C = [C_1 \quad C_2] \quad .$$

The rth order reduced order model is then given by $G_r(s) = C_1(sI-A_{11})^{-1}B_1$, where the partitioning was done such that A_{11} is $r \times r$ and $\sigma_{r+1} < \sigma_r$.

Stability of the Frequency Weighted Reduced Order Model

Consider the two special cases:

Case 1: $W_i(s) = I$ and $W_o(s) \neq I$

Case 2: $W_i(s) \neq I$ and $W_o(s) = I$.

By examining the partitioned form of the grammian equations we have:

For Case 1: the reduced order model satisfies:

$$A_{11}\Sigma_1 + \Sigma_1 A_{11}^T + B_1 B_1^T = 0 \quad .$$

For Case 2: the reduced order model satisfies:

$$A_{11}^T\Sigma_1 + \Sigma_1 A_{11} + C_1^T C_1 = 0 \quad .$$

Since the full order model is assumed to be minimal, the balanced grammian is positive definite i.e.:

Case 1: $A\Sigma + \Sigma A^T + BB^T = 0 \ , \quad \Sigma > 0 \quad .$

Case 2: $A^T\Sigma + \Sigma A + C^T C = 0 \ , \quad \Sigma > 0 \quad .$

Now since Σ_1 is just a leading partition of a positive definite matrix, it too is positive definite, thus for either case $\Sigma_1 > 0$.

It is well known, [Ref. 36] that the partitioned grammian equations (i.e. Lyapunov equations) together with $\Sigma_1 > 0$ implies that $Re[\lambda[A_{11}]] \leq 0$, furthermore if for

Case 1: (A_{11}, B_1) is controllable then $Re[\lambda[A_{11}]] < 0$

Case 2: (A_{11}, C_1) is observable then $Re[\lambda[A_{11}]] < 0 \quad .$

Thus for either case, the reduced order model is guaranteed to be stable and generically (assuming controllability or observability of the reduced order model) the reduced order model is asymptotically stable.

For the general case of non-unity weightings it is not known whether the reduced order model will be stable or not. As will be seen in Chapter IV, the general case will not be required for the remainder of this thesis anyway.

Frequency Weighted Balanced Realization Error Bound

The manipulations leading to the internally balanced (unity weightings) realization model reduction error bound were carried out for the frequency weighted (non-unity weightings) balanced realization. These manipulations are contained in Appendix D and result in

$$E_\infty \triangleq \| W_o(s)[G(s) - G_r(s)] W_i(s) \|_\infty \leq 2(1 + \alpha) tr[\Sigma_2]$$

where unfortunately a simple bound for the positive quantity, α could not be found. The quantity, α is related to the H_∞ norm of the transmission from the weighted input to the neglected states and/or from the neglected states to the weighted output. The premise of the model reduction is that these transmissions are small, hence a conjecture is that: $\alpha < 1$ when $E_\infty < 1$.

Short of knowing something in closed form about α it is probably best to obtain the error, E_∞ for the model reduction by direction computation.

Model Reduction of Full Order Models With Unstable Poles

As we have seen, both the internally and frequency weighted balanced realization model reduction techniques require that the full order model be asymptotically stable. In many cases model reduction is necessary when the full order model contains poles in the closed right half plane. Some work has been done in formally extending the internally balancing technique to include unstable poles [Ref. 42] however these results were deemed to be beyond the scope of this thesis. Rather the following scheme was used and is recommended.

Given the transfer function of the full order model, $G(s)$ it is always possible to perform the decomposition (partial fraction expansion)

$$G(s) = G_s(s) + G_{us}(s)$$

where $G_s(s)$ contains all the asymptotically stable poles of $G(s)$ and $G_{us}(s)$ contains all the unstable poles of $G(s)$.

Now since for control design, the reduced order model must have the same number of unstable poles as the full order model anyway, the reduced order model can be obtained by reducing the order of only the stable part, $G_s(s)$ and leaving the unstable part as is. That is apply the balancing model reduction technique to obtain $G_{sr}(s)$, a reduced order model of $G_s(s)$, then the reduced order model, $G_r(s)$ of $G(s)$ is given by

$$G_r(s) = G_{sr}(s) + G_{us}(s) \quad .$$

The error using this technique will be that due to the order reduction of the stable part only, which can be seen by

$$\begin{aligned} E_\infty &\triangleq \| W_o(s) [G(s) - G_r(s)] W_i(s) \|_\infty \\ &= \| W_o(s) [G_s(s) + G_{us}(s) - G_{sr}(s) - G_{us}(s)] W_i(s) \|_\infty \\ &= \| W_o(s) [G_s(s) - G_{sr}(s)] W_i(s) \|_\infty \quad . \end{aligned}$$

The unanswered question is: could a smaller E_∞ be obtained by allowing the locations of the unstable poles to change but remain in the closed right half plane? A partial answer to the question is obvious for poles on the $j\omega$ axis. In this case, the reduced order model must have poles at exactly the same locations on the $j\omega$ axis as the full order model or E_∞ will not be bounded. A complete answer to the question was not obtained.

Model Reduction Concluding Remarks

This chapter has developed a unique model reduction technique which is an attractive solution to the model reduction for control system design problem. The key idea is that of frequency dependent weightings. The choice of weightings will be discussed in the next chapter.

IV. CHOICE OF MODEL REDUCTION WEIGHTINGS FOR CONTROL DESIGN

This chapter will develop two approaches for choosing model reduction weightings. The first approach assumes that it is the model of the compensator for which a reduced order model is desired and the second assumes that it is the model of the plant for which a reduced order model is desired. Both of these approaches result in a reduced order controller being designed which provides a stable closed loop system for the full order model of the plant.

Motivation For The Choice of Weightings

The two approaches for designing reduced order controllers are motivated by the stability robustness theorem of Chapter II which is repeated here for convenience. Let $P(s)$ be a multivariable transfer function which is stable under unity feedback as shown in Fig. IV.1 with

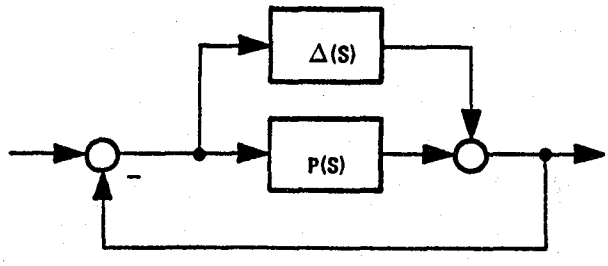

Fig. IV.1 Perturbed Closed Loop System

$\Delta(s) = 0$. The result is that the perturbed closed loop system remains stable for all stable perturbations, $\Delta(s)$ which satisfy either

$$||\Delta(s)[I + P(s)]^{-1}||_\infty < 1$$

or

$$||[I + P(s)]^{-1}\Delta(s)||_\infty < 1$$

and are referred to as input or output uncertainty tests respectively. This theorem is used to derive appropriate weightings for model reduction as part of control system design.

Compensator Order Reduction

Assume a compensator transfer function, $K(s)$ has been designed for the transfer function of the system to be controlled, $G(s)$ by some technique to meet performance and stability robustness specifications of the closed loop system. It is assumed that $K(s)$ has an order large enough to warrant reducing its order to give $K_r(s)$, a reduced order approximation of $K(s)$. Motivated by the stability robustness theorem, consider the block diagram in Fig. IV.2. For the nominal

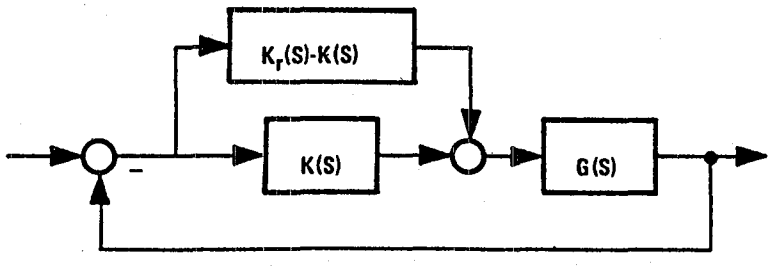

Fig. IV.2 Compensator Order Reduction As a Perturbation

loop (i.e. $K_r(s) - K(s) = 0$) the closed loop system is the result of the full order design. On the other hand the perturbed system corresponds to the closed loop system with the reduced order compensator and the full order model (this is the closed loop system for which stability is required). The stability of the closed loop system with the full order model and the reduced order compensator is guaranteed by

$$E_\infty = \| W_o(s)[K(s) - K_r(s)]\ W_i(s) \|_\infty < 1$$

where to apply the theorem the uncertainty due to the model reduction is represented arbitrarily at the input or the output:

for output uncertainty representation

$$W_o(s) = [I + G(s)K(s)]^{-1}\ G(s) \quad \text{and} \quad W_i(s) = I$$

for input uncertainty representation

$$W_i(s) = G(s)[I + K(s)G(s)]^{-1} \quad \text{and} \quad W_o(s) = I \quad .$$

Actually part of the uncertainty can be put in both places but this generality was not used in this thesis.

The reduced order controller, $K_r(s)$ is now determined by finding the reduced order model of $K(s)$ from the frequency weighted balanced realization of $K(s)$ with the weightings for either the input or output uncertainty representation. The algorithm for this approach is summarized in Table IV.1.

It can be readily verified that the two non-unity weightings are the same i.e. $G(s)[I + K(s)G(s)]^{-1} = [I + G(s)K(s)]^{-1}G(s)$. Thus the difference in the two

Table IV.1 Compensator Order Reduction Algorithm

- Design the full order compensator transfer function, $K(s)$ to meet the design objectives for the plant transfer function, $G(s)$.

- Then choose input and output weightings by arbitrarily representing the model reduction uncertainty at either the input or the output:

Input Uncertainty	Output Uncertainty
$W_i(s) = G(s)\left[I + K(s)G(s)\right]^{-1}$	$W_i(s) = I$
$W_o(s) = I$	$W_o(s) = \left[I + G(s)K(s)\right]^{-1}G(s)$

- Obtain the frequency weighted reduced order model, $K_r(s)$ of $K(s)$ for $W_i(s)$ and $W_o(s)$ such that $E_\infty < 1$. Then the closed loop system will be guaranteed to be stable with the reduced order compensator $K_r(s)$.

uncertainty representations results in the weighting being used either as an input or an output weighting for model reduction of $K(s)$. A realization of this weighting is given in Table IV.2.

Note that for either case the input and output weightings have poles which are those of the closed loop system with the full order compensator and the full order model. This closed loop system will always be stable, hence, the weightings will always be stable.

Some examples of the application of this approach are contained in Chapter V. This approach is quite straightforward and most of the remainder of this chapter will deal with the second approach. Advantages and disadvantages of the two approaches will be discussed and compared at the end of this chapter.

Plant Order Reduction

With this approach, the error due to the reduced order model of $G(s)$ is associated with the perturbation term of the stability robustness theorem. The block diagram shown in Fig. IV.3 results. When the

Table IV.2 Realization of $G(s)[I + K(s)G(s)]^{-1} = [I + G(s)K(s)]^{-1}G(s)$

$$\text{let} \quad G(s) = C(sI-A)^{-1}B$$
$$\text{and} \quad H(s) = H(sI-F)^{-1}G$$

then a realization of

$$W(s) \triangleq G(s)\left[I + K(s)G(s)\right]^{-1} = \left[I + G(s)K(s)\right]^{-1} G(s)$$

is given by

$$W(s) = C_w(sI-A_w)^{-1}B_w$$

where

$$A_w \triangleq \begin{bmatrix} A & -BH \\ GC & F \end{bmatrix} \quad B_w \triangleq \begin{bmatrix} B \\ 0 \end{bmatrix}$$
$$C_w \triangleq [C \quad 0] \quad .$$

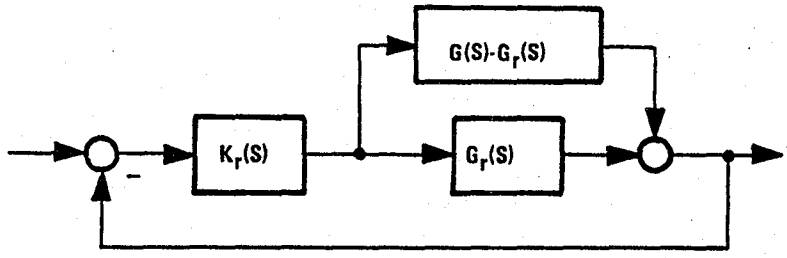

Fig. IV.3 Plant Order Reduction As a Perturbation

perturbation term, $G(s) - G_r(s)$ is zero, the block diagram represents the result of a reduced order compensator design for the reduced order model, $G_r(s)$. That is, assume $K_r(s)$ is designed to satisfy the design objectives for the reduced order model, $G_r(s)$. On the other hand, the perturbed system corresponds to the closed loop system with the reduced order compensator and the full order model (this is the closed loop system for which stability is required).

The stability of the closed loop system with the full order model and the reduced order compensator is guaranteed by

$$E_\infty = \| W_o(s)[G(s) - G_r(s)]\ W_i(s) \|_\infty < 1$$

where to apply the theorem the uncertainty due to the model reduction is represented arbitrarily at the input or the output:

for output uncertainty representation

$$W_i(s) = K_r(s)\,[I + G(s)K_r(s)\,]^{-1} \quad \text{and} \quad W_o(s) = I$$

for input uncertainty representation

$$W_i(s) = I \quad \text{and} \quad W_o(s) = [I + K_r(s)G_r(s)]^{-1}\,K_r(s) \quad .$$

Again, it can be readily verified that the two non-unity weightings are the same i.e. $K_r(s)[I + G_r(s)K_r(s)\,]^{-1} = [I + K_r(s)G_r(s)\,]^{-1}\,K_r(s)$. Thus again, the difference in the two uncertainty representations results in the weighting being used either as an input or an output weighting for model reduction of $G(s)$.

Note that for either case, the input and output weightings have poles which are those of the closed loop system with the reduced order compensator and the reduced order model. This closed loop system will always be stable, hence, the weightings will always be stable.

Unfortunately the weightings for reducing the order of $G(s)$ are not known a priori. The weightings depend on both the compensator and the reduced order model which are not known before the model reduction.

Elimination of Compensator Dependence With Advanced Loop Shaping

Advanced loop shaping, which was discussed in Chapter II is an LQG based design procedure, which for a large class of design problems, allows the designer to a priori specify a desired loop shape for one of the input or output loop transfer functions, $K(s)G(s)$ or $G(s)K(s)$ respectively. That is before actually

computing $K(s)$, the input or output loop transfer function is known.

Assuming that advanced loop shaping will be used to perform the reduced order controller design, it is of interest to make use of the a priori known loop transfer function to determine the a priori unknown model reduction weightings. Towards this end let

$$H_o(s) \triangleq G_r(s)K_r(s)\,[I + G_r(s)K_r(s)\,]^{-1}$$

and

$$H_i(s) \triangleq [I + K_r(s)G_r(s)\,]^{-1}\,K_r(s)G_r(s)$$

then for input uncertainty:

$$\begin{aligned} W_o(s) &= [I + K_r(s)G_r(s)\,]^{-1}\,K_r(s) \\ &= H_i(s)\,G_r^{-1}(s) \end{aligned}$$

and for output uncertainty:

$$\begin{aligned} W_i(s) &= K_r(s)\,[I + G_r(s)K_r(s)\,]^{-1} \\ &= G_r^{-1}(s)\,H_o(s) \quad . \end{aligned}$$

Note that $H_i(s)$ and $H_o(s)$ depend only on the loop transfer functions $K_r(s)\,G_r(s)$ and $G_r(s)\,K_r(s)$ respectively, which are known a priori (with advanced loop shaping). Thus either $H_i(s)$ or $H_o(s)$ will also be known a priori. Thus for either the input or output uncertainty representation, the dependence of the weightings on the reduced order compensator has been eliminated. Unfortunately the weightings still depend on the reduced order model which is

not known a priori.

Plant Order Reduction For Control System Design Problem Statement

To simplify the further discussion assume the model reduction uncertainty is represented at the output. The dual results will be summarized later. Then the problem can be stated:

Given: $G(s)$, $H_o(s)$, r

Find: a reduced order model, $G_r(s)$ of $G(s)$

such that $E_\infty = \| [G(s) - G_r(s)] G_r^{-1}(s) H_o(s) \|_\infty < 1$.

Well the model reduction technique of Chapter III addresses problems like this, however, it assumes that the weightings are known. In this case the weighting $G_r^{-1}(s) H_o(s)$ depends on the result of the model reduction.

Parameterization of the Solution

Without loss of generality assume an n^{th} order, output normal minimal realization, $\{F, G, H\}_n$ of the stable portion, $G_s(s)$ of the plant, $G(s)$ is given. That is

$$F + F^T + H^T H = 0$$

where $G_s(s) = H(sI-F)^{-1}G$ and $G(s) = G_s(s) + G_{us}(s)$ ($G_s(s)$ has poles in

the open left half plane and $G_{us}(s)$ has poles in the closed right half plane). Such a realization (or the input normal, dual) can be readily obtained by performing the steps in Table IV.3.

For the sake of further discussion assume the input weighting, $W_i(s)$ which solves the problem is known. Then let U be the weighted controllability grammian for the stable portion of the plant, $G_s(s)$ and the weighting, $W_i(s)$. This grammian, U can be computed as shown in Table III.1 with a Lyapunov equation, however, note that by using Parseval's Theorem, U is also given by

$$U = \frac{1}{2\pi} \int_{-\infty}^{\infty} (j\omega I - F)^{-1} G W_i(j\omega) W_i^H(j\omega) G^T (-j\omega I - F^T)^{-1} \, d\omega \quad .$$

This is introduced only for the sake of a more compact notation than that of Table III.1 and computations are probably easier with the Lyapunov equation of Table III.1.

The next step of the model reduction is to balance the weighted controllability grammian with the identity observability grammian (i.e. F, G, H is an output normal realization). This balancing is accomplished by finding the eigenvalue decomposition of U i.e.

$$U = W \Lambda W^T$$

where $\Lambda = \text{diag}\,\{\lambda_i\}$, $\lambda_1 \geq \lambda_2 \geq \cdots \geq \lambda_n > 0$, $\lambda_i \epsilon \mathbf{R}$ $\forall i$ and $W^T W = I$. Then the transformation to a frequency weighted balanced realization is obtained by letting

Table IV.3 Input and Output Normal Realizations

Assume an arbitrary, minimal, asymptotically stable realization $\{A,B,C\}$ is given.

Input Normal	Output Normal
solve for U from	solve for Y from
$AU + UA^T + BB^T = 0$	$A^TY + YA + C^TC = 0$
perform the eigenvalue decomposition	perform the eigenvalue decomposition
$U = V\Lambda V^T, \quad \Lambda = \text{diag}\{\lambda_i\} \geq 0$	$Y = V\Lambda V^T, \quad \Lambda = \text{diag}\{\lambda_i\} > 0$
$\lambda_i \varepsilon \mathcal{R}\ \forall i$ and $V^TV = I$	$\lambda_i \varepsilon \mathcal{R}\ \forall i$ and $V^TV = I$
let $T = V\Lambda^{1/2}$	let $T = V\Lambda^{-1/2}$
then	then
$F^T + F + GG^T = 0$	$F + F^T + H^TH = 0$

where $F = T^{-1}AT \quad G = T^{-1}B$

$H = CT$

$$T = W\Lambda^{1/4} \quad .$$

Note

$$T^{-1}UT^{-T} = \Lambda^{-1/4}\, W^T W\Lambda W^T W\Lambda^{-1/4} = \Lambda^{1/2}$$
$$T^T IT = \Lambda^{1/4}\, W^T IW\Lambda^{1/4} = \Lambda^{1/2}$$

and thus $\sum = \text{diag}\,\{\lambda_i^{1/2}\}$ is the balanced grammian. The frequency weighted realization $\{A, B, C\}$ of the stable portion $G_s(s)$ of the plant, $G(s)$ is given by

$$A = T^{-1}FT \qquad B = T^{-1}G$$
$$C = HT \quad .$$

Note that this frequency weighted balanced realization is equivalent to that which would have been obtained by applying the alternate algorithm for computing it, given in Table III.1.

Now then assuming the order, r of the reduced order model is given, the reduced order model is obtained by partitioning

$$A = \begin{bmatrix} A_{11} & A_{12} \\ A_{21} & A_{22} \end{bmatrix} \qquad B = \begin{bmatrix} B_1 \\ B_2 \end{bmatrix}$$

$$C = [C_1 \quad C_2] \qquad \text{where } A_{11} \text{ is } r \times r \quad .$$

The realization of the reduced order model, $G_{sr}(s)$ of the stable portion, $G_s(s)$ of the plant, $G(s)$ is given by

$$G_{sr}(s) = C_1(sI - A_{11})^{-1} B_1 \quad .$$

Note that:

$$
\begin{aligned}
G_{sr}(s) &= C_1(sI - A_{11})^{-1} B_1 \\
&= HW_1 \Sigma_1^{1/2} \left\{ sI - \Sigma_1^{-1/2} W_1^T F W_1 \Sigma_1^{1/2} \right\}^{-1} \Sigma_1^{-1/2} W_1^T G \\
&= HW_1(sI - W_1^T F W_1)^{-1} W_1^T G
\end{aligned}
$$

where $W = [W_1 \;\; W_2]$ and $\Sigma = \begin{bmatrix} \Sigma_1 & 0 \\ 0 & \Sigma_2 \end{bmatrix}$ which are both partitioned compatibly with A, B, C (i.e. W_1 has r columns and Σ_1 is $r \times r$). Thus the reduced order model, $G_{sr}(s)$ does not depend explicitly on Σ and hence only the eigenvectors of U corresponding to the r largest eigenvalues of U are necessary to compute the *rth* order reduced order model.

The reduced order model of the plant is given by

$$G_r(s) = G_{sr}(s) + G_{us}(s) \quad .$$

Since the input weighting from the beginning of this discussion was assumed to be the correct weighting it must also be given by

$$W_i(s) = G_r^{-1}(s) H_o(s) \quad .$$

The previous, hypothetical, discussion is summarized schematically in Fig. IV.4. Note that if either U, W, W_1, $G_{sr}(s)$, $G_r(s)$ or $W_i(s)$ were known the problem would be solved. Note also that the diagram also represents functions of these quantities onto themselves. For example, take any positive definite, $n \times n$ matrix U_{in} as an input to the upper left hand block in Fig. IV.4 and regard the output of the lower left hand block, U_{out} in Fig. IV.4 as the output of the function, $f(U)$ i.e.

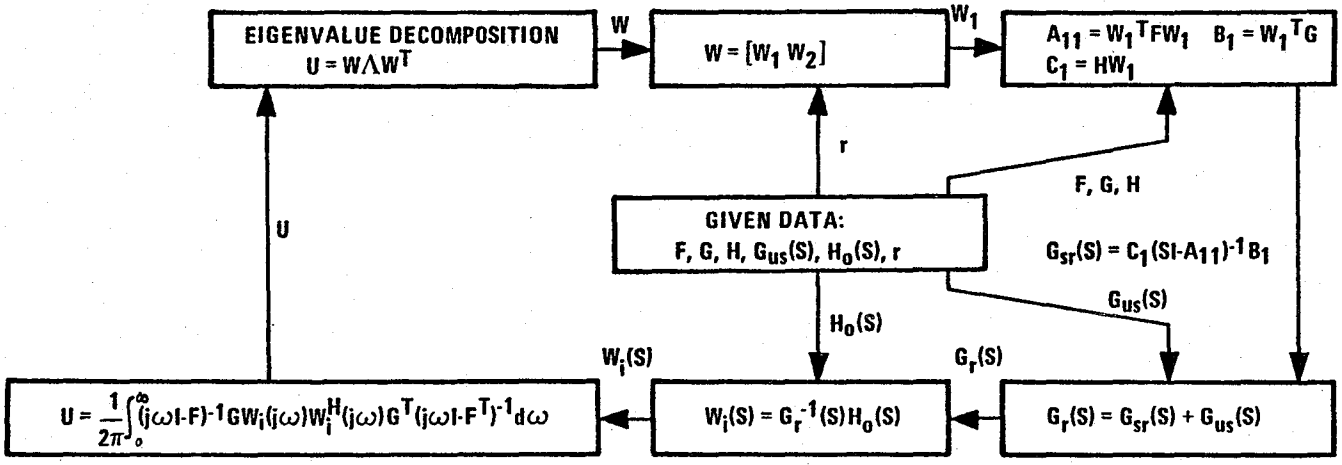

Figure IV.4 Schematic of the Inter-relationships for Plant Order Reduction Solution

That is $f(U)$ is defined algorithmically as (assuming F, G, H, $G_{us}(s)$, $H_o(s)$ and r are given):

$$U = W\Lambda W^T \qquad W = [W_1\ W_2]$$

where W_1 has r columns

$$\begin{aligned} A_{11} &= W_1^T F W_1 \quad B_1 = W_1^T G \quad C_1 = HW_1 \\ G_r(s) &= C_1(sI - A_{11})^{-1} B_1 + G_{us}(s) \\ W_i(s) &= G_r^{-1}(s) H_o(s) \\ f(U) &= \frac{1}{2\pi} \int_{-\infty}^{\infty} (j\omega I - F)^{-1} G W_i(j\omega) W_i^H(j\omega)\ G^T(-j\omega I - F^T)^{-1}\, d\omega \quad . \end{aligned}$$

This series of steps is rather involved but nevertheless does define the function, $f(U)$.

Statement of the Plant Order Reduction Problem as a Fixed Point Problem

The plant order reduction problem can now be stated:

Given: F, G, H, $G_{us}(s)$, $H_o(s)$, r

Find: U such that $U = f(U)$.

Thus the solution to the plant order reduction problem is equivalent to finding the stationary or fixed point of the function $f(U)$ which maps $n \times n$ positive definite matrices onto $n \times n$ positive definite matrices.

Similar functions can be obtained for W, W_1, $G_{sr}(s)$, $G_r(s)$ or $W_i(s)$ as well. The functions involving the transfer functions: $G_{sr}(s)$, $G_r(s)$ or $W_i(s)$ are not of interest, since specifying a transfer function typically involves specifying realizations which are not unique. The function involving W_1 is of interest, since it involves the fewest parameters as unknowns.

The existence and uniqueness of stationary points for these functions is an open question. These issues were deemed to be beyond the scope of this thesis and the following solution technique was used successfully.

Successive Approximation Solution

The successive approximation method to obtain the solution of the equation $x = f(x)$ is to guess an initial x say, x_1 and let

$$x_{i+1} = f(x_i) \qquad i = 1, 2, \cdots$$

then under appropriate conditions

$$x = \lim_{i \to \infty} x_i \quad .$$

The appropriate conditions [Ref. 43] are that the solution exists and that the function, $f(x)$ is a contraction i.e. the first derivative of the function as a matrix should have eigenvalues with magnitudes strictly less than unity in a neighborhood of the solution.

This technique resulted in satisfactory solutions for all the examples tested

for this thesis (see Chapter V). However, the procedure did not always converge to a unique point. In several examples the procedure converged to a limiting set rather than a limiting point. That is a limit cycle was reached:

$$f(x_{i+k}) \cong f(x_i) \qquad i \gg 1$$

where k was the number of elements in the limiting set. In these cases, the value of E_∞ was compared for the k elements of the limiting set and the one corresponding to the smallest E_∞ was taken as an acceptable solution.

Other Solution Techniques

The problem of solving $x = f(x)$ is also theoretically amenable to more advanced iterative solution procedures involving derivative(s) of $f(x)$. These techniques were not used, however, since the computation of the gradient of this function was deemed to be beyond the scope of this thesis.

Obtaining a Realization of $G^{-1}(s)H(s)$

In order to carry out the successive approximation solution procedure, it is necessary to obtain a realization of $G^{-1}(s)H(s)$ where realizations of the square $m \times m$ transfer functions, $G(s)$ and $H(s)$ are given. Although a realization for $G^{-1}(s)$ does not exist in general a realization for $G^{-1}(s)H(s)$ often does exist. The existence depends on the pole-zero excess of both $G(s)$ and $H(s)$. Two special cases were used in this thesis and they will now be discussed.

$G(s)$ With First Order Rolloff

Assume $\{A, B, C\}$ is a state space realization of $G(s)$, i.e. $G(s) = C(sI-A)^{-1}B$. Then first order rolloff is defined to mean that CB has full rank. The connection between this and a rolloff slope of negative one is obtained from the high frequency expansion of $G(s)$:

$$\begin{aligned} G(s) &= C(sI-A)^{-1}B \\ &= C[s(I - \frac{1}{s} A)]^{-1} B \\ &= C\frac{1}{s}(I + \frac{1}{s}A + \frac{1}{s^2} A^2 + ...) B \\ &= \frac{1}{s} CB + \frac{1}{s^2} CAB + \frac{1}{s^3} CA^2B + \cdots \end{aligned}$$

Thus if CB has full rank then all the singular values of $G(j\omega)$ will have a slope of negative one for large ω when plotted on a log-log scale versus ω.

For a realization of $G^{-1}(s)H(s)$ to exist in the full rank CB case, it is necessary that $H(s)$ have a rolloff slope of negative one or less. This will always be true if $H(s)$ has a state space triple (as opposed to quadruple) realization, say, $\{F, G, H\}$ (i.e. zero feed thru or D term).

It can be verified by direct computation that for any $\alpha \epsilon \mathbf{R}$:

$$W(s) = G^{-1}(s)H(s) = C_w(sI-A_w)^{-1} B_w + D_w$$

where $G(s) = C(sI-A)^{-1}B$, CB full rank

$H(s) = H(sI-F)^{-1}G$

$$A_w \triangleq \begin{bmatrix} A + B(CB)^{-1}C(\alpha I - A) & -B(CB)^{-1}H(\alpha I - F) \\ 0 & F \end{bmatrix} \quad B_w \triangleq \begin{bmatrix} B(CB)^{-1}HG \\ G \end{bmatrix}$$

$$C_w \triangleq \begin{bmatrix} (CB)^{-1}C(\alpha I - A) & -(CB)^{-1}H(\alpha I - F) \end{bmatrix} \qquad D_w \triangleq \begin{bmatrix} (CB)^{-1}HG \end{bmatrix} .$$

Thus $\{A_w, B_w, C_w, D_w\}$ is a realization of $W(s) = G^{-1}(s)H(s)$. However, this realization of $W(s)$ is not minimal, in fact, it has m uncontrollable poles at $s = \alpha$ (these poles had to be introduced artificially to produce the realization for $W(s)$). The fact that these poles are uncontrollable can be verified by showing that the left eigenvectors of A_w corresponding to the eigenvalues of A_w at $s = \alpha$ are orthogonal to B_w [Ref. 34]. These eigenvectors are given by

$$V^T = \begin{bmatrix} C & -H \end{bmatrix}$$

and it can be verified that $V^T A_w = \alpha V^T$ and $V^T B_w = 0$.

Thus a non-minimal realization of $W(s)$ has been obtained. There are several ways of eliminating these m uncontrollable poles at $s = \alpha$. In fact, a method using internally balanced realizations for obtaining a minimal realization was discussed in Chapter II.

The realization of the dual, $W(s) = H(s)G^{-1}(s)$ and the realization of $W(s) = G^{-1}(s)H(s)$ are summarized in Table IV.4.

$G(s)$ With Second Order Rolloff

Assume $\{A, B, C\}$ is a state space realization of $G(s)$, i.e.

Table IV.4 Realizations of $G^{-1}(s)H(s)$ and $H(s)G^{-1}(s)$ For G(s) With First Order Rolloff

$G(s) = C(sI-A)^{-1}B$ with CB full rank, $H(s) = H(sI-F)^{-1}G$, $\alpha \varepsilon \mathcal{R}$

$W(s) = G^{-1}(s)H(s)$

$= C_w(sI-A_w)^{-1}B_w+D_w$

Note:

$V^TA_w = \alpha V^T$

$V^TB_w = 0$

$$A_w \triangleq \begin{bmatrix} A + B(CB)^{-1}C(\alpha I-A) & -B(CB)^{-1}H(\alpha I-F) \\ 0 & F \end{bmatrix} \quad B_w \triangleq \begin{bmatrix} B(CB)^{-1}HG \\ G \end{bmatrix}$$

$$C_w \triangleq \begin{bmatrix} (CB)^{-1}C(\alpha I-A) & -(CB)^{-1}H(\alpha I-F) \end{bmatrix} \quad D_w \triangleq \begin{bmatrix} (CB)^{-1}HG \end{bmatrix}$$

$$V^T \triangleq \begin{bmatrix} C & -H \end{bmatrix}$$

$W(s) = H(s)G^{-1}(s)$

$= C_w(sI-A_w)^{-1}B_w+D_w$

Note:

$A_wV = \alpha V$

$C_wV = 0$

$$A_w \triangleq \begin{bmatrix} A + (\alpha I-A)B(CB)^{-1}C & 0 \\ -(\alpha I-F)G(CB)^{-1}C & F \end{bmatrix} \quad B_w = \begin{bmatrix} (\alpha I-A)B(CB)^{-1} \\ -(\alpha I-F)G(CB)^{-1} \end{bmatrix} \quad V \triangleq \begin{bmatrix} B \\ -G \end{bmatrix}$$

$$C_w = \begin{bmatrix} HG(CB)^{-1}C & H \end{bmatrix} \quad D_w = \begin{bmatrix} HG(CB)^{-1} \end{bmatrix}$$

$G(s) = C(sI-A)^{-1}B$. Then second order rolloff is defined to mean that $CB = 0$ but CAB has full rank. Again the connection between this and a rolloff slope of negative two is obtained from the high frequency expansion of $G(s)$:

$$G(s) = \frac{1}{s} CB + \frac{1}{s^2} CAB + \frac{1}{s^3} CA^2B + \cdots \quad .$$

Thus if $CB = 0$ and CAB has full rank then all the singular values of $G(j\omega)$ will have a slope of negative two for large ω when plotted on a log-log scale versus ω.

For a realization of $G^{-1}(s)H(s)$ to exist in the $CB = 0$ and full rank CAB case it is necessary that $H(s)$ have a rolloff slope of negative two or less. Thus if $\{F, G, H\}$ is a realization of $H(s)$, i.e. $H(s) = H(sI-F)^{-1}G$, it is necessary that $HG = 0$.

It can be verified by direct computation that for any $\alpha \neq \beta$ and $\alpha, \beta \epsilon \mathbf{R}$:

$$W(s) = G^{-1}(s)H(s) = C_w(sI-A_w)^{-1} B_w + D_w$$

where $G(s) = C(sI-A)^{-1}B$, $CB = 0$, CAB full rank
$H(s) = H(sI-F)^{-1}G$, $HG = 0$

$$C_g \triangleq C(\alpha I-A)(\beta I-A) \qquad D_g \triangleq CAB$$
$$H_h \triangleq H(\alpha I-F)(\beta I-F) \qquad D_h \triangleq HFG$$

$$A_w \triangleq \begin{bmatrix} A-BD_g^{-1}C_g & BD_g^{-1}H_h \\ 0 & F \end{bmatrix} \qquad B_w \triangleq \begin{bmatrix} BD_g^{-1}D_h \\ G \end{bmatrix}$$
$$C_w \triangleq \begin{bmatrix} -D_g^{-1}C_g & D_g^{-1}H_h \end{bmatrix} \quad D_w \triangleq \begin{bmatrix} D_g^{-1}D_h \end{bmatrix} \quad .$$

Thus $\{A_w, B_w, C_w, D_w\}$ is a realization of $W(s) = G^{-1}(s)H(s)$. However, this realization of $W(s)$ is also not minimal, in fact, it has $2m$ uncontrollable poles: m at $s = \alpha$ and m at $s = \beta$ (these poles had to be introduced artificially to produce the realization for $W(s)$). The fact that these poles are uncontrollable can be verified by showing that the left eigenvectors of A_w corresponding to the eigenvalues of A_w at $s = \alpha$ and $s = \beta$ are orthogonal to B_w [Ref. 34]. These eigenvectors are given by

$$V^T = \begin{bmatrix} C(\beta I - A) & -H(\beta I - F) \\ C(\alpha I - A) & -H(\alpha I - F) \end{bmatrix}$$

and it can be verified that

$$V^T A_w = \begin{bmatrix} \alpha I & 0 \\ 0 & \beta I \end{bmatrix} V^T$$

and

$$V^T B_w = 0 \quad .$$

The realization of the dual, $W(s) = H(s)G^{-1}(s)$ and the realization of $W(s) = G^{-1}(s)H(s)$ are summarized in Table IV.5.

Realizations of $W(s) = G^{-1}(s)H(s)$ and $W(s) = H(s)G^{-1}(s)$ have been given for two special cases which include a large class of transfer functions, $G(s)$. In those cases not included it is still possible to obtain a realization of $W(s)$ by modifying the procedure used to obtain the results in Tables IV.4 and 5.

Table IV.5 Realizations of $G^{-1}(s)H(s)$ and $H(s)G^{-1}(s)$ For G(s) With Second Order Rolloff

$G(s) = C(sI-A)^{-1}B$ with $CB=0$, CAB full rank, $H(s) = H(sI-F)^{-1}G$ with $HG = 0$, $\alpha \neq \beta \in \mathbb{R}$

$W(s) = G^{-1}(s)H(s)$

$= C_w(sI-A_w)^{-1}B_w+D_w$

Note:

$$V^T A_w = \begin{bmatrix} \alpha I & 0 \\ 0 & \beta I \end{bmatrix} V^T$$

$$V^T B_w = 0$$

$C_g \triangleq C(\alpha I-A)(\beta I-A)$, $D_g \triangleq CAB$, $H_h \triangleq H(\alpha I-F)(\beta I-F)$, $D_h \triangleq HFG$

$$A_w \triangleq \begin{bmatrix} A-BD_g^{-1}C_g & BD_g^{-1}H_h \\ 0 & F \end{bmatrix} \quad B_w = \begin{bmatrix} BD_g^{-1}D_h \\ G \end{bmatrix}$$

$$C_w \triangleq \begin{bmatrix} -D_g^{-1}C_g & D_g^{-1}H_h \end{bmatrix} \quad D_w = \begin{bmatrix} D_g^{-1}D_h \end{bmatrix}$$

$$V^T \triangleq \begin{bmatrix} C(\beta I-A) & -H(\beta I-F) \\ C(\alpha I-A) & -H(\alpha I-F) \end{bmatrix}$$

$W(s) = H(s)G^{-1}(s)$

$= C_w(sI-A_w)^{-1}B_w+D_w$

Note:

$$A_w V = V \begin{bmatrix} \alpha I & 0 \\ 0 & \beta I \end{bmatrix}$$

$$C_w V = 0$$

$B_g \triangleq (\alpha I-A)(\beta I-A)B$, $D_g = CAB$, $G_h \triangleq (\alpha I-F)(\beta I-F)G$, $D_h = HFG$

$$A_w \triangleq \begin{bmatrix} A-B_gD_g^{-1}C & 0 \\ G_hD_g^{-1}C & F \end{bmatrix} \quad B_w \triangleq \begin{bmatrix} -B_gD_g^{-1} \\ G_hD_g^{-1} \end{bmatrix} \quad V \triangleq \begin{bmatrix} (\beta I-A)B & (\alpha I-A)B \\ -(\beta I-F)G & -(\beta I-F)G \end{bmatrix}$$

$$C_w \triangleq \begin{bmatrix} D_hD_g^{-1}C & H \end{bmatrix} \quad D_w = \begin{bmatrix} D_hD_g^{-1} \end{bmatrix}$$

Obtaining a Stable Weighting When $G(s)$ is Non-minimum Phase

Often the reduced order model, $G_r(s)$ resulting from a balanced realization will be non-minimum phase (typically at high frequency) and in these cases the weighting, $W(s) = G_r^{-1}(s)H(s)$ or $W(s) = H(s)G_r^{-1}(s)$ will have unstable poles. This is because the transmission zeros of $G_r(s)$ will become poles of $W(s)$. In this case it will be necessary to modify the transfer function of the weighting to make it stable.

Consider the definition of the model reduction error criterion, E_∞

$$E_\infty \triangleq \| W_o(s) \left[G(s) - G_r(s) \right] W_i(s) \|_\infty$$

then by definition of the H_∞ norm

$$E_\infty = \sup_\omega \bar{\sigma} \left[W_o(j\omega) \left[G(j\omega) - G_r(j\omega) \right] W_i(j\omega) \right]$$

then by definition of the maximum singular value

$$E_\infty = \sup_\omega \lambda_{\max}^{1/2} \left[W_o(j\omega) \left[G(j\omega) - G_r(j\omega) \right] W_i(j\omega) W_i^H(j\omega) \right.$$

$$\left. \left[G^H(j\omega) - G_r^H(j\omega) \right] W_o^H(j\omega) \right]$$

then since $\lambda_{\max}[AB] = \lambda_{\max}[BA] \qquad \forall A, B$,

$$E_\infty = \sup_\omega \lambda_{\max}^{1/2} \left[\left[G(j\omega)-G_r(j\omega)\right] W_i(j\omega) W_i^H(j\omega)\right.$$

$$\left.\left[G^H(j\omega)-G_r^H(j\omega)\right] W_o^H(j\omega) W_o(j\omega)\right] \quad .$$

Thus E_∞ depends only on the products $W_i(j\omega)W_i^H(j\omega)$ and $W_o^H(j\omega)\ W_o(j\omega)$ and not on the weightings by themselves.

Spectral Factorization

Consider the product $W(j\omega)W^H(j\omega) = W(s)W^T(-s)\,|_{s=j\omega}$ when $W(s)$ has some poles in the open right half plane. To facilitate the following disscussion let $W_+(s) \triangleq W(s)$ to denote the fact that $W_+(s)$ has poles with positive real parts. It is well known [Ref. 44] that a transfer function $W_-(s)$ always exists with poles in the open left half plane such that

$$W_-(s)W_-^T(-s) = W_+(s)W_+^T(-s) \quad .$$

This is called spectral factorization in the literature. Since E_∞ depends only on products like above, the stable spectral factor can always be used in place of the unstable factor without changing E_∞.

Computation of the Stable Spectral Factor

It is well known [Refs. 1-4] that the minimum input (i.e. minimum of $J = \int_o^\infty u^T(t)u(t)dt$) control (i.e. $u = -K_c x$) required to stabilize the unstable,

controllable system $\dot{x} = Ax + Bu$ just reflects the unstable poles of the system across the imaginary axis. That is the eigenvalues of $A - BK_c$ are the stable eigenvalues of A plus the stable reflections of the unstable eigenvalues of A. The gain K_c is computed by solving for $P \geq 0$ such that

$$A^T P + PA - PBB^T P = 0$$

and then $K_c = B^T P$.

It is not so well known that these facts can be used to solve the spectral factorization problem in the multivariable case (it's trivial in the SISO case). It has been shown in Reference 5 and it can be verified by direct computation that the given transfer function $W_+(s) \triangleq C(sI-A)^{-1}B$ can be factored

$$W_+(s) = W_-(s)A(s)$$

where

$$W_-(s) \triangleq C(sI-A+BK_c)^{-1}B$$
$$A(s) \triangleq I + K_c(sI-A)^{-1}B$$

and where

$$A^T P + PA - PBB^T P = 0 , \qquad P \geq 0$$

and

$$K_c = B^T P \quad .$$

It can also be verified that $A(s)$ is a multivariable all pass, i.e.

$$A^T(-s)A(s) = A(s)A^T(-s) = I \quad .$$

Thus we have

$$\begin{aligned} W_+(s)W_+^T(-s) &= W_-(s)A(s)A^T(-s)W_-^T(-s) \\ &= W_-(s)W_-^T(-s) \end{aligned}$$

which accomplishes the objective.

These results have a dual for the other spectral factorization problem $W_+^T(-s)W_+(s) = W_-^T(-s)W_-(s)$ and both cases are summarized in Table IV.6.

The results for plant order reduction are summarized in Table IV.7 for both representations of the model reduction uncertainty.

Advantages and Disadvantages of the Two Approaches (Compensator vs. Plant Order Reduction)

Compensator order reduction requires that the high order compensator be designed for the high order plant. This is clearly undesirable and is in fact the motivation for searching for reduced order models. The advantage of this method is that implementing the algorithm for compensator order reduction is straightforward (i.e. the model reduction weightings are known a priori). Often a low order approximation to a given compensator is desired and thus this attractive, formal method for obtaining the approximation is a very useful result of this thesis.

Table IV.6 Spectral Factorization

$$W_+(s) = C(sI-A)^{-1}B$$

$W_+(s)W_+^T(-s) = W_-(s)W_-^T(-s)$	$W_+^T(-s)W_+(s) = W_-^T(-s)W_-(s)$
Solve for $P \geq 0$ from	Solve for $P \geq 0$ from
$A^TP + PA - PBB^TP = 0$	$AP + PA^T - PC^TCP = 0$
let $K_c = B^TP$	let $K_f = PC^T$
then $W_+(s) = W_-(s)A(s)$	$W_+(s) = A(s)W_-(s)$
where	where
$W_-(s) = C(sI-A+BK_c)^{-1}B$	$W_-(s) = C(sI-A+K_fC)^{-1}B$
$A(s) = I + K_c(sI-A)^{-1}B$	$A(s) = I + C(sI-A)^{-1}K_f$

and in either case: $A^T(-s)A(s) = A(s)A^T(-s) = I$

Table IV.7 Summary of Plant Order Reduction Results

Preliminary Assumptions	$G(s)=H(sI-F)^{-1}G + G_{us}(s)$ where $Re[\lambda[F]]<0$ and $G_{us}(s)$ has unstable poles	
Use first steps of advanced loop shaping to obtain (Table II.5)	Regulator Loop Transfer Function $= L_i(s)$	Filter Loop Transfer Function $= L_o(s)$
Then the indicated closed loop transfer function is known	$H_i(s) = [I + L_i(s)]^{-1} L_i(s)$	$H_o(s) = L_o(s)[I + L_o(s)]^{-1}$
Assume realization {F,G,H} is (Table IV.3)	input normal: $F+F^T+GG^T = 0$	output normal: $F+F^T+H^TH = 0$
Eigenvalue decomposition of the positive definite input to $f(\cdot)$(to be defined)	$Y = W\Lambda W^T$	$U = W\Lambda W^T$
Select r columns of W corresponding to the largest eigenvalues	$\Lambda = \text{diag}\{\lambda_i\}$ where $\lambda_1 \geq \lambda_2 \geq \ldots \geq \lambda_n$ $W = [W_1 \quad W_2]$	
Compute the reduced order model	$G_r(s) = HW_1(sI-W_1^TFW_1)^{-1}W_1^TG + G_{us}(s)$	
Compute the weightings (Tables IV.4,5)	$W_o(s) = H_i(s)G_r^{-1}(s)$	$W_i(s) = G_r^{-1}(s)H_o(s)$
Spectral Factorization (Table IV.6)	$W_o(s) = A(s)W_{o-}(s)$	$W_i(s) = W_{i-}(s)A(s)$
Solve for grammian (Table III.1)	$f(Y) = \frac{1}{2\pi}\int_{-\infty}^{\infty}(-j\omega I-F^T)^{-1}H^TW_{o-}^H(j\omega)W_{o-}(j\omega)H(j\omega I-F)^{-1}d\omega$	$f(U) = \frac{1}{2\pi}\int_{-\infty}^{\infty}(j\omega I-F)^{-1}GW_{i-}(j\omega)W_{i-}^H(j\omega)G^T(-j\omega I-F^T)^{-1}d\omega$
Solve for stationary point of $f(\cdot)$	$Y = f(Y)$	$U = f(U)$
Use final steps of advanced loop shaping to obtain (Table II.5)	$K_r(s)$ such that $K_r(s)G_r(s) = L_i(s)$	$K_r(s)$ such that $G_r(s)K_r(s) = L_o(s)$

Plant order reduction on the other hand permits the compensator to be designed for the reduced order plant. This is clearly an advantage and satisfies the intentions of model reduction for control design. The disadvantage of this method is that the algorithm for implementing plant order reduction is not closed form (i.e. the model reduction weightings are not known a priori). In some cases it is not possible and in many cases it is not desirable to design a compensator for the high order plant and a reduced order model is required. This attractive, formal approach for obtaining this reduced order model is a very useful result of this thesis.

The examples of the next chapter serve to illustrate the effectiveness of both of these methods.

V. EXAMPLES

The purpose of this chapter is to illustrate by example both the model reduction and control design techniques discussed in the previous chapters. The intent is to use the examples to make specific points. Thus, typically only segments of the model reduction for control system design theory will appear in a given example.

The chapter will illustrate three topics: model reduction, compensator order reduction and plant order reduction. The order of the full order model will vary from 2nd to 168th order.

Model Reduction Examples

The purpose of this section is to: verify some statements made in the section,"On the Question of Optimality" of Chapter III, illustrate graphically the effect of the weighting on the model reduction and to compare results for the balancing model reduction approach to a more classical model reduction approach.

"Simple" H_∞ Example

The SISO second order transfer function for this example is given by

$$G(s) = \frac{2(s+2)}{(s+1)(s+3)} \quad .$$

It can be verified that the first order reduced order model of $G(s)$ obtained with the internally balanced realization technique is given by

$$G_{r,ib}(s) = \frac{1.8320}{s + 1.4453}$$

and the smallest singular value of the balanced grammian, σ_2 is given by $\sigma_2 = 0.032871$. It can also be verified that the error magnitude, $|G(j\omega) - G_{r,ib}(j\omega)|$ is bounded

$$|G(j\omega) - G_{r,ib}(j\omega)| \leq |G(0) - G_{r,ib}(0)| = 2(0.032871) \qquad \forall\omega \quad .$$

It can also be verified that the first order reduced order model of $G(s)$ obtained with the Hankel norm technique is given by

$$G_{r,H}(s) = \frac{1.6514}{s + 1.3028} + 0.032871 \quad .$$

It is of interest to compute the error for the Hankel technique. It can be verified that the error is given by

$$G(j\omega) - G_{r,H}(j\omega) = -0.032871 \frac{(j\omega-1)(j\omega-3)(j\omega-1.3028)}{(j\omega+1)(j\omega+3)(j\omega+1.3028)} \quad .$$

Note that the error magnitude is independent of frequency! That is

$$|G(j\omega) - G_{r,H}(j\omega)| = 0.032871 \qquad \forall\omega \quad !$$

This is the smallest possible error as measured with the H_∞ norm of $G(s) - G_r(s)$ when a D term is allowed [Ref. 14].

Thus this example is consistent with the comments made in the section:

"On the Question of Optimality" of Chapter III. That is the reduced order model obtained with the Hankel technique (where D terms are required) has one half the error magnitude of the reduced order model obtained with the internally balanced realization technique (where D terms are not used). The error bound $\|G(s) - G_r(s)\|_\infty \leq 2tr[\sum_2]$ is also verified for this example.

An Example to Illustrate the Effect of the Weightings

A 46th order, 3 input and 3 output model representing a large space structure with many resonances was reduced to 28th order using both the internally balancing and frequency weighted balancing techniques. The transfer function for this example was of the form

$$G(s) = \sum_{i=1}^{23} \frac{c_i b_i^T}{s^2 + 2\zeta_i \omega_i s + \omega_i^2}$$

where $\omega_1 = \omega_2 = 0$ (rigid body poles), six modes had damping ratios of $\zeta = 0.7$ and the rest had damping ratios of $\zeta = 0.005$. A Bode plot for $G(s)$ (i.e. log $\sigma_i[G(j\omega)]$ vs. ω, $i = 1, 2, 3$) is shown in Fig. V.1.

For the purposes of illustration the model reduction weightings for the frequency weighted balancing case were arbitrarily chosen to be given by

$$W_i(s) = W_o(s) = W(s) = \frac{s}{(s+2)^2} I_3$$

and a Bode plot of $W(s)$ is shown in Fig. V.2.

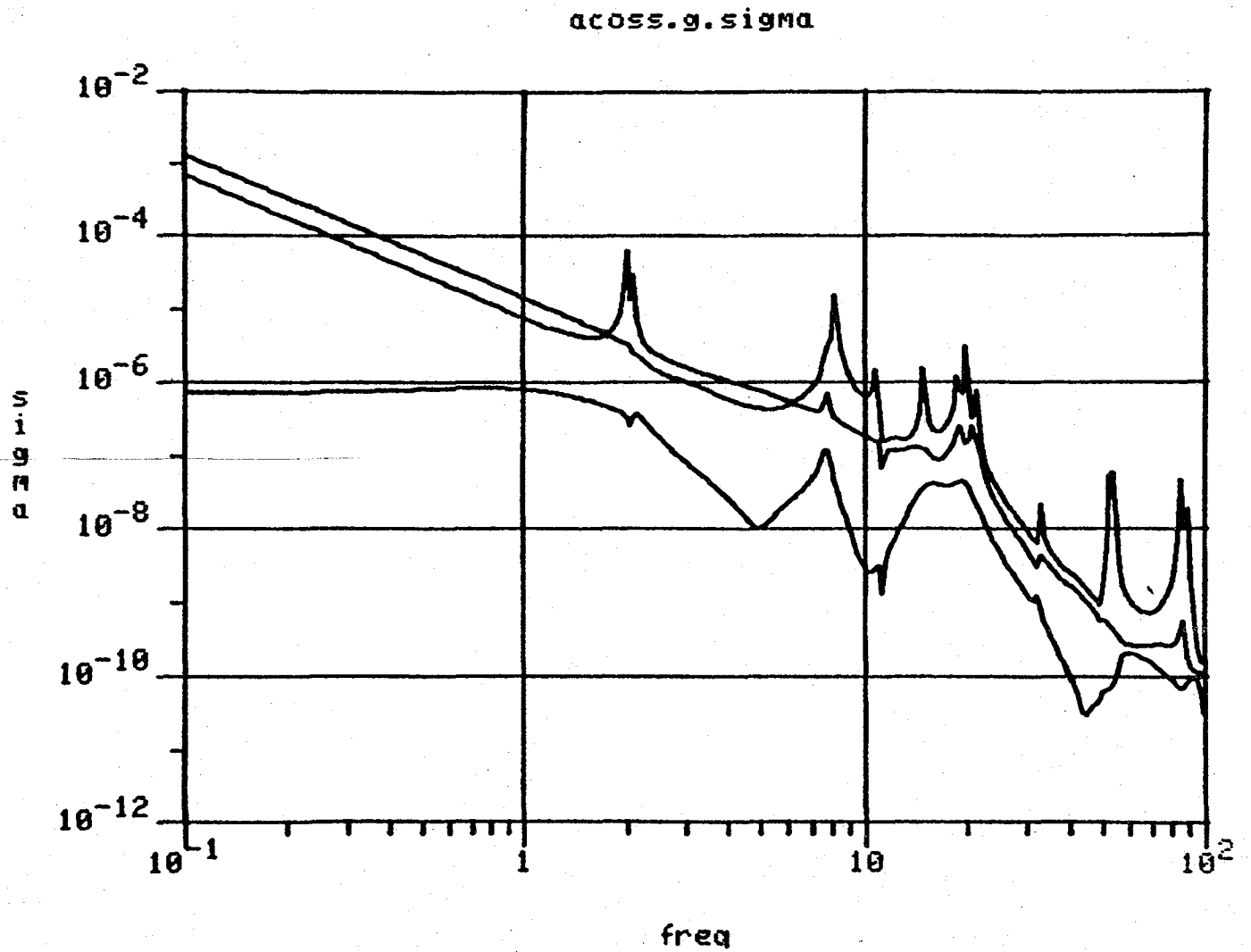

Figure V.1 Flexible Structure Full Order Model

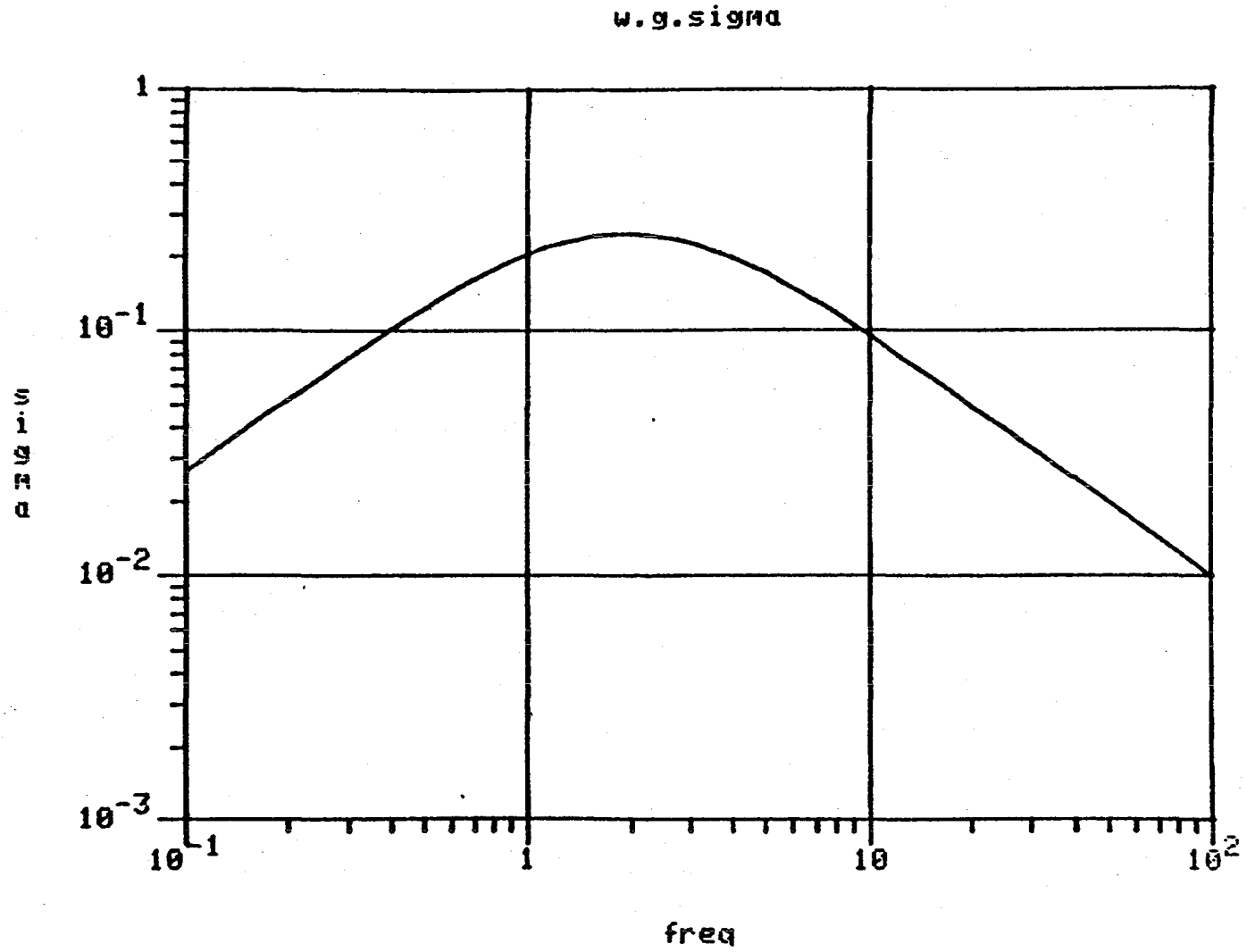

Figure V.2 Flexible Structure Model Reduction Weighting

Bode plots for a 28th order reduced order model, $G_r(s)$ using either balancing technique (weighted or unweighted) look very similar to that for $G(s)$ and thus are not shown. The only noticeable difference is that the peaks in the $G(s)$ plot beyond $\omega = 30$ do not appear in the plots for $G_r(s)$.

Noticeable differences are however apparent in the Bode plots of the error $G(s) - G_r(s)$. These plots are shown in Figs. V.3, 4 for the $G_r(s)$ obtained from the internally balanced realization and the $G_r(s)$ obtained from the frequency weighted balanced realization respectively. Notice that the singular values of the error are relatively flat for the unweighted reduced order model but that they are not flat for the weighted reduced order model. In fact, the singular values of the error are smaller near the peak of the weighting as expected. Note also, that this smaller error is obtained at the expense of larger error at higher frequencies where there is less weighting.

The example clearly shows the effect of the weighting on the model reduction. The example also illustrates the effectiveness of the frequency weighted balanced realization model reduction algorithm in tailoring the error with respect to frequency.

Comparison of Balancing to Classical Model Reduction

To facilitate the comparison of model reduction via balancing to more classical model reduction, an example was chosen for which a classical reduced order model is readily obtained. The example is a 7th order model of a spinning,

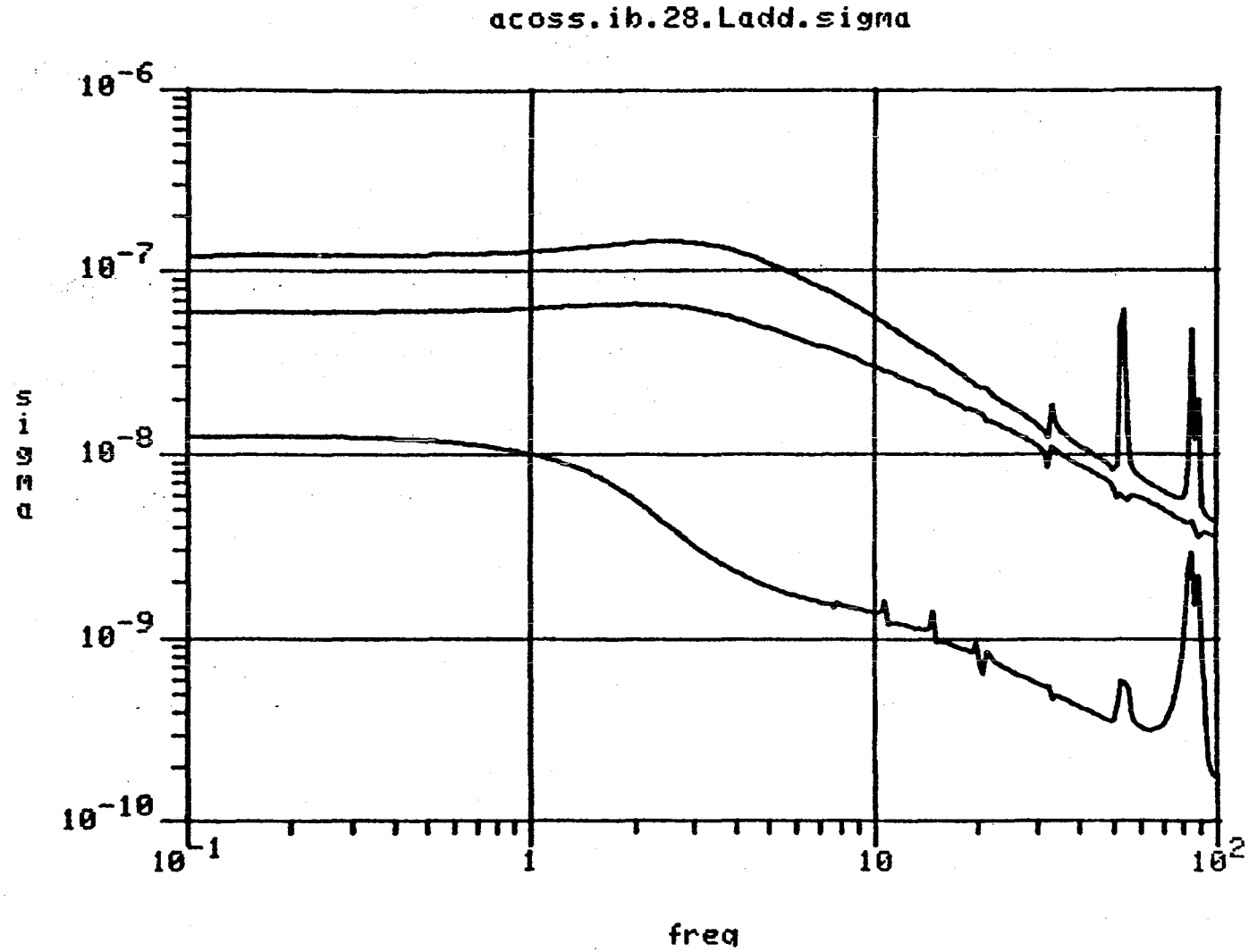

Figure V.3 Flexible Structure Error For Internally Balancing Technique

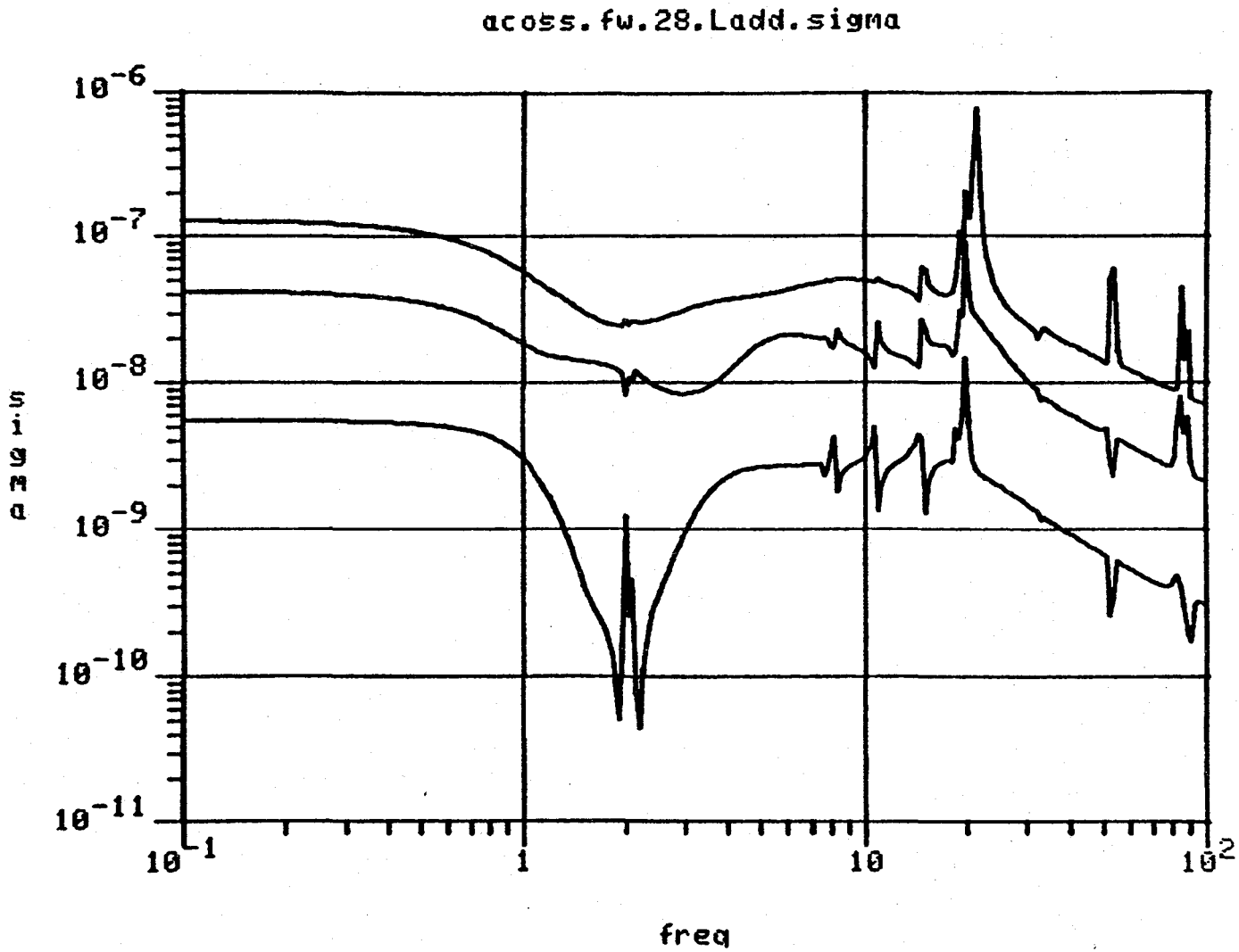

Figure V.4 Flexible Structure Error For Frequency Weighted Balancing Technique

symmetric projectile. The 7 states are: 3 components of velocity, u, v, w, 3 components of angular velocity, p, q, r and pitch angle, θ. The inputs are 2 thrusters perpendicular to the axis of symmetry and the outputs are pitch rate, q and yaw rate, r. The coupling of the 3 states: forward velocity, u, roll rate, p and pitch angle, θ with the other 4 states is typically very small for such a projectile and almost always ignored. This leaves a 4th order model. This 4th order model will be called the classically obtained reduced order model of the 7th order model.

It is of interest to compare this reduced order model to that obtained by internally balancing. The 7th order model was balanced and the 4th order reduced order model was extracted. This reduced order model was for all practical intents and purposes identical to that obtained classically. Detailed data to substantiate this claim are given in Appendix E.

The point here is that balancing is consistent with more classical model reduction when the model reduction is trivial.

Compensator Order Reduction Examples

The purpose of this section is to present some examples of compensator order reduction. Three relatively low order SISO compensators (less than 10th order) were designed and then reduced with the weighting technique discussed in Chapter IV. This technique proved to be effective in obtaining satisfactory (i.e. maintain closed loop stability) reduced order models of these compensators when

other techniques failed, such as: internally balancing (i.e. unity weightings), mode truncation and elimination of modes with small residues. The fact that the integral squared impulse response error criterion is not a good discriminator for model reduction for control design is also demonstrated. The compensator order reduction algorithm is not limited to LQG designs and was used successfully on a non-LQG design.

Four Disk Example

The system to be controlled is the subject of an experimental research project at Stanford [Ref. 45]. The system, indicated in Fig. V.5 consists of

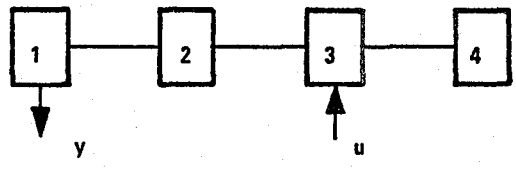

Fig. V.5 Four Disk System

four disks (unity inertia) connected by a flexible wire (unity spring constant) with a motor for applying torques to the third disk and a sensor for measuring angular displacement of the first disk.

The transfer function for this system with non-collocated actuators and

sensors is given by

$$G(s) = \frac{1}{4s^2} \frac{\left(\frac{s^2+2\zeta z s+z^2}{z^2}\right)\left(\frac{s+a}{a}\right)}{\left(\frac{s^2+2\zeta\omega_1 s+\omega_1^2}{\omega_1^2}\right)\left(\frac{s^2+2\zeta\omega_2 s+\omega_2^2}{\omega_2^2}\right)} \times \frac{\left(\frac{s^2-0.8bs+b^2}{b^2}\right)}{\left(\frac{s^2+2\zeta\omega_3 s+\omega_3^2}{\omega_3^2}\right)}$$

where the pole and zero data is given in Table V.1.

Table V.1 Four Disk System Pole and Zero Data

$\omega_1 = 0.765$	$z = 1$
$\omega_2 = 1.41$	$a = 4.84$
$\omega_3 = 1.85$	$b = 5.65$
$\zeta = 0.02$	

Note that the vibratory modes are assumed to have 2% damping and that the system is non-minimum phase.

Note that the vibratory modes are assumed to have 2% damping and that the system is non-minimum phase.

The performance and stability robustness requirements chosen for this example resulted in the constraints for the loop shape shown in Fig. V.6. The

relationship between these requirements and Fig. V.6 was discussed in

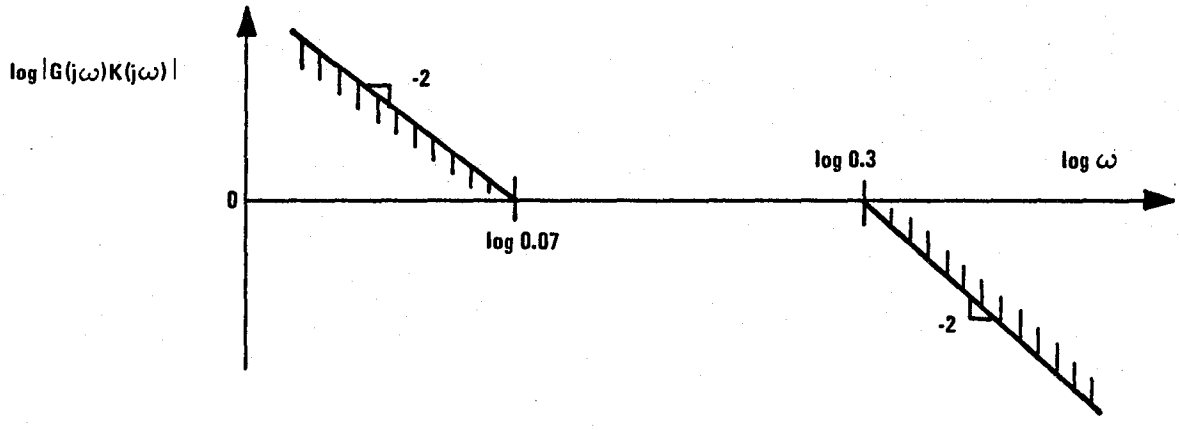

Fig. V.6 Loop Shape Constraints For Four Disk System

Chapter II and Fig. V.6 is just Fig. II.13 for this example. Note, that the frequencies for which high gain is required are significantly less than the magnitude of the non-minimum phase zeros of $G(s)$ (i.e. $0.07 \ll b$) and thus the non-minimum phase zeros will have little impact on the design.

A compensator was designed using the standard LQG loop shaping procedure of Chapter II (see Table II.4). This compensator satisfied the low frequency constraint of Fig. V.6. However, because LQ loop transfer functions rolloff with a slope of negative one it could not satisfy the high frequency constraint. Hence, the compensator was modified by introducing an additional

lag to satisfy this constraint as well. Note that this additional lag does degrade loop properties in the crossover region due to the attendant phase loss of the lag. This degradation (45 deg. compared to 60 deg. of phase margin) was deemed acceptable.

The compensator is given by

$$K_9(s) = 0.0216 \frac{\left(\frac{s+\alpha}{\alpha}\right)\left(\frac{s^2+2\varsigma\omega_1 s+\omega_1^2}{\omega_1^2}\right)}{\left(\frac{s^2+2\varsigma z s+z^2}{z^2}\right)\left(\frac{s^2+1.9\beta_1 s+\beta_1^2}{\beta_1^2}\right)} \times \frac{\left(\frac{s^2+2\varsigma\omega_2 s+\omega_2^2}{\omega_2^2}\right)\left(\frac{s^2+2\varsigma\omega_3 s+\omega_3^2}{\omega_3^2}\right)}{\left(\frac{s^2+1.2s\beta_2 s+\beta_2^2}{\beta_2^2}\right)\left(\frac{s^2+0.4\beta_3 s+\beta_3^2}{\beta_3^2}\right)\left(\frac{s+\beta_4}{\beta_4}\right)}$$

where the pole and zero data is given in Table V.2. Note that the compensator

Table V.2 Four Disk Compensator Pole and Zero Data

$\beta_1 = 2.74$ $\qquad\qquad$ $\alpha = 0.0503$

$\beta_2 = 2.87$

$\beta_3 = 2.99$

$\beta_4 = 0.521$ (additional lag pole)

essentially inverts the plant as discussed in Chapter II.

This 9th order compensator was reduced to 6th order with the compensator

order reduction algorithm given in Table IV.1. The result is given by

$$K_6(s) = 0.0232 \frac{\left(\frac{s+\alpha_r}{\alpha_r}\right)\left(\frac{s^2+3\zeta\omega_1 s+\omega_1^2}{\omega_1^2}\right)}{\left(\frac{s^2+1.7\beta_{4r}s+\beta_{4r}^2}{\beta_{4r}^2}\right)} \times \frac{\left(\frac{s^2+3\zeta\omega_{2r}s+\omega_{2r}^2}{\omega_{2r}^2}\right)}{\left(\frac{s^2+2\zeta z s+z^2}{z^2}\right)\left(\frac{s^2+2\zeta\beta_5 s+\beta_5^2}{\beta_5^2}\right)}$$

where the pole and zero data is given in Table V.3.

Table V.3 Reduced Order Four Disk Compensator Pole and Zero Data

$\beta_{4r} = 0.567 \cong \beta_4$	$\alpha_r = 0.0515 \cong \alpha$
$\beta_5 = 3.29$	$\omega_{2r} = 1.47 \cong \omega_2$

Note that the reduced order compensator essentially inverts only the low frequency behavior of the plant, i.e. the poles with $|s| = \omega_1, \omega_2$ and the zero with $|s| = z$. Results in Appendix E show that ω_1, ω_2 and z must be known to within 10% to guarantee closed loop stability. The zero at $s = -\alpha_r$ is nearly the same as the zero of the full order compensator at $s = -\alpha$. The additional lag pole at $s = -\beta_4$ of the full order compensator is approximated by a 2nd order pole with $|s| = \beta_{4r} \cong \beta_4$.

This compensator is stable (closed loop poles given in Appendix E) with the full order model of the plant and satisfies the loop shape constraints of Fig. V.6. In addition the crossover properties of this compensator are essentially the same as those of the full order compensator (e.g. the compensator has a phase margin of 46 deg. compared to 45 deg. for the full order compensator).

It is of interest to note that reduced order models of $K_9(s)$ for any order obtained with the internally balanced realization of $K_9(s)$ produce an unstable closed loop system. The same would be true for any unweighted model reduction method (e.g. residue technique, covariance cost, minimum integral squared impulse response error, ...). The eighth order reduced order model of $K_9(s)$ obtained by using the internally balanced technique is discussed in Appendix E.

It is also of interest to examine the integral squared impulse response error criterion for this example. This error criterion is defined

$$E_2 \triangleq \sqrt{\frac{||H_e(t)||_2}{||H(t)||_2}}$$

where for this example

$$H_e(t) = \mathrm{L}^{-1}\,[\mathrm{K_9(s)} - \mathrm{K_6(s)}]\,(\mathrm{t})$$
$$H(t) = \mathrm{L}^{-1}\,[\mathrm{K_9(s)}]\,(\mathrm{t})$$

i.e. $H_e(t)$ is the impulse reponse of the error and $H(t)$ is the impulse response of the full order compensator. The error criterion is arbitrarily normalized to make it dimensionless and thus have some meaning with respect to unity.

The value of E_2 was computed for $K_6(s)$, the 6th order reduced order model of $K_9(s)$ obtained from the internally balanced realization of $K_9(s)$. These results are given in Table V.4. Note that while the reduced order model obtained

Table V.4 Comparison of E_2 and Closed Loop Stability

Model Reduction Technique	E_2	Closed Loop System Stability
Frequency Weighted Balancing	0.956	stable
Internally Balancing	0.119	unstable

with the internally balancing technique has an E_2 error criterion eight times smaller than that of the reduced order model obtained with the frequency weighted balancing technique, it results in an unstable closed loop system, whereas the weighted reduced order model results in a stable closed loop system.

These results clearly suggest that E_2 is not a good discriminator for model reduction for control system design. It is also clear that properly selected frequency dependent weightings are critical in obtaining a reduced order model for this example.

This example is somewhat academic because there really isn't any need to reduce the order of the compensator. However, the example has served to illustrate the procedure and make the following points: frequency dependent weightings are critical and E_2 is the wrong error criterion.

Robust Four Disk Design

The above design for the four disk system, although satisfactory with respect to the constraints of Fig. V.6 and the crossover requirements (say, phase margin $\geq 45 deg.$), it is not satisfactory with respect to more stringent stability robustness requirements. For instance, more robustness would be required if the disk inertias were significantly uncertain. This in turn would lead to uncertain natural frequencies ω_1, ω_2, ω_3 as well as overall gain. The above design based on plant inversion would be suspect in this case.

In another study by this author the inertia of the fourth disk was taken to be uncertain but bounded between one and four. The pole-zero configurations for these two extremes are shown in Fig. V.7

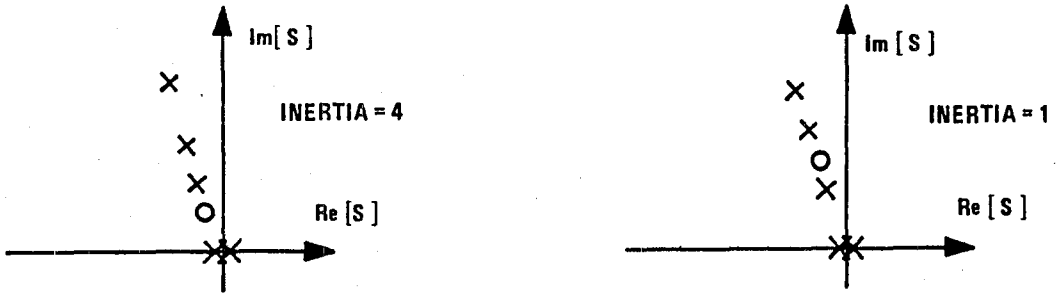

Fig. V.7 Four Disk System Pole-Zero Configurations

Note that the inertia variation between the extremes causes the lowest frequency pole and zero to interchange locations in the s plane. Since the system exhibits such significant variation, a rigid body model was used for the following.

$$G(s) = \frac{0.2}{s^2}$$

The intent of the previous study was to maximize performance subject to satisfactory robustness requirements (including robustness with respect to the uncertain 4th inertia). The loop shape requirements for this problem are shown in Fig. V.8. Note that the

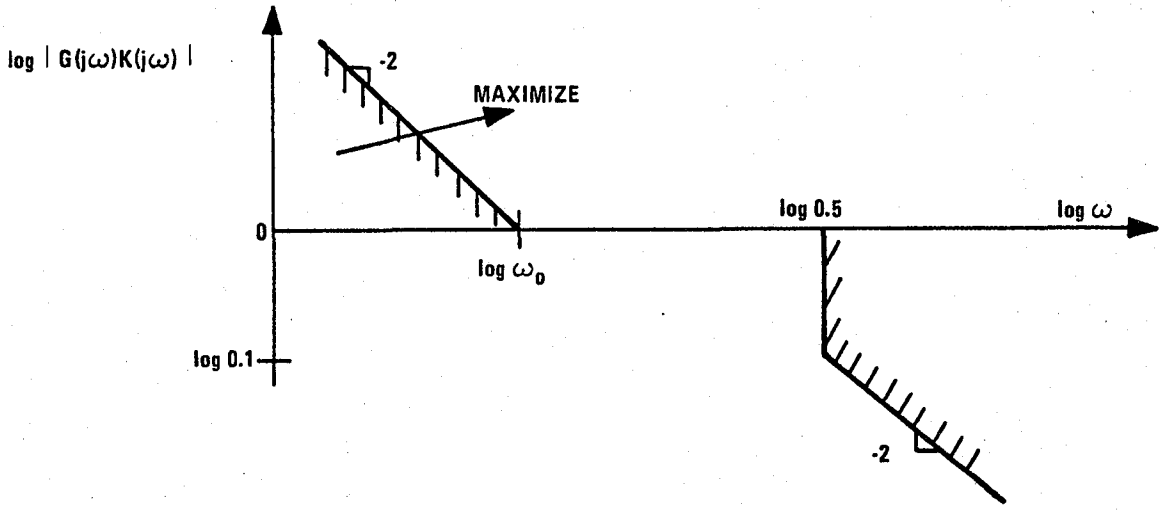

Fig. V.8 Four Disk Robust Design Loop Shape Requirements

high frequency constraint of Fig. V.6 was modified. The loop is required to have more attenuation for frequencies greater than 0.5 compared to Fig. V.6, to satisfy the uncertain inertia requirement (more details are given in App. E). However, the loop is permitted to have less attenuation for frequencies just less than 0.5 compared to Fig. V.6 to facilitate achieving maximum performance. Satisfactory crossover is also required, say phase margin should be 45 deg. or more.

The design technique of the previous study resulted in $\omega_o = 0.13$ as the maximum performance subject to the above constraints. It is of interest to note that this performance is even higher than that of the previous design! An 8th order compensator which achieves this performance is given by

$$K_8(s) = 0.0639 \frac{\left(\frac{s^2+1.41\alpha_1 s+\alpha_1^2}{\alpha_1^2}\right)\left(\frac{s+\alpha_2}{\alpha_2}\right)}{\left(\frac{s+\alpha_1}{\alpha_1}\right)\left(\frac{s^2+1.93\alpha_2 s+\alpha_2^2}{\alpha_2^2}\right)} \times$$

$$\frac{\left(\frac{s^2+1.93\alpha_3 s+\alpha_3^2}{\alpha_3^2}\right)\left(\frac{s^2+0.52\alpha_3 s+\alpha_3^2}{\alpha_3^2}\right)}{\left(\frac{s^2+1.41\alpha_2 s+\alpha_2^2}{\alpha_2^2}\right)\left(\frac{s^2+0.52\alpha_2 s+\alpha_2^2}{\alpha_2^2}\right)\left(\frac{s+\alpha_4}{\alpha_4}\right)}$$

where the pole and zero data is given in Table V.5. The magnitude of the pole

Table V.5 Four Disk Robust Design Pole and Zero Data

$\alpha_1 = 0.0850$	$\alpha_3 = 0.500$
$\alpha_2 = 0.403$	$\alpha_4 = 200$

at $s = -\alpha_4$ was arbitrarily made very large to make the compensator strictly proper.

This 8th order compensator was reduced to 5th order with the compensator

order reduction algorithm given in Table IV.1. The result is given by

$$K_5(s) = 0.0638 \frac{\left(\frac{s^2+1.35\alpha_{1r}s+\alpha_{1r}^2}{\alpha_{1r}^2}\right)}{\left(\frac{s+\gamma_1}{\gamma_1}\right)\left(\frac{s+\gamma_2}{\gamma_2}\right)} \times \frac{\left(\frac{s^2+0.752\alpha_{3r}s+\alpha_{3r}^2}{\alpha_{3r}^2}\right)}{\left(\frac{s^2+0.552\alpha_{2r}s+\alpha_{2r}^2}{\alpha_{2r}^2}\right)\left(\frac{s+\alpha_{4r}}{\alpha_{4r}}\right)}$$

where the pole and zero data is given in Table V.6.

Table V.6 Reduced Order Four Disk Robust Design Pole and Zero Data

$\alpha_{1r} = 0.0872 \cong \alpha_1$		$\alpha_{4r} = 32.1$	
$\alpha_{2r} = 0.382 \cong \alpha_2$		$\gamma_1 = 0.107$	
$\alpha_{3r} = 0.531 \cong \alpha_3$		$\gamma_2 = 0.310$	

This compensator provides essentially the same closed loop properties as the full order compensator. That is the loop satisfies the constraints of Fig. V.8 and hence the closed loop system is stable for any inertia of the fourth disk between one and four (a root locus is shown in App. E). In addition, the compensator provides essentially the same performance and crossover properties as the full order compensator.

Again this example did not really require model reduction, however, it shows

that the procedure of Table IV.1 can be applied to a compensator designed with any method, not necessarily LQG designs. Also it demonstrates that performance and robustness properties are not compromised as a result of the reduction.

Flexible Beam Example

The system to be controlled is also the subject of an experimental research project at Stanford. The system, indicated in Fig. V.9 consists of a flexible beam with a motor for applying torques at one

Fig. V.9 Flexible Beam System

end and a sensor for measuring tip displacement at the other end.

The transfer function for an 8th order model of this system with non-collocated actuators and sensors is given by

$$G(s) = \frac{2.98}{s^2} \frac{\left(\frac{s+\alpha_1}{\alpha_1}\right)\left(\frac{s-\alpha_2}{\alpha_2}\right)}{\left(\frac{s^2+2\zeta_1\omega_1 s+\omega_1^2}{\omega_1^2}\right)} \times$$

$$\frac{\left(\frac{s^2-0.72\alpha_3 s+\alpha_3^2}{\alpha_3^2}\right)\left(\frac{s^2+0.74\alpha_4 s+\alpha_4^2}{\alpha_4^2}\right)}{\left(\frac{s^2+2\zeta_2\omega_2 s+\omega_2^2}{\omega_2^2}\right)\left(\frac{s^2+2\zeta_3\omega_3 s+\omega_3^2}{\omega_3^2}\right)}$$

where the pole and zero data is given in Table V.7. Note that this system is also non-minimum phase.

Table V.7 Flexible Beam System Pole and Zero Data

$\alpha_1 = 10.3$	$\omega_1 = 11.3$	$\zeta_1 = 0.05$
$\alpha_2 = 11.7$	$\omega_2 = 22.0$	$\zeta_2 = 0.02$
$\alpha_3 = 36.1$	$\omega_3 = 52.8$	$\zeta_3 = 0.02$
$\alpha_4 = 37.6$		

The performance and stability robustness requirements chosen for this example resulted in the constraints for the loop shape shown in Fig. V.10. Note

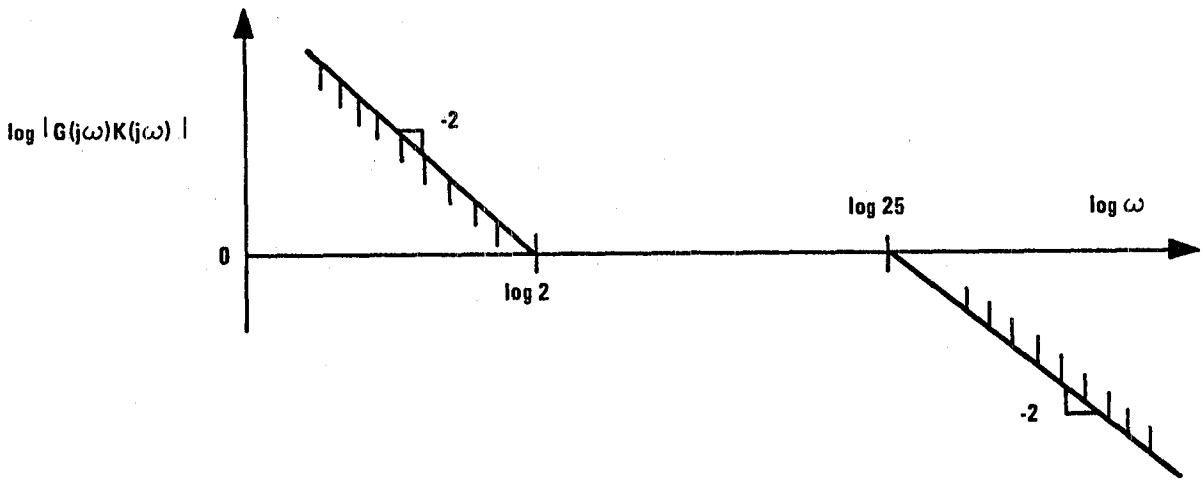

Fig. V.10 Loop Shape Constraints For Flexible Beam System

that the minimum phase zeros for this problem will seriously degrade the crossover properties for designs obtained by any technique. This is because of the proximity of the non-minimum phase zeros to the crossover region.

A compensator was designed using the standard LQG loop shaping procedure of Chapter II (see Table II.4). An additional lag was appended as in the LQG design for the four disk system. This compensator satisfied the constraints of Fig. V.10. The loop crossover properties were seriously degraded (only 24 deg. of phase margin and 5 dB of gain margin) due to the non-minimum phase zeros and the additional compensator lag. The compensator is given by

$$K_9(s) = 1.91 \frac{\left(\frac{s+\beta_1}{\beta_1}\right)\left(\frac{s^2-2\hat{\varsigma}_1\hat{\omega}_1 s+\hat{\omega}_1^2}{\hat{\omega}_1^2}\right)}{\left(\frac{s+\alpha_1}{\alpha_1}\right)\left(\frac{s+\beta_2}{\beta_2}\right)\left(\frac{s^2+0.3\beta_3 s+\beta_3^2}{\beta_3^2}\right)} \times$$

$$\frac{\left(\frac{s^2+2\hat{\varsigma}_2\hat{\omega}_2 s+\hat{\omega}_2^2}{\hat{\omega}_2^2}\right)\left(\frac{s^2+2\hat{\varsigma}_3\hat{\omega}_3 s+\hat{\omega}_3^3}{\hat{\omega}_3^2}\right)}{\left(\frac{s^2+0.74\alpha_4 s+\alpha_4^2}{\alpha_4^2}\right)\left(\frac{s+\beta_4}{\beta_4}\right)\left(\frac{s^2+1.4\beta_5 s+\beta_5^2}{\beta_5^2}\right)}$$

where the pole and zero data is given in Table V.8. Note that the compensator essentially inverts the

Table V.8 Flexible Beam Compensator Pole and Zero Data

$\beta_1 = 1.56$	$\hat{\omega}_1 = 11.4 \cong \omega_1$	$\hat{\varsigma}_1 = 0.057 \cong \varsigma_1$
$\beta_2 = 22.9$	$\hat{\omega}_2 = 22.4 \cong \omega_2$	$\hat{\varsigma}_2 = 0.009 \cong \varsigma_2$
$\beta_3 = 32.2$	$\hat{\omega}_3 = 52.8 \cong \omega_3$	$\hat{\varsigma}_3 = 0.02 \cong \varsigma_3$
$\beta_4 = 53.4$		
$\beta_4 = 470.$		

minimum phase behavior of the plant as discussed in Chapter II.

This 9th order compensator was reduced to 6th order with the compensator order reduction algorithm given in Table IV.1. The result is given by

$$K_6(s) = 1.93 \frac{\left(\frac{s+\beta_{1r}}{\beta_{1r}}\right)\left(\frac{s^2-2\hat{\zeta}_{1r}\hat{\omega}_{1r}s+\hat{\omega}_{1r}^2}{\hat{\omega}_{1r}^2}\right)}{\left(\frac{s^2+1.72\alpha_{1r}s+\alpha_{1r}^2}{\alpha_{1r}^2}\right)\left(\frac{s^2+0.12\gamma_1 s+\gamma_1^2}{\gamma_1^2}\right)} \times \frac{\left(\frac{s^2+2\hat{\zeta}_{2r}\hat{\omega}_{2r}s+\hat{\omega}_{2r}^2}{\hat{\omega}_{2r}^2}\right)}{\left(\frac{s^2+0.1\gamma_2 s+\gamma_2^2}{\gamma_2^2}\right)}$$

where the pole and zero data is given in Table V.9.

Table V.9

Reduced Order Flexible Beam Compensator Pole and Zero Data

$\alpha_{1r} = 8.66 \cong \alpha_1$	$\hat{\omega}_{1r} = 11.6 \cong \omega_1$	$\hat{\zeta}_{1r} = 0.08 \cong \zeta_1$
$\beta_{1r} = 1.59 \cong \beta_1$	$\hat{\omega}_{2r} = 21.3 \cong \omega_2$	$\hat{\zeta}_{2r} = 0.01 \cong \zeta_2$
$\gamma_1 = 22.3$		
$\gamma_2 = 41.8$		

Note that this compensator essentially inverts the low frequency, minimum phase behavior of the plant, i.e. the poles with $|s| = \omega_1, \omega_2$ and the zero at $s = -\alpha_1$.

This compensator is stable (closed loop poles given in App. E) with the full order model of the plant and satisfies the loop shape constraints. The crossover properties of this compensator were however degraded (only 17 deg of phase margin and 3 dB of gain margin).

It is of interest to compare this 6th order compensator to one that would be obtained by neglecting the third mode (i.e. the plant pole with $|s| = \omega_3$). This is referred to as modal truncation and is often done in practice. An LQG design was carried out for a 6th order plant model obtained by truncating the ω_3 term of the partial fraction expansion of $G(s)$. The design was carried out such that the low frequency constraint of Fig. V.10 was satisfied to facilitate a meaningful comparison. The closed loop system with this compensator and the full order model was found to be unstable. Details of this design are given in App. E.

Again this example does not really require model reduction, however, it shows that the procedure of Table IV.1 can design a reduced order compensator that is closed loop stable with the full order model when the classical modal truncation technique fails. This is not meant to be an indictment of the modal truncation technique. It is a useful technique when used carefully. For example it is used successfully in a later example of this chapter.

Plant Order Reduction Examples

The purpose of this section is to present some examples of the plant order reduction algorithm discussed in Chapter IV (see Table IV.7). A couple simple SISO (less than 3rd order) examples as well as a MIMO (6th order) example will be used to demonstrate the successive approximation solution procedure. This technique was found to be acceptable for these examples. The section concludes with a significant design/demonstration example, utilizing a 168th order, MIMO

non-collocated model of a flexible spacecraft. The model reduction and design techniques of this thesis are shown to be very effective in performing this design.

Simple Low Order Examples

The plant order reduction algorithm was exercised with the "simple H_∞ example" (i.e. the first example of this chapter) with transfer function given by

$$G(s) = \frac{2(s+2)}{(s+1)(s+3)} \quad .$$

The closed loop transfer function was chosen to be

$$H(s) = \frac{0.5}{s + 0.5} \quad .$$

An initial weighting was determined from

$$W(s) = G^{-1}(s)H(s)$$

and the successive approximation algorithm (Table IV.7) converged after five iterations. The resulting reduced order model is given by

$$G_r(s) = \frac{1.78}{s + 1.36} \quad .$$

The compensator, $K(s) = G_r^{-1}(s)\,\frac{0.5}{s}$ is guaranteed to produce a stable closed loop system with $G(s)$ since $E_\infty = 0.024 < 1$.

Third Order Example

The plant order reduction algorithm was also exercised with the 3rd order transfer function:

$$G(s) = \frac{(s+0.8)(s+2)}{(s+1.5)(s^2+1.4s+1)} \quad .$$

For this example the closed loop transfer function was chosen to be

$$H(s) = \frac{1}{s+1} \quad .$$

An initial weighting was determined from

$$W(s) = G^{-1}(s)\,H(s)$$

and after 3 and 5 iterations the successive approximation algorithm (Table IV.7) converged for the 2nd and 1st order reduced order models respectively. These reduced order models are given by

$$G_2(s) = \frac{0.822(s+1.14)}{s^2+1.34s+1.07}$$

$$G_1(s) = \frac{1.16}{(s+0.819)} \quad .$$

The compensators, $K_r(s) = G_r^{-1}(s)\frac{1}{s}$ $r = 1, 2$ are guaranteed to produce stable closed loop systems with $G(s)$ since $E_\infty = 0.0085, 0.249 < 1$ for $r = 1, 2$ respectively.

The only significance of these two examples is that the successive approximation solution procedure was successful.

C5A Example

The successive approximation solution procedure was also demonstrated with a more realistic example. The plant transfer function for this example is a 6th order representation of the C5A aircraft wing root bending and torsion moments measured in in-lbs due to aileron and elevator commands measured in radians [Ref. 46]. The MIMO system with two inputs and two outputs has the poles and transmission zeros given in Table V.10. A Bode plot of the singular values of the 2×2 6th order plant transfer function, $G(s)$ is shown in Fig. V.11 and an output normal realization of the transfer function is given in Table V.11.

Fourth Order Reduced Order Model

To obtain a 4th order reduced order model, the following output closed loop system was used

$$H_o(s) = \frac{1}{s+1} I_2 \quad .$$

An initial input weighting was determined from

$$W_i(s) = G^{-1}(s)\, H_o(s) \quad .$$

The successive approximation algorithm converged after 5 iterations. The resulting 2×2 4th order reduced order model poles and transmission zeros are given in Table V.12. A realization of this reduced

Table V.10 C5A Poles and Transmission Zeros

Poles

$s^2;\ \omega = 1.4,\ \varsigma = 0.6$	short period mode
$s^2;\ \omega = 5.5,\ \varsigma = 0.09$	flexible mode
$s = -6.0$	aileron actuator
$s = -7.5$	elevator actuator

Transmission Zeros

$s^2;\ \omega = 8.1,\quad \varsigma = 0.69$

$s^2;\ \omega = 11.3,\quad \varsigma = 0.44$

where the notation $s^2;\ \omega = \omega, \varsigma = \varsigma$ means the complex conjugate pair $s = -\varsigma\omega \pm j\omega\sqrt{1-\varsigma^2}$.

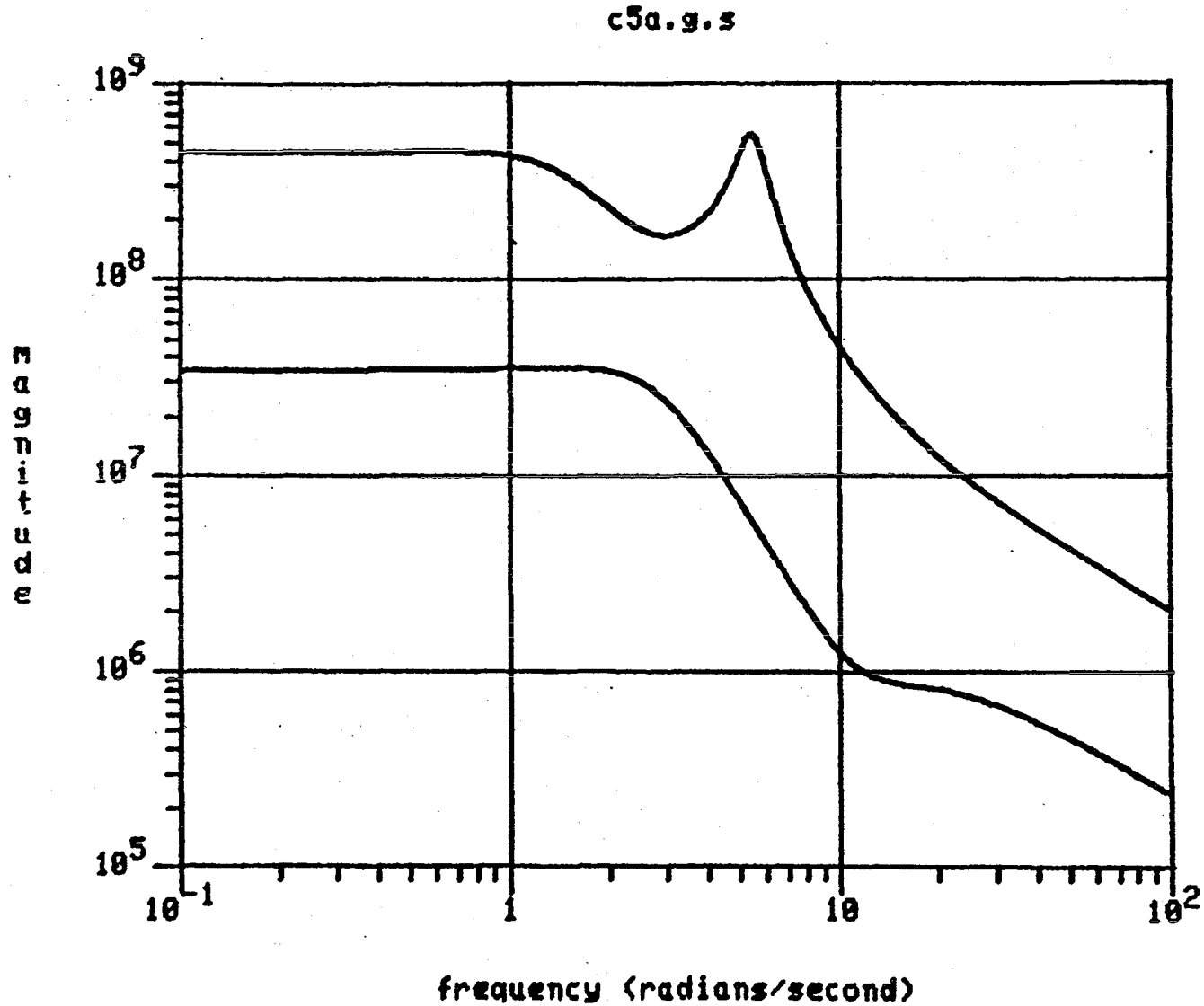

Figure V.11 Bode Plot of the Singular Values of $G(j\omega)$

Table V.11 C5A Transfer Function Realization

$$\dot{x} = Fx + Gu \qquad G(s) = H(sI-F)^{-1}G$$
$$y = Hx \qquad F + F^T + H^TH = 0$$

$$u = \begin{bmatrix}\text{aileron command}\\ \text{elevator command}\end{bmatrix} \qquad y = \begin{bmatrix}\text{Bending moment}\\ \text{Torsion moment}\end{bmatrix}$$

$$F = \begin{bmatrix} -1.192e-01 & 5.806e-01 & 4.758e+00 & -1.464e+00 \\ -4.412e-01 & -4.414e-02 & -1.014e-01 & 1.343e+00 \\ -5.366e+00 & 5.039e-01 & -9.381e-01 & -2.174e+00 \\ 7.003e-01 & -8.856e-01 & 1.491e-01 & -1.232e+00 \\ -9.315e-01 & -3.954e-01 & -1.598e-01 & -4.563e-01 \\ 2.980e-02 & -2.697e-01 & 2.673e-02 & -4.245e-01 \end{bmatrix}$$

$$\begin{bmatrix} 2.060e+00 & 1.640e+00 \\ -4.941e-01 & -5.637e-01 \\ 4.632e+00 & 3.238e+00 \\ 4.452e+00 & 5.533e+00 \\ -6.579e+00 & -2.592e+00 \\ -4.385e-01 & -7.364e+00 \end{bmatrix}$$

$$G = \begin{bmatrix} -2.577e+08 & 2.985e+08 \\ 1.865e+08 & 2.345e+08 \\ -2.491e+07 & -8.587e+07 \\ -1.875e+07 & -2.817e+07 \\ -1.139e+07 & -1.851e+07 \\ -3.218e+06 & -2.683e+06 \end{bmatrix}$$

$$H = \begin{bmatrix} -4.682e-01 & -2.971e-01 & -1.356e+00 & -1.538e+00 \\ -1.386e-01 & 2.364e-03 & 1.932e-01 & -3.131e-01 \end{bmatrix}$$

$$\begin{bmatrix} 3.010e+00 & 2.784e+00 \\ -2.024e+00 & 2.642e+00 \end{bmatrix}$$

Table V.12
C5A 4th Order Reduced Order Model Poles and Transmission Zeros

Poles

$s^2;\ \omega = 1.25,\ \varsigma = 0.511$ short period mode

$s^2;\ \omega = 5.30,\ \varsigma = 0.0925$ flexible mode

Transmission Zeros

$s^2;\ \omega = 10.5,\ \varsigma = 0.395$

order model is given in Table V.13. Clearly the algorithm has just eliminated

Table V.13 C5A 4th Order Reduced Order Model Realization

$$G_r(s) = C(sI-A)^{-1}B$$

$$A = \begin{bmatrix} -1.003e{-}03 & 1.140e{+}00 & 2.218e{-}01 & 1.170e{-}01 \\ -3.387e{+}00 & -8.392e{-}03 & -1.280e{+}00 & -3.100e{-}01 \\ -5.146e{+}00 & 9.648e{+}00 & -1.320e{-}01 & -5.580e{-}01 \\ -2.574e{+}01 & 2.352e{+}01 & 5.203e{+}00 & -2.114e{+}00 \end{bmatrix}$$

$$B = \begin{bmatrix} 2.759e{+}05 & -7.092e{+}07 \\ -8.895e{+}07 & 4.467e{+}07 \\ 1.195e{+}08 & 3.905e{+}07 \\ 3.512e{+}08 & 7.355e{+}06 \end{bmatrix}$$

$$C = \begin{bmatrix} -4.413e{-}02 & 3.680e{-}02 & 1.251e{-}01 & 6.998e{-}01 \\ -2.261e{-}01 & -3.854e{-}01 & -5.397e{-}01 & 9.998e{-}02 \end{bmatrix}$$

the actuator dynamics, leaving the short period and flex mode dynamics essentially unchanged.

Second Order Reduced Order Model

To obtain a 2nd order reduced order model, the following output closed loop transfer function was used

$$H_o(s) = \frac{0.1}{s + 0.1} I_2 \quad .$$

An initial input weighting was determined from

$$W_i(s) = G^{-1}(s) H_o(s) \quad .$$

The successive approximation algorithm did not converge to a single point in this case. Rather, the algorithm resulted in a limit cycle containing three points. A graphical representation of the limit cycle is shown in Fig. V.12a, b where the balanced grammian's singular values are plotted versus iteration. Clearly after the 10th iteration, the successive approximation algorithm cycles between three points.

As discussed in Chapter IV, when this happens, the solution is the reduced order model of the limit set corresponding to the minimum error, E_∞. Recall that the error criterion in this case is defined

$$E_\infty = \| [G(s) - G_r(s)] \, G_r^{-1}(s) H_o(s) \|_\infty \quad .$$

Bode plots of the maximum singular value of $[G(j\omega) - G_r(j\omega)] \, G_r^{-1}(j\omega) \, H_o(j\omega)$ versus ω are shown in Figs. 13a, b, c for the three points of the limit set respectively. Recall, from the definition of the H_∞ norm that E_∞ is just the peak value of these plots. Thus Fig. V.13c corresponds to the reduced order model which is the solution by definition. Note that $E_\infty > 1$ here and thus a control design based on this reduced order model is not guaranteed to be successful.

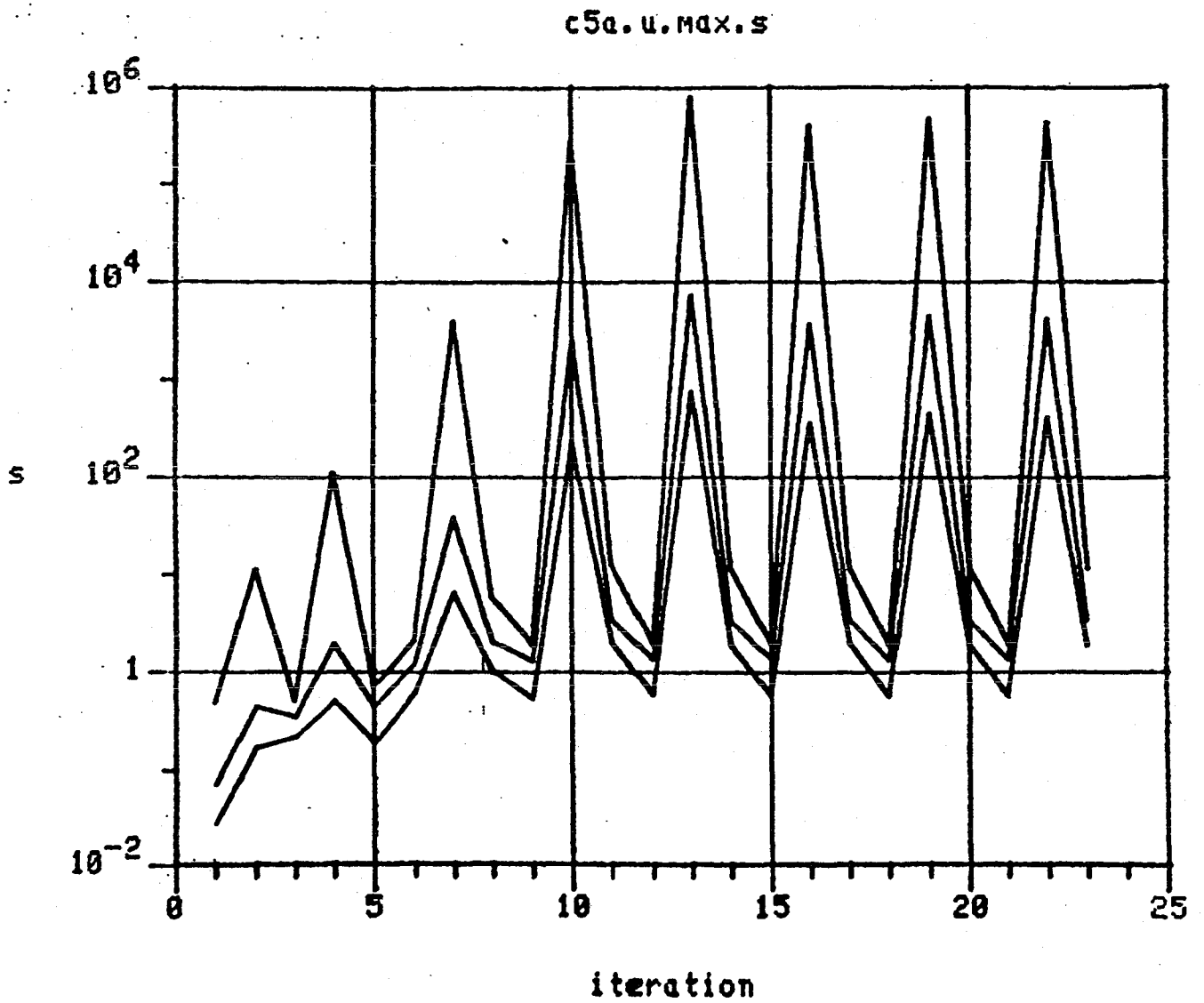

Figure V.12a The 3 Largest Singular Values of the Balanced Grammian

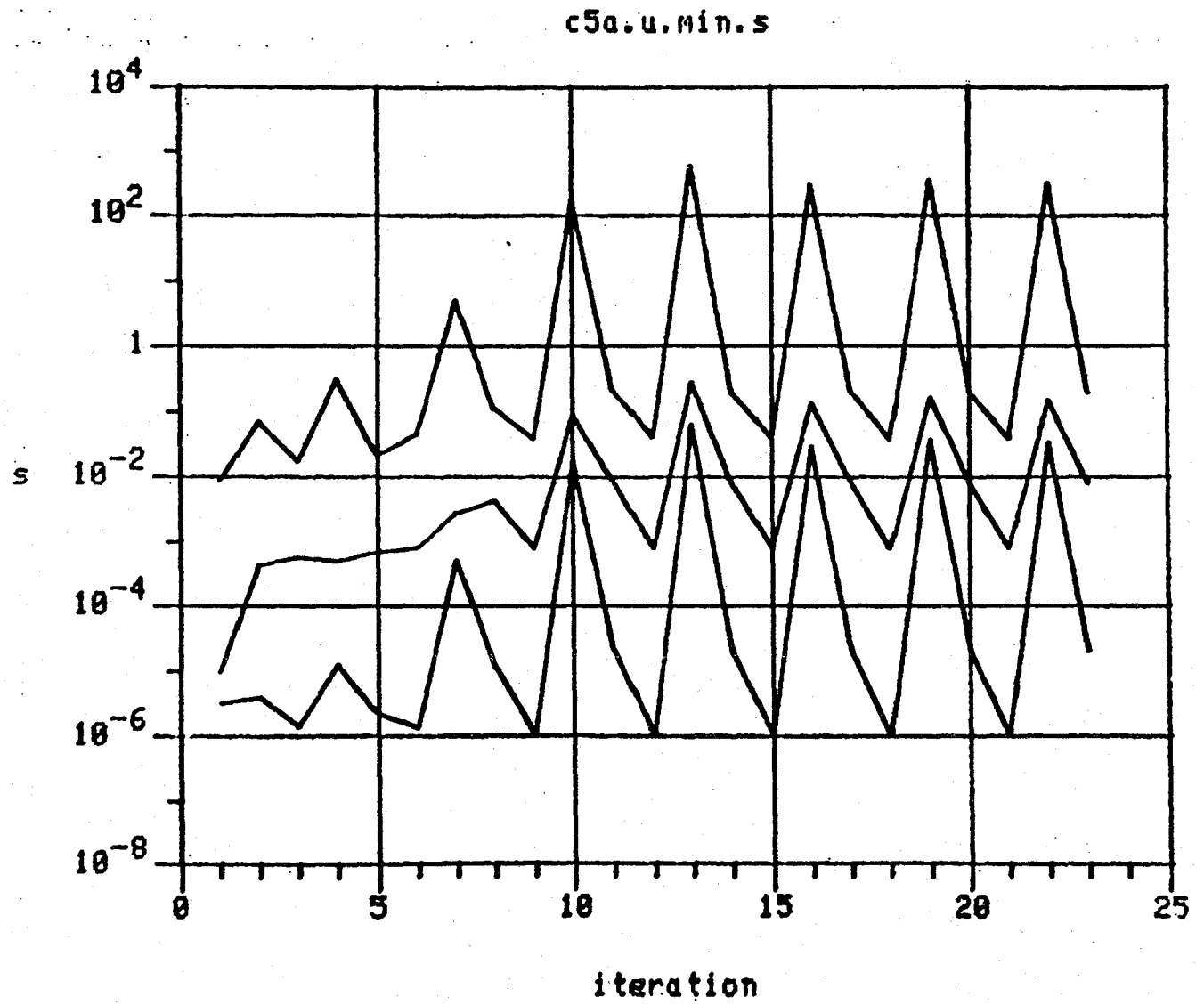

Figure V.12b The 3 Smallest Singular Values of the Balanced Grammian

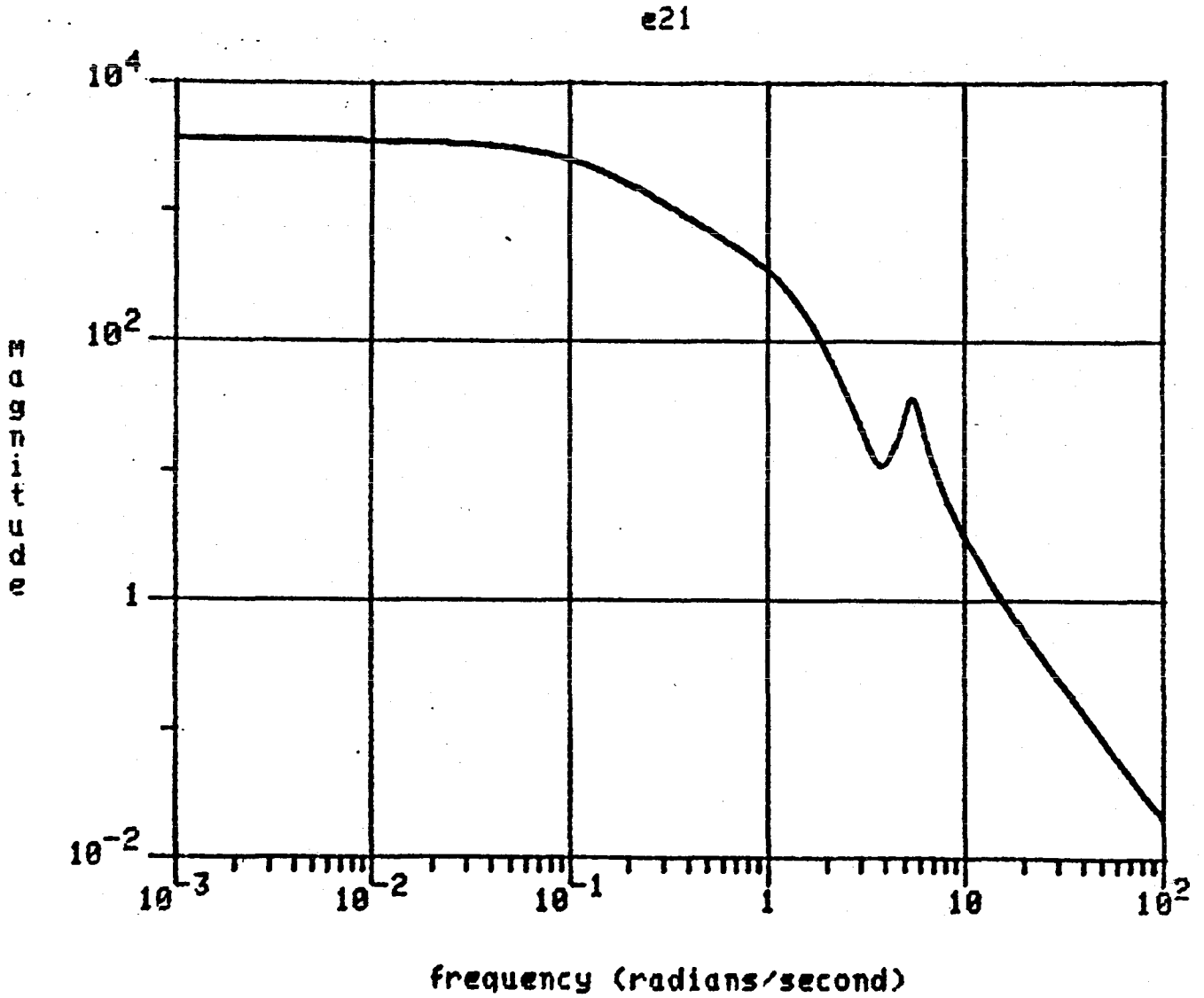

Figure V.13a Error Plot For 21st Point of the Iterations

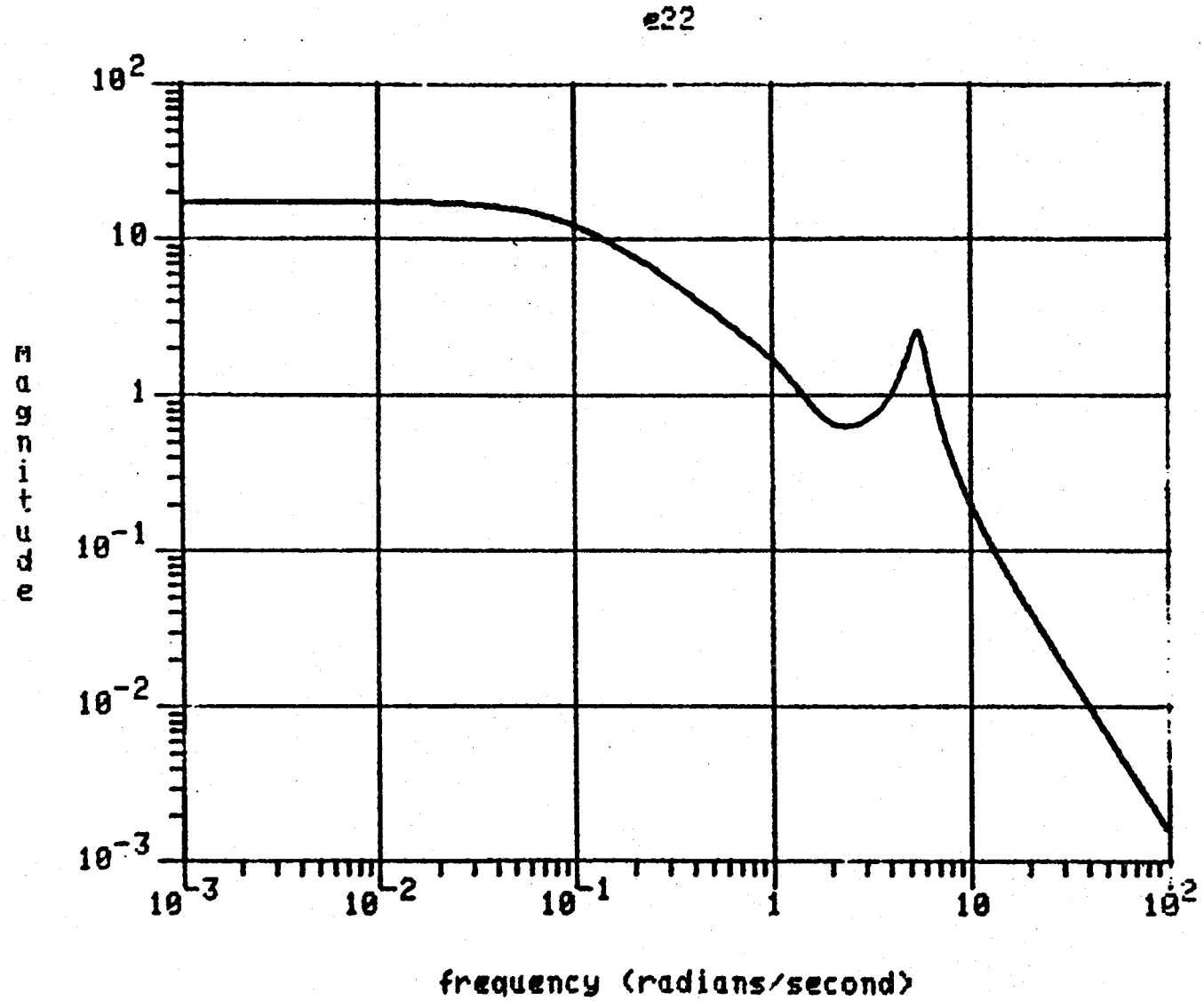

Figure V.13b Error Plot For 22nd Point of the Iterations

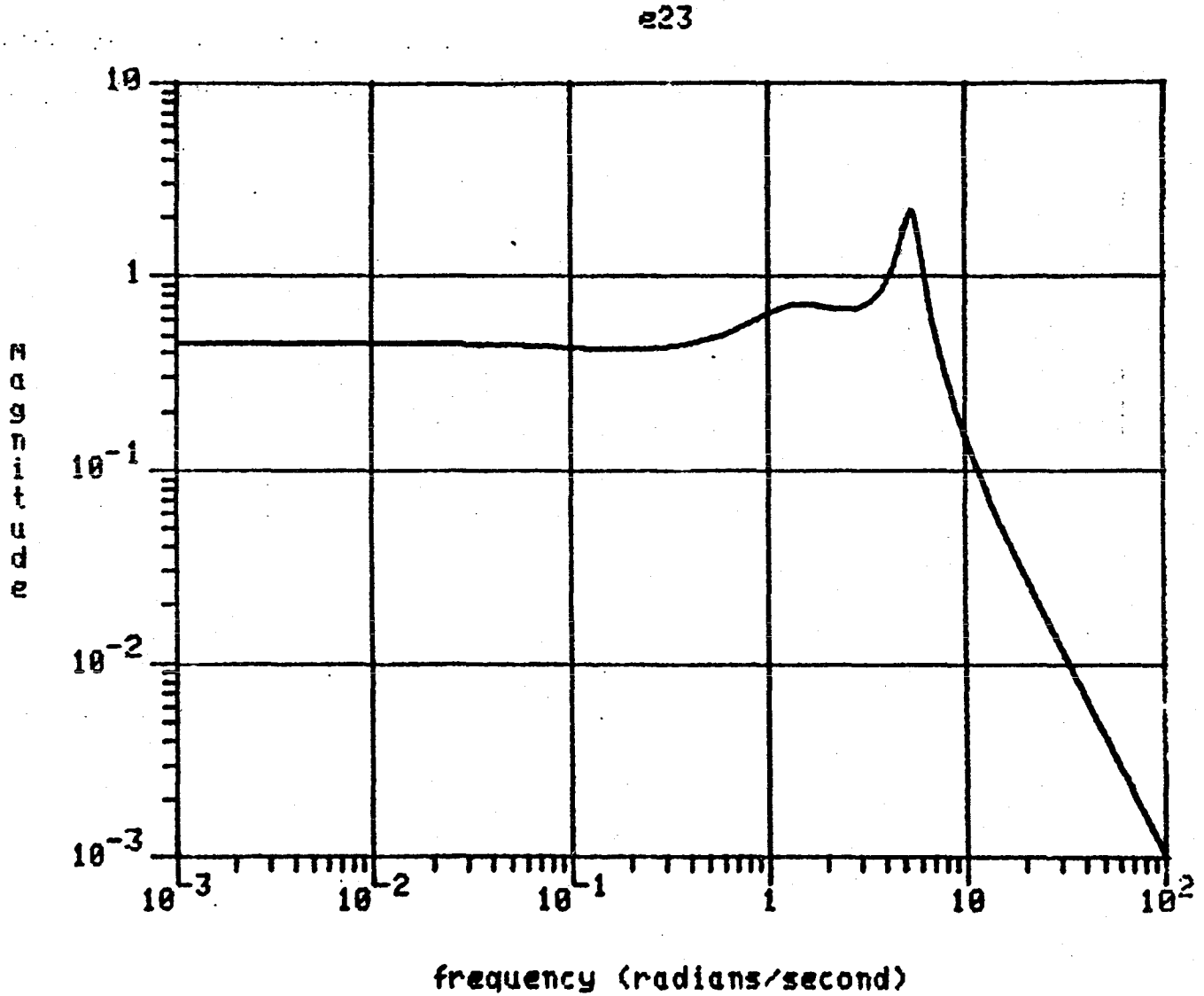

Figure V.13c Error Plot For 23rd Point of the Iterations

This reduced order model has no transmission zeros and a 2nd order pair of poles with magnitude of 0.755 and a damping ratio of 0.728. Thus the 2nd order reduced order model retains the short period dynamics. A realization of this reduced order model is given in Table V.14.

Table V.14

C5A 2nd Order Reduced Order Model Realization

$$
\begin{aligned}
G_r(s) &= C(sI-A)^{-1}B \\
A &= \begin{bmatrix} -5.554e{-}01 & 1.142e{-}01 \\ -2.344e{+}00 & -5.438e{-}01 \end{bmatrix} \\
B &= \begin{bmatrix} -1.186e{+}07 & 1.026e{+}07 \\ 5.073e{+}07 & 1.700e{+}08 \end{bmatrix} \\
C &= \begin{bmatrix} 3.498e{+}00 & 1.851e{+}00 \\ -8.419e{-}01 & 2.896e{-}01 \end{bmatrix}
\end{aligned}
$$

This example has illustrated the use of the plant order reduction algorithm on a realistic example. The results obtained are consistent with intuition. That is for the 4th order reduced order model, throwing out the actuator dynamics seems reasonable. The fact that a compensator designed with the 2nd order reduced order model is not guaranteed to be successful is also reasonable. The procedure for dealing with non-convergence of the successive approximation solution procedure was also illustrated.

ACOSS EXAMPLE

The purpose of this example was to demonstrate all the steps of the plant

order reduction and reduced order controller design algorithm on a realistic example problem where model reduction was necessary. The example chosen was the ACOSS II large space structure [Ref. 47]. The spacecraft, as illustrated in Fig. V.14, consists of an equipment section, solar panels and an optical structure to support the optical hardware for the surveillance mission of the satellite.

The control problem is to provide acceptable line of sight errors in the face of the disturbance environment. Line of sight error is the focal plane x–y position error of the image of the optical system of this surveillance satellite. The disturbance environment consists of external disturbances: solar, gravity gradient, aerodynamic and thermal and internal disturbances: imperfectly balanced rotating machinery on board the equipment section (cryogenic coolers for the mirrors and control moment gyros).

Sensors and Actuators

Three actuators for solving the control problem are located near the center of the equipment section (Node 44). They are control moment gyros (CMG) and provide torque inputs about the x, y and z axes. The sensors for solving the control problem are located on the optical structure near the focal plane (Node 11). They are rate-integrating gyros and provide angular position measurements about the x, y and z axes. Note that the sensors and actuators are non-collocated.

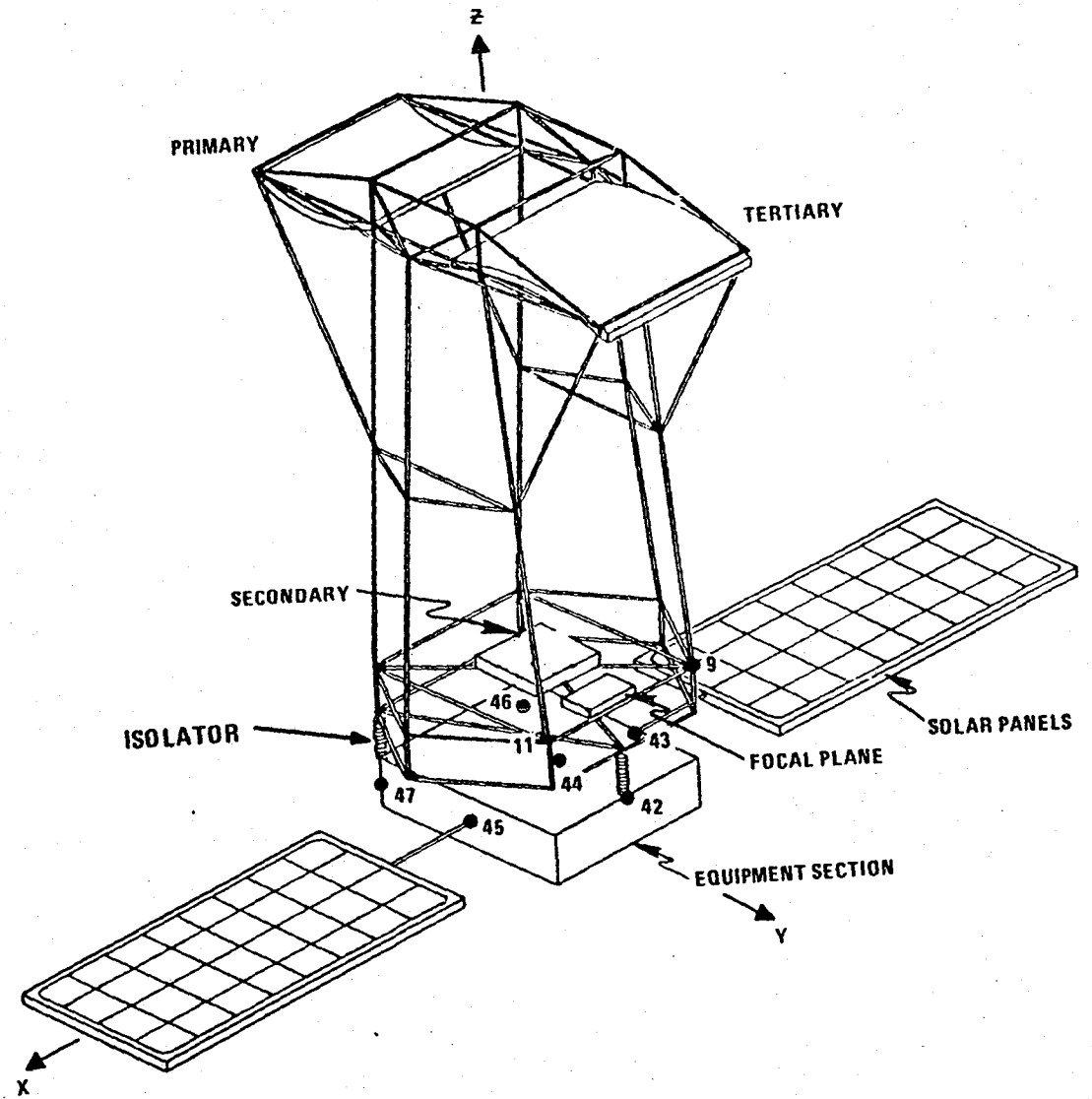

Figure V.14 ACOSS II Large Space Structure

Full Order Model

A finite element model of the spacecraft was developed at Draper Labs [Ref. 48] and is given by

$$G_{84}(s) = \sum_{i=1}^{84} \frac{c_i b_i^T}{s^2 + 2\zeta_i \omega_i s + \omega_i^2}$$

where ω_i, b_i, c_i and ζ_i $i = 1, 2, ..., 84$ are given in Appendix G. A Bode plot of the singular values of $G_{84}(j\omega)$ is shown in Fig. V.15. That is $G(s)$ is the 3×3 transfer function relating the CMG inputs to the gyro outputs. The first six of the modes are rigid body modes and thus $\omega_i = 0$ i=1, 2, ..., 6. Six of the remaining modes have damping ratios of $\zeta_i = 0.7$ (see App. G) and the rest have damping ratios of $\zeta_i = 0.005$. The higher damping ratios reflect the presence of passive isolators connecting the equipment section to the optical structure. The lighter damping is just that due to structural damping.

Loop Shape Constraints

The loop shape constraints for this control problem are shown in Fig. V.16 and would apply for either the input or the output loop shapes.

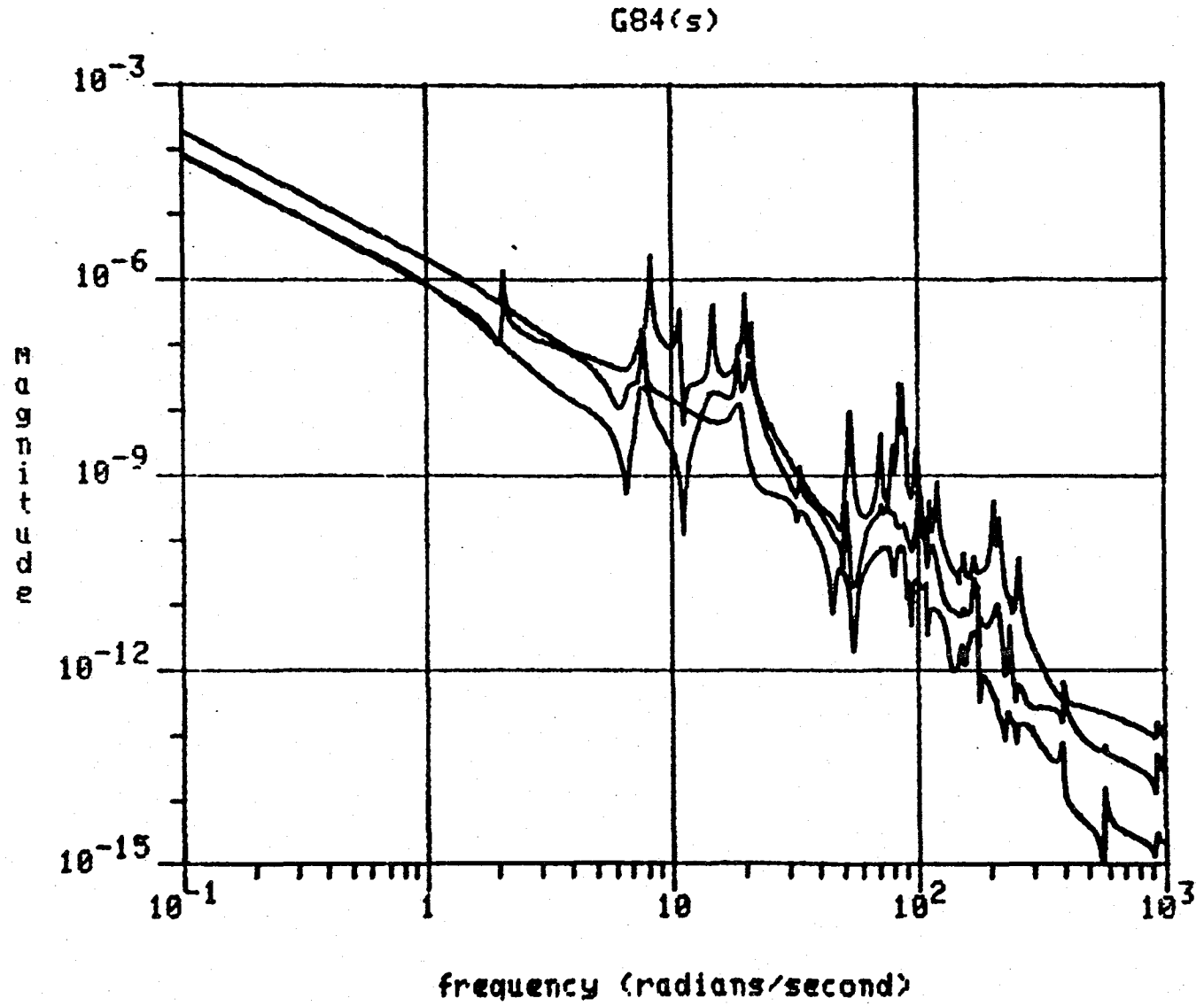

Figure V.15 Bode Plot of the Singular Values of $G_{84}(j\omega)$

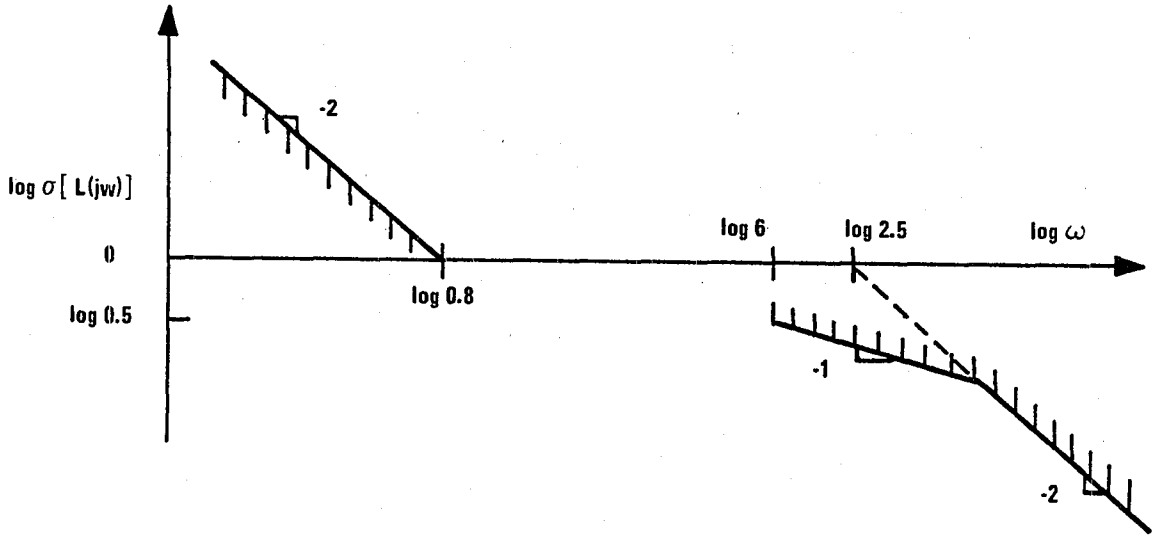

Fig. V.16 Loop Shape Constraints

The low frequency portion of the figure reflects the requirements for maintaining acceptable line of sight error in the presence of the disturbances. The high frequency constraint is due to sensor noise and high frequency modeling errors. The section of negative one slope is due to non-minimum phase zeros and will be discussed shortly. The crossover requirements are that the minimum singular values of the return difference and inverse-return difference for either the input or the output remain greater than 0.5.

Constraints Due To Actuator Dynamics

Actuator dynamics impose additional loop requirements which are expressed in terms of the input inverse-return difference. This requirement is due to the

fact that the design will be done neglecting the actuator dynamics. Requirements for closed loop stability with respect to neglected actuator dynamics can be generated with the stability robustness theorem of Chapter II.

Consider the block diagram of the actuator dynamics shown in Fig. V.17.

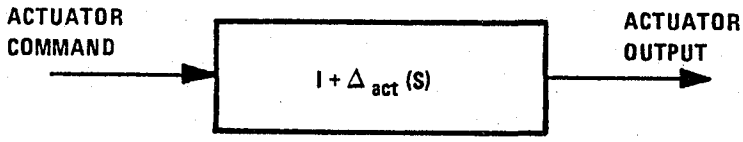

Fig. V.17 Actuator Dynamics

The actuator dynamics are nominally modeled as an identity (i.e. $\Delta_{act}(s) = 0$ nominally) and $\Delta_{act}(s)$ accounts for the actual dynamics of the actuator. The point is that although $\Delta_{act}(s)$ is not known exactly it can be bounded. The bound for this problem is given by

$$\bar{\sigma}[\Delta_{act}(j\omega)] \leq l_{act}(\omega)$$

and the scalar function of frequency, $l_{act}(\omega)$ is plotted in Fig. V18. To fix ideas this representation includes

$$G_{act}(s) = \frac{a}{s + a} I$$

$$G_{act}(s) = \frac{a^2}{s^2 + 1.4as + a^2} I$$

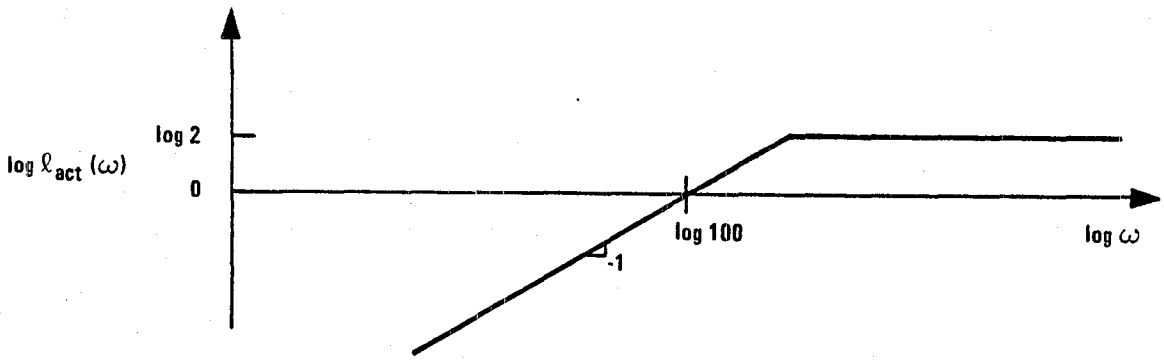

Fig. V.18 Actuator Uncertainty Bound

and

$$G_{act}(s) = \frac{a(s+a)}{s^2 + 1.4as + a^2} I$$

where $a \geq 200$ r/sec as potential actuator dynamics.

To guarantee closed loop stability for any of the actuator dynamics included in the above representation it is necessary that

$$\underline{\sigma}\left[I + \left[K(j\omega)G(j\omega)\right]^{-1}\right] > \mathbf{l}_{act}(\omega) \qquad \forall\omega \quad .$$

Thus, this additional requirement is imposed on the input inverse-return difference.

Motivation For Using Methodology of Chapter IV

A compensator was designed using LQG and a model of only the rigid body portion of the transfer function $G_{84}(s)$, i.e. neglecting the flexibility effects. This

design satisfied the performance imposed high gain constraint of Fig. V.16. However, the closed loop system was unstable when the flexible effects were added. Clearly the design process must take into account the flexible modes. But, there are 78 2nd order flexible modes to take account of ! Surely not all 78 are important for the control design, but which ones of the 78 are critical? The plant order reduction methodology of Chapter IV addresses this question.

Preliminary Model Simplification

The three rigid body modes corresponding to translation are neither controllable nor observable with the actuators and sensors and thus were discarded (see App. G). The modes of the model with $\omega_i \geq 100$ r/sec and $||b_i|| \cdot ||c_i|| \cong 0$ were also discarded (see App. G). Note that the modes beyond 100 r/sec are sufficiently far beyond the crossover region and thus it should not be necessary to include them in the model. The closed loop stability of the system in the presence of these discarded modes, will however, have to be checked, after completing the design. The justification for eliminating the modes with small residues and those with magnitudes greater than 100 r/sec (roughly two decades greater than the desired bandwidth) is that this model reduction is trivial and the formal balancing would eliminate these modes anyway.

The preliminary simplification resulted in a model with 29 2nd order modes. The transfer function for this model will be denoted by $G_{29}(s)$. A Bode plot of the singular values of $G_{29}(j\omega)$ is shown in Fig. V.19. Note that this plot is

essentially the same as that for $G_{84}(s)$ except that peaks are missing for $\omega \geq 100$ r/sec.

Minimum Phase Approximation of $G_{29}(s)$

The 58th order reduced order model, $G_{29}(s)$ has 15 transmission zeros in the right half plane. The non-minimum phase zeros all have magnitudes greater than 6 r/sec and all but one are very close to the $j\omega$ axis. It is desirable to approximate the system with a minimum phase model, $G(s)$. This will satisfy the technical requirements for using the LQG loop shaping design procedure discussed in Chapter II.

This is accomplished by factoring

$$G_{29}(s) = G(s)P(s)$$

where $G(s)$ is minimum phase and $P(s)$ is a MIMO all pass, i.e. $P(s)P^T(-s) = P^T(-s)P(s) = I$. In addition $P(s)$ was chosen such that $\lim_{s\to\infty} [P(s)-I] = 0$. This can always be done and a general procedure for performing this factorization is discussed in Appendix F. This of course, introduces additional uncertainty into the design process. The stability of the closed loop system with $G_{29}(s)$ can however be guaranteed by satisfying

$$\underline{\sigma}\left[I + \left[K(j\omega)G(j\omega)\right]^{-1}\right] > \bar{\sigma}\left[P(j\omega) - I\right] \quad .$$

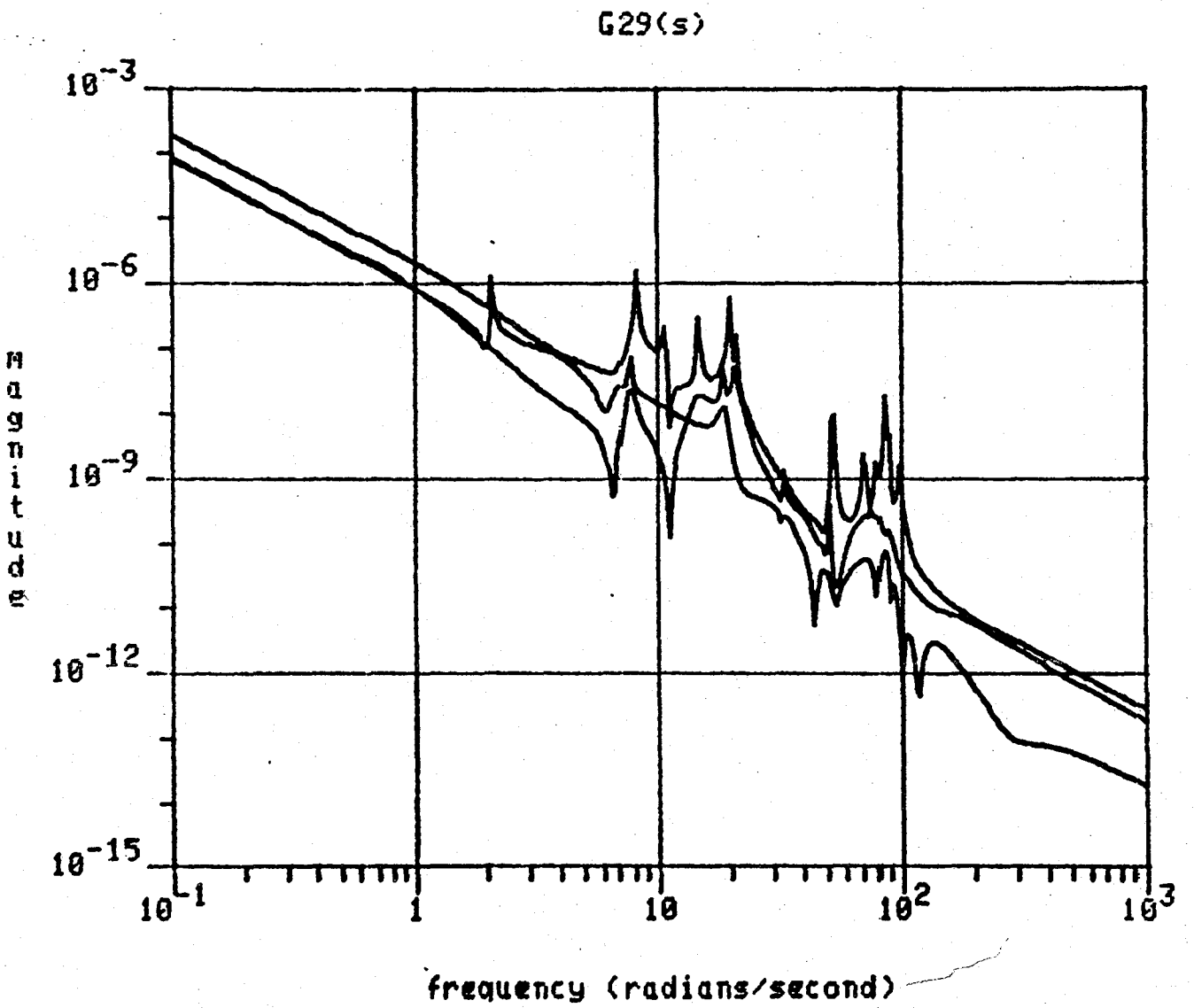

Figure V.19 Bode Plot of the Singular Values of $G_{29}(s)$

A Bode plot of the maximum singular value of $P(j\omega)-I$ is shown in Fig. V.20

This leads to the portion of the mid frequency loop shape constraint with -1 slope. In other words, the loop must be rolled off for frequencies greater than the magnitude of the smallest non-minimum phase zero.

Stable and Unstable Decomposition of $G(s)$

The transfer function $G(s)$ can be expanded into stable and unstable (rigid body poles for this example) parts:

$$G(s) = G_s(s) + G_{us}(s) \quad .$$

That is

$$G_{us}(s) = \frac{R}{s^2}$$

where R^{-1} is the full rank 3×3 inertia matrix for the center of mass of the structure about the x, y and z axes and $G_s(s)$ represents the flexible characteristics of the satellite.

Preliminary Design Steps

A filter loop transfer function was designed using the standard LQG loop shaping procedure (2nd column of Table II.4) to satisfy the high gain constraint of Fig. V.16. A satisfactory high gain characteristic was obtained using only the rigid body dynamics, i.e. $G_{us}(s)$. In other words, for this step of the design, the

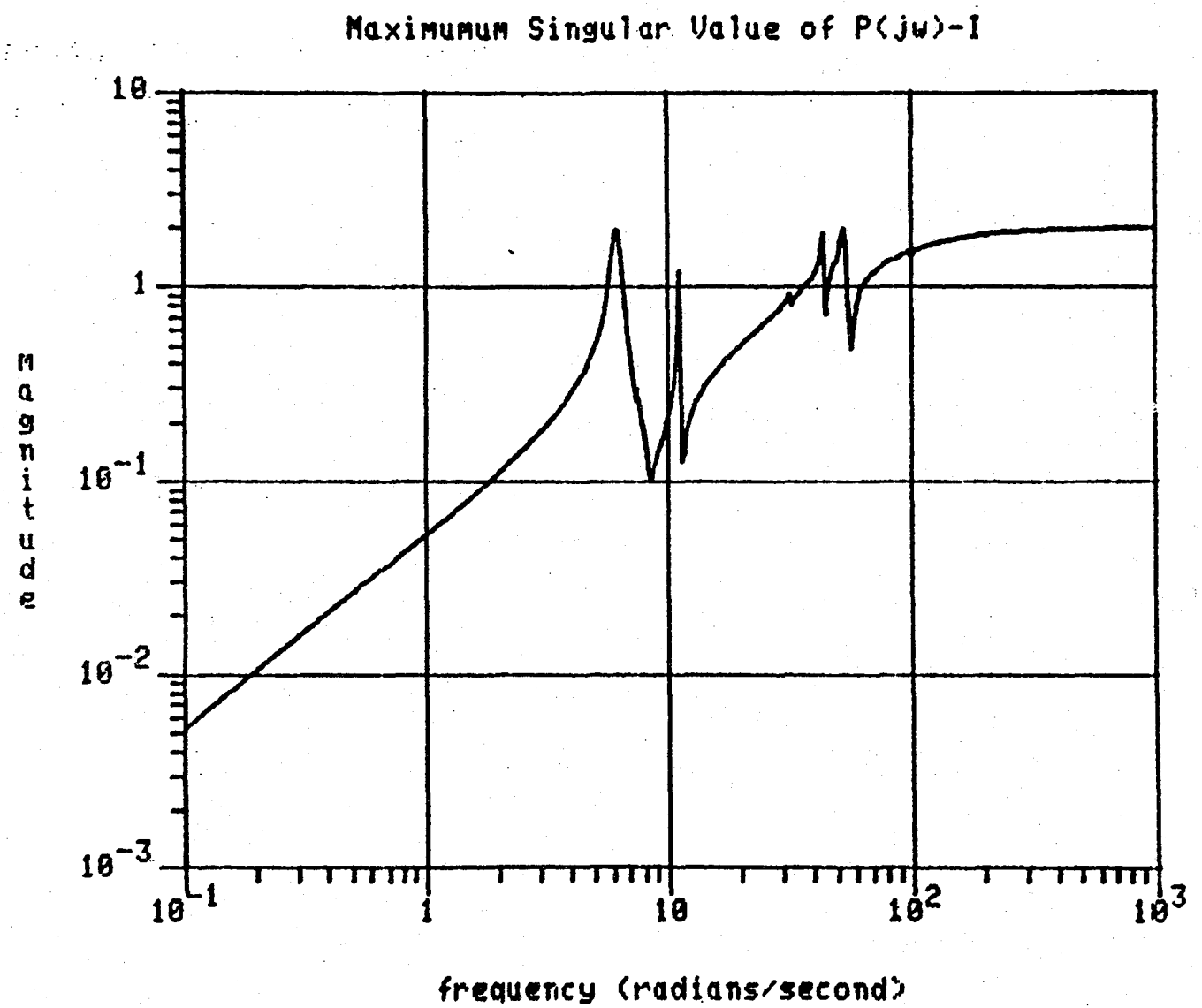

Figure V.20 Bode Plot of the Maximum Singular Value of P(jω) - I

process noise driving the flexible mode states was taken to be zero.

To be more precise let $G_{us}(s) = C(sI-A)^{-1}B$ then the scalar ρ was chosen such that $W_f(s) = C(sI-A)^{-1}\Gamma$ satisfied the high gain constraints of Fig. V.16 where $\Gamma = \rho B$. Then the filter ricatti equation was solved for $P_f > 0$:

$$AP_f + P_f A^T + \Gamma\Gamma^T - P_f C^T C P_f = 0$$

and the filter gain, $K_f = P_f C^T$ was computed. This resulted in the filter loop transfer function $L_f(s) = C(sI-A)^{-1}K_f$ and a Bode plot of the singular values of $L_f(j\omega)$ is shown in Fig. V.21. Note that as discussed in Chapter II this transfer function also satisfies the high gain loop shape constraint, since $W_f(s) = C(sI-A)^{-1}\Gamma$ did.

Plant Order Reduction

The filter loop transfer function was then used to obtain the output closed loop transfer function

$$\begin{aligned} H_o(s) &= L_o(s)[I + L_o(s)]^{-1} \\ &= C(sI-A+K_f C)^{-1}K_f \end{aligned}$$

An initial input weighting was obtained from

$$W_i(s) = G_{us}^{-1}(s)H_o(s)\frac{100}{s+100} \qquad \text{where}$$

the lag at $s = -100$ (actually three lags since $W_i(s)$ is a 3×3 matrix transfer function) was needed such that the initial weighting would be proper.

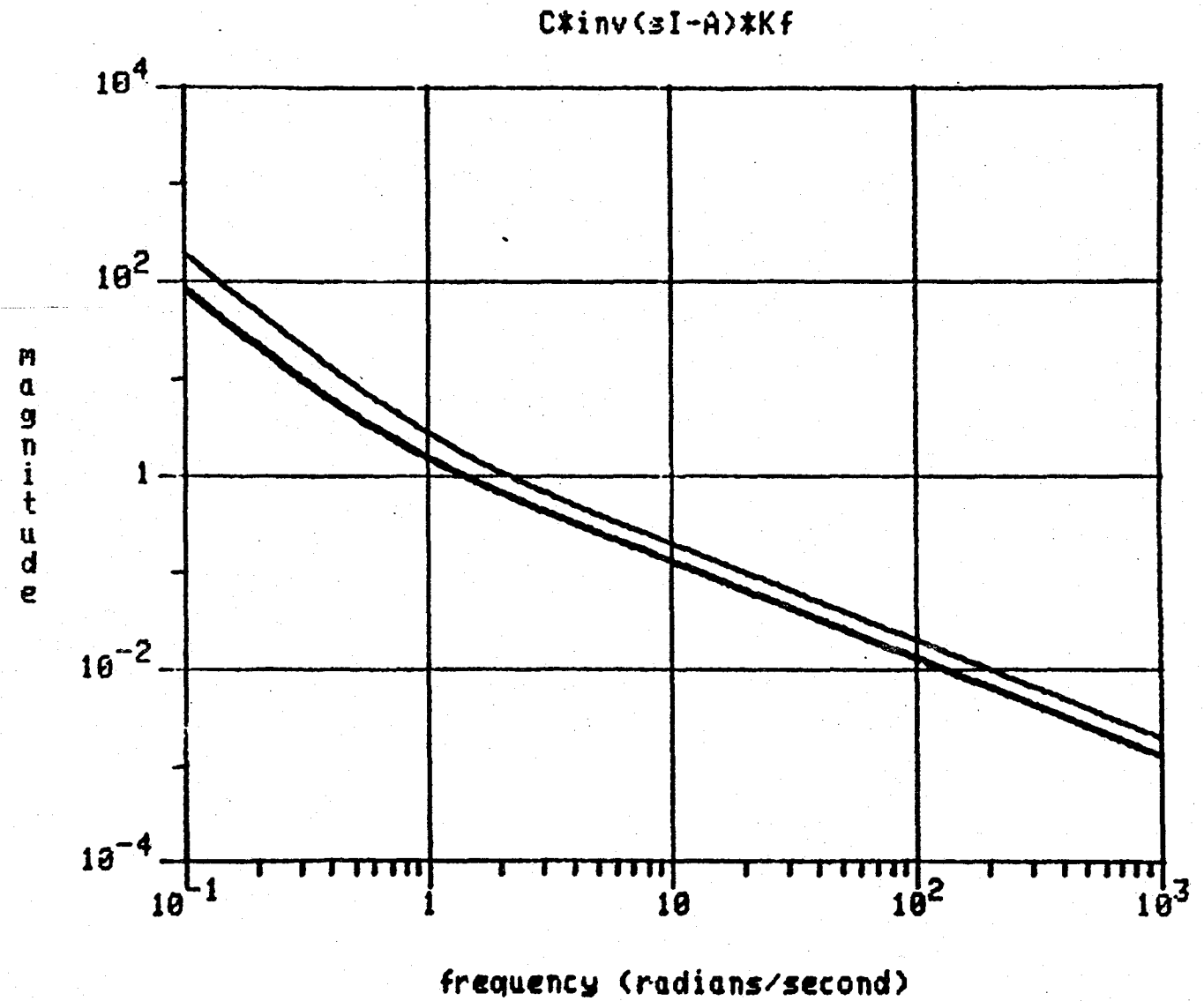

Figure V.21 Bode Plot of the Singular Values of the Filter Loop Transfer Function

The successive approximation solution procedure resulted in a satisfactory 32nd order reduced oder model, $G_r(s)$ of the 58th order $G(s)$. The iterations had not converged after 32 (32nd order and 32 iterations is just a coincidence) iterations but the values of E_∞ were changing very little and hence the process was stopped. The error plot, i.e. $\bar{\sigma}[[G(j\omega) - G_r(j\omega)]\ G_r^{-1}(j\omega)\ H(j\omega)\ ]$ versus ω is shown in Fig. V.22. Note that E_∞ is less than one and thus a satisfactory design based on $G_r(s)$ is expected. A Bode plot of the singular values of $G_r(j\omega)$ is shown in Fig. V.23.

Recall that the model reduction algorithm produces a reduced order model, $G_{sr}(s)$ of $G_s(s)$ and that $G_r(s)$ is obtained from

$$G_r(s) = G_{sr}(s) + G_{us}(s) \quad .$$

A realization of $G_{sr}(s)$ is given by

$$G_{sr}(s) = C_1(sI - A_{11})^{-1} B_1 \quad .$$

Letting

$$\bar{A} \triangleq \begin{bmatrix} A & 0 \\ 0 & A_{11} \end{bmatrix} \qquad \bar{B} \triangleq \begin{bmatrix} B \\ B_1 \end{bmatrix}$$

$$\bar{C} \triangleq [C \quad C_1]$$

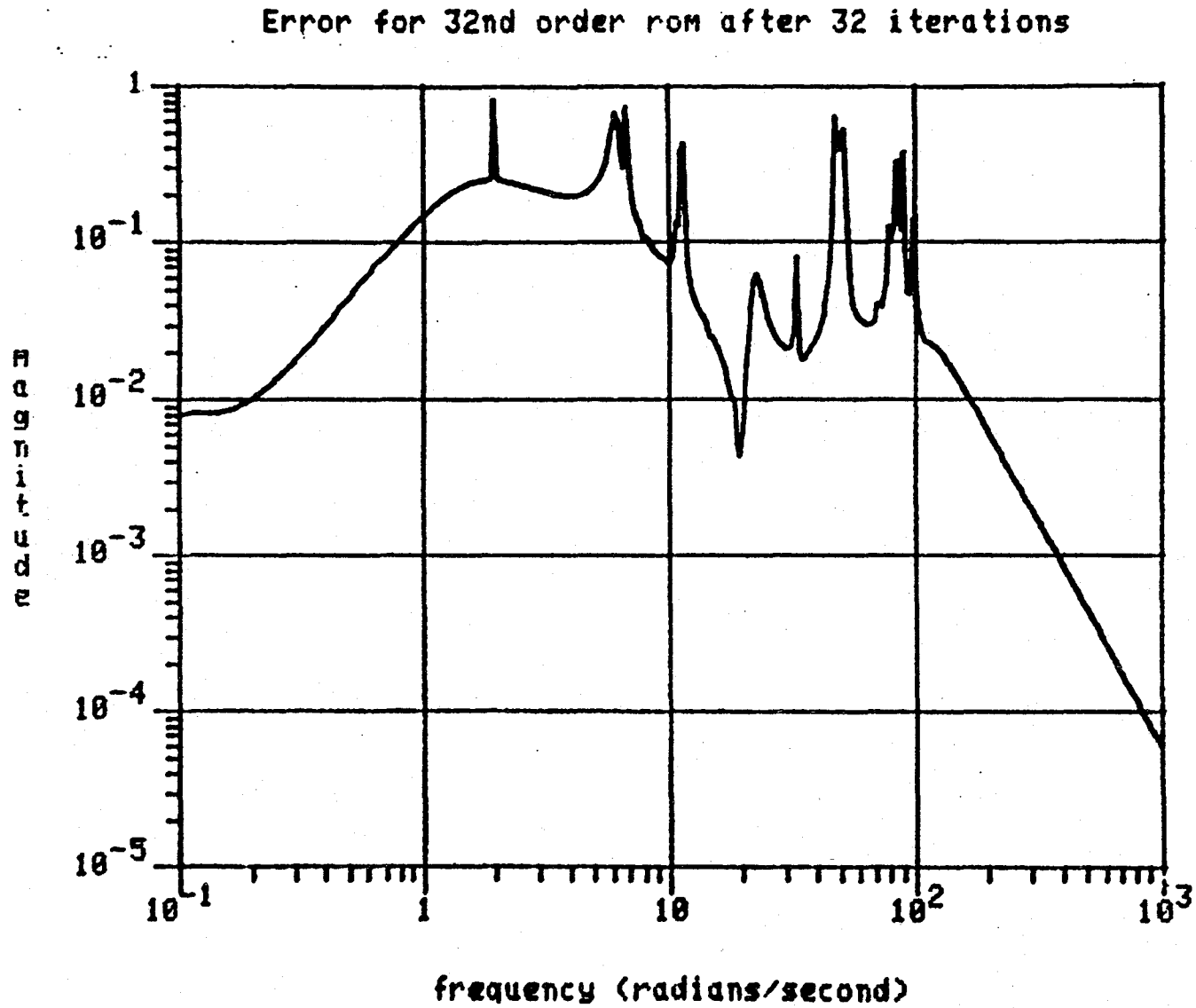

Figure V.22 Error Plot For 32nd Order Reduced Order Model of 58th Order Full Order Model

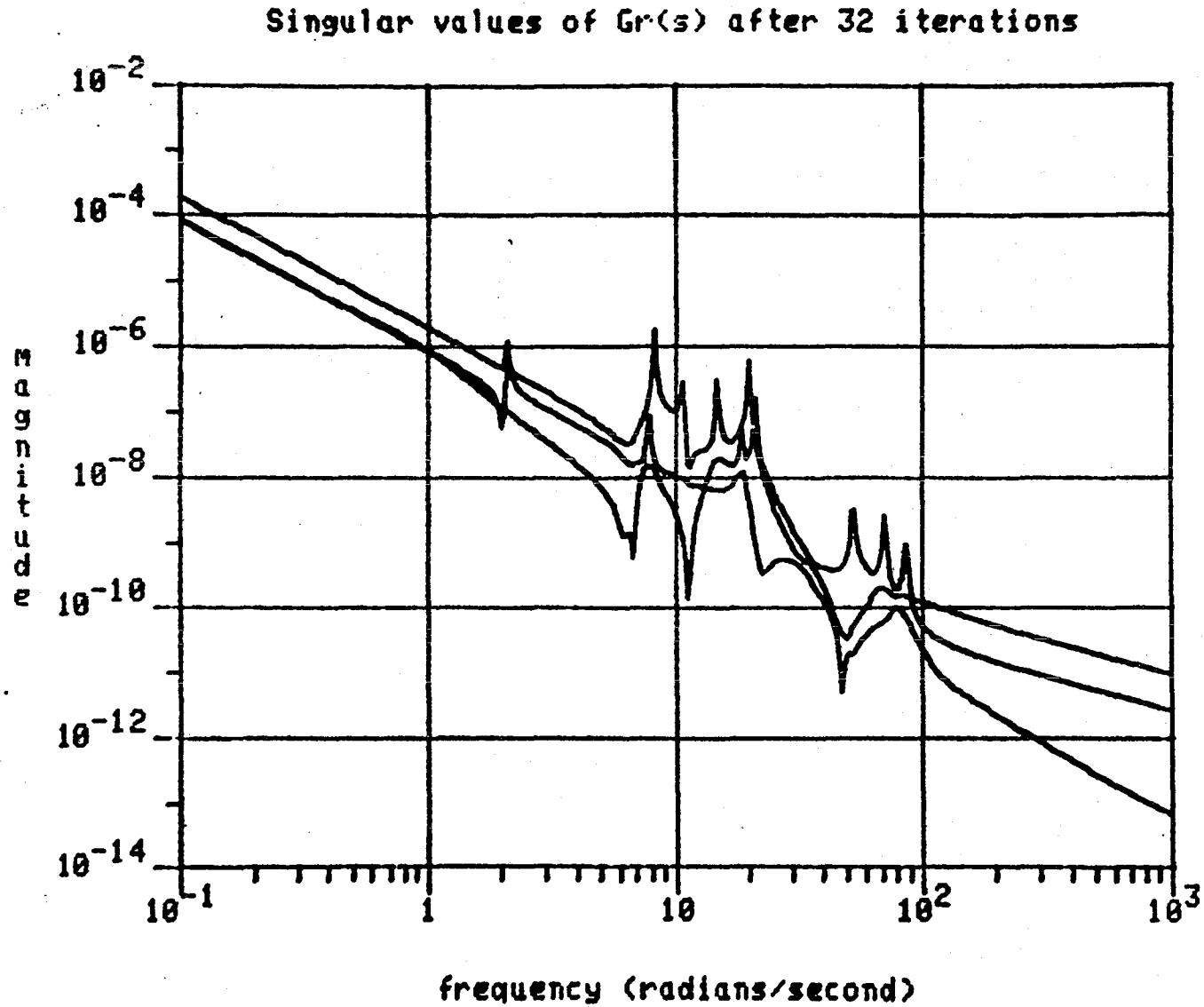

Figure V.23 Bode Plot of the Singular Values of $G_r(j\omega)$

we have

$$G_r(s) = \overline{C}(sI-\overline{A})^{-1}\overline{B} \quad .$$

Final Design Steps

To complete the design of the compensator, $K(s)$ the filter loop transfer function $L_f(s) = C(sI-A)^{-1}K_f$ is recovered with the remaining steps of Table II.4. That is the regulator Riccati equation is solved for $\overline{P}_c > 0$:

$$\overline{A}^T\overline{P}_c + \overline{P}_c\overline{A} + q^2\overline{C}^T\overline{C} - \overline{P}_c\overline{B}\overline{B}^T\overline{P}_c = 0$$

and the regulator gain is obtained from

$$\overline{K}_c = \overline{B}^T\overline{P}_c \quad .$$

The scalar q was chosen large enough to satisfy the loop shape constraints of Fig. V.16.

Finally the compensator transfer function is given by

$$K(s) = \overline{K}_c(sI-\overline{A}+\overline{B}\overline{K}_c+\overline{K}_f\overline{C})^{-1}\overline{K}_f$$

where

$$\overline{K}_f \triangleq \begin{bmatrix} K_f \\ 0 \end{bmatrix} \quad .$$

A Bode plot of the singular values of $K(j\omega)$ is shown in Fig. V.24. Note that the overall shape is that of the familiar lead compensator. Note also that considerable notch filtering is going on (i.e. plant inversion). The sensitivity of

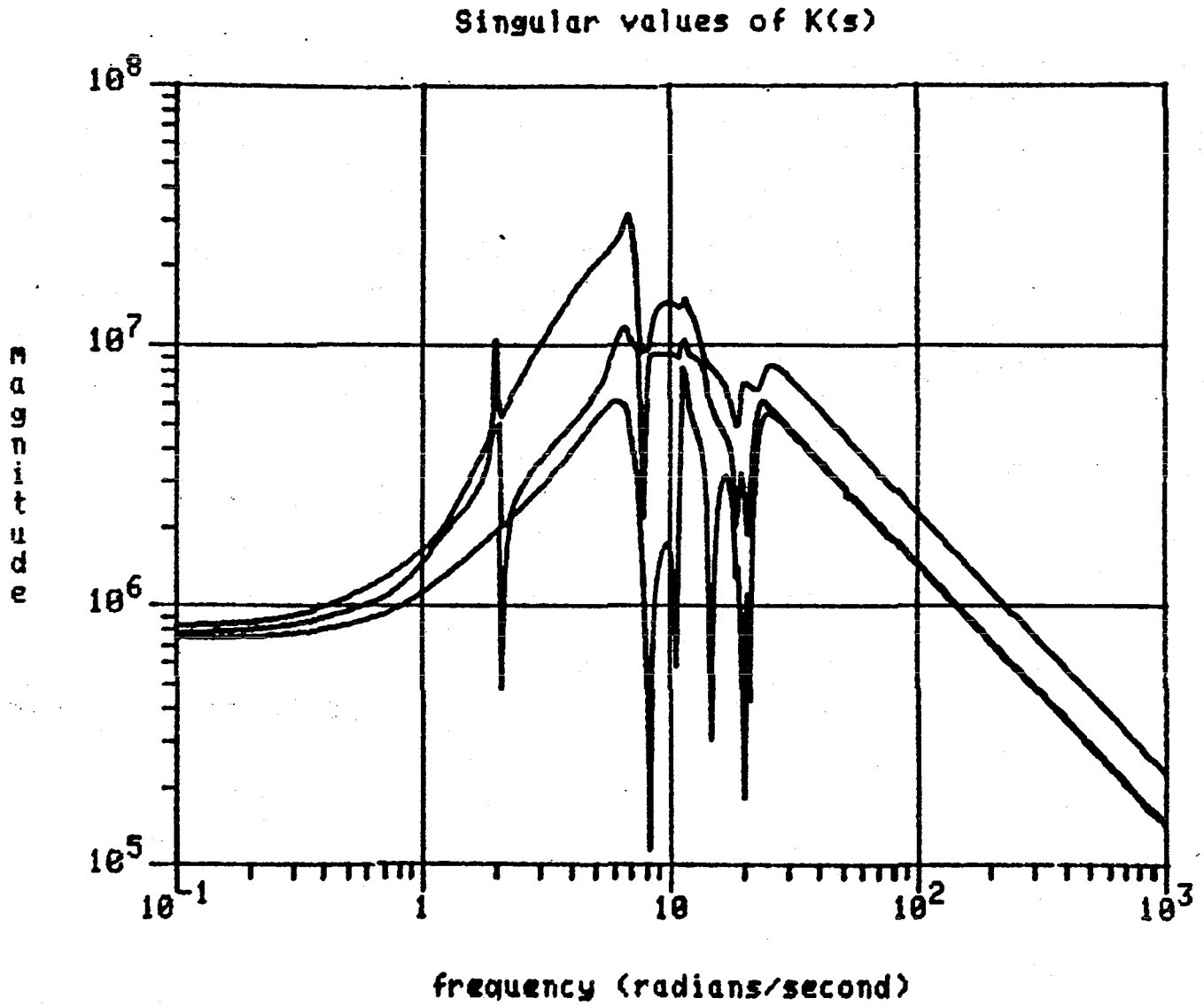

Figure V.24 Bode Plot of the Singular Values of K(jω)

this plant inversion is an issue. Hence an analysis is presented in Appendix E for how accurately the resonant frequencies must be known to guarantee closed loop stability.

Verification of Stability

Well the compensator is certainly closed loop stable with the reduced order model, $G_r(s)$ (it is an LQG design). However the stability with the actual system $G_{84}(s)$ must still be ascertained. The stability of the compensator, $K(s)$ with the 58th order non-minimum phase model, $G_{29}(s)$ was verified with an eigenvalue check (results are tabulated in App. E). Finally the stability of the compensator, $K(s)$ with $G_{84}(s)$ was verified by checking that

$$\| \left[G_{84}(s) - G_{29}(s) \right] K(s) \left[I + G_{29}(s)K(s) \right]^{-1} \|_\infty < 1 \quad .$$

This is just the stability robustness theorem of Chapter II applied to this problem. A plot of $\bar{\sigma}[[G_{84}(j\omega) - G_{29}(j\omega)]\, K(j\omega)[I + G_{29}(j\omega)K(j\omega)]^{-1}\,]$ versus ω is shown in Fig. V.25. Note that its peak value is less than one and thus the closed loop system is stable with the full order model, $G_{84}(s)$.

It remains to verify that the neglected actuator dynamics do not cause an instability. This can also be verified with the stability robustness theorem of Chapter II. In this case the following inequality must be satisfied

$$\underline{\sigma}\left[I + [K(j\omega)G_{84}(j\omega)]^{-1} \right] > l_{act}(\omega) \qquad \forall\omega \quad .$$

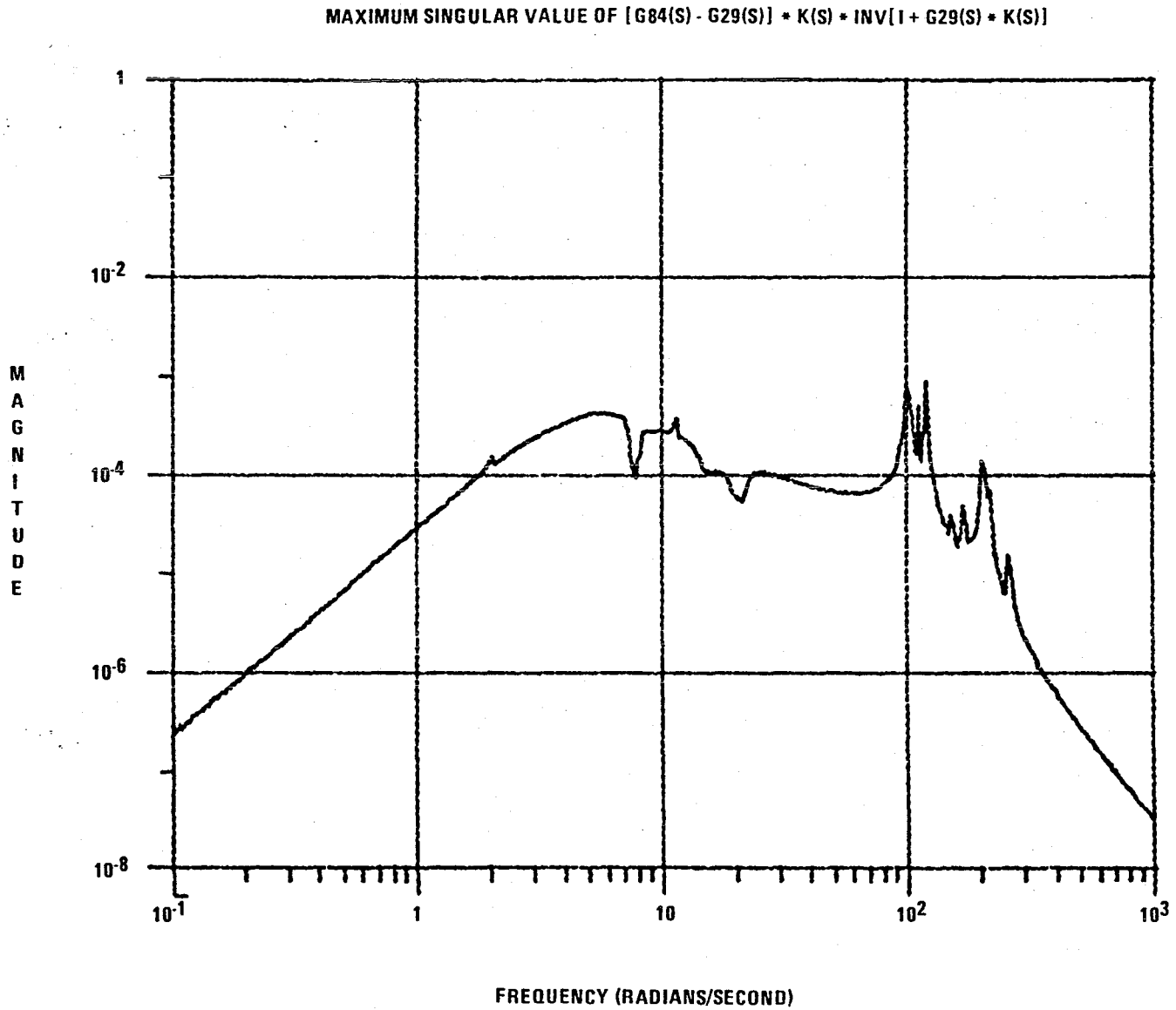

Figure V.25 Bode Plot of the Maximum Singular Value of $[G_{84}(j\omega) - G_{29}(j\omega)]K(j\omega)[I + G_{29}(j\omega)K(j\omega)]^{-1}$

By comparing the plot of $\underline{\sigma}\left[I + [K(j\omega)G_{84}(j\omega)]^{-1}\right]$ versus ω shown in Fig. V.30 to the plot of $l_{act}(\omega)$ shown in Fig. V.18, it can be verified that this condition is satisfied.

In conclusion with regard to stability, the 32nd order compensator is closed loop stable with the 168th order full order model $G_{84}(s)$ in the presence of the actuator uncertainty.

Verification of the Other Loop Requirements

Bode plots for the input loop transfer function, $K(s)G_{84}(s)$ and the output loop transfer function, $G_{84}(s)K(s)$ are shown in Figs. V.26 and 27 respectively. By comparing these plots to the constraints of Fig. V.16 it can be seen that the low and high frequency constraints are satisfied but the mid frequency constraint with negative one slope is not. Recall that this constraint was imposed for stability requirements due to the minimum phase approximation used for design. Since stability was checked and found to be satisfactory (i.e. stable closed loop system) violation of this constraint is of no concern.

Bode plots of the input return difference, $I + K(s)G(s)$ and the output return difference $I + G(s)K(s)$ are shown in Figs. V.28 and 29 respectively. Recall that the loop shape constraints required that the minimum singular value of these return differences be greater than 0.5 for all frequencies. It can be seen

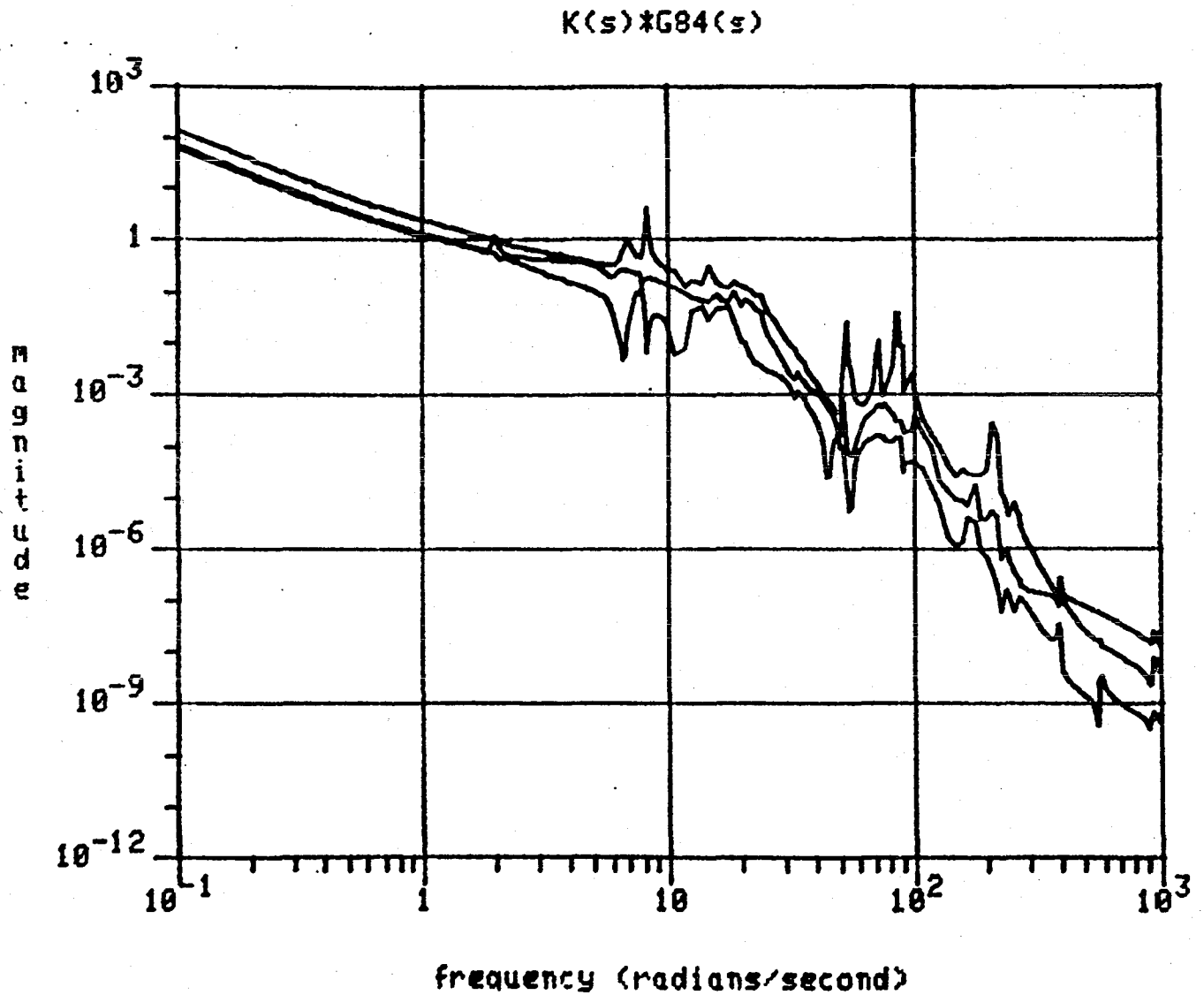

Figure V.26 Bode Plot of the Singular Values of $K(j\omega)G_{84}(j\omega)$

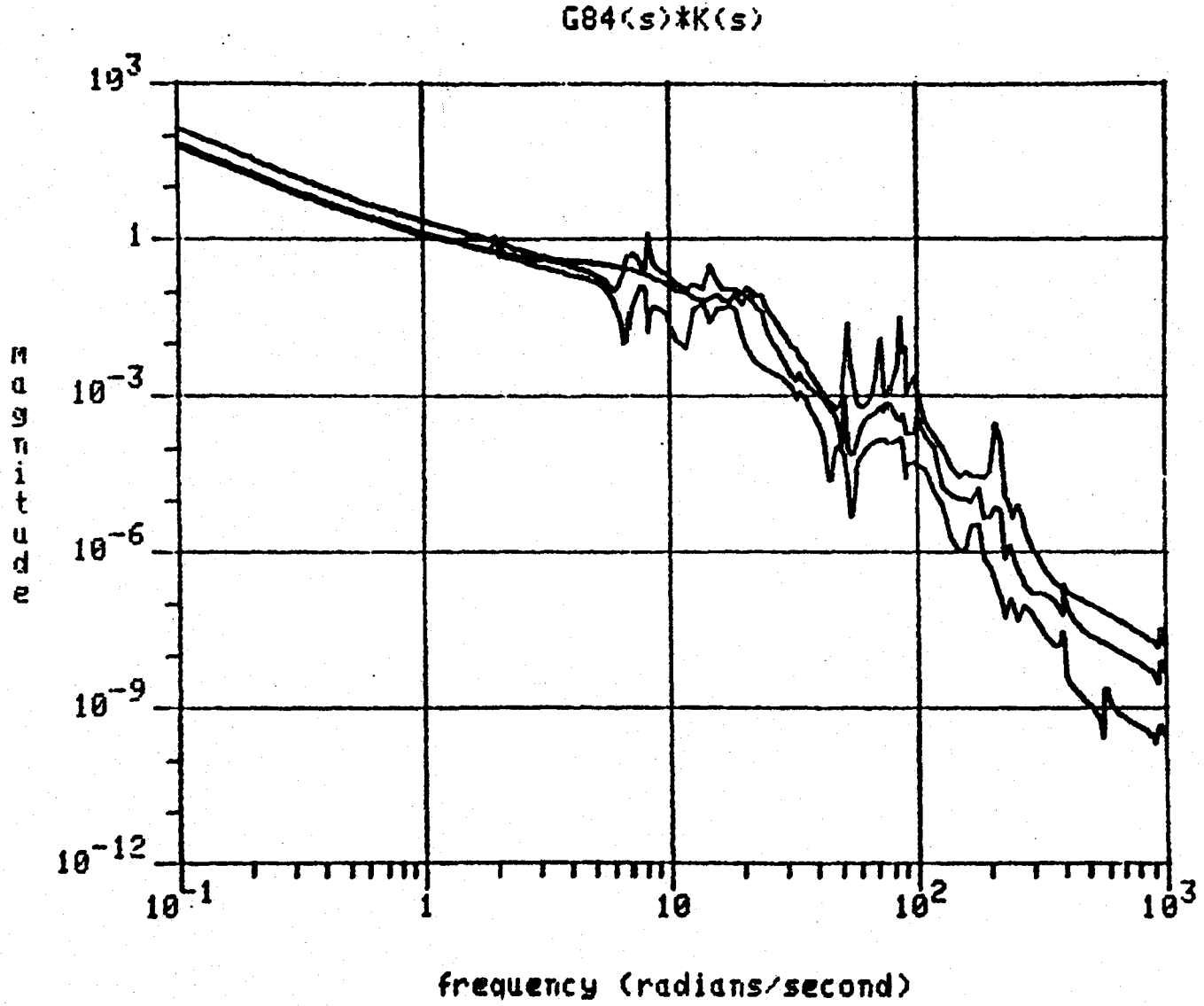

Figure V.27 Bode Plot of the Singular Values of $G_{84}(j\omega)K(j\omega)$

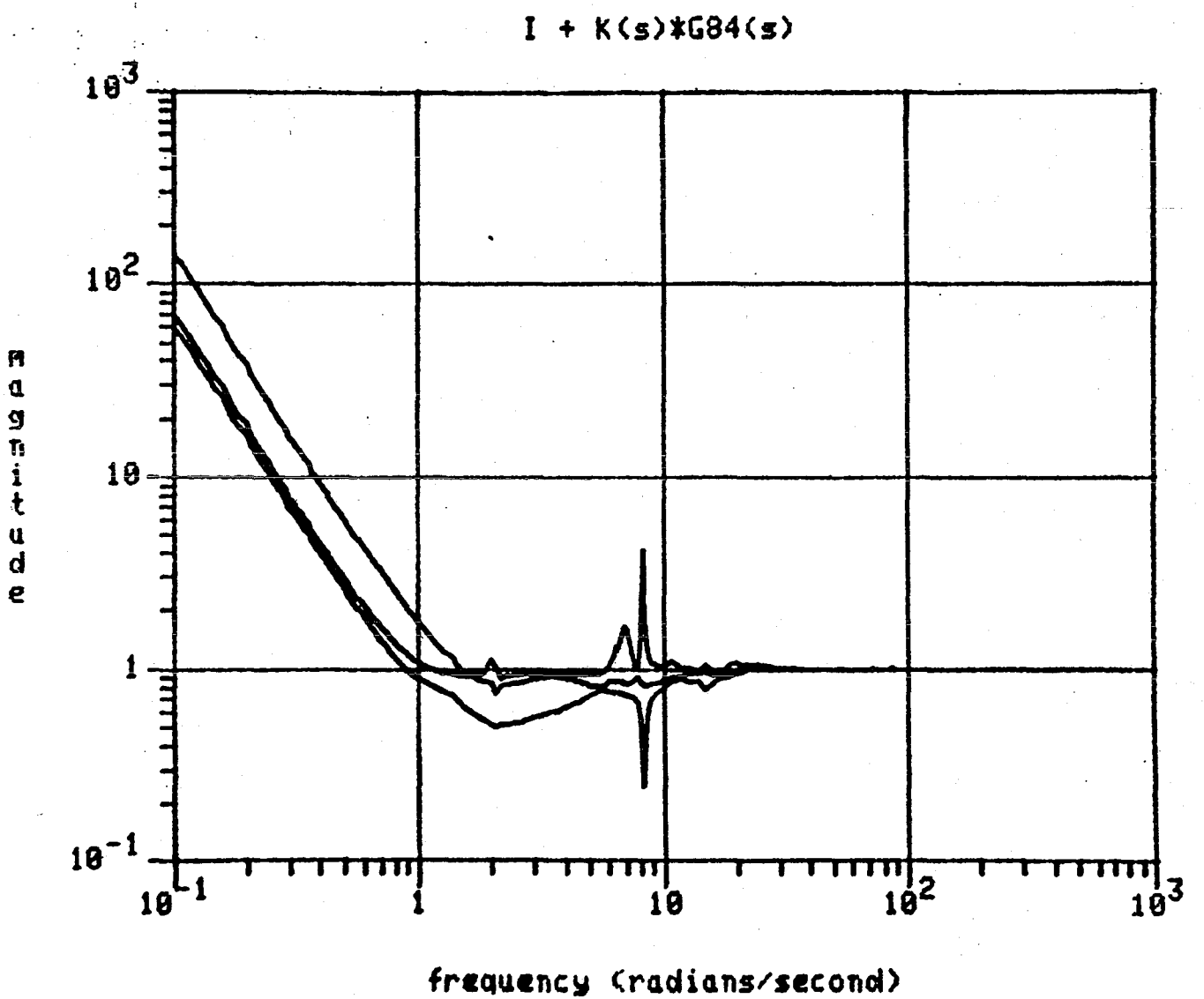

Figure V.28 Bode Plot of the Singular Values of $I + K(j\omega)G_{84}(j\omega)$

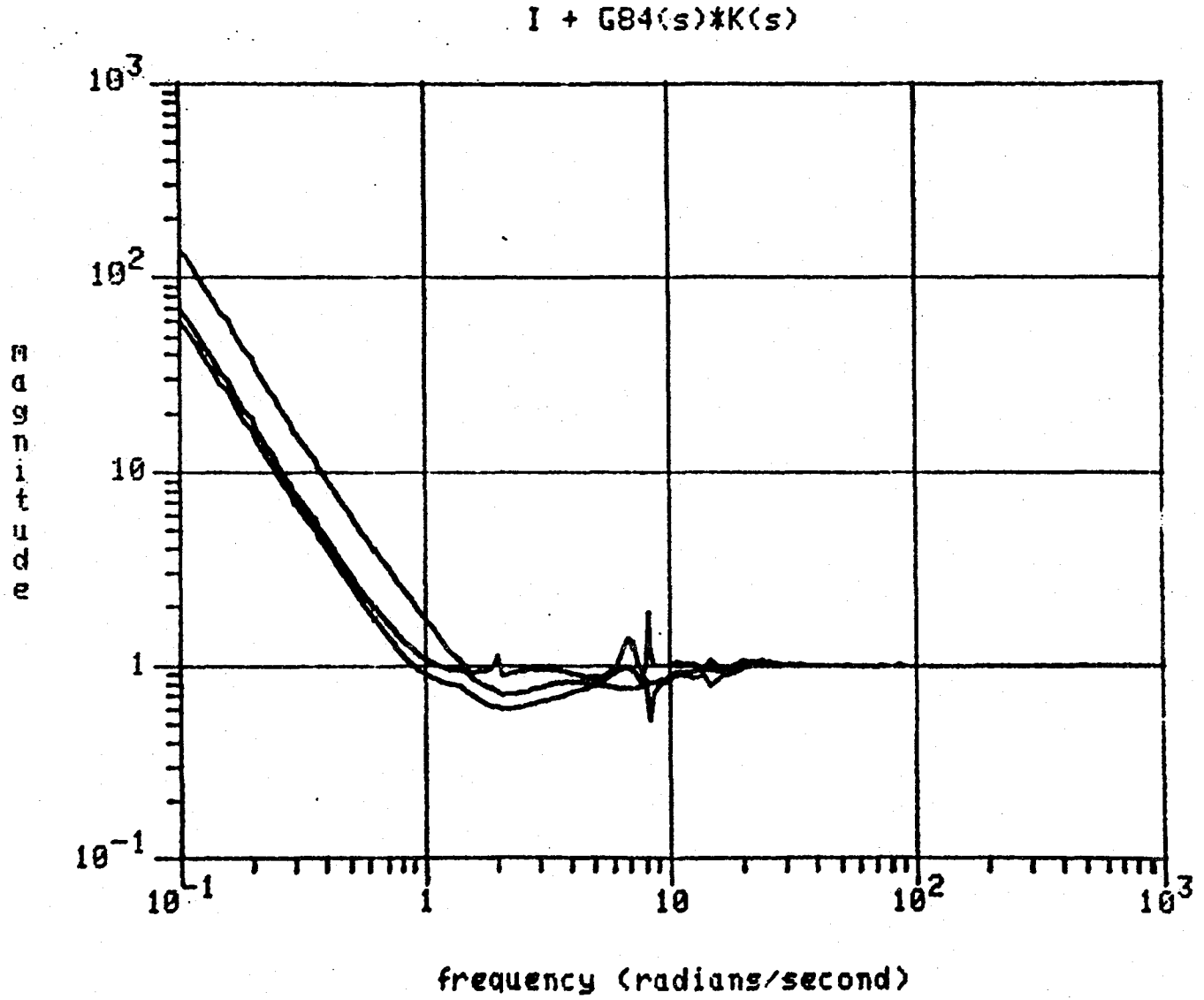

Figure V.29 Bode Plot of the Singular Values of $I + G_{84}(j\omega)K(j\omega)$

from the plots that while the output return difference satisfies this constraint, the input return difference is in violation of the constraint for a narrow band of frequencies near 8 rad/sec.

Similar remarks apply to the input inverse-return difference, $I + [K(s)G(s)]$-1 and the output inverse-return difference $I + [G(s)K(s)]^{-1}$ with Bode plots shown in Figs. V.30 and 31 respectively.

Note that the input loop properties are not as good as the output loop properties. This is a consequence of the LQG loop shaping design methodology. That is the desirable properties of the output loop were designed formally (i.e. 2nd column of Table II.4 and Table IV.7) but the input loop properties are just a consequence of the design.

Step Responses

Time histories (see App. E) were computed for step commands and were found to compare favorably with expected results based on the performance specification.

Conclusions For ACOSS Design

The plant order reduction and reduced order compensator design methodology of Chapter IV has been shown to be effective on a realistic, high order design example.

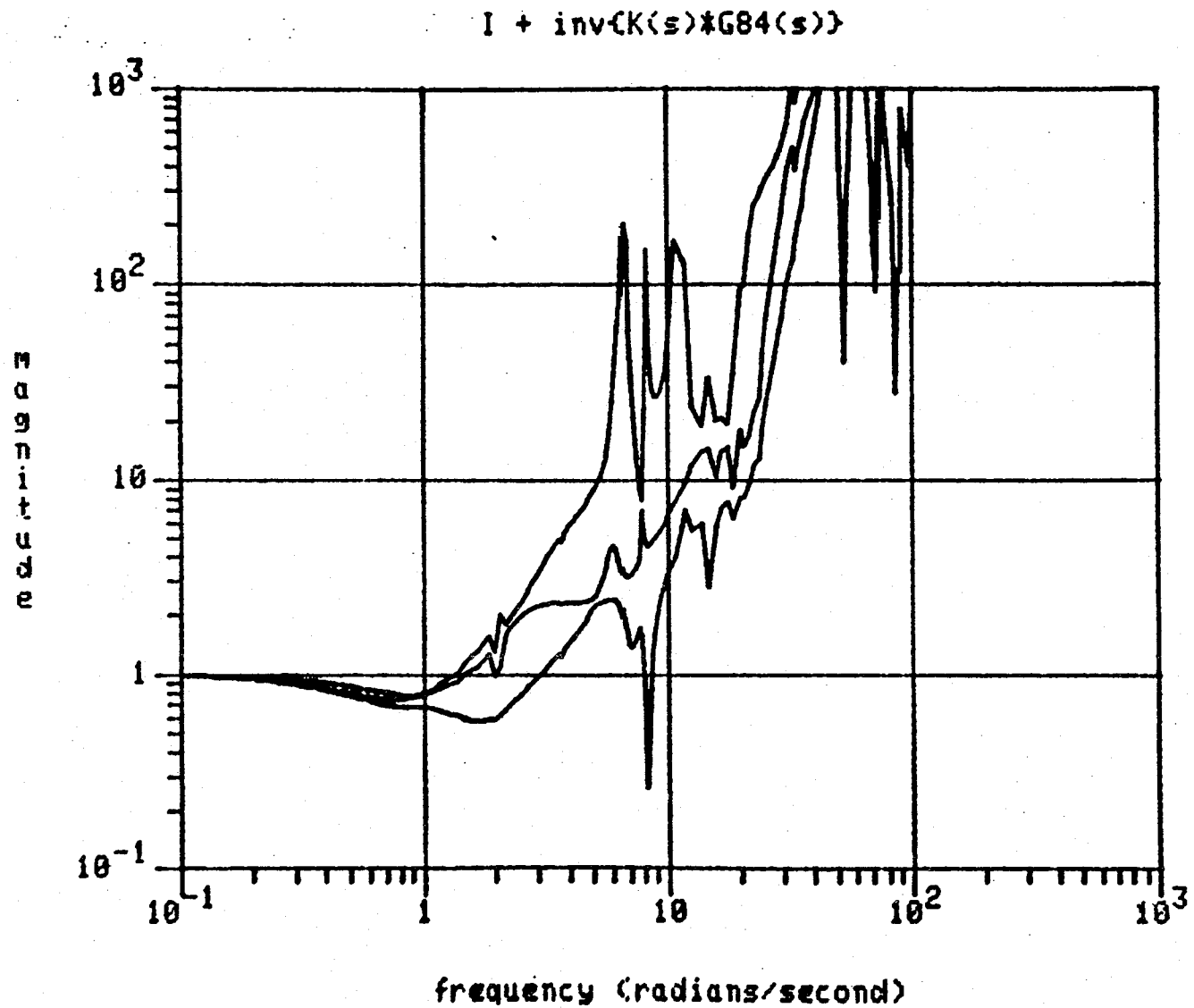

Figure V.30 Bode Plot of the Singular Values of $I + [K(j\omega)G_{84}(j\omega)]^{-1}$

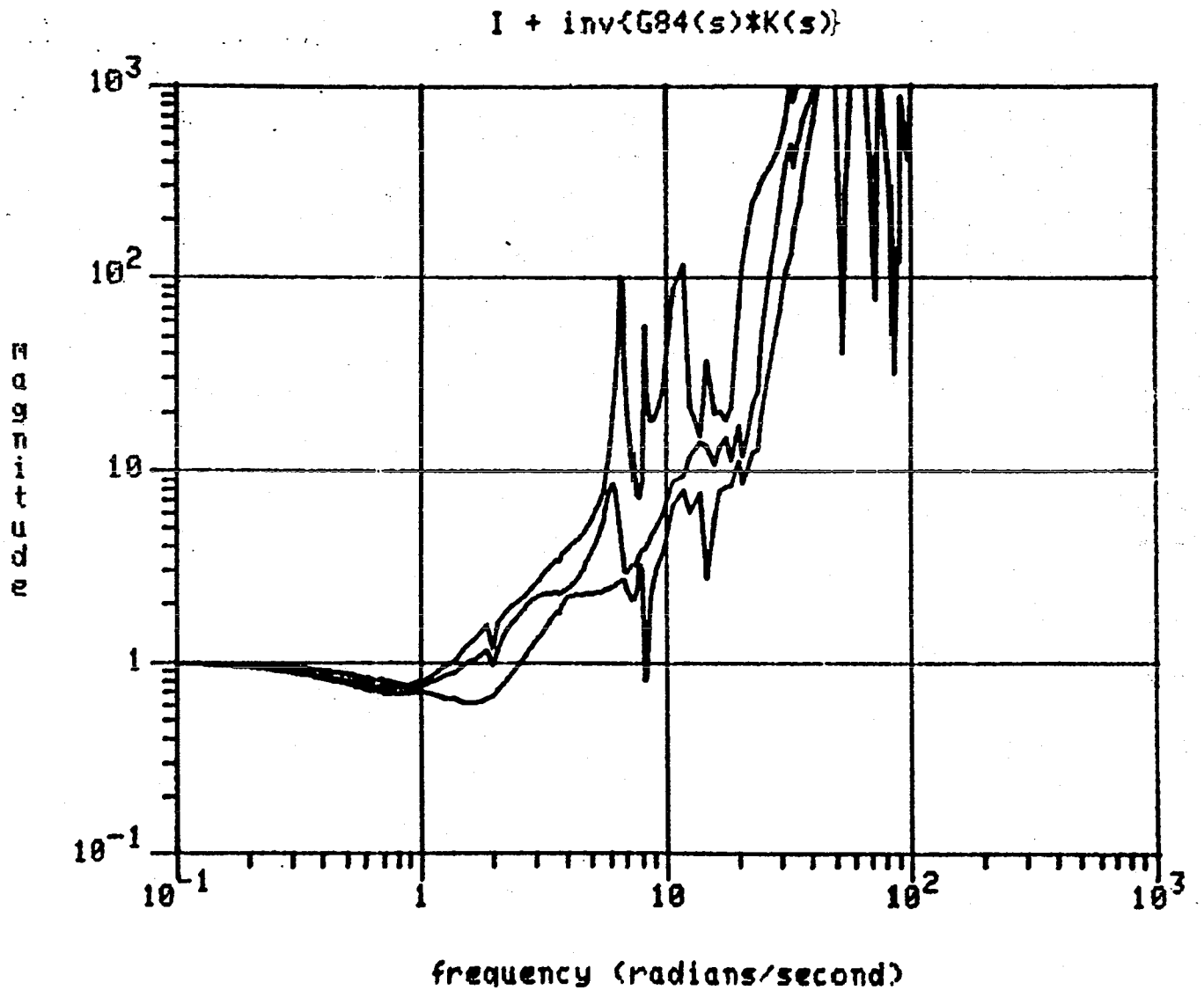

Figure V.31 Bode Plot of the Singular Values of $I + [G_{84}(j\omega)K(j\omega)]^{-1}$

VI. CONCLUSIONS AND RECOMMENDATIONS FOR FURTHER RESEARCH

Conclusions

The major conclusion of this thesis is that model reduction and control design, which have long been treated tacitly as independent design steps, can be successfully interrelated through a formal design process developed in the thesis.

The formal process combines frequency weighted model reduction with modern linear quadratic gaussian loop shaping design. The model reduction approach involves a frequency weighted error between the full and reduced order model. An important point is that the size of this error is measured by the peak value of its frequency response. This criterion is important because it enables the size of the model reduction error and closed loop stability to be related by appropriate choice of frequency weightings.

Internally balanced realizations were investigated and found to have desirable properties as a model reduction tool. A new theoretical result for bounding the peak value of the error frequency response was obtained. The balancing mechanics was extended to include frequency dependent weightings. Appropriate weightings for control system design were derived.

Several example problems demonstrated the effectiveness of the model reduction technique for obtaining successful control designs. The examples illustrate that the frequency weightings and peak value error criterion are critical

for non-trivial model reduction problems. For trivial (i.e. near pole-zero cancellations, small residues, modes with frequencies far beyond control bandwidth) model reduction problems any reasonable model reduction method will give acceptable results.

Recommendations For Further Research

There are always some open questions left at the end of a research endeavor. Some of the open questions of this thesis and the author's comments regarding them are:

1. Are reduced order models obtained from frequency weighted balanced realizations asymptotically stable if both the input and output weightings are non-unity? The author believes that they are stable (possibly a weak condition on the weightings is required, say no transmission zeros on the $j\omega$ axis).

2. Can a simple error bound for frequency weighted balanced realizations be proved? The author's opinion is that this is hopeless.

3. Would a scalar transfer function times an identity used as an input weighting produce the same reduced order model if it were used as an output weighting? Intuitively the answer is yes and a proof should be possible.

4. Can the theoretical properties of the plant order reduction fixed point problem be established (existence and uniqueness of solutions)? The author's opinion is that solutions do exist and probably more than one in many cases.

5. What are the similarities and differences of plant and compensator order reduction in terms of the resulting control system design? It would be pleasing if the results were the same but the author's opinion is that they won't be the same.

6. Can the Hankel results be generalized to include the frequency dependent weightings? Certainly a weighted Hankel model reduction can be done. The interesting question is: can an error bound be proved?

7. Can the plant order reduction problem be solved with something other than the linear quadratic gaussian synthesis procedure? Combining the model reduction ideas with the recent results in H_∞ optimization is a fruitful area for several Ph.D. dissertations.

8. Can better numerical algorithms for solving the model reduction problem be obtained? Any progress in this area would be of great value to the practicing control engineer.

9. Can model reduction weightings be chosen for purposes other than guaranteeing closed loop stability? Certainly weightings can be chosen for other purposes e.g. to satisfy performance objectives.

REFERENCES

1. Bryson, A. E. and Y-C. Ho, *Applied Optimal Control,* John Wiley & Sons, New York, 1975.

2. Kwakernaak, H. and R. Sivan, *Linear Optimal Control Systems,* John Wiley & Sons, New York, 1972.

3. Athans, M. and P. L. Falb, *Optimal Control,* McGraw Hill Inc., New York, 1966.

4. Anderson, B. D. O. and J. B. Moore, *Linear Optimal Control,* Prentice-Hall Inc., New Jersey, 1971.

5. Doyle, J.C., "Advances in Multivariable Control," Proc. of the Office of Naval Research/Honeywell Workshop on Advances in Multivariable Control, Oct. 1984.

6. Genesio, R. and M. Milanese, "A Note on the Derivation and Use of Reduced-Order Models," *IEEE Transactions on Automatic Control,* Vol. AC-21, Feb. 1976.

7. Wilson, D. A., "Optimum Solution of Model Reduction Problem," *Proc. IEE,* Vol. 117, June 1970.

8. Wilson, D. A., "Model Reduction for Multivariable Systems," *International Journal of Control,* Vol. 20, 1974.

9. Skelton, R. E., "Cost-Decomposition of Linear Systems with Application to Model Reduction," *International Journal of Control,* Vol. 32, Dec. 1980.

10. Meier, Lewis, III and D. G. Luenberger, "Approximation of Linear Constant Systems," *IEEE Transactions on Automatic Control,* Vol. AC-12, Oct. 1967.

11. Moore, B. C., "Principal Component Analysis in Linear Systems: Controllability, Observability and Model Reduction," *IEEE Transactions on Automatic Control,* Vol. AC-26, Feb. 1981.

12. Adamjan, V. M., D. Z. Arov, and M. G. Krein, "Analytic Properties of Schmidt Pairs for a Hankel Operator and the Generalized Schur-Takagi Problem," *Math. USSR Sbornik,* Vol. 15, 1971.

13. Kung, S-Y. and D. W. Lin, "Optimal Hankel-Norm Model Reductions: Multivariable Systems," *IEEE Transactions on Automatic Control,* Vol. AC-26, Aug. 1981.

14. Bettayeb, M., L. M. Silverman, and M. G. Safonov, "Optimal Approximation of Continuous-Time Systems," *Proc. of the 19th IEEE Conference on Decision and Control,* Vol. 1, Dec. 1980.

15. Glover, K. and D. J. N. Limebeer, "Robust Multivariable Control System Design Using Optimal Reduced Order Plant Models," *Proc. American Control Conference,* Vol. 2, June 1983.

16. Stein, G. and J. C. Doyle, "Singular Values and Feedback: Design Examples," *Proc. 16th Allerton Conference on Communication, Control and Computing,* Oct. 1980.

17. Doyle, J. C., "Analysis of Feedback Systems with Structured Uncertainties," *Proc. IEE,* Vol. 129, Nov. 1982.

18. Doyle, J. C., J. E. Wall, and G. Stein, "Performance and Robustness Analysis for Structured Uncertainty," *Proc. of the 21st IEEE Conference on Decision and Control,* Vol. 2, Dec. 1982.

19. Doyle, J. C. "Synthesis of Robust Controllers and Filters," *Proc. of the 22nd IEEE Conference on Decision and Control,* Vol. 1, Dec. 1983.

20. Wall, J. E., J. C. Doyle, G. L. Hartmann, N. A. Lehtomaki, and G. Stein, "Performance and Robustness Aspects of Digital Control Systems," *AGARD Lecture Series No. 128: Computer-Aided Design and Analysis of Digital Guidance and Control Systems,* Sept. 1983.

21. Cruz, J. B. and W. R. Perkins, "A New Approach to the Sensitivity Problem in Multivariable Feedback System Design," *IEEE Transactions on Automatic Control, Vol. AC-9, July 1964.*

22. Doyle, J. C. "Limitations on Achievable Performance of Multivariable Feedback Systems," *AGARD Lecture Series No. 117: Multi-Variable Analysis and Design Techniques,* Sept.-Oct., 1981.

23. Bode, H. W., *Network Analysis and Feedback Amplifier Design,* D. Van Nostrand, Princeton, 1945.

24. Doyle, J. C. and G. Stein, "Multivariable Feedback Design: Concepts for a Classical/Modern Synthesis," *IEEE Transactions on Automatic Control,* Vol. AC-26, Feb. 1981.

25. Harvey, C. A. and G. Stein, "Quadratic Weights for Asymptotic Regulator Properties," *IEEE Transactions on Automatic Control,* Vol. AC-23, June 1978.

26. Gupta, N. K., "Frequency-Shaped Cost Functionals: Extension of Linear-Quadratic-Gaussian Designs Methods," *Journal of Guidance and Control,* Vol. 3, Nov.-Dec. 1980.

27. Safonov, M. G. and M. Athans, "Gain and Phase Margin for Multiloop LQG Regulators," *IEEE Transactions on Automatic Control,* Vol. AC-22, April 1977.

28. Lehtomaki, N. A., N. R. Sandell, Jr. and M. Athans, "Robustness Results in Linear-Quadratic Gaussian Based Multivariable Control Designs," *IEEE Transactions on Automatic Control,* Vol. AC-26, Feb. 1981.

29. Horowitz, I. M., *Synthesis of Feedback Systems,* Academic Press, New York, 1963.

30. Doyle, J. C. and G. Stein, "Robustness with Observers," *IEEE Transactions on Automatic Control,* Vol. AC-24, Aug. 1979.

31. Wall, J. E., J. C. Doyle, and C. A. Harvey, "Tradeoffs in the Design of Multivariable Feedback Systems," *Proc. 18th Allerton Conference on Communication, Control and Computing,* Oct. 1980.

32. Gangsaas, D., U. Ly, and D. C. Norman, "Practical Gust Load Alleviation and Flutter Suppression Control Laws Based on a LQG Methodology," Paper: AIAA-81-0021 presented at AIAA 19th Aerospace Sciences Meeting, Jan. 1981.

33. Moore, J. B., D. Gangsaas, and J. D. Blight, "Performance and Robustness Trades in LQG Regulator Design," *Proc. of the 20th Conference on Decision and Control,* Vol. 3, Dec. 1981.

34. Kailath, T., *Linear Systems,* Prentice Hall, New Jersey, 1980.

35. Brockett, R., *Finite Dimensional Linear Systems,* John Wiley and Sons, New York, 1970.

36. Pernebo, L. and L. M. Silverman, "Model Reduction via Balanced State Space Representations," *IEEE Transactions on Automatic Control,* Vol. AC-27, April 1982.

37. Stewart, G. W. *Introduction to Matrix Computations,* Academic Press, New York, 1973.

38. Martin, G. D. "On the Control of Flexible Mechanical Systems," Ph.D. dissertation, Dept. of Aeronautics and Astronautics, Stanford University, SUDAAR 511, May 1978.

39. Jonckheere, E. A., M. G. Safonov, and L. M. Silverman, "Topology Induced By the Hankel Norm in the Space of Transfer Matrices," *Proc. of the 20th Conference on Decision and Control,* Vol. 1, Dec. 1981.

40. Jonckheere, E. A. and L. M. Silverman, "Singular Value Analysis of Deformable Systems," *Proc. of the 20th Conference on Decision and Control,* Vol. 2, Dec. 1981.

41. Gregory, C. Z. Jr., "Reduction of Large Flexible Spacecraft Models Using Internal Balancing Theory," *AIAA Guidance and Control Conference,* AIAA No. 83-2292, Aug. 1983.

42. Bernard, D.E., "Control System Design for Lightly Coupled Large Space Structures," Ph.D. dissertation, Dept. of Aeronautics and Astronautics, Stanford University, January 1985.

43. Luenberger, D. G., *Optimization By Vector Space Methods,* John Wiley and Sons, New York, 1969.

44. Anderson, B. D. O. "An Algebraic Solution to the Spectral Factorization Problem," *IEEE Transactions on Automatic Control,* Vol. AC-12, Aug. 1967.

45. Rosenthal, D.E., "Experiments in Control of Flexible Structures With Uncertain Parameters," Ph.D. dissertation, Dept. of Aeronautics and Astronautics, Stanford University, SUDAAR 542, March 1984.

46. Harvey, C. A. and R. E. Pope, "Insensitive Control Technology Development," NASA Contractor Report 2947, Feb. 1978.

47. Barrett, M. F. and D. F. Enns, "Maximum Likelihood Identification For Large Space Structures," Paper: AIAA No. 83-2243 CP presented at AIAA Guidance and Control Conference, Aug. 1983.

48. Strunce, R. R., et al, "Active Control of Space Structures," C. S. Draper Laboratory Interim Report No. RK-1404, Contract No. F30602-80-C-0096, Sept. 1980.

APPENDIX A

SINGULAR VALUES

The singular values of a complex, $n \times m$ matrix, A are denoted by $\sigma_i[A]$ (or just σ_i when context permits) and are defined to be the k largest, nonnegative square roots of the eigenvalues of $A^H A$ (or equivalently AA^H) where $k = \min(n,m)$. That is

$$\sigma_i[A] \triangleq \lambda_i^{1/2}[A^H A] \qquad i = 1, 2, \ldots, k$$

and the ordering is such that $\sigma_i \geq \sigma_{i+1}$.

The maximum and minimum singular values of A, denoted by $\bar{\sigma}[A]$ and $\underline{\sigma}[A]$ respectively are equivalently given by

$$\bar{\sigma}[A] = \max_{x \neq 0} \frac{||Ax||}{||x||} = \max_{||x||=1} \frac{||Ax||}{||x||}$$

$$\underline{\sigma}[A] = \min_{x \neq 0} \frac{||Ax||}{||x||} = \min_{||x||=1} \frac{||Ax||}{||x||} \quad .$$

If A^{-1} exists, the minimum singular value is also equivalently given by

$$\underline{\sigma}[A] = \frac{1}{\bar{\sigma}[A^{-1}]} \quad .$$

By the definition of singular values it is also clear that

$$\bar{\sigma}[\alpha A] = |\alpha| \, \bar{\sigma}[A]$$

for any complex scalar, α.

The complex, $n \times m$ matrix, A can be decomposed in terms of its singular values, σ_i as follows

$$A = U\Sigma V^H = \sum_{i=1}^{k} \sigma_i u_i v_i^H$$

where

$$U = [u_1\ u_2\ \cdots\ u_n]$$
$$V = [v_1\ v_2\ \cdots\ v_m]$$
$$\Sigma = \begin{cases} \begin{bmatrix} \Sigma_1 \\ 0 \end{bmatrix} & n \geq m \\ [\Sigma_1 \quad 0] & n \leq m \end{cases}$$

and $\Sigma_1 = \text{diag}\ \{\sigma_1, \sigma_2, ..., \sigma_k\}$.

The columns of U and V are right eigenvectors of AA^H and A^HA, respectively and are known as the left and right singular vectors of the matrix A. In addition the matrices U and V are unitary, that is

$$U^HU = UU^H = I$$
$$V^HV = VV^H = I \quad .$$

Several standard inequalities and theorems involving singular values are stated in Table A.1.

Table A.1 Singular Values: Some Inequalities and Theorems

Inequalities:

$$\begin{aligned}
\bar{\sigma}[A+B] &\leq \bar{\sigma}[A] + \bar{\sigma}[B] \\
\bar{\sigma}[AB] &\leq \bar{\sigma}[A]\,\bar{\sigma}[B] \\
\underline{\sigma}[A] - 1 &\leq \underline{\sigma}[I+A] \leq \underline{\sigma}[A] + 1 \\
\underline{\sigma}[A] &\leq |\lambda[A]| \leq \bar{\sigma}[A]
\end{aligned}$$

Theorems:

$$\begin{aligned}
\underline{\sigma}[A], \underline{\sigma}[B] \neq 0 &\Rightarrow \underline{\sigma}[AB] \geq \underline{\sigma}[A]\underline{\sigma}[B] \\
\bar{\sigma}[E] < \underline{\sigma}[A] &\Rightarrow \underline{\sigma}[A+E] > 0 \\
\bar{\sigma}[A] < 1 &\Rightarrow \underline{\sigma}[I+A] \geq 1 - \bar{\sigma}[A]
\end{aligned}$$

APPENDIX B

STABILITY ROBUSTNESS CONDITIONS

This appendix will give proofs that either of

1) $\underline{\sigma}[I + G(j\omega)] > \bar{\sigma}[\Delta(j\omega)] \qquad \forall\omega$

2) $\underline{\sigma}[I + G^{-1}(j\omega)] > \bar{\sigma}[G^{-1}(j\omega)\Delta(j\omega)] \qquad \forall\omega$

3) $\underline{\sigma}[I + G^{-1}(j\omega)] > \bar{\sigma}[\Delta(j\omega)G^{-1}(j\omega)] \qquad \forall\omega$

implies that there exists an $L(s)$ and an $R(s)$ such that

$$||L(s)\Delta(s)R^{-1}(s)||_\infty < 1$$

and

$$||R(s)[I + G(s)]^{-1} L^{-1}(s)||_\infty < 1 \quad .$$

Proof for 1):

$$\underline{\sigma}[I + G(j\omega)] > \bar{\sigma}[\Delta(j\omega)] \qquad \forall\omega$$

$$\Leftrightarrow \quad \frac{1}{\underline{\sigma}[I + G(j\omega)]}\,\bar{\sigma}[\Delta(j\omega)] < 1 \qquad \forall\omega$$

$$\Leftrightarrow \quad \bar{\sigma}[[I + G(j\omega)]^{-1}]\,\bar{\sigma}[\Delta(j\omega)] < 1 \qquad \forall\omega$$

$$\Rightarrow \quad ||[I + G(s)]^{-1}\,\Delta(s)||_\infty < 1$$

$$\Leftrightarrow \quad ||[I + G(s)]^{-1}\,\Delta(s)||_\infty < 1$$

let $\quad L(s) = \Delta^{-1}(s) \quad \text{and} \quad R(s) = I \qquad$ Q.E.D.

Proof for 2):

$$\underline{\sigma}[I + G^{-1}(j\omega)] > \bar{\sigma}[G^{-1}(j\omega)\Delta(j\omega)] \qquad \forall\omega$$

$$\Leftrightarrow \quad \frac{1}{\underline{\sigma}[I + G^{-1}(j\omega)]}\,\bar{\sigma}[G^{-1}(j\omega)\Delta(j\omega)] < 1 \qquad \forall\omega$$

$$\Leftrightarrow \quad \bar{\sigma}[[I + G^{-1}(j\omega)]^{-1}]\,\bar{\sigma}[G^{-1}(j\omega)\Delta(j\omega)] < 1 \qquad \forall\omega$$

$$\Rightarrow \quad \bar{\sigma}[[I + G^{-1}(j\omega)]^{-1}\,G^{-1}(j\omega)\Delta(j\omega)] < 1 \qquad \forall\omega$$

$$\Leftrightarrow \quad \bar{\sigma}[[I + G(j\omega)]^{-1}\Delta(j\omega)] < 1 \qquad \forall\omega$$

$$\Leftrightarrow \quad \|[I + G(s)]^{-1}\Delta(s)\|_\infty < 1$$

let $\quad L(s) = \Delta^{-1}(s) \quad$ and $\quad R(s) = I \qquad$ Q.E.D.

Proof for 3):

$$\underline{\sigma}[I + G^{-1}(j\omega)] > \bar{\sigma}[\Delta(j\omega)G^{-1}(j\omega)] \qquad \forall\omega$$

$$\Leftrightarrow \quad \bar{\sigma}[\Delta(j\omega)G^{-1}(j\omega)]\,\frac{1}{\underline{\sigma}[I + G^{-1}(j\omega]} < 1 \qquad \forall\omega$$

$$\Leftrightarrow \quad \bar{\sigma}[\Delta(j\omega)G^{-1}(j\omega)]\,\bar{\sigma}[[I + G^{-1}(j\omega)]^{-1}] < 1 \qquad \forall\omega$$

$$\Rightarrow \quad \bar{\sigma}[\Delta(j\omega)G^{-1}(j\omega)[I + G^{-1}(j\omega)]^{-1}] < 1 \qquad \forall\omega$$

$$\Leftrightarrow \quad \bar{\sigma}[\Delta(j\omega)[I + G(j\omega)]^{-1}] < 1 \qquad \forall\omega$$

$$\|\Delta(s)[I + G(s)]^{-1}\|_\infty < 1$$

let $\quad L(s) = I \quad$ and $\quad R(s) = \Delta(s) \qquad$ Q.E.D.

APPENDIX C

DETAILS OF BALANCING THE CONTROLLABILITY AND OBSERVABILITY GRAMMIANS WITH EIGENVECTORS OF THEIR PRODUCT

Lemma C1: Product of Positive Semi-Definite Matrices is Similar to a Positive Semi-Definite Matrix

Let A and B be positive semi-definite matrices, i.e. $A, B \geq 0$. Since A is positive semi-definite it has the singular value decomposition:

$$A = V \Lambda V^T$$

where

$$\Lambda = \begin{bmatrix} \Lambda_1 & 0 \\ 0 & 0 \end{bmatrix} , \qquad \Lambda_1 > 0$$

and

$$V V^T = I \quad .$$

Let

$$S = V^T B V = \begin{bmatrix} S_{11} & S_{12} \\ S_{12}^T & S_{22} \end{bmatrix}$$

where S_{11} has the same dimensions as Λ_1. Note that:

$$B \geq 0 \Rightarrow S \geq 0 \Rightarrow S_{11} \geq 0 \quad .$$

Hence S_{11} has the singular value decomposition:

$$S_{11} = U\Sigma U^T$$

where

$$\Sigma = \begin{bmatrix} \Sigma_1 & 0 \\ 0 & 0 \end{bmatrix}$$

$$U = [U_1 \quad U_2]$$

and

$$UU^T = I \quad .$$

Let

$$C(X) = \begin{bmatrix} U_2^T & X^T \end{bmatrix} \begin{bmatrix} S_{11} & S_{12} \\ S_{12}^T & S_{22} \end{bmatrix} \begin{bmatrix} U_2 \\ X \end{bmatrix} \quad .$$

Note that:

$$S \geq 0 \Rightarrow \qquad C(X) \geq 0 \qquad \forall X \quad .$$

From the singular value decomposition of S_{11} it can be seen that

$$U_2^T S_{11} = 0$$

and thus

$$C(X) = U_2^T S_{12} X + X^T S_{12}^T U_2 + X^T S_{22} X \quad .$$

From this expression for $C(X)$ and the fact that $C(X) \geq 0$ for any X it can be seen that $U_2^T S_{12} = 0$ or else it would be possible to find an X such that $C(X)$ was not positive semi-definite. To be precise, say $U_2^T S_{12} \neq 0$, then there exists a z such that $\delta \triangleq z^T U_2^T S_{12} S_{12}^T U_2 z > 0$. Next let $\gamma \triangleq z^T U_2^T S_{12} S_{22} S_{12}^T U_2 z$, then

$S \geq 0$, implies $S_{22} \geq 0$, implies $\gamma \geq 0$. Then let

$$\epsilon \triangleq \begin{cases} \frac{\delta}{\gamma} & \gamma \neq 0 \\ 1 & \gamma = 0 \end{cases} .$$

Finally let $X = -\epsilon S_{12}^T U_2$, then

$$\begin{aligned} z^T C(X) z &= -2\epsilon\delta + \epsilon^2\gamma \\ &= \begin{cases} -\frac{\delta^2}{\gamma} & \gamma \neq 0 \\ -2\delta & \gamma = 0 \end{cases} . \end{aligned}$$

In either case $z^T C(X) z < 0$ and hence if $U_2^T S_{12} \neq 0$ it is always possible to choose X such that $C(X)$ is not positive semi-definite. Since $C(X) \geq 0$ for $\forall X$ it follows that $U_2^T S_{12} = 0$.

Let

$$T \triangleq V \begin{bmatrix} \Lambda_1^{1/2} & -U_1 \Sigma_1^{-1} U_1^T S_{12} \\ 0 & I \end{bmatrix}$$

then it can be verified that

$$T^{-1} A B T = \begin{bmatrix} \Lambda_1^{1/2} S_{11} \Lambda_1^{1/2} & 0 \\ 0 & 0 \end{bmatrix} .$$

This completes the proof since $S_{11} \geq 0$ and $\Lambda_1 > 0$ imply that $T^{-1} A B T \geq 0$.

Lemma C2: Nonzero Off-Diagonal Elements of Two Symmetric Matrices Whose Product is Diagonal Correspond to Repeated Elements of Their Diagonal Product

Let A with elements, a_{ij} and B with elements, b_{ij} be $n \times n$ symmetric matrices, i.e. $A = A^T$ and $B = B^T$ where $AB = \Lambda = \text{diag}\{\lambda_i\}$. Then it will be proved that $a_{ij}(\lambda_i - \lambda_j) = 0$ and $b_{ij}(\lambda_i - \lambda_j) = 0$ for $\forall\, i,j$.

Firstly note that it is sufficient to prove the result for A since

$$BA = B^T A^T = (AB)^T = \Lambda \quad .$$

Next partition A, B and Λ compatibly:

$$A = \begin{bmatrix} A_{11} & A_{12} \\ A_{12}^T & A_{22} \end{bmatrix} \quad B = \begin{bmatrix} B_{11} & B_{12} \\ B_{12}^T & B_{22} \end{bmatrix} \quad \Lambda = \begin{bmatrix} \Lambda_1 & 0 \\ 0 & \Lambda_2 \end{bmatrix}$$

where A_{11}, B_{11}, Λ_1 are $r \times r$ with $1 < r < n$ but r is otherwise arbitrary. The equation $AB = \Lambda$ is then equivalent to the following four equations:

$$\begin{aligned} A_{11} B_{11} + A_{12} B_{12}^T &= \Lambda_1 && (1,1) \\ A_{11} B_{12} + A_{12} B_{22} &= 0 && (1,2) \\ A_{12}^T B_{11} + A_{22} B_{12}^T &= 0 && (2,1) \\ A_{12}^T B_{12} + A_{22} B_{22} &= \Lambda_2 && (2,2) \quad . \end{aligned}$$

Multiplying the transpose of equation (1,2) by A_{22} on the left and equation (2,1) by A_{11} on the right and then subtracting the two equations results in

$$A_{22} B_{22} A_{12}^T = A_{12}^T B_{11} A_{11} \quad .$$

Using this result to substitute for $A_{12}^T B_{11} A_{11}$ in the equation obtained by

multiplying the transpose of equation (1,1) by A_{12}^T on the left results in

$$\begin{aligned} A_{22}\, B_{22}\, A_{12}^T + A_{12}^T\, B_{12}\, A_{12}^T &= A_{12}^T \Lambda_1 \\ \left[A_{22}\, B_{22} + A_{12}^T\, B_{12}\right] A_{12}^T &= A_{12}^T\, \Lambda_1 \\ \Lambda_2\, A_{12}^T &= A_{12}^T\, \Lambda_1 \end{aligned}$$

where equation (2,2) was used to substitute for the term in brackets. Examining the final equation for all r between 1 and n implies that

$$a_{ij}(\lambda_i - \lambda_j) = 0 \qquad \forall \;\; i,j \quad .$$

Q.E.D.

Lemma C3: Transformation Always Exists Which Diagonalizes Both Grammians, U and Y

Lemma C1 shows that a transformation, T_1 always exists such that $T_1^{-1} U Y T_1 = \Lambda = \text{diag}\,\{\lambda_i\}$. In fact T_1 is any eigenvector matrix of UY. Let

$$A \triangleq T_1^{-1} U T_1^{-T}$$

and

$$B \triangleq T_1^T Y T_1$$

then

$$AB = T_1^{-1} U T_1^{-T} T_1^T Y T_1 \quad .$$

Noting that $A = A^T$ and $B = B^T$, Lemma C2 shows that the elements of A and B, a_{ij} and b_{ij} respectively satisfy

$$a_{ij}(\lambda_i - \lambda_j) = 0$$

and

$$b_{ij}(\lambda_i - \lambda_j) = 0 \quad .$$

Clearly if $\lambda_i \neq \lambda_j$ for $i \neq j$ then T_1 is a transformation with satisfies Lemma C3. Otherwise without loss of generality, order the elements of Λ such that

$$\lambda_1 = \lambda_2 = \cdots = \lambda_{k_1} > \lambda_{k_1+1} = \lambda_{k_1+2} = \cdots = \lambda_{k_1+k_2} > \cdots$$
$$\cdots > \lambda_{k_1+k_2+\ldots+k_{q-1}+1} = \cdots = \lambda_{k_1+k_2+\ldots+k_q} \quad .$$

That is Λ has k_i elements equal to $\lambda_{k_1+k_2+\ldots+k_i}$ for $i=1, 2, \ldots, q$ and $n = \sum_{i=1}^{q} k_i$.

Then Lemma C2 shows that

$$A = \text{block diag } \{A_i\}$$
$$B = \text{block diag } \{B_i\}$$
$$\Lambda = \text{block diag } \left\{\lambda_{k_1+\ldots+k_i} I_{k_i}\right\}$$

where A_i and B_i are $k_i \times k_i$. Then let V_j be any eigenvector matrix for A_j, i.e.

$$V_j^{-1} A_j V_j = \text{diag } \left\{\alpha_{k_1+k_2+\ldots+k_{j-1}+i}\right\} \quad .$$

The fact that A_j can be diagonalized is a consequence of the symmetry of A_j which is a consequence of the symmetry of A. Another consequence of the

symmetry of A_j is that V_j can be chosen such that $V_j = V_j^{-T}$.

Next let

$$T_2 = \text{block diag } \{V_i\}$$

then let

$$\hat{A} = T_2^{-1} A T_2^{-T}$$

and $$\hat{B} = T_2^T B T_2 \quad .$$

Then $\hat{A} = \text{diag } \{\alpha_i\}$ and

$$\begin{aligned} \hat{A}\hat{B} &= T_2^{-1} A T_2^{-T} T_2^T B T_2 \\ &= T_2^{-1} AB T_2 \\ &= T_2^{-1} \Lambda T_2 \\ &= \Lambda \end{aligned}$$

but since $\hat{A}$ and Λ are diagonal $\hat{B}$ must also be diagonal, i.e. $\hat{B} = \text{diag } \{\beta_i\}$. In conclusion $T_1 T_2$ is a transformation which satisfies Lemma C3.

Q.E.D.

Choice of Scaling Such That Controllable and Observable Portions of Balanced Diagonal Grammains Are Equal

It has been shown in Lemma C3 that there exists a transformation, T such that

$$T^{-1}UT^{-T} = \text{diag}\,\{\alpha_i\}$$
$$T^{T}YT = \text{diag}\,\{\beta_i\}$$
$$T^{-1}UYT = \Lambda = \text{diag}\,\{\lambda_i\}$$

and $\lambda_i = \alpha_i\beta_i$; $i=1, 2, \ldots, N$. Without loss of generality assume the λ_i have been ordered such that

$$\lambda_1 \geq \lambda_2 \geq \cdots \geq \lambda_n > \lambda_{n+1} = \lambda_{n+2} = \cdots = \lambda_N = 0 \quad .$$

Let

$$d_i = \begin{cases} \left[\dfrac{\alpha_i}{\beta_i}\right]^{1/4} & \alpha_i,\ \beta_i \neq 0 \\ \\ 1 & \alpha_i = 0 \quad \text{or} \quad \beta_i = 0 \end{cases}$$

and

$$D = \text{diag}\,\{d_i\}$$

and

$$T_b = TD$$

then

$$
\begin{aligned}
T_b^{-1} U T_b^{-T} &= D^{-1} T^{-1} U T^{-T} D^{-1} \\
&= D^{-1} \text{ diag } \{\alpha_i\} D^{-1} \\
&= \text{diag } \left\{ \frac{\alpha_i}{d_i^2} \right\} \\
&= \text{block diag } \{\Sigma, \Sigma_y\}
\end{aligned}
$$

and

$$
\begin{aligned}
T_b^T Y T_b &= D T^T Y T D \\
&= D \text{ diag } \{\beta_i\} D \\
&= \text{diag } \{\beta_i d_i^2\} \\
&= \text{block diag } \{\Sigma, \Sigma_y\}
\end{aligned}
$$

where

$$
\begin{aligned}
\Sigma &= \text{diag } \left\{ \sqrt{\lambda_1}, \sqrt{\lambda_2}, \ldots, \sqrt{\lambda_n} \right\} \\
\Sigma_u &= \text{diag } \left\{ \alpha_{n+1}, \alpha_{n+2}, \ldots, \alpha_N \right\} \\
\Sigma_y &= \text{diag } \left\{ \beta_{n+1}, \beta_{n+2}, \ldots, \beta_N \right\} \quad .
\end{aligned}
$$

APPENDIX D

CONJECTURE REGARDING E_∞ BOUND FOR FREQUENCY WEIGHTED BALANCED REALIZATIONS

The objective of this appendix is to carry out the manipulations leading to the conjecture about the E_∞ bound for frequency weighted balanced realizations. The notation and results of Chapter III for the proof of the unweighted error bound for internally balanced realizations will be used.

From Chapter III we have that

$$G(s) - G_r(s) = \tilde{C}(s)\Delta^{-1}(s)\tilde{B}(s) \quad .$$

Let $E(s) \triangleq W_o(s)[G(s) - G_r(s)]W_i(s)$ where $W_o(s)$ and $W_i(s)$ are the specified output and input model reduction weightings. Letting

$$B_w(s) \triangleq \tilde{B}(s)W_i(s)$$

and

$$C_w(s) \triangleq W_o(s)\tilde{C}(s)$$

it can be seen that

$$E(s) = C_w(s)\Delta^{-1}(s)B_w(s) \quad .$$

From the definition of the maximum singular value we have

$$\bar{\sigma}\left[E(j\omega)\right] = \lambda_{\max}^{1/2}\left[C_w(j\omega)\Delta^{-1}(j\omega)B_w(j\omega)B_w^T(-j\omega)\Delta^{-T}(-j\omega)C_w^T(-j\omega)\right]$$
$$= \lambda_{\max}^{1/2}\left[\Delta^{-1}(j\omega)B_w(j\omega)B_w^T(-j\omega)\Delta^{-T}(-j\omega)C_w^T(-j\omega)C_w(j\omega)\right] .$$

The fact that the realization is balanced with respect to the model reduction weightings: $W_o(s)$ and $W_i(s)$ is then used to derive expressions for $B_w(j\omega)\,B^T(-j\omega)$ and $C_w^T(-j\omega)\,C_w(j\omega)$. This requires an enormous amount of algebra which will only be sketched here.

The basic idea is the same as that for the proof of the bound for the unweighted case given in Chapter III. That is the two grammian equations:

$$\bar{A}_i\bar{U} + \bar{U}\bar{A}_i^T + \bar{B}_i\bar{B}_i^T = 0$$
$$\bar{A}_o^T\bar{Y} + \bar{Y}\bar{A}_o + \bar{C}_o^T\bar{C}_o = 0$$

are partitioned into six equations each, by substituting

$$\bar{A}_i = \begin{bmatrix} A_{11} & A_{12} & B_1H_i \\ A_{21} & A_{22} & B_2H_i \\ 0 & 0 & F_i \end{bmatrix} \qquad \bar{B}_i = \begin{bmatrix} B_1D_i \\ B_2D_i \\ G_i \end{bmatrix}$$

$$\bar{A}_o = \begin{bmatrix} A_{11} & A_{12} & 0 \\ A_{21} & A_{22} & 0 \\ G_oC_1 & G_oC_2 & F_o \end{bmatrix} \qquad \bar{C}_o = \begin{bmatrix} D_oC_1 & D_oC_2 & H_o \end{bmatrix}$$

$$\bar{U} = \begin{bmatrix} \Sigma_1 & 0 & U_{31}^T \\ 0 & \Sigma_2 & U_{32}^T \\ U_{31} & U_{32} & U_{33} \end{bmatrix} \qquad \bar{Y} = \begin{bmatrix} \Sigma_1 & 0 & Y_{13} \\ 0 & \Sigma_2 & Y_{23} \\ Y_{13}^T & Y_{23}^T & Y_{33} \end{bmatrix} .$$

The result for $B_w(s)$ will be discussed and the result for $C_w(s)$ will follow by

duality. Using the definition of $B_w(s)$ and $\tilde{B}(s)$ to expand $B_w(s)\,B_w^T(-s)$ results in terms involving $B_1D_iD_i^TB_1^T$, $B_1D_iD_i^TB_2^T$, $B_1H_iU_{33}$, $B_2D_iD_i^TB_2^T$, $B_2H_iU_{33}$ and GG^T. Substitutions are made for these six terms using the six equations for the weighted controllability grammian.

This results in an expression involving Σ_2 and U_{22} (the Σ_1, U_{31}, U_{33} terms exactly cancel). This final expression and its dual for $C_w^T(-s)C_w(s)$ are given by

$$\begin{aligned} B_w(s)B_w^T(-s) &= \Delta(s)\Sigma_2 + \Sigma_2\Delta^T(-s) + N_i(s) \\ C_w^T(-s)C_w(s) &= \Delta^T(-s)\Sigma_2 + \Sigma_2\Delta(s) + N_o(s) \end{aligned}$$

where

$$\begin{aligned} N_i(s) &\triangleq \Delta(s)U_{32}^T(-sI-F_i^T)^{-1}H_i^T\tilde{B}^T(-s) + \tilde{B}(s)H_i(sI-F_i)^{-1}U_{32}\Delta^T(-s) \\ N_o(s) &\triangleq \Delta^T(-s)Y_{23}(sI-F_o)^{-1}G_o\tilde{C}(s) + \tilde{C}^T(-s)G_o^T(-sI-F_o^T)^{-1}Y_{23}^T\Delta(s) \quad . \end{aligned}$$

With these expressions for $B_w(s)B_w^T(-s)$ and $C_w^T(-s)C_w(s)$ we have

$$\begin{aligned} \bar{\sigma}[E(j\omega)] = \lambda_{\max}^{1/2} \Big[\Big[\Big[\Sigma_2 &+ \Delta^{-1}(j\omega)\Sigma_2\Delta^T(-j\omega) + \Delta^{-1}(j\omega)N_i(j\omega)\Big] \\ &\Big[\Sigma_2 + \Delta^{-T}(-j\omega)\Sigma_2\Delta(j\omega) \\ &+ \Delta^{-T}(-j\omega)N_o(j\omega)\Big]\Big] \quad . \end{aligned}$$

If $N_i(j\omega) = N_o(j\omega) = 0$ then with the same steps as in Chapter III it can be shown that

$$\bar{\sigma}\Big[E(j\omega)\Big] \leq 2tr\Big[\Sigma_2\Big] \qquad \forall\omega \quad ,$$

however, $N_i(j\omega)$ and $N_o(j\omega)$ are not zero in general. A bound for the general case could not be found but a conjecture is that

$$E_\infty = \sup_\omega \bar{\sigma}[E(j\omega)] \leq 2(1+\alpha)\ tr[\Sigma_2]$$

where the conjecture is that

$$\alpha < 1 \quad \text{when} \quad E_\infty < 1 \quad .$$

APPENDIX E

SUBSTANTIATING DATA

Spinning Projectile Data

A seventh order realization of the rigid body dynamics of a spinning projectile is given by

$$\begin{aligned} \dot{x} &= Ax + Bu \\ y &= Cx \end{aligned}$$

where

$$\begin{aligned} x^T &= [u \;\; v \;\; w \;\; p \;\; q \;\; r \;\; \theta] \\ u^T &= [F_y \quad F_z] \\ y^T &= [q \quad\quad r] \quad . \end{aligned}$$

The matrices, A, B, C are tabulated in Table E.1.

The units of the velocity components, u, v, w are measured in terms of the magnitude of the velocity, V (=1053 ft/sec). That is $\frac{u}{V}$ which is dimensionless and $\frac{v}{V}\,\frac{180}{\pi}$ and $\frac{w}{V}\,\frac{180}{\pi}$ which represent sideslip and angle of attack in degrees respectively. The units of the components of the angular velocity p, q and r are measured in degrees/sec, the units of the pitch angle, θ are measured in degrees and the units of F_y and F_z are measured in pounds (lbs).

Table E.1 A, B, C Matrices For Spinning Projectile

$$A = \begin{bmatrix}
-4.757e-02 & 8.817e-04 & 2.594e-05 & 0.000e+00 & -4.013e-04 & -8.310e-04 & -4.616e-04 \\
-5.777e-01 & -1.554e-01 & -1.376e-02 & -2.285e-07 & 0.000e+00 & -9.853e-01 & -5.350e-04 \\
-1.204e+00 & 1.410e-02 & -1.551e-01 & -9.307e-07 & 9.986e-01 & 2.749e-02 & 1.416e-02 \\
-3.855e+02 & 3.208e-01 & -1.549e-01 & -5.487e-03 & 0.000e+00 & 0.000e+00 & 0.000e+00 \\
3.621e+02 & -4.036e+00 & 6.359e+02 & -1.438e-03 & -2.200e-01 & -1.278e+02 & -4.062e-04 \\
1.729e+03 & -6.433e+02 & -7.576e+00 & -2.000e-03 & 1.278e+02 & -2.099e-01 & -4.062e-04 \\
0.000e+00 & 0.000e+00 & 0.000e+00 & 0.000e+00 & 1.000e+00 & 0.000e+00 & 0.000e+00
\end{bmatrix}$$

$$B = \begin{bmatrix}
0.000e+00 & 0.000e+00 \\
1.701e-02 & 0.000e+00 \\
0.000e+00 & 1.701e-02 \\
0.000e+00 & 0.000e+00 \\
0.000e+00 & 4.584e+01 \\
-4.584e+01 & 0.000e+00 \\
0.000e+00 & 0.000e+00
\end{bmatrix}$$

$$C = \begin{bmatrix}
0.000e+00 & 0.000e+00 & 0.000e+00 & 0.000e+00 & 1.000e+00 & 0.000e+00 & 0.000e+00 \\
0.000e+00 & 0.000e+00 & 0.000e+00 & 0.000e+00 & 0.000e+00 & 1.000e+00 & 0.000e+00
\end{bmatrix}$$

Fourth order reduced order models were obtained with the internally balancing technique and the "classical" technique of neglecting the u, p and θ states. These two reduced order models are compared below. To facilitate the comparison of the two reduced order models and the full order model let the transfer function relating $u(s)$ and $y(s)$ be parameterized as shown in Table E.2. Then the differences between the two reduced order models can be seen by examining the data in Table E.3.

Note that all the parameters differ by less than a few percentage for the two reduced order models. The only exception is the precession damping for which the internally balanced reduced order model is in closer agreement with the full order model than the classical reduced oder model. The authors opinion is that for all practical intents and purposes the two reduced order models are identical.

Four Disk Example

Sensitivity With Respect To Knowledge of ω_1, ω_2 and z

The fact that the compensator, $K_6(s)$ involves pole-zero cancellation near the $j\omega$ axis is a concern. The poles of $G(s)$ with $|s| = \omega_1, \omega_2$ and the zero of $G(s)$ with $|s| = z$ are cancelled. Hence, an analysis was performed to assess the stability of the closed loop system in the face of simultaneous $\pm 10\%$ uncertainty in these three critical parameters, ω_1, ω_2 and z (sensitivity to other parameters would be less severe). The analysis was performed assuming that for any uncertainty the DC gain of $G(s)$ was known exactly.

Table E.2 Parameterization of Spinning Projectile Transfer Function

$$G(s) = \frac{1}{(s^2+2\zeta_p\omega_p s+\omega_p^2)(s^2+2\zeta_n\omega_n s+\omega_n^2)} \begin{bmatrix} g_{11}(s)(s^2+2\zeta_{11}\omega_n s+\omega_{11}^2) & g_{12}(s)(s+a_{12})(s-b_{12})(s+c_{12}) \\ -g_{21}(s)(s+a_{21})(s-b_{21})(s+c_{21}) & g_{22}(s)(s^2+2\zeta_{22}\omega_{22} s+\omega_{22}^2) \end{bmatrix}$$

For Full Order Model:

let $d(s) = (s+5.2e-3)[s^2+5.8e-2s+1.1e-3]$

then $g_{11}(s) = K_{11}s(s+4.5e-3)(s-2.3e-2)/d(s)$

$g_{12}(s) = K_{12}s(s+5.5e-3)(s+4.5e-2)/d(s)$

$g_{21}(s) = K_{21}(s+5.2e-3)(s^2+6.1e-2s+1.1e-3)/d(s)$

$g_{22}(s) = K_{22}(s+5.6e-3)(s-6.1e-2)(s+0.1)/d(s)$

For Reduced Order Model:

$g_{ij}(s) = K_{ij} \qquad i,j = 1,2$

Table E.3 Comparison of Full Order Model, Internally Balanced and "Classical" Reduced Order Models

Description	Parameter	Full Order Model	Internally Balanced	Classical	% Difference in Reduced Order Models
precession poles	ζ_p	0.0045631	0.0045631	0.0056017	-22.76
	ω_p	5.1780	5.1780	5.1860	-0.15
nutation poles	ζ_n	0.0027824	0.0027824	0.0027816	0.03
	ω_n	122.66	122.66	122.65	0.01
Fy to q numerator	K11	5859.2	5859.2	5859.2	0
	ζ_{11}	0.70813	0.70741	0.71171	-0.61
	ω_{11}	0.39345	0.26611	0.26782	-0.64
Fz to q numerator	K12	45.842	45.842	45.842	0
	a12	0.39231	0.37864	0.39244	-3.64
	b12	24.952	24.955	24.982	-0.11
	c12	25.319	25.322	25.346	-0.09
Fy to r numerator	K21	45.842	45.842	45.842	0
	a21	0.39529	0.39835	0.39483	0.98
	b21	25.009	25.009	25.009	0
	c21	25.369	25.369	25.383	-0.06
Fz to r numerator	K22	5859.6	5859.6	5859.6	0
	ζ_{22}	0.69610	0.71724	0.70056	2.33
	ω_{22}	0.34805	0.32858	0.34772	-5.83
MIMO Transmission zeros	ζ	0.09896	0.09956	0.09917	0.04
	ω	0.39302	0.39759	0.39282	-1.35

Note: The % difference was computed by subtracting the classical parameter from the internally balanced parameter, dividing by the internally balanced parameter and then multiplying by 100.

Consider the multiplicative perturbation implied by the uncertainty in ω_1, ω_2 and z

$$\Delta(s) = \frac{G(s;\, \omega_1,\, \omega_2,\, z) - G(s;\, \hat{\omega}_1,\, \hat{\omega}_2,\, \hat{z})}{G(s;\, \hat{\omega}_1,\, \hat{\omega}_2,\, \hat{z})}$$

$$= \left(\frac{\hat{z}}{z}\,\frac{\omega_1}{\hat{\omega}_1}\,\frac{\omega_2}{\hat{\omega}_2}\right)^2 \left(\frac{s^2 + 2\varsigma z s + z^2}{s^2 + 2\varsigma \hat{z} s + \hat{z}^2}\right) \left(\frac{s^2 + 2\varsigma \hat{\omega}_1 s + \hat{\omega}_1^2}{s^2 + 2\varsigma \omega_1 s + \omega_1^2}\right)\left(\frac{s^2 + 2\varsigma \hat{\omega}_2 s + \hat{\omega}_2^2}{s^2 + 2\varsigma \omega_2 s + \omega_2^2}\right) - 1$$

where $G(s;\, \omega_1,\, \omega_2,\, z)$ represents a possible true system and $G(s;\, \hat{\omega}_1,\, \hat{\omega}_2\, \hat{z})$ represents the nominal system. Note that the other poles and zeros cancel out of the expression for $\Delta(s)$. Also note that $\Delta(0) = 0$.

Let $l(\omega)$ be a bound for the magnitude of the perturbation, i.e.

$$l(\omega) = \max_{\substack{0.9 \le \frac{\alpha}{\hat{\alpha}} \le 1.1 \\ (\alpha = \omega_1, \omega_2, z}} |\Delta(j\omega)| \quad .$$

The bound, $l(\omega)$ is plotted versus ω in Fig. E.1.

The stability robustness theorem of Chapter II (see also App. B) guarantees stability of the closed loop system in the presence of the uncertainty if

$$\left|1 + \left[G(j\omega;\, \hat{\omega}_1,\, \hat{\omega}_2,\, \hat{z})\; K_6(j\omega)\right]^{-1}\right| > l(\omega) \qquad \forall\omega \quad .$$

This condition can be seen to be satisfied by examining Fig. E.1 where the left and right hand sides of the inequality are plotted versus ω. Thus the closed loop

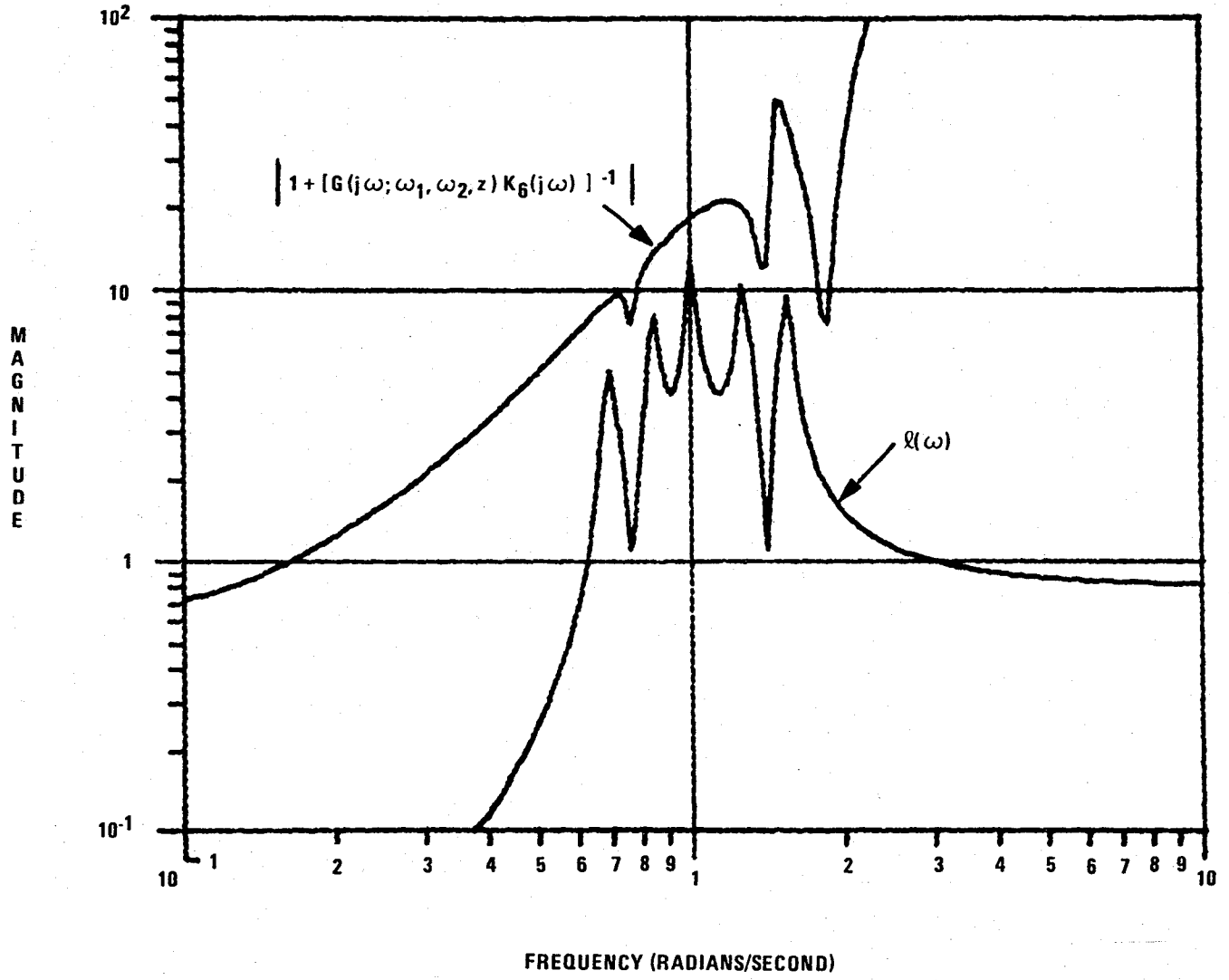

Fig. E.1 Stability Robustness Test For Four Disk System With $K_6(s)$

system is stable in the face of simultaneous $\pm 10\%$ uncertainty in ω_1, ω_2 and z.

Closed Loop Poles

The closed loop poles for the control system with $G(s)$ and $K_6(s)$ are given in Table E.4. Note that all have negative real parts which is guaranteed by the fact that $E_\infty \leq 0.2$ (i.e. less than unity) for the weighted model reduction of $K(s)$ to $K_6(s)$.

Results With Internally Balanced Model Reduction

An eighth order reduced order model of $K(s)$ was found using unity weighting or the internally balanced method. This compensator produces an unstable system with closed loop poles shown in Table E.5.. The fact that unity weighting produced an unstable closed loop system is easily seen by comparing the Bode gain plots of the three compensators $K(s)$ or $K_9(s)$, $K_8(s)$ and $K_6(s)$ shown in Fig. E.2. While $K_8(s)$ (unity weighting) captures the high gain portion of $K(s)$ nicely it sacrifices low frequency model fidelity, whereas, $K_6(s)$ (non-unity weighting) with only six poles matches the low frequency behavior and produces a stable closed loop system.

Robust Four Disk Design

For zero damping the transfer function of the four disk system as a function

Table E.4 Four Disk System
Closed Loop Poles for G(s) and $K_6(s)$
(Non-unity model reduction weighting)

	real	imaginary	frequency	damping
1	-7.3074e-02	6.4415e-02	9.7412e-02	7.5016e-01
2	-7.3074e-02	-6.4415e-02	9.7412e-02	7.5016e-01
3	-4.0331e-01	1.8681e-01	4.4447e-01	9.0739e-01
4	-4.0331e-01	-1.8681e-01	4.4447e-01	9.0739e-01
5	-1.4689e-02	7.6457e-01	7.6471e-01	1.9209e-02
6	-1.4689e-02	-7.6457e-01	7.6471e-01	1.9209e-02
7	-2.0000e-02	9.9980e-01	1.0000e+00	2.0000e-02
8	-2.0000e-02	-9.9980e-01	1.0000e+00	2.0000e-02
9	-2.9580e-02	1.4082e+00	1.4085e+00	2.1001e-02
10	-2.9580e-02	-1.4082e+00	1.4085e+00	2.1001e-02
11	-4.2471e-02	1.8470e+00	1.8475e+00	2.2988e-02
12	-4.2471e-02	-1.8470e+00	1.8475e+00	2.2988e-02
13	-6.5126e-02	3.2895e+00	3.2901e+00	1.9794e-02
14	-6.5126e-02	-3.2895e+00	3.2901e+00	1.9794e-02

Table E.5 Four Disk System
Closed Loop Poles for G(s) and $K_8(s)$
(Unity model reduction weighting)

	real	imaginary	frequency	damping
1	1.4037e-02	1.6785e-01	1.6843e-01	-8.3338e-02
2	1.4037e-02	-1.6785e-01	1.6843e-01	-8.3338e-02
3	-1.2746e-02	7.6926e-01	7.6937e-01	1.6567e-02
4	-1.2746e-02	-7.6926e-01	7.6937e-01	1.6567e-02
5	-1.9501e-02	1.0012e+00	1.0014e+00	1.9474e-02
6	-1.9501e-02	-1.0012e+00	1.0014e+00	1.9474e-02
7	-2.7707e-02	1.4088e+00	1.4091e+00	1.9663e-02
8	-2.7707e-02	-1.4088e+00	1.4091e+00	1.9663e-02
9	-3.6872e-02	1.8496e+00	1.8500e+00	1.9932e-02
10	-3.6872e-02	-1.8496e+00	1.8500e+00	1.9932e-02
11	-1.4981e+00	2.1873e+00	2.6512e+00	5.6508e-01
12	-1.4981e+00	-2.1873e+00	2.6512e+00	5.6508e-01
13	-5.9795e-01	2.9355e+00	2.9958e+00	1.9960e-01
14	-5.9795e-01	-2.9355e+00	2.9958e+00	1.9960e-01
15	-3.0948e+00	1.9086e+00	3.6360e+00	8.5115e-01
16	-3.0948e+00	-1.9086e+00	3.6360e+00	8.5115e-01

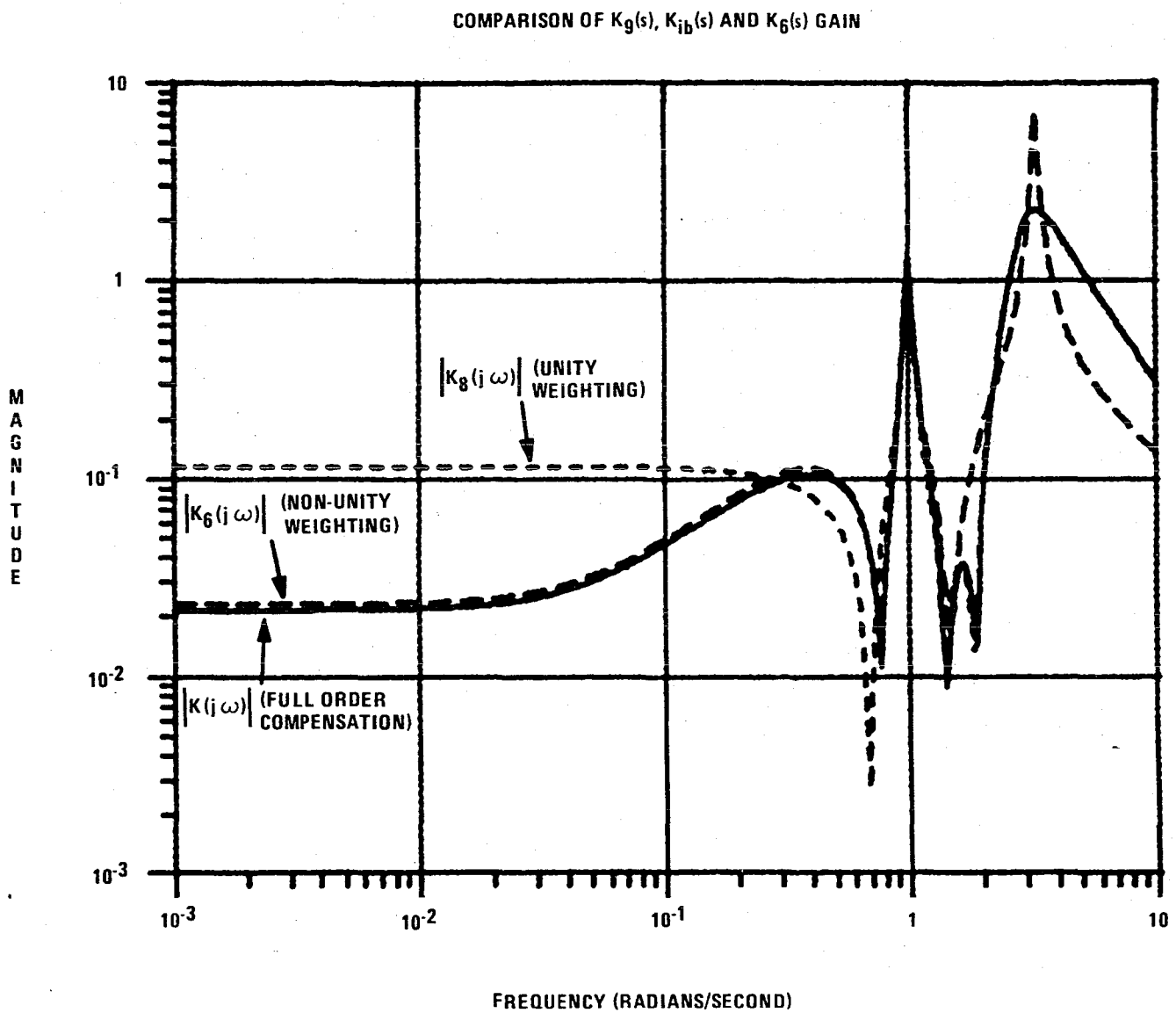

Figure E.2 Comparison of Compensators For Four Disk System

of the inertia of the fourth disk is given by

$$G_0\left(s;\frac{1}{\gamma^2}\right) = \frac{(s^2+\gamma^2)}{s^2\left[s^6 + (5+\gamma^2)s^4 + (6+4\gamma^2)s^2 + (1+3\gamma^2)\right]}$$

where $\frac{1}{\gamma^2}$ is the inertia of the fourth disk. A partial fraction expansion of $G_0(s;\frac{1}{\gamma^2})$ is given by

$$G_0\left(s;\frac{1}{\gamma^2}\right) = \sum_{i=0}^{3}\frac{R_i}{s^2+\omega_i^2}$$

where the residues, $R_i \quad i = 0, 1, 2, 3$ and $\omega_i \quad i=1, 2, 3$ are functions of the inertia of the fourth disk and $\omega_0 = 0$. The constant damping ratio $\varsigma = 0.02$ was introduced to produce the transfer function

$$G_1\left(s;\frac{1}{\gamma^2}\right) = \sum_{i=0}^{3}\frac{R_i}{s^2+2\varsigma\omega_i s+\omega_i^2} \quad .$$

Consider the multiplicative perturbation given by

$$\Delta(s) = \frac{G_1\left(s;\frac{1}{\gamma^2}\right) - G(s)}{G(s)}$$

where the nominal model, $G(s)$ was chosen to be given by

$$G(s) = \frac{0.2}{s^2} \quad .$$

Let $l(\omega)$ be a bound for the magnitude of the perturbation, i.e.

$$l(\omega) = \max_{1 \leq \frac{1}{\gamma^2} \leq 4} |\Delta(j\omega)| \quad .$$

This bound is plotted versus ω in Fig. E.3 and resulted in the high frequency constraint of Fig. V.8.

The stability robustness theorem of Chapter II (see also App. B) guarantees stability of the closed loop system in the presence of the uncertain but bounded inertia of the fourth disk if

$$|1 + [G(j\omega)K_5(j\omega)]^{-1}| > l(\omega) \qquad \forall\omega$$

where $K_5(s)$ is the compensator of Chapter V. This condition can be seen to be satisfied by examining Fig. E.3 where the left and right hand sides of the inequality are plotted versus ω.

It may also be of interest to examine the closed loop pole locations as a function of the inertia of the fourth disk. A root locus plot is shown in Fig. E.4 for $1 \leq \frac{1}{\gamma^2} \leq 4$. Note that all the poles are in the left half plane as guaranteed by the stability robustness theorem. Also note that a closed loop pole at $s \cong -\alpha_{4_r} = -32.1$ is not shown.

Flexible Beam Example

Closed Loop Poles

The closed loop poles for the control system with $G(s)$ and $K_6(s)$ are given in Table E.6. Note that all have negative real parts.

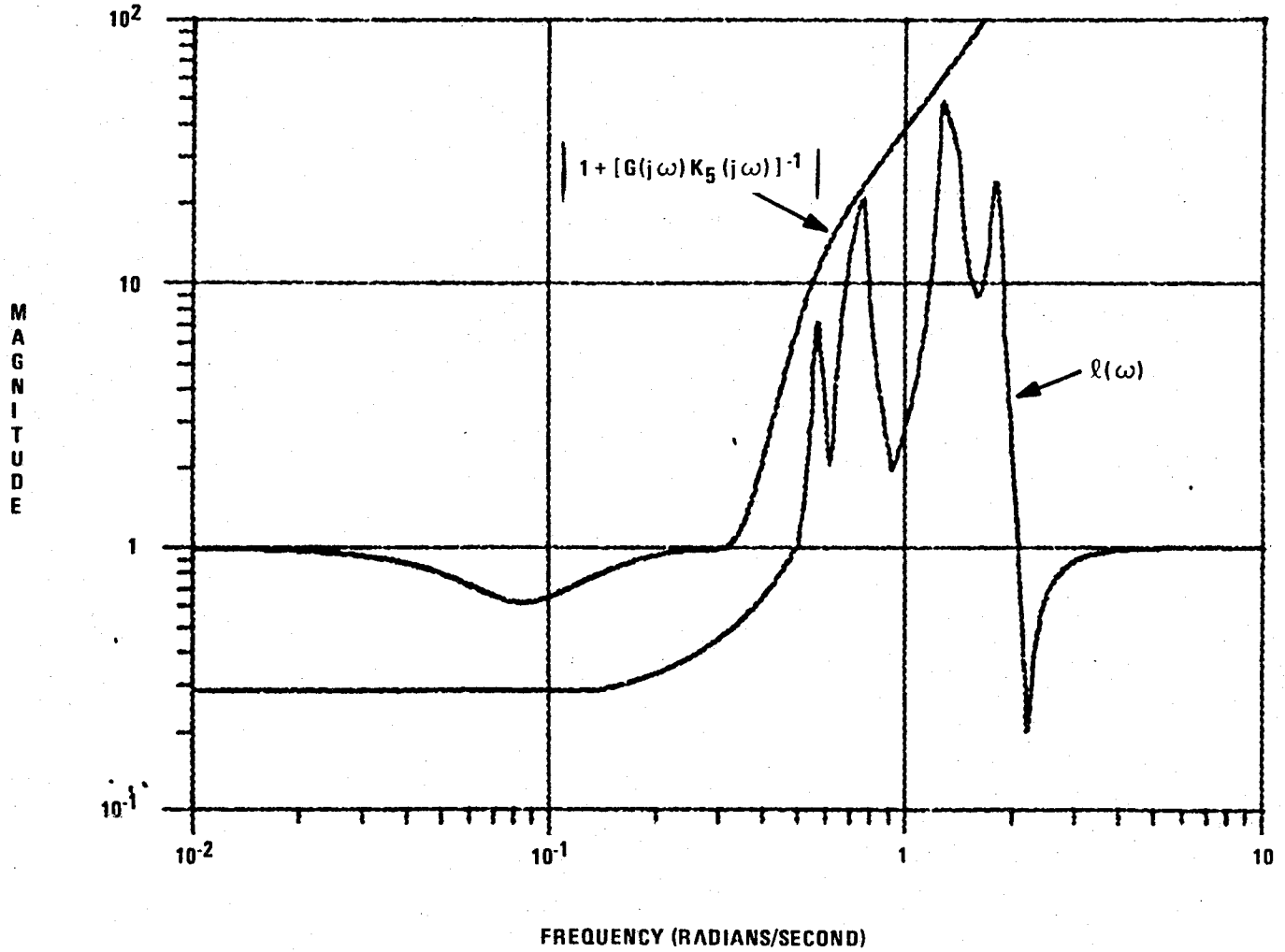

Figure E.3 Stability Robustness Test For Uncertain Fourth Disk Inertia

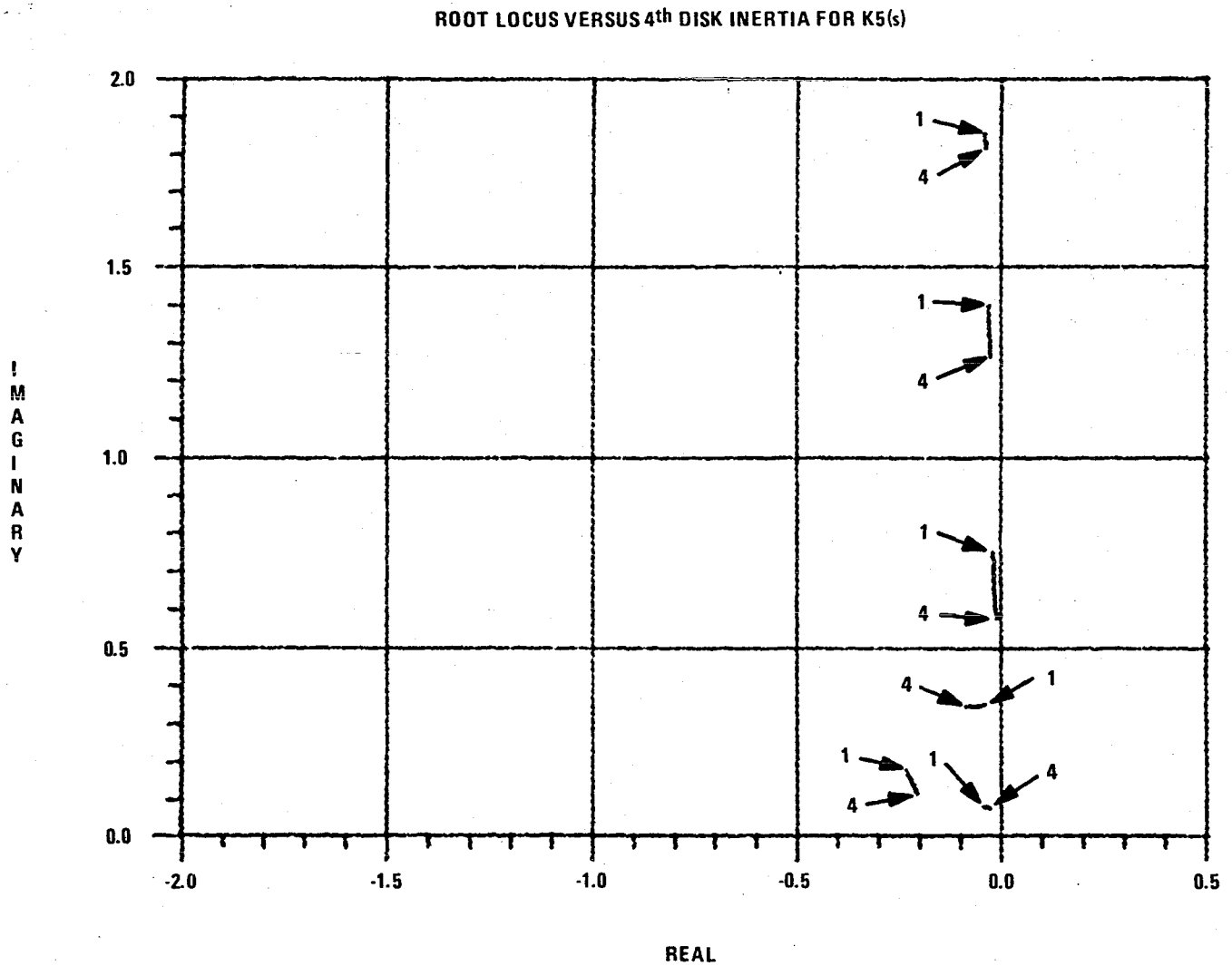

Figure E.4 Root Locus For Robust Four Disk Design

Table E.6 Flexible Beam Closed Loop Poles for G(s) and $K_6(s)$ (Non-unity model reduction weighting)

	real	imaginary	frequency	damping
1	-2.8533e+00	0.0000e+00	2.8533e+00	1.0000e+00
2	-9.9263e-01	4.6585e+00	4.7631e+00	2.0840e-01
3	-9.9263e-01	-4.6585e+00	4.7631e+00	2.0840e-01
4	-6.3522e+00	0.0000e+00	6.3522e+00	1.0000e+00
5	-1.1824e+00	1.1811e+01	1.1870e+01	9.9610e-02
6	-1.1824e+00	-1.1811e+01	1.1870e+01	9.9610e-02
7	-9.8649e-02	2.1721e+01	2.1721e+01	4.5417e-03
8	-9.8649e-02	-2.1721e+01	2.1721e+01	4.5417e-03
9	-2.9323e+00	2.1774e+01	2.1971e+01	1.3347e-01
10	-2.9323e+00	-2.1774e+01	2.1971e+01	1.3347e-01
11	-1.1634e+00	4.2174e+01	4.2190e+01	2.7575e-02
12	-1.1634e+00	-4.2174e+01	4.2190e+01	2.7575e-02
13	-1.9634e+00	5.2381e+01	5.2417e+01	3.7458e-02
14	-1.9634e+00	-5.2381e+01	5.2417e+01	3.7458e-02

Table E.7 Flexible Beam Closed Loop Poles for G(s) and $K_{mt}(s)$ (LQG design based on reduced order model of G(s) obtained with mode truncation)

	real	imaginary	frequency	damping
1	-3.4733e+00	2.4961e+00	4.2772e+00	8.1206e-01
2	-3.4733e+00	-2.4961e+00	4.2772e+00	8.1206e-01
3	-1.0143e+01	3.4765e+00	1.0722e+01	9.4598e-01
4	-1.0143e+01	-3.4765e+00	1.0722e+01	9.4598e-01
5	-2.1691e+00	1.1628e+01	1.1829e+01	1.8338e-01
6	-2.1691e+00	-1.1628e+01	1.1829e+01	1.8338e-01
7	-7.3621e-01	2.2054e+01	2.2066e+01	3.3364e-02
8	-7.3621e-01	-2.2054e+01	2.2066e+01	3.3364e-02
9	-4.0673e+00	3.6747e+01	3.6971e+01	1.1001e-01
10	-4.0673e+00	-3.6747e+01	3.6971e+01	1.1001e-01
11	1.5150e+01	6.0890e+01	6.2746e+01	-2.4145e-01
12	1.5150e+01	-6.0890e+01	6.2746e+01	-2.4145e-01
13	-2.0670e+02	2.0346e+02	2.9003e+02	7.1267e-01
14	-2.0670e+02	-2.0346e+02	2.9003e+02	7.1267e-01

Results With Modal Truncation

Another sixth order compensator, $K_{mt}(s)$ was obtained by truncating the second order mode with $|s| = \omega_3$ in the partial fraction expansion of $G(s)$ and doing a LQG loop shaping design with this sixth order reduced order model. This compensator produces an unstable system with closed loop poles shown in Table E.7. The differences between the two designs involving $K_6(s)$ and $K_{mt}(s)$ are readily seen from the loop gain plots for the two designs shown in Fig. E.5. While both loops have the same low frequency performance characteristics, the peak at $s = j\omega_3$ is less than one for $K_6(s)$ and greater than ten for $K_{mt}(s)$. Note that the unstable pole has a magnitude of approximately ω_3.

ACOSS Example

Sensitivity With Respect To Knowledge of Resonant Frequencies

The transmission zeros of the compensator $K(s)$ are given in Table E.8. Comparing these zeros with the poles of $G_{84}(s)$ it can be seen that the compensation involves pole-zero cancellation near the $j\omega$ axis which is a concern. An analysis was performed to assess the stability of the closed loop system in the face of simultaneous uncertainty in the critical resonant frequencies given in Table E.9 (sensitivity to other resonant frequencies would be less severe). The analysis was performed assuming that for any uncertainty the DC gain of $G_{84}(s)$ was known exactly.

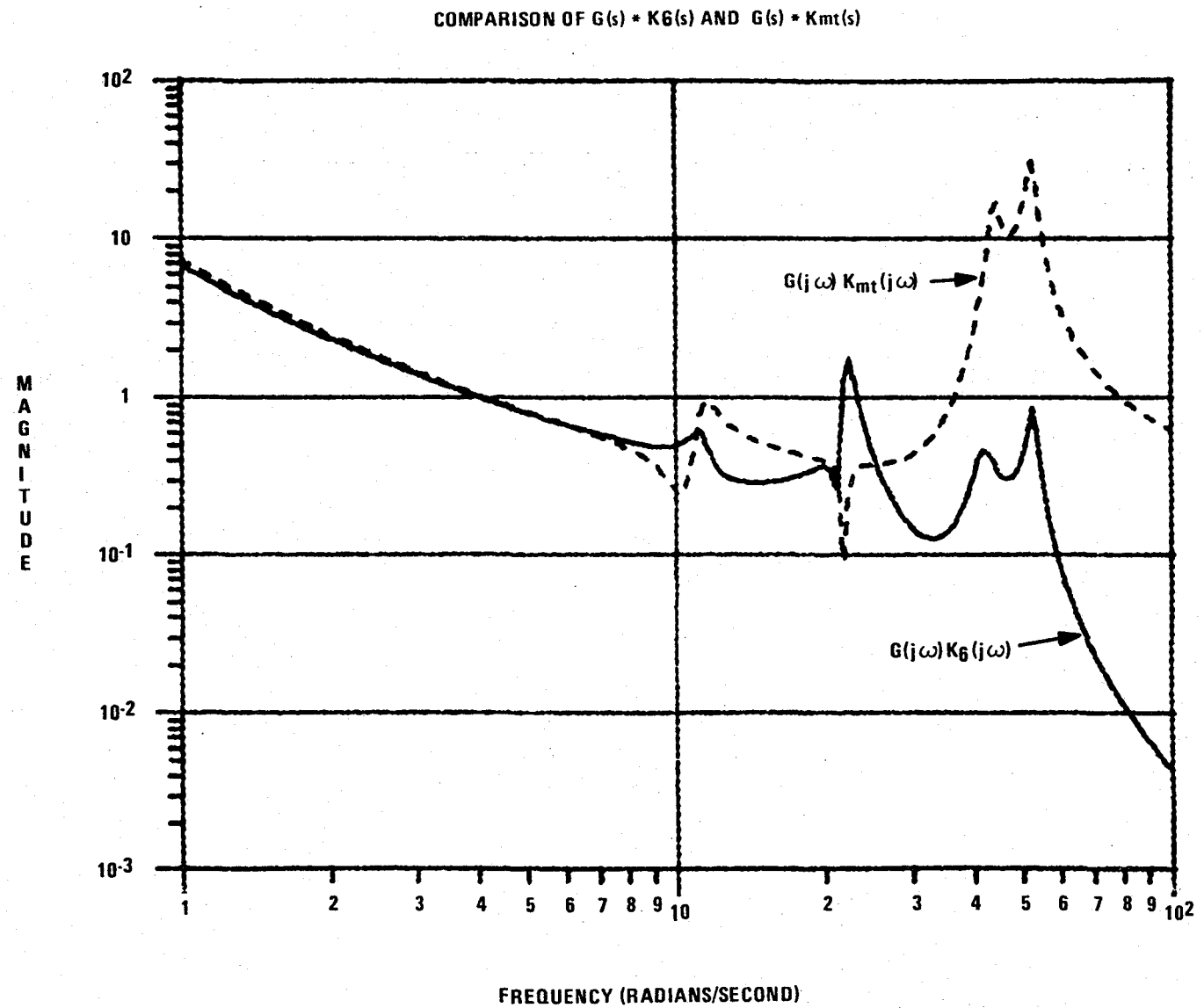

Figure E.5 Comparison of Loop Shapes For Flexible Beam System

Table E.8 Transmission Zeros of K(s)

	real	imaginary	frequency	damping
1	-2.9816e-02	8.8096e-02	9.3005e-02	3.2059e-01
2	-2.9816e-02	-8.8096e-02	9.3005e-02	3.2059e-01
3	-5.5829e-01	0.0000e+00	5.5829e-01	1.0000e+00
4	-5.9824e-01	0.0000e+00	5.9824e-01	1.0000e+00
5	-8.5396e-01	0.0000e+00	8.5396e-01	1.0000e+00
6	-5.8649e-01	7.9556e-01	9.8838e-01	5.9339e-01
7	-5.8649e-01	-7.9556e-01	9.8838e-01	5.9339e-01
8	-1.2038e-02	-2.0914e+00	2.0915e+00	5.7559e-03
9	-1.2038e-02	2.0914e+00	2.0915e+00	5.7559e-03
10	-4.4255e-02	-7.7002e+00	7.7004e+00	5.7471e-03
11	-4.4255e-02	7.7002e+00	7.7004e+00	5.7471e-03
12	-3.7544e-02	-8.1589e+00	8.1590e+00	4.6016e-03
13	-3.7544e-02	8.1589e+00	8.1590e+00	4.6016e-03
14	-9.0018e-02	1.0757e+01	1.0757e+01	8.3680e-03
15	-9.0018e-02	-1.0757e+01	1.0757e+01	8.3680e-03
16	-6.8857e-02	1.4851e+01	1.4852e+01	4.6363e-03
17	-6.8857e-02	-1.4851e+01	1.4852e+01	4.6363e-03
18	-1.0316e-01	-1.8770e+01	1.8770e+01	5.4960e-03
19	-1.0316e-01	1.8770e+01	1.8770e+01	5.4960e-03
20	-1.0340e-01	-1.9954e+01	1.9955e+01	5.1816e-03
21	-1.0340e-01	1.9954e+01	1.9955e+01	5.1816e-03
22	-1.0712e-01	2.1283e+01	2.1283e+01	5.0329e-03
23	-1.0712e-01	-2.1283e+01	2.1283e+01	5.0329e-03
24	-1.2568e-01	5.3099e+01	5.3099e+01	2.3668e-03
25	-1.2568e-01	-5.3099e+01	5.3099e+01	2.3668e-03
26	-3.4154e-01	-7.1233e+01	7.1234e+01	4.7946e-03
27	-3.4154e-01	7.1233e+01	7.1234e+01	4.7946e-03
28	-4.1136e-04	8.5839e+01	8.5839e+01	4.7922e-06
29	-4.1136e-04	-8.5839e+01	8.5839e+01	4.7922e-06

Table E.9 Critical Resonant Frequencies and Their Uncertainty

Mode	ω_i	% Uncertainty
10	2.09	0.5
14	7.69	0.2
15	8.17	0.2
17	10.8	1.0
21	14.9	2.0
22	18.8	2.0
23	20.0	2.0
24	21.3	2.0
29	52.5	20.
30	53.9	20.
33	71.3	20.
36	85.3	20.
37	86.2	20.

Recall that $G_{84}(s)$ can be written

$$G_{84}(s;\Omega) = \frac{R}{s^2} + \sum_{i=7}^{84} \frac{c_i b_i}{\omega_i^2} \frac{\omega_i^2}{s^2 + 2\zeta_i\omega_i s + \omega_i^2}$$

where Ω denotes the actual values of the thirteen resonant frequencies given in Table E.9. Let the nominal system be given by

$$G_{84}(s;\hat{\Omega}) = \frac{R}{s^2} + \sum_{i=7}^{84} \frac{c_i b_i}{\omega_i^2} \frac{\hat{\omega}_i^2}{s^2 + 2\zeta_i\hat{\omega}_i s + \hat{\omega}_i^2}$$

where $\hat{\Omega}$ denotes the nominal values of the thirteen resonant frequencies given in Table E.9. Note that in general $\omega_i \neq \hat{\omega}_i$ for $\omega_i \epsilon \Omega$ and $\omega_i = \hat{\omega}_i$ for $\omega_i \notin \Omega$.

Consider the additive perturbation implied by the uncertainty in $\omega_i \epsilon \Omega$

$$\begin{aligned}\Delta(s) &= G_{84}(s;\Omega) - G_{84}(s;\hat{\Omega}) \\ &= \sum_{\substack{i \ s.t. \\ \omega_i \epsilon \Omega}} \frac{c_i b_i}{\omega_i^2} \frac{s[(\omega_i^2 - \hat{\omega}_i^2)s + 2\zeta_i\omega_i\hat{\omega}_i(\omega_i - \hat{\omega}_i)]}{(s^2 + 2\zeta_i\omega_i s + \omega_i^2)(s^2 + 2\zeta_i\hat{\omega}_i s + \hat{\omega}_i^2)}\end{aligned}$$

Note that the resonant frequencies not included in Ω do not appear in the expression for $\Delta(s)$. Also note that $\Delta(0) = 0$.

The stability robustness theorem of Chapter II guarantees stability of the closed loop system in the presence of the uncertainty if

$$\max_{\Omega \epsilon \overline{\Omega}} \left\{ \bar{\sigma} \left[\Delta(j\omega) K(j\omega) \left[I + G_{84}(j\omega;\hat{\Omega}) K(j\omega) \right]^{-1} \right] \right\} < 1 \qquad \forall \omega$$

where $\overline{\Omega}$ represents any Ω such that

$$1 - p_i \leq \frac{\omega_i}{\hat{\omega}_i} \leq 1 + p_i \qquad \omega_i \epsilon \Omega$$

and the percentage uncertainties, 100 p_i are given in Table E.9. This condition can be seen to be satisfied by examining Fig. E.6 where the left hand side is plotted versus ω and can be seen to be less than unity for any frequency. Thus the closed loop system is stable in the face of simultaneous percent uncertainty given in Table E.9 for the thirteen critical resonant frequencies.

Closed Loop Poles

The closed loop poles for the control system with $G_{29}(s)$ and $K(s)$ are given in Table E.10. Note that all have negative real parts.

Step Responses

Consider the closed loop system shown in Fig. E.7 where y is a 3×1 vector containing

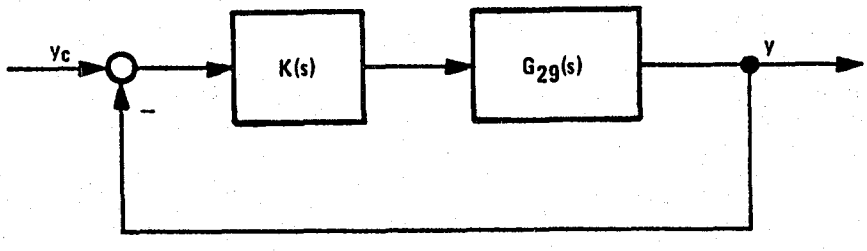

Fig. E.7 ACOSS Closed Loop System

Table E.10 ACOSS Closed Loop Poles for $G_{29}(s)$ and K(s)

	real	imaginary	frequency	damping
1	-2.9816e-02	8.8100e-02	9.3009e-02	3.2058e-01
2	-2.9816e-02	-8.8100e-02	9.3009e-02	3.2058e-01
3	-6.1360e-01	3.0984e-01	6.8739e-01	8.9265e-01
4	-6.1360e-01	-3.0984e-01	6.8739e-01	8.9265e-01
5	-4.0492e-01	7.9540e-01	8.9254e-01	4.5367e-01
6	-4.0492e-01	-7.9540e-01	8.9254e-01	4.5367e-01
7	-6.4070e-01	6.9728e-01	9.4694e-01	6.7660e-01
8	-6.4070e-01	-6.9728e-01	9.4694e-01	6.7660e-01
9	-9.3599e-01	6.1517e-01	1.1201e+00	8.3567e-01
10	-9.3599e-01	-6.1517e-01	1.1201e+00	8.3567e-01
11	-7.2532e-01	1.7343e+00	1.8798e+00	3.8584e-01
12	-7.2532e-01	-1.7343e+00	1.8798e+00	3.8584e-01
13	-1.3664e-02	1.9930e+00	1.9930e+00	6.8558e-03
14	-1.3664e-02	-1.9930e+00	1.9930e+00	6.8558e-03
15	-6.8568e-03	2.0257e+00	2.0257e+00	3.3849e-03
16	-6.8568e-03	-2.0257e+00	2.0257e+00	3.3849e-03
17	-1.0646e-02	2.0926e+00	2.0927e+00	5.0874e-03
18	-1.0646e-02	-2.0926e+00	2.0927e+00	5.0874e-03
19	-1.3639e+00	1.9261e+00	2.3601e+00	5.7790e-01
20	-1.3639e+00	-1.9261e+00	2.3601e+00	5.7790e-01
21	-1.9663e+00	1.9916e+00	2.7988e+00	7.0258e-01
22	-1.9663e+00	-1.9916e+00	2.7988e+00	7.0258e-01
23	-3.3905e+00	1.2301e+00	3.6067e+00	9.4005e-01
24	-3.3905e+00	-1.2301e+00	3.6067e+00	9.4005e-01
25	-3.6342e+00	4.1695e-01	3.6580e+00	9.9348e-01
26	-3.6342e+00	-4.1695e-01	3.6580e+00	9.9348e-01
27	-2.5629e+00	4.8492e+00	5.4848e+00	4.6727e-01
28	-2.5629e+00	-4.8492e+00	5.4848e+00	4.6727e-01
29	-7.9609e-01	6.7097e+00	6.7568e+00	1.1782e-01
30	-7.9609e-01	-6.7097e+00	6.7568e+00	1.1782e-01
31	-3.4522e+00	6.0854e+00	6.9964e+00	4.9343e-01
32	-3.4522e+00	-6.0854e+00	6.9964e+00	4.9343e-01
33	-5.2997e-01	7.4876e+00	7.5063e+00	7.0603e-02
34	-5.2997e-01	-7.4876e+00	7.5063e+00	7.0603e-02
35	-3.7437e-02	7.6858e+00	7.6859e+00	4.8709e-03
36	-3.7437e-02	-7.6858e+00	7.6859e+00	4.8709e-03
37	-5.3200e-02	8.1980e+00	8.1981e+00	6.4893e-03
38	-5.3200e-02	-8.1980e+00	8.1981e+00	6.4893e-03
39	-5.1140e-02	1.0824e+01	1.0824e+01	4.7248e-03
40	-5.1140e-02	-1.0824e+01	1.0824e+01	4.7248e-03
41	-2.0123e-01	1.1277e+01	1.1279e+01	1.7841e-02
42	-2.0123e-01	-1.1277e+01	1.1279e+01	1.7841e-02
43	-8.6668e+00	7.3510e+00	1.1364e+01	7.6262e-01
44	-8.6668e+00	-7.3510e+00	1.1364e+01	7.6262e-01
45	-1.6999e+00	1.4005e+01	1.4107e+01	1.2050e-01
46	-1.6999e+00	-1.4005e+01	1.4107e+01	1.2050e-01
47	-7.8180e-02	1.4847e+01	1.4847e+01	5.2658e-03
48	-7.8180e-02	-1.4847e+01	1.4847e+01	5.2658e-03
49	-1.2081e+01	8.9556e+00	1.5039e+01	8.0335e-01
50	-1.2081e+01	-8.9556e+00	1.5039e+01	8.0335e-01
51	-9.6233e-02	1.8783e+01	1.8783e+01	5.1234e-03
52	-9.6233e-02	-1.8783e+01	1.8783e+01	5.1234e-03

Table E.10 ACOSS Closed Loop Poles for $G_{29}(s)$ and K(s) (continued)

53	-7.8238e-01	1.8999e+01	1.9015e+01	4.1146e-02
54	-7.8238e-01	-1.8999e+01	1.9015e+01	4.1146e-02
55	-9.7238e-02	1.9954e+01	1.9955e+01	4.8730e-03
56	-9.7238e-02	-1.9954e+01	1.9955e+01	4.8730e-03
57	-1.0795e-01	2.1283e+01	2.1283e+01	5.0723e-03
58	-1.0795e-01	-2.1283e+01	2.1283e+01	5.0723e-03
59	-1.9858e+00	2.1922e+01	2.2012e+01	9.0213e-02
60	-1.9858e+00	-2.1922e+01	2.2012e+01	9.0213e-02
61	-3.7302e+00	2.2085e+01	2.2398e+01	1.6654e-01
62	-3.7302e+00	-2.2085e+01	2.2398e+01	1.6654e-01
63	-1.6470e-01	3.3051e+01	3.3052e+01	4.9830e-03
64	-1.6470e-01	-3.3051e+01	3.3052e+01	4.9830e-03
65	-2.5546e-01	5.0998e+01	5.0999e+01	5.0091e-03
66	-2.5546e-01	-5.0998e+01	5.0999e+01	5.0091e-03
67	-2.5671e-01	5.2528e+01	5.2528e+01	4.8871e-03
68	-2.5671e-01	-5.2528e+01	5.2528e+01	4.8871e-03
69	-2.3095e-01	5.3103e+01	5.3103e+01	4.3490e-03
70	-2.3095e-01	-5.3103e+01	5.3103e+01	4.3490e-03
71	-2.7437e-01	5.3848e+01	5.3849e+01	5.0951e-03
72	-2.7437e-01	-5.3848e+01	5.3849e+01	5.0951e-03
73	-3.6814e-01	7.1237e+01	7.1238e+01	5.1678e-03
74	-3.6814e-01	-7.1237e+01	7.1238e+01	5.1678e-03
75	-3.5867e-01	7.1286e+01	7.1287e+01	5.0313e-03
76	-3.5867e-01	-7.1286e+01	7.1287e+01	5.0313e-03
77	-3.6135e-01	7.2242e+01	7.2243e+01	5.0019e-03
78	-3.6135e-01	-7.2242e+01	7.2243e+01	5.0019e-03
79	-4.0078e-01	7.9957e+01	7.9958e+01	5.0124e-03
80	-4.0078e-01	-7.9957e+01	7.9958e+01	5.0124e-03
81	-4.4628e-01	8.5342e+01	8.5343e+01	5.2293e-03
82	-4.4628e-01	-8.5342e+01	8.5343e+01	5.2293e-03
83	-6.7891e-02	8.5837e+01	8.5837e+01	7.9092e-04
84	-6.7891e-02	-8.5837e+01	8.5837e+01	7.9092e-04
85	-4.1536e-01	8.6172e+01	8.6173e+01	4.8201e-03
86	-4.1536e-01	-8.6172e+01	8.6173e+01	4.8201e-03
87	-4.4261e-01	8.8972e+01	8.8973e+01	4.9746e-03
88	-4.4261e-01	-8.8972e+01	8.8973e+01	4.9746e-03
89	-4.9289e-01	9.8345e+01	9.8346e+01	5.0118e-03
90	-4.9289e-01	-9.8345e+01	9.8346e+01	5.0118e-03

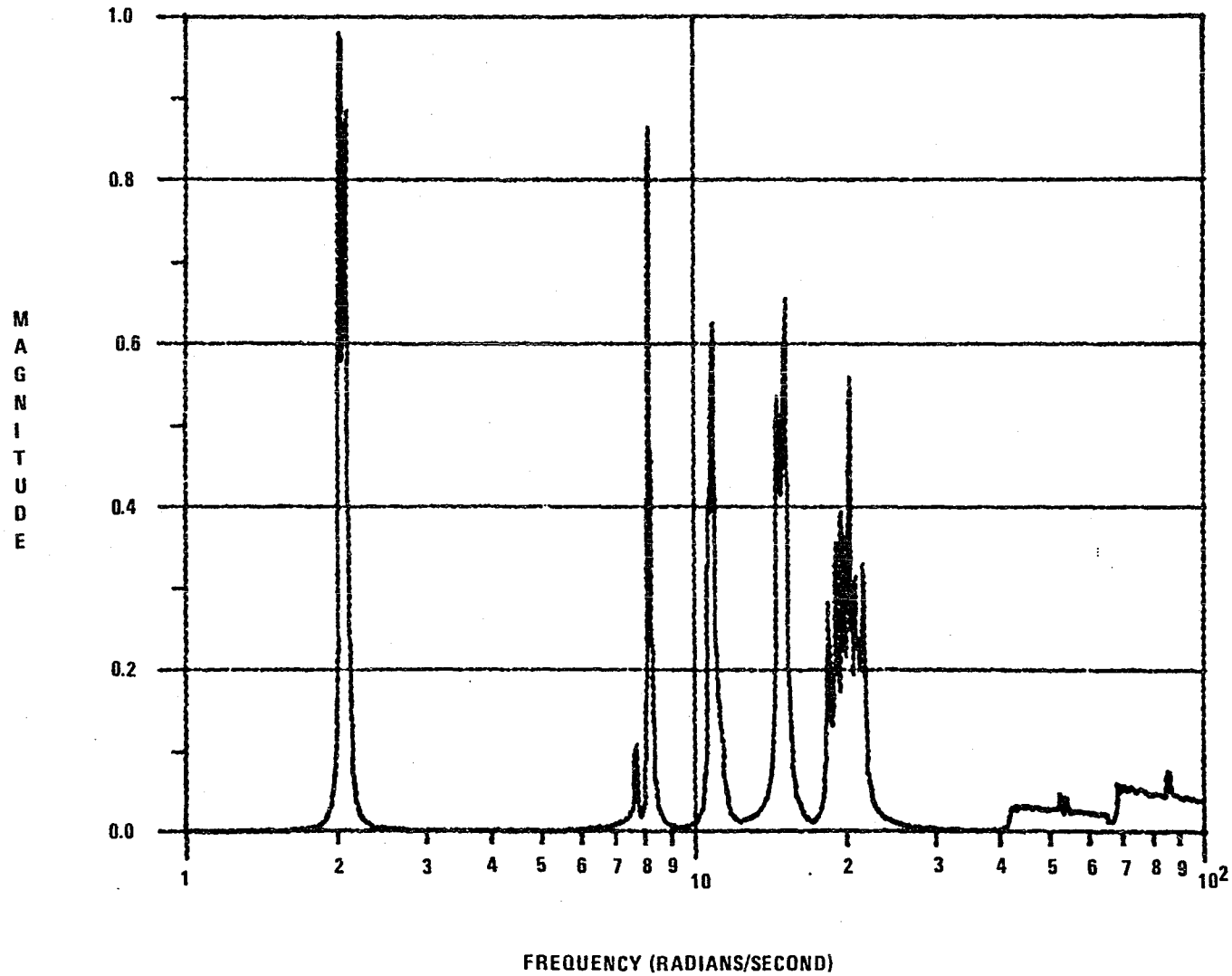

Figure E.6 Stability Robustness Test For ACOSS

the Node 11 gyro outputs for attitude about the x, y, z axes measured in radians and y_c is the commanded value of y.

Based on the low frequency performance specification of Fig. V.16, the design of $K(s)$ was carried out such that

$$y(s) \cong C(sI-A+K_f C)^{-1}K_f \; y_c(s)$$

where A, K_f, C are defined in the "Preliminary Design Steps" section of Chapter V and are based on rigid body characteristics of the space structure. The poles of this rigid body closed loop transfer function are given in Table E.11.

It is of interest to compare the step responses of the actual closed loop system with $K(s)$ and $G_{29}(s)$ to the rigid body response, i.e. that of $C(sI-A+K_f C)^{-1}K_f$. The x, y, z gyro responses are shown in Figs. E.8a, b for an x command, i.e. $y_c^T = [1 \;\; 0 \;\; 0]$. The x, y, z gyro responses are shown in Figs. E.9a, b for a y command, i.e. $y_c^T = [0 \;\; 1 \;\; 0]$. The x, y, z gyro responses are shown in Figs. E.10a, b for a z command, i.e. $y_c^T = [0 \;\; 0 \;\; 1]$.

Note that the actual responses are basically the same as the rigid body responses. The actual response is a little slower, has a little more overshoot and takes a little longer to settle out compared to the rigid body responses. Note also that the off axis coupling Figs. E.8b, E.9b, E.10b is always less than 8% of the command and less than 2% of the command after 6 sec.

Table E.11 Poles of the Rigid Body Closed Loop Transfer Function

	real	imaginary	frequency	damping
1	-6.3465e-01	6.3465e-01	8.9753e-01	7.0711e-01
2	-6.3465e-01	-6.3465e-01	8.9753e-01	7.0711e-01
3	-6.6044e-01	6.6044e-01	9.3400e-01	7.0711e-01
4	-6.6044e-01	-6.6044e-01	9.3400e-01	7.0711e-01
5	-9.8923e-01	9.8923e-01	1.3990e+00	7.0711e-01
6	-9.8923e-01	-9.8923e-01	1.3990e+00	7.0711e-01

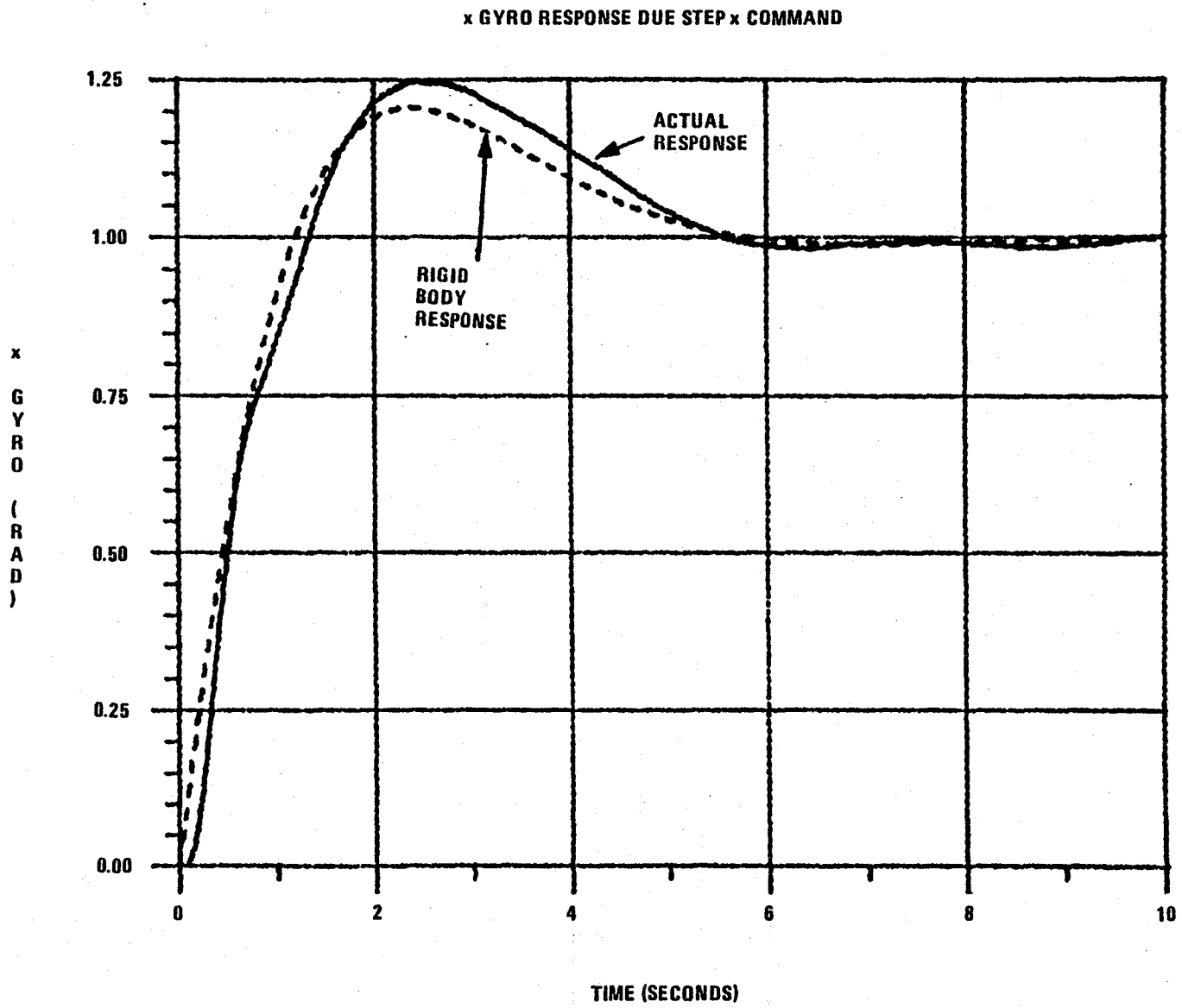

Figure 8a Response of x Gyro to Step x Command

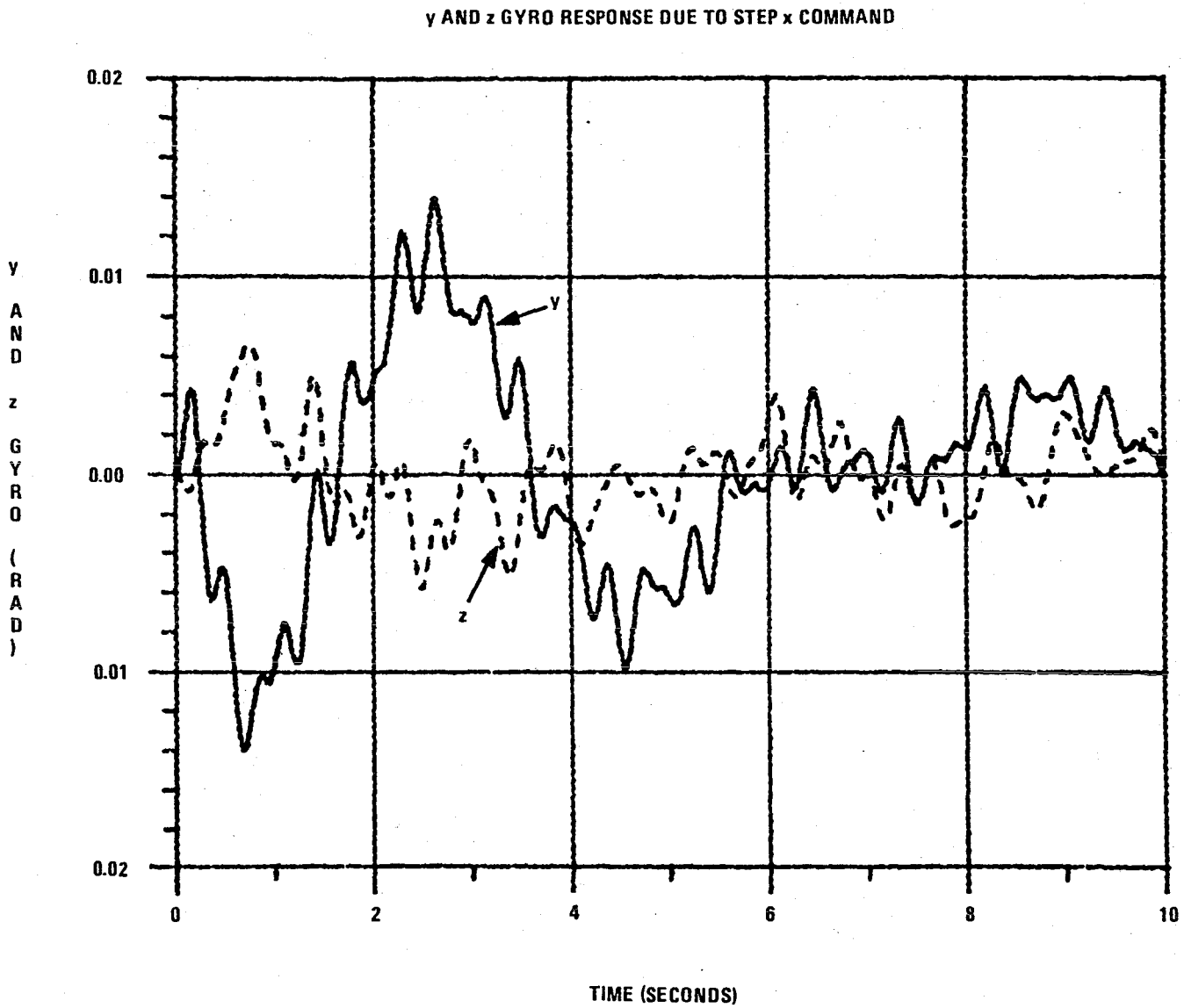

Fig. E.8b Response of y and z Gyros Due To Step x Command

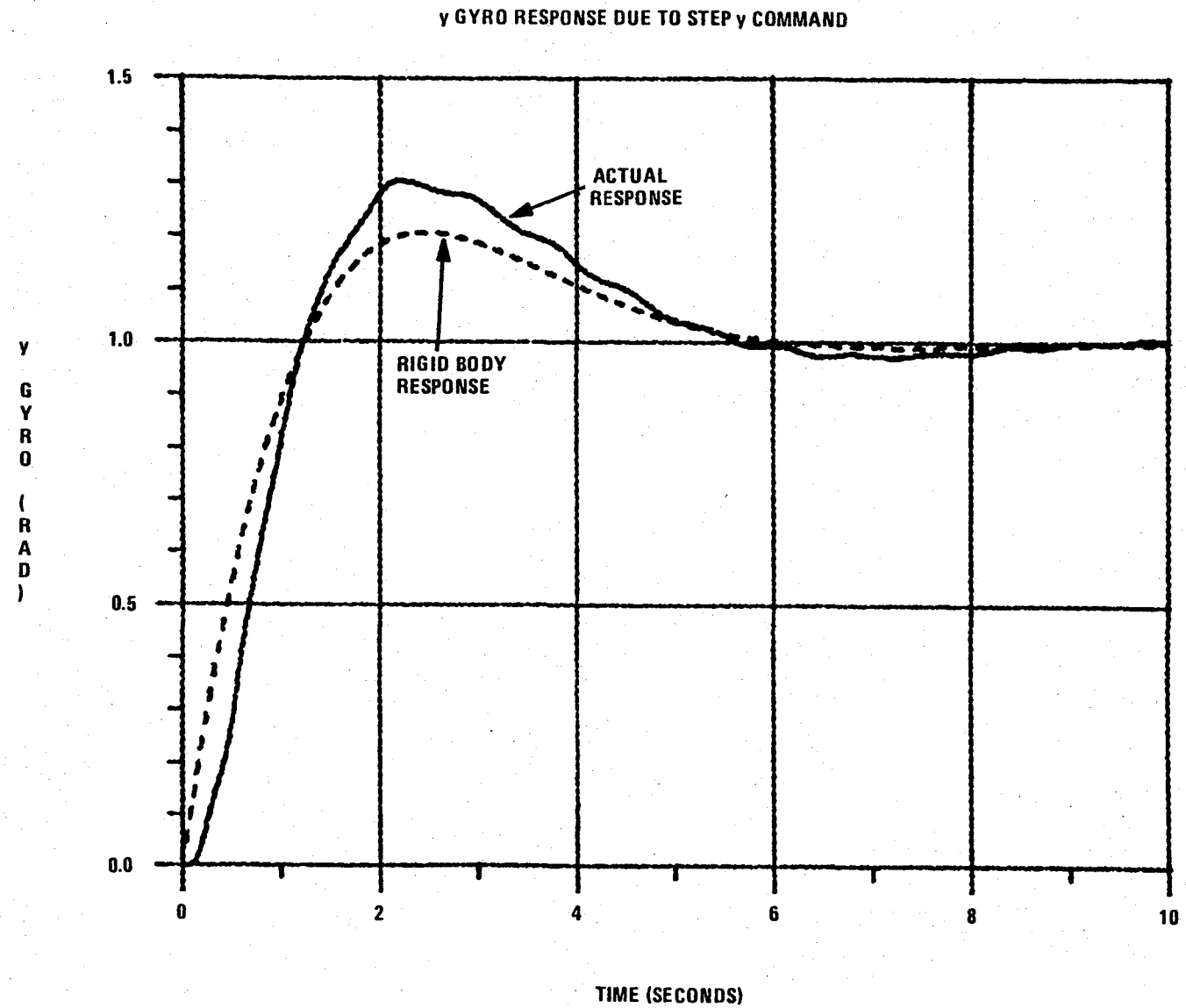

Figure E.9a Response of y Gyro to Step y Command

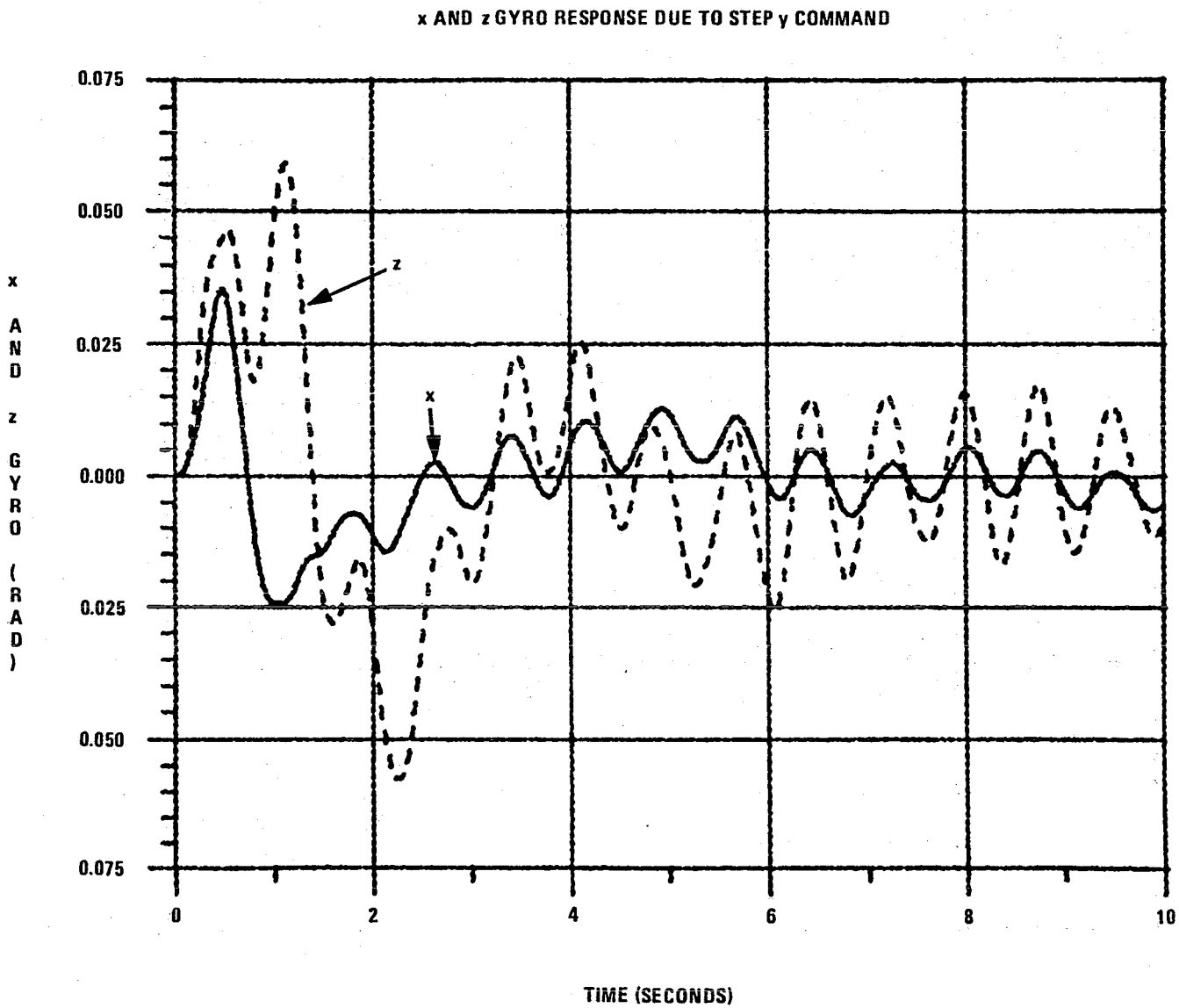

Figure E.9b Response of x and z Gyros Due To Step y Command

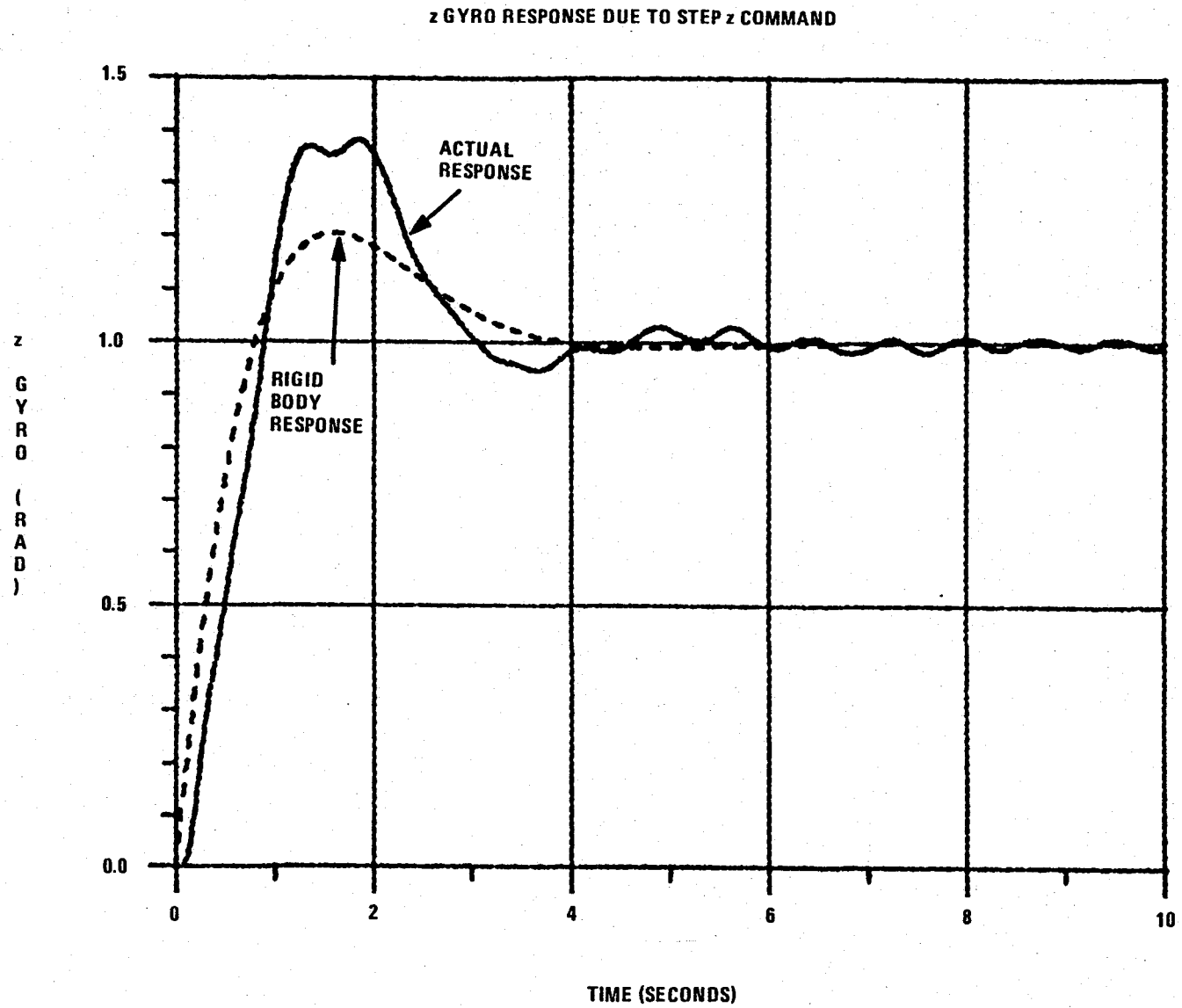

Figure E.10a Response of z Gyro to Step z Command

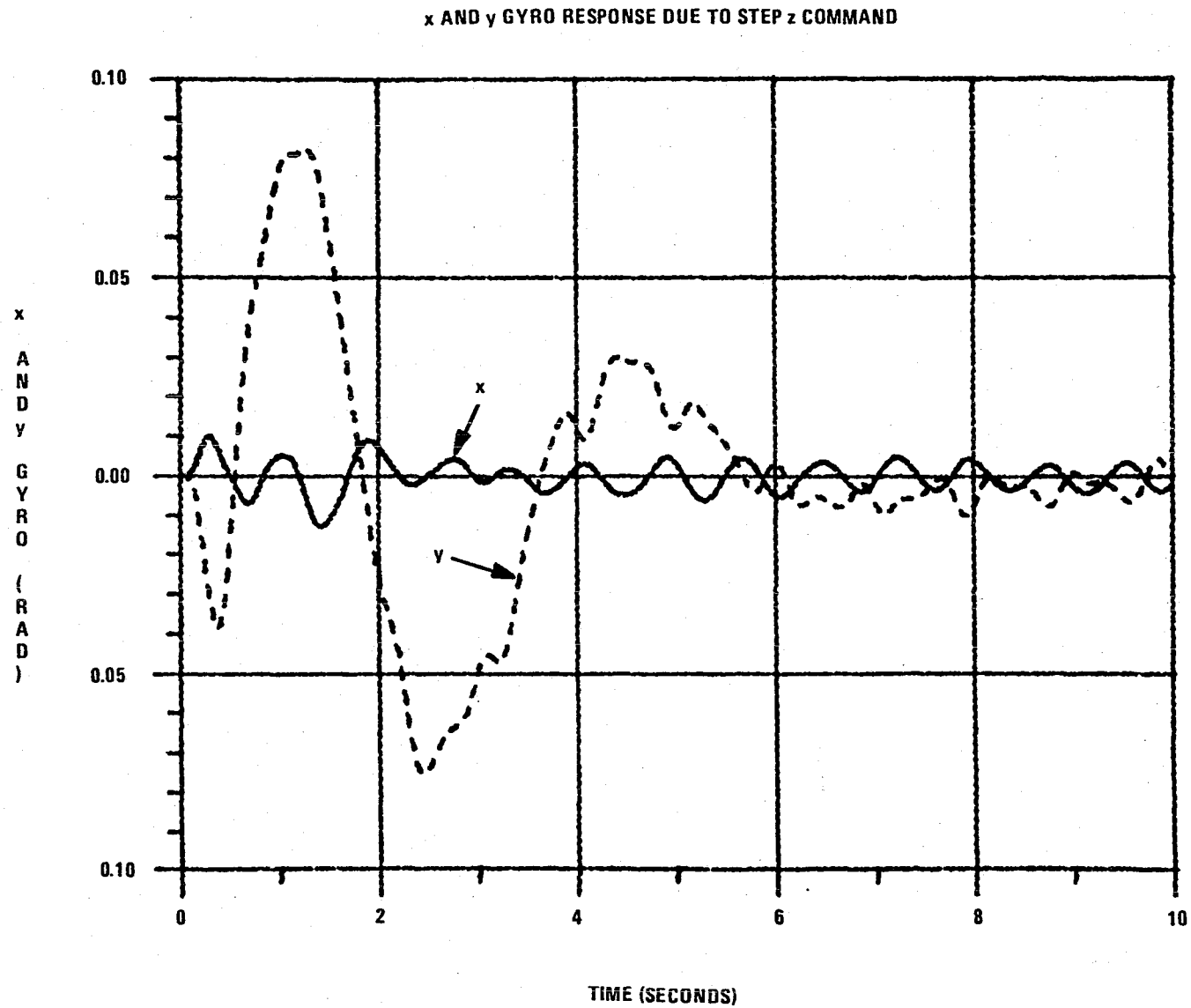

Figure E.10b Response of x and y Gyros Due To Step z Command

APPENDIX F

TRANSFER FUNCTION FACTORIZATION INVOLVING TRANSMISSION ZEROS

An nth order MIMO transfer function, $G(s)$ with $q \leq n$ transmission zeros at $s = z_1, z_2, ..., z_q$ can always by factored in the two ways:

$$G(s) = \hat{G}_i(s)P_i(s) = P_o(s)\hat{G}_o(s)$$

where $\hat{G}_i(s)$ and $\hat{G}_o(s)$ have transmission zeros at $s = -z_1, -z_2, ..., -z_q$ and $P_i(s)$ and $P_o(s)$ are MIMO all pass transfer functions with transmission zeros at $s = z_1, z_2, ..., z_q$ and poles at $s = -z_1, -z_2, ..., -z_q$. MIMO all pass transfer functions have the property that

$$\begin{aligned} P_i(s)P_i^T(-s) &= P_i^T(-s)P_i(s) = I \\ P_o(s)P_o^T(-s) &= P_o^T(-s)P_o(s) = I \quad . \end{aligned}$$

These factorizations are not unique. Consider a unitary transformation, i.e. a matrix V such that $V^T V = I$. Let

$$\begin{aligned} \tilde{G}_i(s) &= \hat{G}_i(s)V_i^T \quad \tilde{P}_i(s) = V_i P_i(s) \qquad V_i^T V_i = I \\ \tilde{P}_o(s) &= P_o(s)V_o^T \quad \tilde{G}_o(s) = V_o \hat{G}_o(s) \quad V_o^T V_o = I \end{aligned}$$

then

$$G(s) = \tilde{G}_i(s)\tilde{P}_i(s) = \tilde{P}_o(s)\tilde{G}_o(s)$$

for any unitary matrices V_i and V_o. Thus the factorizations are only unique up to a unitary transformation.

These factorizations can be expressed in state space terms [Ref. 31]. Let $\{A,B,C,D\}$ be a realization of $G(s)$ i.e. $G(s) = C(sI-A)^{-1}B + D$. The factorizations are expressed in terms of the generalized eigenvectors for the transmission zeros generalized eigenvalue problem. The results for a single ($q = 1$) real zero at $s = z$ and a complex pair ($q = 2$) of zeros at $s = z$ and $s = z^*$ are given in Table F.1. More than one zero or one complex pair can be handled by repeated application of the formulas in Table F.1.

These factorizations are particularly useful for obtaining a minimum phase approximation of a non-minimum phase transfer function. The factorizations are applied for the non-minimum phase zeros of $G(s)$ resulting in a minimum phase approximation $\hat{G}_i(s)V_i^T$ or $V_o\hat{G}_o(s)$ for any V_i, V_o such that $V_i^TV_i = I$ and $V_o^TV_o = I$. Important measures of the approximation error are defined by

$$\Delta_i(s) \triangleq \left[\hat{G}_i(s)V_i^T\right]^{-1}\left[G(s) - \hat{G}_i(s)V_i^T\right] = V_iP_i(s) - I$$
$$\Delta_o(s) \triangleq \left[G(s) - V_o\hat{G}_o(s)\right]\left[V_o\hat{G}_o(s)\right]^{-1} = P_o(s)V_o^T - I \quad .$$

Typically the unitary transformations, V_i and V_o are chosen such that $\Delta_i(0) = \Delta_o(0) = 0$. This is accomplished by letting

$$V_i = P_i^T(0)$$
$$V_o = P_o(0) \quad .$$

Table F.1

Transfer Function Factorization

Involving Zeros In State Space Terms

Input or Output Factorization	$G(s) = P(s)\hat{G}(s)$	$G(s) = \hat{G}(s)P(s)$
Generalized Eigenvalue Problem	$\begin{bmatrix} x^T & w^T \end{bmatrix} \begin{bmatrix} (zI-A) & -B \\ -C & -D \end{bmatrix} = 0$	$\begin{bmatrix} (zI-A) & -B \\ -C & -D \end{bmatrix} \begin{bmatrix} x \\ w \end{bmatrix} = 0$
Eigenvector Normalization	$w^H w = 1$	
$\hat{G}(s)$	$\hat{G}(s) = \hat{C}(sI-A)^{-1}B + D$	$\hat{G}(s) = C(sI-A)^{-1}\hat{B} + D$
	$\mathrm{Im}[z] = 0$	Special Case
$\hat{B}$, $\hat{C}$	$\hat{C} = C - 2zwx^T$	$\hat{B} = B - 2zxw^T$
$P(s)$	$P(s) = I - \frac{2z}{s+z} ww^T$	
	$\mathrm{Im}[z] \neq 0$	Special Case
Definitions	$\alpha \triangleq \mathrm{Re}[z]$ $\quad \beta \triangleq w^T w$ $\quad \gamma \triangleq \left(1 - \frac{\alpha^2 \lvert\beta\rvert^2}{\lvert z\rvert^2}\right)^{-1}$	
$\hat{B}$, $\hat{C}$	$\hat{C} = C - 4\alpha\gamma \mathrm{Re}\left[wx^H - \frac{\alpha\beta}{z} w^* x^H\right]$	$\hat{B} = B - 4\alpha\gamma \mathrm{Re}\left[xw^H - \frac{\alpha\beta}{z} x^* w^H\right]$
$P(s)$	$P(s) = I - \frac{4\alpha\gamma}{s^2+2\alpha s+\lvert z\rvert^2} \left\{ s\mathrm{Re}\left[ww^H - \frac{\alpha\beta}{z} w^* w^H\right] + \mathrm{Re}\left[zww^H - \alpha\beta w^* w^H\right] \right\}$	

Note: The expressions for $\hat{B}$ and γ in Reference 31 have typographical errors. The above expressions are correct.

APPENDIX G

ACOSS II MODEL DATA

The ACOSS II transfer function is given by

$$G(s) = \sum_{i=1}^{84} \frac{c_i b_i^T}{s^2 + 2\zeta_i \omega_i s + \omega_i^2}$$

where b_i is a 3×1 vector corresponding to x,y and z torque inputs at node 44, c_i is a 3×1 vector corresponding to x, y and z attitude outputs at node 11, ω_i is the frequency and ζ_i is the damping ratio for the ith mode. The data for ω_i, b_i and c_i is tabulated in Table G.1. The damping ratios are 0.005 for all modes except: 7, 8, 11, 12, 13, 16 which have damping ratios equal to 0.7.

The three rigid body modes corresponding to translation were eliminated by letting

$$B_R \triangleq \text{block row } \left[b_i^T\right] \qquad i=1, 2, \ldots, 6$$
$$C_R \triangleq \text{block col } \left[c_i\right] \qquad i=1, 2, \ldots, 6 \quad .$$

Then

$$G(s) = \frac{R}{s^2} + \sum_{i=7}^{84} \frac{c_i b_i^T}{s^2 + 2\zeta_i \omega_i s + \omega_i^2}$$

where

$$R \triangleq C_R B_R \quad .$$

Note that R^{-1} is the 3×3 inertia matrix for the center of mass of the structure

Table G.1 ACOSS II Data

Mode	Freq	Torque Inouts at Node 44			Attitude Outputs at Node 11		
		x	y	z	x	y	z
	rad/sec	1/Nm	1/Nm	1/Nm	rad	rad	rad
1	0.00e+00	1.38e-05	-3.84e-04	-6.09e-04	1.38e-05	-3.84e-04	-6.09e-04
2	0.00e+00	-4.69e-04	-4.59e-05	2.29e-04	-4.69e-04	-4.59e-05	2.29e-04
3	0.00e+00	4.83e-05	3.45e-05	-1.45e-04	4.83e-05	3.45e-05	-1.45e-04
4	0.00e+00	1.31e-04	-2.20e-04	1.21e-03	1.31e-04	-2.20e-04	1.21e-03
5	0.00e+00	-7.93e-04	4.56e-05	6.02e-05	-7.93e-04	4.56e-05	6.02e-05
6	0.00e+00	-6.01e-05	-7.84e-04	-2.01e-04	-6.01e-05	-7.84e-04	-2.01e-04
7	9.14e-01	2.83e-08	1.54e-03	-8.85e-05	-1.35e-06	-3.84e-04	-1.76e-05
8	1.65e+00	-7.32e-08	-2.37e-05	-5.49e-04	-1.39e-05	2.26e-04	1.15e-03
9	1.99e+00	4.76e-04	-1.04e-11	-5.41e-11	3.58e-06	1.14e-06	-5.81e-08
10	2.09e+00	2.52e-04	1.33e-09	5.66e-09	2.27e-04	2.59e-07	4.03e-07
11	2.78e+00	-1.49e-03	-7.99e-10	-3.32e-09	-9.31e-06	-3.45e-06	1.64e-07
12	3.63e+00	-9.28e-04	-5.43e-07	1.21e-06	-7.09e-04	-4.92e-05	-3.08e-06
13	3.65e+00	2.96e-06	-1.29e-04	5.17e-04	-5.55e-06	-8.67e-04	1.05e-04
14	7.69e+00	-3.07e-08	5.54e-03	7.70e-05	-3.68e-06	1.18e-05	1.09e-05
15	8.17e+00	2.14e-06	6.79e-05	-4.81e-03	-9.96e-05	8.51e-05	-2.82e-04
16	8.47e+00	-9.85e-03	6.05e-09	-9.79e-07	9.41e-05	-5.02e-06	2.65e-06
17	1.08e+01	-3.96e-07	-8.22e-07	1.41e-04	-6.42e-04	1.12e-03	-2.67e-03
18	1.14e+01	-2.72e-05	-4.22e-10	6.32e-09	-7.46e-07	1.53e-07	2.70e-07
19	1.14e+01	-1.03e-05	1.50e-09	-2.51e-08	7.87e-06	9.98e-07	-9.56e-07
20	1.19e+01	1.96e-12	3.69e-16	6.66e-16	-8.27e-15	9.10e-16	-3.42e-16
21	1.49e+01	1.55e-07	-2.71e-04	-2.48e-04	2.60e-04	-2.29e-03	-7.04e-04
22	1.88e+01	-1.72e-02	-3.76e-08	-4.96e-08	1.81e-05	-8.95e-06	3.87e-06
23	2.00e+01	-5.25e-08	-4.16e-05	1.03e-02	-2.54e-05	6.32e-06	-2.29e-04
24	2.13e+01	5.69e-08	-1.20e-02	-2.81e-05	-9.98e-06	7.91e-05	2.47e-05
25	3.24e+01	1.55e-12	-2.16e-15	7.04e-15	4.97e-16	6.45e-15	-3.76e-16
26	3.31e+01	-4.45e-03	1.63e-09	-7.45e-10	-1.75e-06	-2.18e-06	1.05e-06
27	4.95e+01	9.82e-14	5.54e-17	-1.04e-15	2.11e-16	-8.10e-18	1.07e-18
28	5.10e+01	-9.91e-07	3.25e-06	-7.63e-06	1.24e-03	-2.26e-03	9.77e-04
29	5.25e+01	-7.82e-03	-3.75e-10	2.27e-09	-2.95e-05	8.11e-06	-2.48e-06
30	5.39e+01	1.39e-04	-1.83e-09	3.26e-08	-1.78e-03	9.19e-04	-4.00e-04
31	5.54e+01	-1.07e-05	3.60e-12	2.39e-11	3.37e-06	-1.69e-05	1.17e-06
32	5.54e+01	2.99e-05	1.27e-11	5.75e-11	4.28e-06	-2.63e-06	9.30e-07
33	7.13e+01	1.65e-08	-5.02e-08	1.03e-02	-5.55e-06	1.20e-05	-1.59e-05
34	7.22e+01	1.72e-05	7.90e-07	-9.05e-06	-7.09e-04	3.50e-04	-4.15e-05
35	8.00e+01	-8.96e-05	6.84e-07	-1.79e-05	1.02e-03	-1.24e-03	-1.20e-03
36	8.53e+01	2.72e-07	1.72e-02	-1.52e-07	2.05e-05	-1.04e-04	-4.99e-05
37	8.62e+01	5.14e-05	-1.24e-03	-4.80e-05	-9.02e-05	-1.19e-03	-6.80e-04
38	8.90e+01	2.19e-05	1.49e-04	-1.12e-05	-1.96e-03	1.77e-03	2.23e-04
39	9.83e+01	5.43e-05	1.62e-06	1.27e-05	-2.46e-03	-3.56e-03	-5.47e-04
40	1.01e+02	-2.85e-05	5.77e-05	-2.20e-06	-2.08e-03	-7.68e-04	-4.39e-04
41	1.04e+02	1.97e-05	-7.47e-06	-6.19e-07	-1.01e-03	1.95e-03	-3.46e-05
42	1.05e+02	2.39e-05	3.19e-06	1.77e-05	-7.34e-04	-4.77e-05	-2.26e-04
43	1.08e+02	3.45e-05	-4.30e-05	4.93e-06	3.72e-04	-8.58e-05	-2.49e-04
44	1.12e+02	2.75e-05	-1.17e-06	6.77e-07	-1.78e-03	-1.31e-05	-1.91e-04
45	1.20e+02	3.05e-06	2.11e-05	-1.21e-05	-2.85e-03	3.64e-03	1.62e-05
46	1.49e+02	6.20e-05	4.27e-06	-6.21e-07	-2.36e-04	5.09e-04	-1.19e-04
47	1.53e+02	4.09e-06	-1.13e-05	2.17e-06	-2.73e-04	1.01e-03	-2.62e-04
48	1.63e+02	2.28e-07	-3.96e-06	9.39e-07	2.16e-05	2.87e-04	-5.33e-05
49	1.66e+02	-6.47e-06	-4.45e-08	-4.46e-07	6.96e-04	-3.49e-05	2.39e-04
50	1.66e+02	-7.41e-16	3.24e-17	-5.35e-17	-6.12e-16	-9.61e-17	1.77e-16
51	1.69e+02	2.39e-06	7.97e-06	7.46e-09	-1.76e-03	-1.75e-04	3.23e-05

Table G.1 ACOSS II Data (continued)

Mode	Freq	Torque Inputs at Node 44			Attitude Outputs at Node 11		
		x	y	z	x	y	z
	rad/sec	1/Nm	1/Nm	1/Nm	rad	rad	rad
52	1.75e+02	-9.32e-08	3.63e-06	-3.70e-06	1.16e-03	-3.18e-04	-6.35e-04
53	1.75e+02	2.72e-06	-8.45e-07	-5.57e-07	-2.49e-04	1.06e-04	-4.19e-04
54	1.79e+02	1.95e-06	-3.87e-06	7.66e-07	2.30e-04	2.11e-04	-1.00e-04
55	1.80e+02	-1.84e-09	5.09e-09	-1.48e-06	-5.09e-07	8.92e-08	9.68e-08
56	1.93e+02	-8.64e-07	-6.03e-07	4.60e-08	-2.32e-05	3.37e-04	1.76e-05
57	2.06e+02	1.59e-05	4.55e-07	-9.78e-07	5.42e-03	-9.34e-03	1.39e-03
58	2.11e+02	-1.66e-06	-3.41e-07	6.51e-08	-1.49e-04	7.05e-04	-3.26e-04
59	2.17e+02	-1.00e-05	2.64e-07	-1.50e-06	7.99e-03	4.57e-03	-3.84e-03
60	2.36e+02	-1.33e-07	-2.18e-08	9.56e-08	-4.23e-04	3.03e-05	-1.62e-04
61	2.40e+02	4.44e-07	-1.59e-07	-7.13e-07	5.40e-03	1.01e-04	7.32e-04
62	2.55e+02	-1.31e-07	-3.36e-07	1.70e-07	1.76e-04	-1.43e-04	2.00e-04
63	2.59e+02	-3.98e-06	7.45e-08	6.09e-07	-6.75e-03	4.81e-03	-1.42e-03
64	2.91e+02	3.94e-07	-2.05e-07	8.13e-09	1.31e-06	-1.57e-04	-5.18e-05
65	3.01e+02	-2.40e-08	-1.63e-08	5.34e-08	8.30e-05	-1.55e-04	-1.18e-04
66	3.21e+02	-2.17e-07	-1.58e-08	-4.46e-09	1.08e-04	6.69e-05	-1.71e-05
67	3.97e+02	-1.74e-07	-2.92e-07	-1.54e-08	-1.58e-03	-4.47e-04	-9.11e-04
68	3.97e+02	-6.46e-07	7.11e-08	-4.09e-08	-9.70e-04	3.30e-04	-5.39e-04
69	4.54e+02	9.75e-19	-3.61e-18	-5.26e-17	-4.91e-20	4.31e-17	-4.94e-17
70	4.55e+02	1.03e-13	-1.78e-13	4.61e-08	-6.67e-09	-7.56e-08	1.14e-08
71	5.79e+02	-1.97e-07	-4.69e-09	3.67e-09	4.31e-05	-3.36e-04	7.59e-04
72	5.79e+02	8.13e-09	-1.24e-07	6.28e-09	3.20e-05	-3.66e-04	4.52e-04
73	6.92e+02	5.02e-19	-1.33e-19	-2.87e-18	5.22e-17	2.43e-17	-4.99e-18
74	7.00e+02	-3.43e-14	-1.17e-12	-3.53e-08	7.41e-09	1.47e-07	-2.04e-08
75	9.47e+02	1.85e-12	2.52e-08	-1.96e-07	-3.84e-03	-3.36e-03	-1.51e-03
76	9.51e+02	-4.39e-08	1.48e-09	1.44e-08	3.24e-03	2.18e-03	2.31e-03
77	1.01e+03	-2.89e-08	-1.48e-08	1.34e-09	-5.67e-04	-5.85e-05	-3.26e-04
78	1.02e+03	1.48e-08	-2.95e-08	6.60e-10	-1.94e-04	9.00e-05	-2.25e-05
79	1.19e+03	1.15e-09	-4.69e-10	3.94e-08	1.87e-03	1.27e-03	2.38e-04
80	1.19e+03	5.27e-09	3.76e-10	-9.05e-09	-2.31e-03	-1.06e-03	-6.91e-04
81	1.31e+03	4.09e-09	-1.02e-08	4.33e-08	2.78e-03	3.29e-03	1.65e-04
82	1.31e+03	-8.02e-09	-6.49e-10	1.75e-08	4.57e-03	2.72e-03	1.18e-03
83	1.55e+03	-1.33e-10	-3.33e-09	6.55e-09	1.04e-03	8.63e-05	1.21e-04
84	1.55e+03	3.33e-09	7.37e-11	-5.86e-10	-1.02e-03	-8.33e-05	-1.58e-04

about the x, y and z axes. Finally a minimal realization of $\frac{R}{s^2}$ with 6 states is obtained as

$$\frac{R}{s^2} = C(sI-A)^{-1}B$$

where

$$A = \begin{bmatrix} 0 & I_3 \\ 0 & 0 \end{bmatrix} \quad B = \begin{bmatrix} 0 \\ R \end{bmatrix}$$
$$C = \begin{bmatrix} I_3 & 0 \end{bmatrix} \quad .$$

The modes with small residues: 18, 19, 20, 25, 27, 31, 32 and the modes with frequencies greater than 100 r/sec: 40, 41, ..., 84 were also eliminated as part of the preliminary simplification to form $G_{29}(s)$.

1. Report No.	2. Government Accession No.	3. Recipient's Catalog No.
NASA CR-170417		

4. Title and Subtitle	5. Report Date
MODEL REDUCTION FOR CONTROL SYSTEM DESIGN	March 1985
	6. Performing Organization Code

7. Author(s)	8. Performing Organization Report No.
Dale Enns	
	10. Work Unit No.
9. Performing Organization Name and Address Stanford Electronics Laboratories Stanford University Stanford, California 94305	11. Contract or Grant No. NAG2-223
	13. Type of Report and Period Covered Contractor Report-Final
12. Sponsoring Agency Name and Address National Aeronautics and Space Administration Washington, D.C. 20546	14. Sponsoring Agency Code RTOP 505-34-01

15. Supplementary Notes

NASA Technical Monitor: Kevin L. Petersen, Ames Research Center, Dryden Flight Research Facility, Edwards, California 93523

16. Abstract

In a number of applications areas, the control engineer is faced with controlling a physical system for which an analytical model can be derived in the form of a very large number of coupled, first order, linear, time invariant differential equations. This high order analytical model is an input to the controller design process for any design technique.

This thesis develops an approach and a technique for effectively obtaining reduced order mathematical models of a given large order model for the purposes of synthesis, analysis and implementation of control systems. This approach involves the use of an error criterion which is the H-infinity norm of a frequency weighted error between the full and reduced order models. The weightings are chosen to take into account the purpose for which the reduced order model is intended.

A previously unknown error bound in the H-infinity norm for reduced order models obtained from internally balanced realizations was obtained. This motivated further development of the balancing technique to include the frequency dependent weightings. This resulted in the frequency weighted balanced realization and a new model reduction technique.

Two new approaches to designing reduced order controllers were also developed. The first involves reducing the order of a high order controller with an appropriate weighting. The second involves linear-quadratic-Gaussian synthesis based on a reduced order model obtained with an appropriate weighting.

Several numerical examples are used to illustrate the theoretical developments of the thesis. These examples include aircraft and large space structure problems. The examples clearly illustrate the usefulness of this research for practical problems.

17. Key Words (Suggested by Author(s))	18. Distribution Statement
Model reduction technique Control law design	Unclassified-Unlimited STAR category 08

19. Security Classif. (of this report)	20. Security Classif. (of this page)	21. No. of Pages	22. Price*
Unclassified	Unclassified	277	A13

For sale by the National Technical Information Service, Springfield, Virginia 22161.

End of Document